The energetics and mechanics of jet propulsion swimming in European common cuttlefish (*Sepia officinalis*)

Nicholas William Gladman

Submitted in accordance with the requirements for the degree of
Doctor of Philosophy

The University of Leeds
Faculty of Biological Sciences
School of Biology

September 2018

Intellectual property rights

The candidate confirms that the work submitted is his own and that appropriate credit has been given where reference has been made to the work of others.

This copy has been supplied on the understanding that it is copyright material and that no quotation from the thesis may be published without proper acknowledgement.

© 2018 The University of Leeds and Nicholas William Gladman

Declaration

The work carried out in this thesis could not have taken place without the assistance of, and collaboration with, others. Dr Thomas Neil played a role in the initial setup of experiments, and implementation of some equations in chapter 2. Dr Graham Askew assisted in the collection and analysis of data presented in chapters 3 and 4.

Acknowledgements

I would initially like to thank Dr Graham Askew, for his supervision and guidance which proved invaluable throughout this project, I am particularly grateful for Graham's willingness to adapt the project after a shaky start at the university. I would also like to thank my co-supervisor Dr Steve Sait for his insightful comments and reminding me to see the bigger picture. My thanks also go to Dr Sarah Zylinski for giving me this opportunity in the first place, and The University of Leeds 110 Anniversary Scholarship for supporting me through the course of my PhD.

I would also like to thank my lab mates past and present, for providing support and discussions throughout this project. Thanks also to those with whom I have shared an office, you have made this journey an enjoyable one, and probably had to put up with me talking about cuttlefish for far longer than anyone should talk about cuttlefish for!

Finally I'd like to thank my family for all their support and encouragement throughout, even if they had no idea what I was talking about half the time.

Abstract

The locomotive systems of animals play a key role in behaviours such as foraging, predator avoidance and migrations. The range of behaviours and morphologies exhibited by animals have led to a variety of locomotor strategies. This thesis investigates the jet propulsion of cuttlefish (*Sepia officinalis*), where water is taken into a compressible cavity, this is compressed by surrounding musculature, forcing water out and forming a jet. This process involves the transfer of chemical energy into mechanical energy, before mechanical energy is transferred into the wake, propelling the animal through the water. Here the energy transduction chain is investigated from the biochemical level through the mechanical and ultimately into the wake of the animal, providing the most complete investigation into the energy transduction chain during locomotion to date.

Investigations into the structure and function of cuttlefish jet propulsion swimming found cuttlefish produced two distinct jet modes. Jet mode use differed between hatchlings and juveniles. Differential use of jet modes may relate to flow environments inhabited by animals. Different flow environments may impact propulsive efficiency, where hatchlings are more efficient than juveniles. Juvenile propulsive efficiency was ~73 %, the highest reported value among cephalopods to date. Further investigations into the mechanical properties of mantle musculature found shortening velocities scale weakly with animal age, while cyclic measures revealed frequencies which produce the greatest net mechanical power decreased with age. Mechanical and hydrodynamic data reveal a transfer efficiency of ~26 %. Biochemical analyses of mantle muscle worked at three cycle frequencies revealed musculature heavily utilised ATP and phosphagen stores, however, no significant differences were seen between cycle frequencies, with the contractile efficiency being ~26 %. Taken together, these data revealed ~19 % of the available biochemical energy was successfully transferred into useful movement, this seems to question the idea of jet propulsion swimming being an inefficient mode of

locomotion; this value does not account for recovery processes, suggesting efficiency may be lower.

Table of Contents

Intellectual property rights ..... **ii**

Declaration ..... **iii**

Acknowledgements ..... **iv**

Abstract ..... **v**

Table of Contents ..... **vii**

List of Tables ..... **xi**

List of Figures ..... **xii**

List of Abbreviations ..... **xiv**

Chapter 1. General introduction **1**

1.1 Fuel to high-energy phosphates 2

1.1.1 Molluscan muscle physiology 8

1.2 ATP to work 10

1.2.1 Muscle morphology 10

1.2.2 The cross-bridge cycle 12

1.2.3 Contractile efficiency of muscle 14

1.2.4 Contractile properties of molluscan muscle 17

1.2.5 Measuring muscle mechanics 18

1.2.5.1 *In vitro* approaches 19

1.2.5.1.1 Isometric muscle performance 19

1.2.5.1.2 Dynamic muscle performance 21

1.2.5.1.3 Cyclic muscle performance 23

1.2.5.2 *In vivo* approaches 25

1.2.6 Transfer efficiency of muscle 27

1.3 Energy to the environment 28

1.3.1 Swimming through jet propulsion 28

1.3.2 The efficiency of jet propulsion swimming 30

1.3.3 Molluscan locomotion 33

1.3.4 Visualisation of flow 35

1.3.5 Propulsive efficiency 35

1.4 Summary 37

Chapter 2. The hydrodynamics of jet propulsion swimming in European cuttlefish: wake structure and propulsive efficiency **40**

2.1 Abstract 40

2.2 Introduction 41
2.3 Methods 46
2.3.1 Animals 46
2.3.1.1 Animal housing facilities 46
2.3.2 Wake visualisation and analysis 47
2.3.3 Jet properties and propulsive efficiency 49
2.3.4 Swimming kinematics 53
2.3.5 Statistical analysis 53
2.4 Results 54
2.4.1 Animal morphology and swimming kinematics 54
2.4.2 Wake structure 59
2.4.3 Whole cycle propulsive efficiency 64
2.4.4 Allometric scaling of cuttlefish swimming 64
2.5 Discussion 69
2.5.1 Wake structure 69
2.5.2 Propulsive efficiency 71
2.5.3 Scaling of animal swimming mechanics and hydrodynamics 72
2.6 Summary 77
Chapter 3. The mechanical properties of the cuttlefish jet locomotor muscle……. 78
3.1 Abstract 78
3.2 Introduction 78
3.3 Methods 84
3.3.1 Animals 84
3.3.1.1 Juvenile cuttlefish 84
3.3.1.2 Adult cuttlefish 84
3.3.1.3 Animal housing facilities 85
3.3.2 Muscle preparation 85
3.3.3 Isometric contractile properties 87
3.3.4 Isotonic contractile properties 88
3.3.4.1 The force-velocity relationship 88
3.3.5 Cyclic contractile properties 89
3.3.5.1 The work-loop technique 89
3.3.6 *In vivo* estimation of muscle strain 90
3.3.7 Statistical analysis 91

3.4 Results 92
3.4.1 Isometric contractile properties 92
3.4.2 Isotonic contractile properties 98
3.4.2.1 The force-velocity relationship 98
3.4.3 Scaling dynamics of mantle muscle function 99
3.4.3.1 Muscle performance during cyclical contractions 103
3.4.3.1.1 The muscular stress during cyclical contractions 105
3.4.4 *In vivo* muscle activity 107
3.5 Discussion 107
3.5.1 Contractile characteristics of obliquely striated musculature 107
3.5.1.1 Ontogenetic scaling of mechanical performance 110
3.5.1 Performance of obliquely striated muscle under cyclical contractions 112
3.5.1.1 Interspecific comparisons 112
3.5.2 Limitations of this study 115
3.5.3 Transfer efficiency of muscular energy into the wake 118
3.6 Summary 119
Chapter 4. The efficiency of the mantle muscle during cyclical contractions 121
4.1 Abstract 121
4.2 Introduction 122
4.3 Methods 126
4.3.1 Animals 126
4.3.2 Muscle preparation 126
4.3.3 Sample preparation 128
4.3.3.1 Measurement of ATP 129
4.3.3.2 Measurement of arginine and arginine phosphate 130
4.3.3.3 Estimation of ATP used during exercise 132
4.3.4 Contractile efficiency 132
4.3.5 Statistical analysis 133
4.4 Results 133
4.4.1 Anaerobic metabolite concentrations 133
4.4.2 Total anaerobic ATP use during exercise 136
4.4.3 Contractile properties of mantle musculature 139
4.4.4 Contractile efficiency 141

4.5 Discussion 141
4.5.1 The contractile efficiency of cephalopod musculature 141
4.5.1.1 The impact of cycle frequency on contractile efficiency 144
4.5.2 The impact of work on metabolite levels 144
4.5.2.1 Interspecific comparisons 146
4.5.3 Metabolite profiles and muscle cycle frequency 147
4.5.3.1 Interspecific comparisons 148
4.6 Summary 149
Chapter 5. General Discussion 151
5.1 The contractile efficiency, and biochemical changes of mantle muscle during cyclical contractions 151
5.2 The mechanical properties and scaling of cuttlefish muscle 153
5.3 The hydrodynamics and scaling of cuttlefish jet propulsion swimming 155
5.4 How efficiently do cuttlefish utilise energy? 157
5.5 Future work 158
References 160
Appendix 1 188
Appendix 2 190
Appendix 3 192

List of Tables

Table 1. Morphology and swimming kinematics 55

Table 2. Differences in L_j/D_j of juvenile cuttlefish swimming either anterior- or posterior-first 60

Table 3. Regression results for selected parameters. 65

Table 4. Allometric scaling relationships of swimming parameters with respect to mantle length of cuttlefish. Significant relationships are highlighted in bold. 67

Table 5. Allometric scaling relationships of swimming parameters with respect to mantle length of hatchling and juvenile cuttlefish. Significant relationships are highlighted in bold. 67

Table 6. Modified parameters used for work loop experiments. 90

Table 7. Contractile properties of the locomotory musculature of several mollusc species. 95

Table 8. Differences in P_{tw}/P_0 following exercise of mantle musculature. 97

Table 9. Parameters of the hyperbolic linear equations for juvenile and adult mantle muscle preparations. 98

Table 10. Allometric scaling relationships of isometric and isotonic contractile properties and mantle length of cuttlefish. Significant relationships are highlighted in bold. 100

Table 11. Allometric scaling relationships of isometric and isotonic contractile properties and mantle length of juvenile and adult cuttlefish. Significant relationships are highlighted in bold. 101

Table 12. Content of ATP, arginine phosphate and arginine present in control and exercised mantle preparations. 135

Table 13. Pairwise comparisons between cycle frequencies. 137

Table 14. Contractile efficiency at different muscle cycle frequencies. ... 141

Table 15. Parameters tested during the optimisation process. 188

Table 16. Comparison of the work and power output of juvenile preparations from Chapters 3 and 4. 193

List of Figures

Figure 1. Illustrative diagram of the energy cascade during locomotion. 2

Figure 2. Schematic diagram indicating key aerobic processes. 5

Figure 3. Pathways of glycolysis. 6

Figure 4. Example phosphagen systems used within animal tissues. 7

Figure 5. Dehydrogenase pathways typically utilised by animals 7

Figure 6. Comparative diagram of striated (A.) and obliquely striated (B.) muscle structure. 11

Figure 7. Key stages during cross-bridge cycling. 14

Figure 8. Diagram indicating the relationship between the different efficiency measures. 16

Figure 9. Typical relationship between muscle force and the velocity of shortening. 22

Figure 10. Representative work loop. 25

Figure 11. The underlying structure of jets of mode I (A) and II (B). 31

Figure 12. Simplified diagram showing the mechanisms involved in the creation of a jet by a typical cephalopod. 43

Figure 13. Simplified diagram showing the arrangement of muscle fibres through the cephalopod mantle. 44

Figure 14. Typical setup for the PIV experiments. 49

Figure 15. Simplified diagram outlining the data taken to estimate refill area. 52

Figure 16. The mean swimming speed of hatchling and juvenile cuttlefish swimming anteriorly or posteriorly. 56

Figure 17. The estimated mean drag forces experienced by juvenile and hatchling cuttlefish during anterior- or posterior-first swimming. 57

Figure 18. Example profile of changes in velocity of a swimming cuttlefish… 58

Figure 19. Comparisons of instantaneous flow and vorticity between jet modes I (a, b) and II (c, d) 61

Figure 20. The relationship between relative swimming speed and jet angle of juvenile cuttlefish. 62

Figure 21. Relationship between cycle frequency and animal swimming speed. 63

Figure 22. Relationship between animal swimming speed and propulsive efficiency in hatchling and juvenile cuttlefish. 66

Figure 23. Allometric relationships between mantle length and selected swimming parameters. 68

Figure 24. Schematic diagram showing dissected cuttlefish muscle bundle within the muscle rig setup. 87

Figure 25. Example twitch and tetanic stress profiles from one adult (a) and juvenile (b) mantle preparation. 94

Figure 26. Example profiles from two twitch contractions from a 13 mm juvenile preparation. 97

Figure 27. Mean relationship between relative force and velocity of shortening from 5 juvenile and 6 adult cuttlefish preparations. 99

Figure 28. Scaling relationships between mantle length and mechanical properties of cuttlefish musculature. 102

Figure 29. Relationship between mantle muscle cycle frequency and net muscular power of juvenile (black) and adult (red) preparations subject to sinusoidal work. 104

Figure 30. Relationship between mantle muscle cycle frequency and net muscular work of juvenile (black) and adult (red) preparations subject to sinusoidal work. 105

Figure 31. The peak (± sem) stress of mantle muscle preparations during cyclic and isometric stimuli. 106

Figure 32. Diagram indicating the relationship between the different efficiency measures. 123

Figure 33. Boxplot showing the concentration of arginine, arginine-phosphate and ATP in control (unworked) and worked muscle (1 cycle at 0.8 (n=8), 1.4 (n=12) or 2 (n=9) Hz). 134

Figure 34. Boxplots showing the total ATP consumption by cuttlefish mantle muscle. 138

Figure 35. Boxplots of mechanical work and power per cycle at 0.8 (n=8), 1.4 (n=8) and 2 (n=9) Hz. 140

Figure 36. The energy cascade during contractile activity of the circular muscle of the cuttlefish mantle. 151

Figure 37. Example work loop traces from juvenile cuttlefish. Work loops consist of 5 loops at frequencies ranging from 0.8 to 2 Hz. 190

Figure 38. Example force produced by work loops ranging from 0.8 to 2 Hz…… 191

Figure 39. Comparison of the work output of muscle from juvenile preparations from Chapter 3 (red) and 4 (black) 192

Figure 40. Comparison of the power output of muscle from juvenile preparations from Chapter 3 (red) and 4 (black) 193

List of Abbreviations

Abbreviation	Meaning	Units
A	Constant	-
A_j	Jet area	cm^2
ATP_{total}	Total ATP use during exercise	$\mu mol\ g^{-1}$
A_r	Refill orifice area	cm
B	Constant	-
C	Constant	-
C_m	Mantle circumference	cm
C_{mmax}	Maximum mantle circumference	cm
d_{jet}	Distance travelled during a jet	cm
d_m	Mantle diameter	cm
D_{cf}	Diameter of the collar flaps	cm
D_j	Jet diameter	cm
f	Cycle frequency	Hz
L_0	Length of muscle which produced maximum twitch force	mm
L_b	Body length	cm and mm
L_j	Jet length	cm
L_m	Mantle length	cm and mm
P_0	Peak tetanic force	mN
P_{tw}	Peak twitch force	mN
P_{tw} / P_0	Twitch to tetanus ratio	-
r_{cf}	Radius of the collar flaps	cm
Re	Reynolds number	-

Abbreviation	Meaning	Units
RT_{50}	Half relaxation time following a twitch	Seconds
S	Slip	-
t	Time	Seconds
t_j	Time jetting	Seconds
tP_{tw}	Time to peak twitch	Seconds
t_r	Time refilling	Seconds
T	Thrust	mN
$\bar{u}_j$	Mean jet velocity	cm s^{-1}
$\bar{u}_r$	Refill velocity	cm s^{-1}
$\bar{U}$	Mean body velocity	cm s^{-1}
U_{Body}	Velocity in body lengths per second	Body lengths per second
V_{max}	Maximum velocity of muscle shortening	L s^{-1}
W_c	Mechanical work	J g^{-1} and J kg^{-1}
W_m	Free energy from ATP metabolism	J g^{-1}
η_c	Contractile efficiency	-
η_f	Froude efficiency	-
η_r	Rocket efficiency	-
η_T	Total efficiency	-
η_t	Transfer efficiency	-
η_{wc}	Whole cycle efficiency	-
Π_c	Peak net cyclic power	W kg^{-1}
Π_i	Peak net isotonic power	W kg^{-1}
ρ	Water density	kg m^{-3}
P_i	Inorganic phosphate	-
St	Strouhal number	-

Abbreviation	Meaning	Units
σ	Stress	kN m^{-3}
σ_0	Tetanic stress	kN m^{-3}
σ_{tw}	Twitch stress	kN m^{-3}

Chapter 1. General introduction

The locomotion of animals is shaped by aspects of its environment, behaviour, as well as underlying morphology and physiology (Alexander, 1999). The importance of locomotion is highlighted through its involvement in a variety of key behaviours ranging from foraging (Krauel *et al.*, 2018; Shipley *et al.*, 2018; Staniland *et al.*, 2018), and mate searching (Kasumovic and Seebacher, 2018; Muniz *et al.*, 2018; Wexler *et al.*, 2017), to migrations (Mullowney *et al.*, 2018; Staniland *et al.*, 2018) and escape responses (Fukutomi and Ogawa, 2017; Hessel and Nishikawa, 2017; Svetlichny *et al.*, 2018). While locomotion represents a key element of an animal's behaviour and physiology, selective pressures upon locomotive systems act to maximise locomotor performance while minimising the energetic costs of such systems (Alexander, 1999; Li *et al.*, 2018; Zamora-Camacho, 2018). The energetics of locomotion are ultimately driven by the effective utilisation of chemical stores in the form of ATP (Li *et al.*, 2018; Morris and Adamczewska, 2002; Willmer *et al.*, 2004), which is hydrolysed by muscle tissues to provide energy for muscular contraction (Willmer *et al.*, 2004; Woledge *et al.*, 1985). Muscle contraction enables the movement of morphological structures, which transfer energy to the environment (Alexander, 1999; Vogel, 1994; Willmer *et al.*, 2004). This energy cascade ultimately sees chemical energy, ultimately derived from food, being transferred to mechanical energy in the environment (Figure 1; Dabiri, 2009; Vogel, 1994). The efficiency with which animals are able to transfer chemical energy into useful movement is of key importance, where energy waste can have fitness consequences (Li *et al.*, 2018; Muller and van Leeuwen, 2006). More efficient locomotive systems are less costly to maintain and fuel, enabling animals to divert greater resources towards other tasks such as growth and reproduction (Muller and van Leeuwen, 2006).

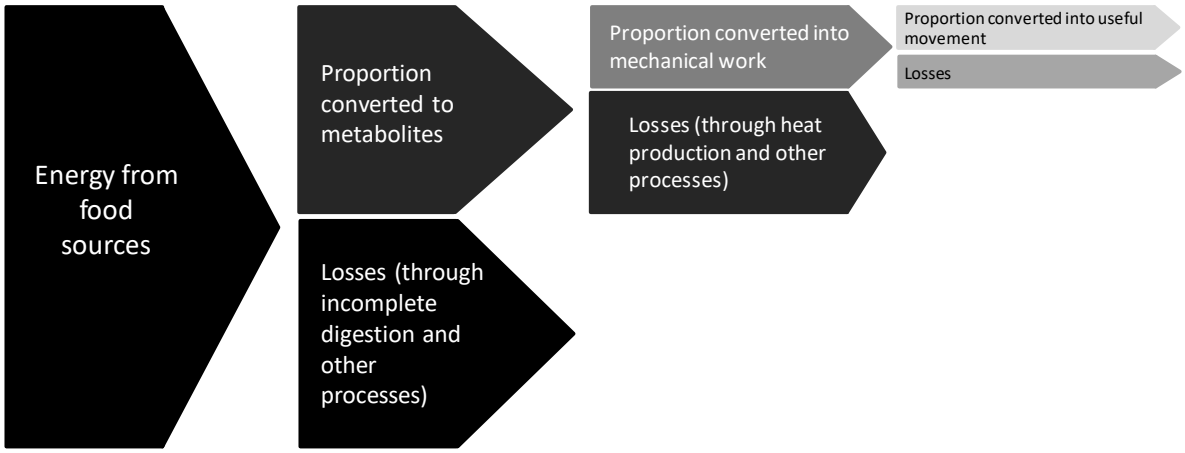

Figure 1. Illustrative diagram of the energy cascade during locomotion. Energetic losses occur between stages as a result of inefficiencies in processes. Energy is input from food sources, with a proportion of this energy lost as a result of incomplete digestion. Of this energy further losses are incurred when converting to phosphate stores, such as ATP, these occur as a result of heat production and the need to input energy into these processes. This ATP is then hydrolysed to fuel mechanical work, a proportion of this released energy is lost through internal processes, such as fuelling Ca^{2+} pumps, and the production of heat. Finally, only a proportion of this mechanical work results in useful movement, with losses incurred due to energy lost in the wake of the animal (such as in vortices), as well as energy loss associated with frictional forces.

1.1 Fuel to high-energy phosphates

The high-energy ATP and other compounds required for muscle activity derive originally from food sources (Alexander, 1999; Greig and Jones, 2016; Woledge *et al.*, 1985). ATP stores within tissues are usually low, with this replenished through the hydrolysis of stored molecules such as glycogen, phosphagens (e.g. creatine-phosphate, arginine-phosphate), fatty acids, and in some cases proteins/amino acids (Muller and van Leeuwen, 2006; Storey and Storey, 1979; Woledge *et al.*, 1985). During muscular activity ATP reserves are consumed necessitating their replenishment (Askew and Marsh, 2002; Curtin and Woledge, 1993a; Curtin and Woledge, 1993b; Morris and Adamczewska, 2002); routine activity (typically low intensity activities),

such as the slow or steady swimming of Atlantic cod (*Gadus morhua*) (Reidy *et al.*, 2000), largemouth bass (*Micropterus salmoides*) (Coughlin, 2002) and chub mackerel (*Scomber japonicas*) (Coughlin, 2002) utilises aerobic processes to replenish these ATP stores (citric acid cycle and oxidative phosphorylation systems; Figure 2), ensuring muscle can continue to work. The slow and steady work of aerobic muscle fibres means ATP demand is not as great as during high intensity work (Curtin and Woledge, 1993a; Curtin and Woledge, 1993b). The slow or steady swimming of dogfish (*Scyliorhinus canicula*), smooth hounds (*Mustelus vulgaris*), tope (*Galerohinus galeus*) and spur dogs (*Squalus acanthius*) is driven by the activity of red (aerobic) muscle. These muscle fibres make up ~18 % of the locomotory musculature, yet account for much of the routine swimming; unlike fast-twitch fibres these muscles utilise lipid reserves during sustained rather than glycogen stores (Bone, 1966). As an animal's swimming velocity increases muscle recruitment begins to shift in favour of muscle fibres which are fuelled anaerobically, as noted with bluegill sunfish (*Lepomis macrochirus*) and American eels (*Anguilla rostrata*), where increasing swimming speeds lead to an increase in the recruitment of fast-twitch fibres in the longitudinal and caudal fin musculature of animals (Flammang and Lauder, 2008; Gillis, 1998; Jayne and Lauder, 1994). Fast fibre types drive processes where force must be developed rapidly, such as those involved in escape (Johnson *et al.*, 1993; Ruegg, 1987). Under such circumstances aerobic processes are unlikely to provide sufficient ATP due to the rapidity of processes (Coughlin, 2002; Reidy *et al.*, 2000). Under these circumstances locomotory muscles rely upon anaerobic mechanisms, utilising both glycolytic pathways (Figure 3) and phosphagen systems (Figure 4) to replenish ATP and maintain locomotory function.

The onset of anaerobiosis within muscle tissues leads to the immediate utilisation of available ATP; this ATP is rapidly hydrolysed to ADP and AMP, requiring tissues to replenish this to continue to fuel musculature (Bailey *et al.*, 2003; Portner *et al.*, 1996). Immediate replenishment is met through de-phosphorylation of phosphagen stores (Figure 4), such as creatine phosphate and arginine phosphate (Arthur *et al.*, 1992; Storey and Storey, 1979). Phosphagens are important phosphate sources, acting to immediately replenish ATP stores, and typically act more quickly than replenishment

through glycolytic pathways (Johnston and Goldspink, 1973). Further replenishment is met through glycolytic pathways where glucose and other monomers are degraded to release ATP (Willmer *et al.*, 2004); this pathway can however lead to acidosis within tissues as a result of H^+ release (Portner *et al.*, 1996; Willmer *et al.*, 2004). This acidosis of tissues can damage myocyte cells and slow muscle function, to minimise damage and maintain muscle function pathways have evolved to minimise $[H^+]$; these pathways act to replenish NAD^+ stores while also maintaining osmotic balance within tissues (Greig and Jones, 2016; Storey, 1977; Willmer *et al.*, 2004). Of these pathways perhaps the most widespread are those facilitated through the action of lactate dehydrogenase (LDH) (Johnston and Goldspink, 1973) and octopine dehydrogenase (ODH) (Capaz *et al.*, 2017; Storey, 1977; Figure 5).

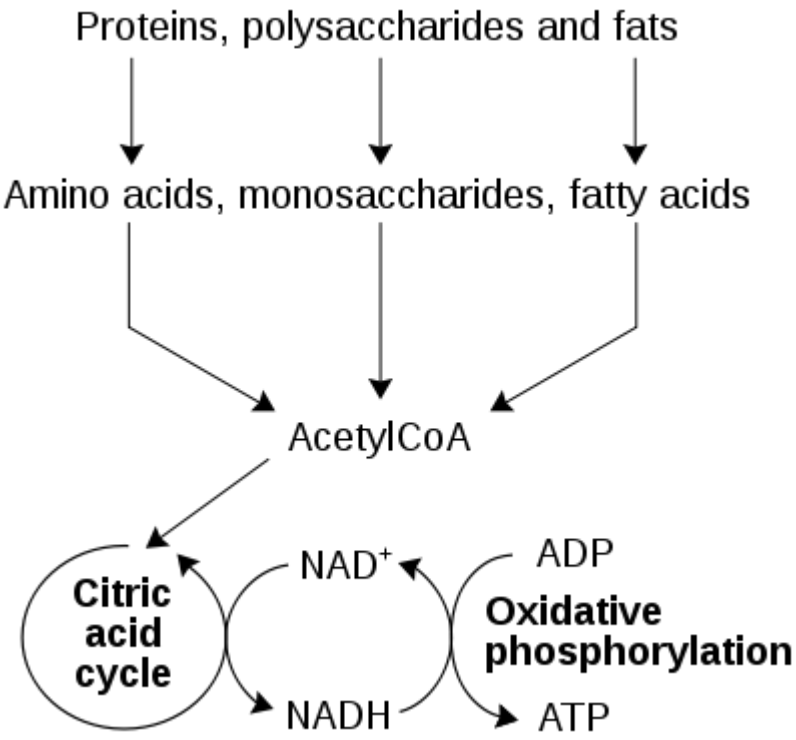

Figure 2. Schematic diagram indicating key aerobic processes. Dietary compounds (Proteins, polysaccharides and fats) are degraded to simpler forms through glycolysis, before entering the link reaction where ultimately acetyl coenzyme A allows compounds to enter the citric acid cycle. The NADH produced through the citric acid cycle is utilised by ATP synthase during oxidative phosphorylation to produce ATP. This process produces a maximum yield of 38 ATP per monomer (eg glucose) input. Diagram adapted from Vickers (2007; https://commons.wikimedia.org/wiki/File:Catabolism_schematic.svg) under a Creative Commons licence.

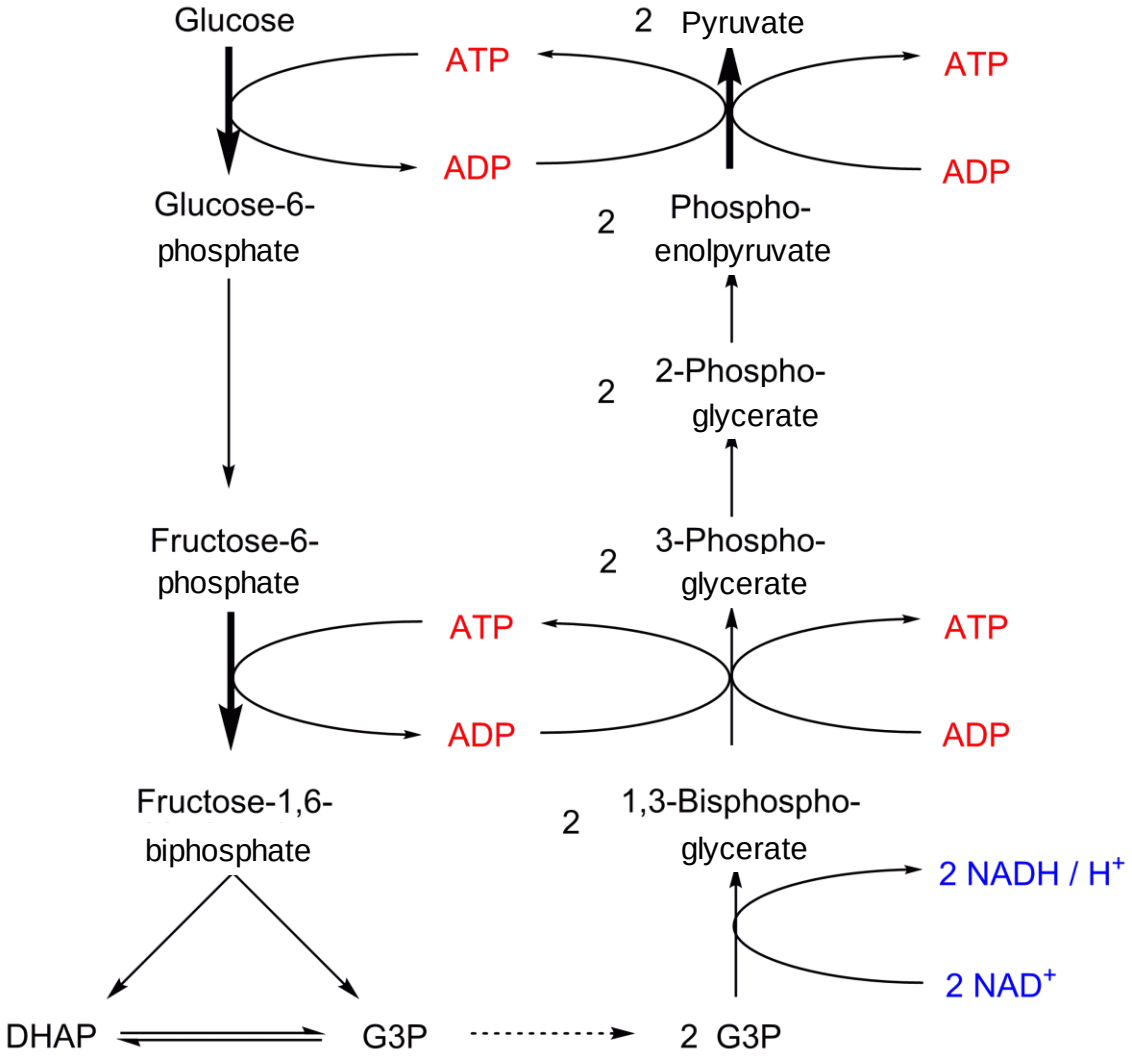

Figure 3. Pathways of glycolysis. Glycolysis yields 2 ATP molecules per glucose used. DHAP is dihydrooxacetone and G3P is glyceraldehyde-3-phosphate. Diagram adapted from Yikrazuul (2009; https://commons.wikimedia.org/w/index.php?curid=7694214) under a Creative Commons licence.

$$Arginine\ phosphate \xleftrightarrow[Arginine\ kinase]{} Arginine + P_i$$

$$Creatine\ phosphate \xleftrightarrow[Creatine\ kinase]{} Creatine + P_i$$

Figure 4. Example phosphagen systems used within animal tissues. Kinases remove phosphate (P_i) groups from donor molecules, typically arginine or creatine phosphate, yielding 1 ATP per molecule hydrolysed. This reaction is reversed when ATP is freely available within tissues, hydrolysing ATP to ADP adding phosphate groups back to arginine or creatine (Arthur *et al.*, 1992; Johnston and Goldspink, 1973; Morris and Adamczewska, 2002; Storey and Storey, 1979).

$$Pyruvate + NADH + H^+ \underset{LDH}{\longleftrightarrow} Lactate + NAD^+$$

$$Arginine + Pyruvate + NADH + H^+ \underset{ODH}{\longleftrightarrow} Octopine + Water + NAD^+$$

Figure 5. Dehydrogenase pathways typically utilised by animals to reduce acidosis within tissues and replenish NAD^+ levels. Lactate pathway is common among vertebrate lineages (LDH is lactate dehydrogenase), Octopine pathway is typically used by invertebrate lineages such as arthropods and molluscs (ODH is octopine dehydrogenase). The ODH pathway yields 3 ATP molecules for every 2 arginine input, LDH pathway yields 1 ATP molecule per pyruvate input (Arthur *et al.*, 1992; Capaz *et al.*, 2017; Morris and Adamczewska, 2002; Storey, 1977).

Despite these processes, anaerobic muscle activity cannot be maintained over a prolonged period of time (Greig and Jones, 2016; Morris and Adamczewska, 2002; Willmer *et al.*, 2004). This results from a variety of limitations within these systems, in particular the finite phosphagen and glycogen stores and the interference associated with the accumulation of various molecules, such as inorganic phosphates, and H^+ (Greig and Jones, 2016; Westerblad *et al.*, 2002). The resulting muscle fatigue leads to reduced force generation, impairing the work of musculature and slowing muscle

relaxation. This ultimately leads to exhaustion, and processes coming to an end, upon this anaerobic by-products are cleared through aerobic means (Arthur *et al.*, 1992; Greig and Jones, 2016; Willmer *et al.*, 2004). Despite these limitations, some animals are able to further maximise anaerobic potential through the degradation of lactate, cyprinoid fish, such as crucian carp (*Carassius carassius*) and goldfish (*C. auratus*), have demonstrated this ability reducing lactate to ethanol (Fagernes *et al.*, 2017). Despite these limitations, anaerobic pathways are used as a result of simple reactions which are able to rapidly provide ATP, fuelling escape responses (Greig and Jones, 2016).

The reliance upon anaerobic pathways to fuel muscle contraction is seen across biological lineages. The fast-start swimming of many fish is one such example of how anaerobic pathways are utilised to achieve predator escape and/or prey capture (Domenici and Blake, 1997). Behaviourally, these processes are identified as C- or S-starts, whereby the animal bends its body prior to a sudden change in speed and sometimes direction (Domenici and Blake, 1997). Powering such responses is typically achieved through the action of anaerobic fast-twitch fibres, which produce high forces, resulting in movement of surrounding fluid and thus thrust. The underlying metabolic changes associated with the use of such musculature has been investigated in a variety of species, work with rainbow trout (*Oncorhynchus mykiss*) has demonstrated ATP, glycogen and phosphocreatine significantly decrease, while lactate accumulates following exercise (Pearson *et al.*, 1990). Similarly, whole animal experiments in cuttlefish (*Sepia officinalis*) have revealed significant declines in ATP, and arginine-phosphate levels, but significant increases in arginine and octopine levels within muscle tissues (Storey and Storey, 1979).

1.1.1 Molluscan muscle physiology

The molluscs are one of the largest and most diverse of the animal taxa (Hickman, 2009; Wilbur, 1983). These animals are found throughout the world's oceans and to some extent on land with a range of behaviours, and most notably, morphological features which enable these animals to successfully inhabit these niches (Hickman, 2009; Wilbur, 1983). The underlying muscle physiology of molluscs differs to that of

vertebrates; energy stores within molluscan muscle are heavily dominated by arginine-phosphate, glycogen and amino acids (particularly arginine and proline) (Ballantyne, 2004). Molluscs lack the triglyceride reserves seen in vertebrate muscle, with the breakdown of amino acids playing a larger part in the metabolism of these animals (Ballantyne, 2004).

Despite the variety of morphological adaptations seen between molluscan lineages, the underlying physiology remains broadly similar (Bailey *et al.*, 2003; Capaz *et al.*, 2017; Denny, 1980; Wilbur, 1983). Studies upon the movement of gastropods, bivalves and cephalopods all suggest much of the movement of these animals is driven through anaerobic processes. Where the movement of banana slugs (*Ariolimax columbianus*) is followed by long recovery periods over which oxygen uptake is increased (Denny, 1981). Bivalves present a somewhat different case, as most animals within this group are sessile (Hickman, 2009). However, some species are mobile, utilising jet propulsion swimming powered by the adductor muscle, such as scallops (Pectinidae) and fragile file clams (*Limaria fragilis*) (Bailey and Johnston, 2005; Baldwin and Lee, 1979; Donovan *et al.*, 2004; Marsh *et al.*, 1992). The scallop adductor muscle is primarily anaerobic in nature with escape responses associated with the utilisation of ATP, arginine-phosphate and accumulation of octopine (Olson and Marsh, in preparation), while the jet propulsion swimming of fragile file clams (*L. fragilis*) is primarily aerobic (Baldwin and Lee, 1979; Donovan *et al.*, 2004). The locomotory muscle of cephalopods is somewhat more developed than that of other molluscan linages. The mantle of coleoid cephalopods shows two distinct cell types arranged into distinct layers (Kier, 1988; Kier and Schachat, 2008; Kier and Thompson, 2003). Despite this high degree of organisation, the mantle is dominated by anaerobic muscle fibres (accounting for as much as 80 % of the mantle volume) (Kier and Thompson, 2003; Moltschaniwskyj, 1994). The high degree of anaerobic fibres is thought to reflect the growth dynamics of these animals (Moltschaniwskyj, 2004), as well as the importance of escape responses. Despite these observations of muscle structure, the picture of cephalopod muscle physiology is mixed. Storey and Storey (1979) have suggested the mantle muscle of cuttlefish (*S. officinalis*) is largely fuelled through anaerobic metabolism when swimming, while the mantle muscle of longfin (*Doryteuthis pealeii*) and opalescent

inshore (*Doryteuthis opalescens*) squid are fuelled primarily through aerobic metabolism (Ballantyne, 2004; Storey and Storey, 1978). These differences between cephalopod lineages highlight the role of evolution in shaping the locomotory systems of animals, and also likely reflect the nature of the squid locomotive system where respiration and jet propulsion are intimately linked (Storey and Storey, 1978).

1.2 ATP to work

1.2.1 Muscle morphology

The structure and function of muscle are closely linked, with different muscle types differing in their mechanical properties (Maddock *et al.*, 1994; Willmer *et al.*, 2004). Of these animal muscle types, the striated (or skeletal) muscle is perhaps the most widely studied, with its involvement in the locomotion of vertebrates and invertebrates, with examples ranging from the myotomal muscle of dogfishes (*Scyliorhinus canicula*) (Curtin and Woledge, 1993a; Curtin and Woledge, 1993b; Curtin and Woledge, 1996), to the body wall muscle of fruit flies (*Drosophila melanogaster*) (Ormerod *et al.*, 2017), the flight musculature of magnificent hummingbirds (*Eugenes fulgens*) (Cheng *et al.*, 2016) and adductor muscle of scallops (Pectinidae) (Marsh and Olson, 1994; Olson and Marsh, 1993). The locomotory muscle of other lineages, particularly those lacking hard skeletal systems, are dominated by obliquely striated muscle (Haba, 2016; Ono, 2014; Thompson and Kier, 2006). This muscle type is common in many invertebrates (Burr and Gans, 1998; Milligan *et al.*, 1997; Toida *et al.*, 1975; Wissocq and Boilly, 1977), particularly in molluscs (Denny, 1980; Thompson *et al.*, 2008), such as cuttlefishes (*Sepiidae*) (Curtin *et al.*, 2000; Kier, 1988; Milligan *et al.*, 1997; Storey and Storey, 1979) and slugs (*Ariolimax columbianus*) (Denny, 1980; Denny, 1981), and annelids (Greidinger, 2012; Quillin, 1998; Quillin, 1999; Quillin, 2000), such as earthworms (*Lumbricus terrestris*) (Mill and Knapp, 1970; Quillin, 2000). Obliquely striated muscle structure differs somewhat to that of striated muscle, where filaments are staggered as opposed to the uniform distribution of striated muscle (Figure 6; Kier, 1988; Milligan *et al.*, 1997; Toida *et al.*, 1975).

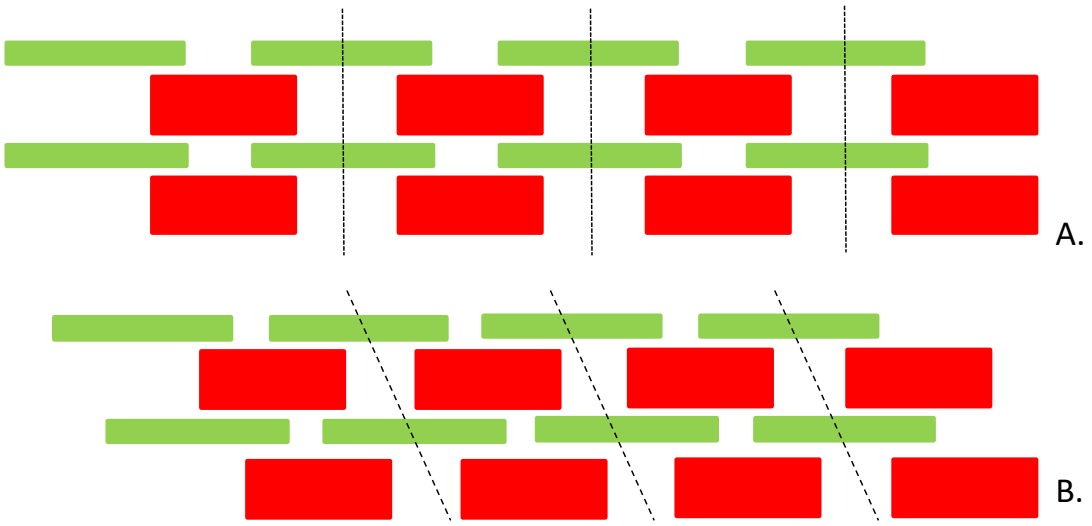

Figure 6. Comparative diagram of striated (A.) and obliquely striated (B.) muscle structure. Thin filaments are shown in green and thick in red, dashed lines indicate Z-lines. Thin and thick filaments run parallel in striated muscle, while these are slightly offset in obliquely striated muscle (Burr and Gans, 1998; Campbell and Reece, 2008; Thompson *et al.*, 2008; Toida *et al.*, 1975; Willmer *et al.*, 2004). This offset leads to Z-lines being at an angle in this muscle type.

This underlying muscle structure likely influences the mechanical properties of the muscle, this is particularly influenced by muscle fibre types (Kier and Thompson, 2003; Rome *et al.*, 1988; Thompson *et al.*, 2010; Willmer *et al.*, 2004) and the elasticity of such muscle structures (Curtin *et al.*, 2000; Woledge *et al.*, 1985). Muscle fibres can broadly be divided into slow- and fast-twitch fibres. Aerobic slow- and fast-twitch fibres house an increased number of mitochondria, relative to anaerobic fast-twitch fibres, to fuel mechanical processes through aerobic means (Kier and Thompson, 2003; Muller and van Leeuwen, 2006; Ruegg, 1987), this increased area inhabited by mitochondria decreases myofibrillar area, a decrease in myofibrillar cross-sectional area affects the mechanical properties of musculature, where muscle stress, net work and power per cycle are affected (Maughan *et al.*, 1983). Anaerobic fast-twitch fibres maximise myofibrillar cross-sectional area with decreased mitochondrial density, this enables muscle myocytes to rapidly contract with high muscular power. Muscle cells may also express different myosin isoforms, these different isoforms differ in the

heavy chain portion of the myosin molecule, which impacts cross-bridge formation, with different isoforms known to differ in myosin ATPase (mATPase) activity and shortening velocities (Pette and Staron, 2000; Schiaffino and Reggiani, 1994; Willmer *et al.*, 2004). The expression of different myosin isoforms and recruitment of different muscle fibre types is noted to occur as a result of endurance training in mammals such as mice (*Mus musculus*) (Waters *et al.*, 2004) and humans (*Homo sapiens*) (Andersen and Henriksson, 1977; Hawley, 2002), where the recruitment of muscle fibres is altered to favour type I and type IIa fibre types (Andersen and Henriksson, 1977; Waters *et al.*, 2004). These fibre types are oxidatative in nature, favouring the sustained activity associated with endurance running. Crucian carp (*Cyprinus carpio*) on the other hand are shown to alter the local recruitment of muscle fibres in response to temperature where fast-twitch fibres are recruited more rapidly by cold-adapted fish thought to be as a result of reduced mechanical power generated by slow-twitch fibres (Johnson and Johnston, 1991; Rome *et al.*, 1985). The elasticity of muscle structures is also noted to impact the underlying mechanical properties of musculature. This is particularly evident where muscle elasticity is high, where muscle may benefit from elastic recoil following shortening, this reduces the work required to re-lengthen a muscle, but may increase the initial work required to lengthen the muscle (Curtin *et al.*, 2000).

1.2.2 The cross-bridge cycle

Despite these different muscle forms, the underlying contractile properties are all fuelled by ATP hydrolysis (Alexander, 1999; Campbell and Reece, 2008; Ipata and Balestri, 2012; Willmer *et al.*, 2004). ATP is utilised during cross-bridge cycling where the energy from ATP acts to break actin-myosin bonds while also providing the energy for force generation (Alexander, 1999; Willmer *et al.*, 2004). This process is cyclic, where cross-bridges are formed and broken and force generated many times during typical muscle activity (Figure 7; Alexander, 1999; Josephson, 1985; Willmer *et al.* 2004). This process is controlled by the presence or absence of calcium ions (Ca^{2+}) within the muscle (Alexander, 1999; Greig and Jones, 2016; Willmer *et al.*, 2004), Ca^{2+} acts upon troponin causing tropomyosin to be moved away from actin binding sites

(Greig and Jones, 2016; Willmer *et al.*, 2004). Once these active sites are uncovered, myosin heads can bind to actin beginning the power stroke of cross-bridge cycling (Greig and Jones, 2016; Willmer *et al.*, 2004). The power stroke acts to pull actin towards the centre of the sarcomere, resulting in muscle shortening; ADP is released following the power stroke leaving the muscle in a rigor state. ATP can be hydrolysed at this point, breaking actin-myosin bonds and leaving myosin in a high-energy state, the cycle then begins again with myosin heads binding to actin active sites. This process is stopped through the action of Ca^{2+}-ATPase pumps, which act to actively remove calcium ions into the sarcoplasmic reticulum in the presence of Mg^{2+} (Greig and Jones, 2016), the removal of calcium ions utilises ATP, incurring additional metabolic costs when fuelling muscular activity. Once Ca^{2+} is removed tropomyosin is able to bind to actin binding sites, stopping further cross-bridge cycling.

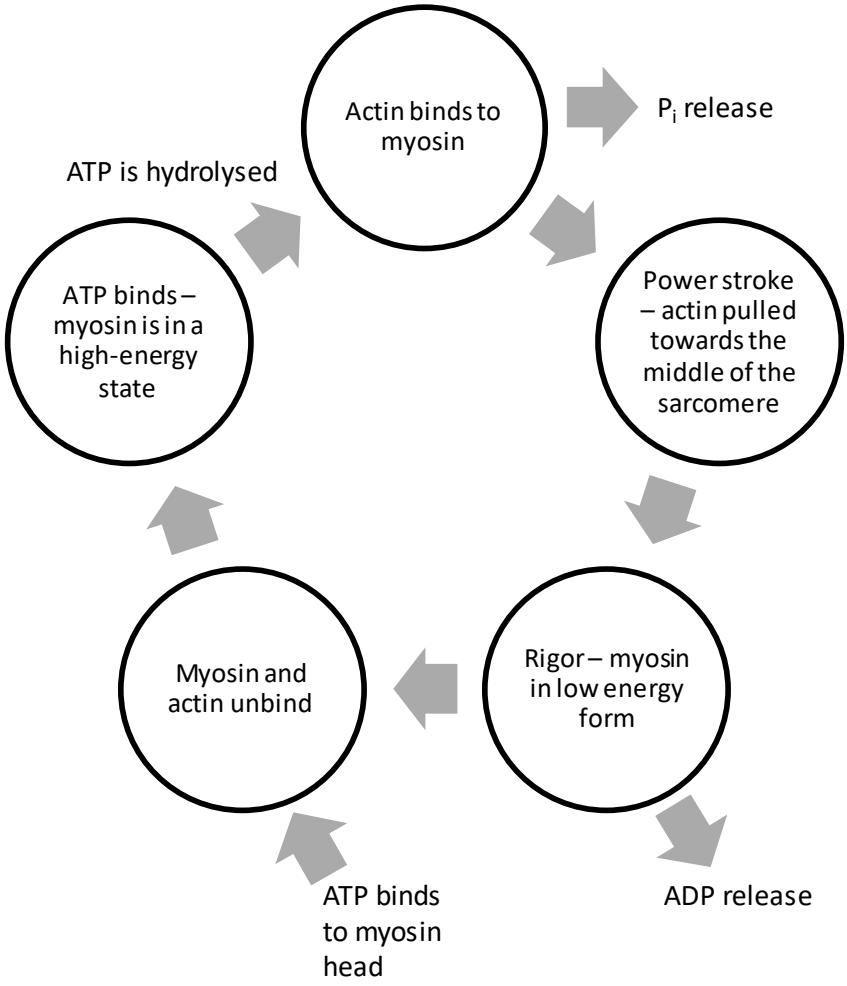

Figure 7. Key stages during cross-bridge cycling. Ca^{2+} is released prior to processes beginning, acting upon troponin to move tropomyosin enabling actin active sites to be revealed and myosin heads to bind. Upon binding, force is generated during the power stroke where actin is pulled by myosin towards to centre of the sarcomere, once this process is complete muscle enters a rigor state, where actin-myosin cross-bridges have formed. ATP is input to break these bonds enabling the process to start again (Greig and Jones, 2016; Willmer *et al.*, 2004; Woledge *et al.*, 1985).

1.2.3 Contractile efficiency of muscle

As described previously, the energy released through metabolic processes is utilised by musculature for mechanical work. The efficiency with which metabolic energy is transferred into mechanical work is of key importance to many animals; more efficient musculature is able to maximise the proportion of this energy which is useful,

minimising losses (Kraskura and Nelson, 2018; Li *et al.*, 2018; Muller and van Leeuwen, 2006; Smith *et al.*, 2005). Selective processes play a key role in refining contractile efficiency whereby efficient musculature may be favoured in animals which utilise near-constant swimming (Curtin and Woledge, 1993a; Priede, 1977; Webb, 1971), whereas animals which rely more heavily upon burst performance may not be under such pressure to increase contractile efficiency (Curtin and Woledge, 1993b; Priede, 1977).

Defining and measuring the contractile efficiency of muscle requires knowledge upon the energy input to move musculature, the work output by muscle, and in some cases knowledge relating to recovery processes (Smith *et al.*, 2005). Measurement of energy input can be achieved by measuring biochemical changes within musculature as well as the oxygen consumption of muscle (Curtin and Woledge, 1993a; Curtin and Woledge, 1993b; Smith *et al.*, 2005). Measurement of biochemical changes in this manner enables the measurement of different components in the energy conversion process, these steps are described as various types of contractile efficiencies (Figure 8; Smith *et al.* 2005; See Chapter 4). Of these definitions, the initial efficiency is perhaps the most simplistic; where the initial efficiency is calculated as the ratio of the mechanical work to the chemical energy (the Gibbs free energy of ATP hydrolysis or the change in enthalpy) (Smith *et al.*, 2005; Whipp and Wasserman, 1969), giving an estimate of the proportion of chemical energy resulting in mechanical work. This method is however unsuitable for muscle with particularly high recovery rates, where reactions may not be stopped quickly enough, the pectoralis muscle of many birds is one such example, where the high metabolic rates of birds enable rapid recovery (Jenni-Eiermann, 2017), as seen across bird lineages, such as Rufous hummingbirds (*Selasphorus rufus*) (Suarez *et al.*, 1990), Adélie penguins (*Pygoscelis adeliae*) (Fongy *et al.*, 2013) and American robins (*Turdus Migratorius*) (Gerson and Guglielmo, 2013). The musculature of ectotherms, is however more suitable due to slow recovery times, as such rapidly freezing tissues of animals such as the mantle muscle of cephalopods (Melzner *et al.*, 2007; Storey and Storey, 1978; Storey and Storey, 1979) or the myotomal muscle of dogfishes (*Scyliorhinus canicula*) (Curtin and Woledge, 1993a; Curtin and Woledge, 1993b) can give an accurate estimation of changes in muscle metabolites (Smith *et al.*,

2005). Other models of contractile efficiency account for recovery processes, as well as the relative inputs of aerobic and anaerobic metabolism and heat production by musculature (summarised in Figure 8; discussed in further detail in Chapter 4).

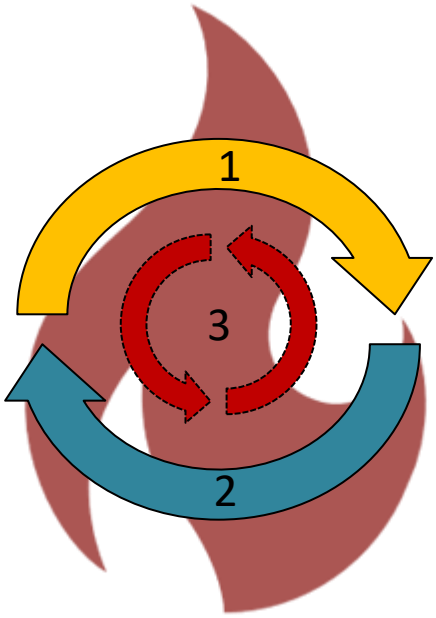

Figure 8. Diagram indicating the relationship between the different efficiency measures. 1. Indicates the initial efficiency, where biochemical energy is converted to mechanical energy. 2. Indicates the aerobic recovery phase acting against the processes of 1., taken together 1. and 2. yield the net efficiency. The overall efficiency takes the underlying metabolism of the animal into account (3.), overall efficiency is the sum of basal metabolism + the energy used for muscle activity + energy use through recovery processes. Processes can also be measured through the production of heat during the catabolism of ATP during muscular activity, termed the thermodynamic efficiency of cross-bridge cycling (Smith *et al.*, 2005).

The two key muscle types discussed previously, namely fast and slow twitch fibres, differ in their contractile efficiency (Curtin and Woledge, 1993a; Curtin and Woledge, 1993b; Smith *et al.*, 2005). As discussed previously slow twitch muscle is aerobic in nature and used primarily in routine activities of animals (Curtin and Woledge, 1993a; Flammang and Lauder, 2008; Gillis, 1998). These fibres are generally more efficient than the fast-twitch fibres of animals which are fuelled through either aerobic or

anaerobic mechanisms (Curtin and Woledge, 1993a; Curtin and Woledge, 1993b; Woledge *et al.*, 1985); where the use of anaerobic fibre-types is primarily involved in escape or burst responses, as a result efficiency may be less important than the process of escape itself. Yalcinkaya *et al.* (2016) provided the first estimates of the contractile efficiency of cephalopod swimming, noting the steady state swimming of brief squid (*Lolliguncula brevis*) may be more efficient than escape responses (0.28 and 0.23 respectively). Quantitative comparisons seem to support this, with the contractile efficiency of dogfish (*Scyliorhinus canicula*) myotomal white (fast twitch) muscle being less efficient than red (slow twitch) muscle (0.379 ± 0.022 (corrected to 0.41 by Smith *et al.* 2005); and 0.507 ± 0.045 respectively) (Curtin and Woledge, 1993a; Curtin and Woledge, 1993b; Smith *et al.*, 2005). The differences in contractile efficiency likely relate to underlying differences in the distribution of red muscle fibres, as well as evolutionary forces driving the mechanical properties muscle fibres and/or mitochondria within muscle fibres display (Coughlin, 2002; Coughlin *et al.*, 2001).

1.2.4 Contractile properties of molluscan muscle

The muscles of molluscs play a key role in both acting as locomotive elements as well as providing support (Kier, 1988; Wilbur, 1983). The function of this musculature relies heavily upon fluid-filled cavities for musculature to act against (Kier, 1988). The contraction of molluscan locomotory muscle leads to dimensional changes of animals during locomotive events (Kier, 1988). These body deformations are strongly related to the underlying mechanical properties of musculature, where elongations of an animal's body results from displacement of internal fluid elongating the body of the animal. Elongations are typical of the action of circular muscles, such as those of the cephalopod mantle cavity. These muscles compress the cavity, increasing pressure within the mantle cavity, forcing water out through the siphon, as the muscle contracts the internal fluid, non-contractile elements and inactive musculature (such as the radial muscles, involved in expanding the mantle) are displaced resulting in elongation of the animal. This water forms a jet, which acts to create thrust propelling the animal through the water (Gosline *et al.*, 1983; O'Dor and Webber, 1991; Thompson *et al.*, 2010).

Other locomotory systems can lead to processes such as body shortening, this occurs where internal structures and fluid are displaced increasing cross-sectional area. If these internal structures resist or create forces themselves this can lead to bending. Decreases in length are seen during the crawling locomotion of many gastropod molluscs where waves of shortening and subsequent lengthening are seen across the muscular foot of animals, this process acts to facilitate the crawling seen in these animals (Denny, 1980; Denny, 1981). The musculature of molluscs is also capable of torsional movements, where muscle can twist around its longitudinal axis during movement; these torque processes are of key importance, particularly in obliquely striated muscle due to the differences in fibre angles.

Studies upon the function of this muscle have primarily focused upon squids, with studies revealing the mantle muscle of European common squid (*Alloteuthis subulata*) behaves in much the same way as vertebrate cross-striated muscle (Milligan *et al.*, 1997). Wider studies, such as those investigating the function of the bay scallop (*Argopecten irradians*) adductor muscle have found somewhat different contractile properties when compared to vertebrate musculature; this is particularly evident when looking at the twitch responses of this muscle, which seem to be broadly similar to the tetani produced. The lack of differentiation between twitch and tetanic contractile properties likely result from the role of the adductor in escape responses, where an all-or-nothing response is favoured (Marsh and Olson, 1994; Marsh *et al.*, 1992).

1.2.5 Measuring muscle mechanics

Muscle function is a key determinate of locomotor performance of animals (Gerry and Ellerby, 2014). The underlying mechanical properties of musculature are likely to have undergone selection to maximise locomotor performance under a certain set of conditions dictated through environmental, predation and mating pressures amongst others (Alexander, 1999; Alexander, 2003; Wells, 1994). These selective forces impact the design and function of locomotory musculature. To understand the impacts of this,

muscle function can be assessed through a variety of approaches, these broadly being divided into *in vitro* and *in vivo* approaches.

1.2.5.1 *In vitro* approaches

In vitro approaches assess the function of musculature under controlled conditions. This is achieved through the isolation of muscle bundles and/or individual fibres (Alexander, 1999; Willmer *et al.*, 2004). These muscle bundles are kept alive through immersion in a saline solution (such as Ringers), and are electrically stimulated to produce contractile forces (Josephson, 1985; Willmer *et al.*, 2004). In measuring and implementing such procedures an ergometer is used, enabling the measurement of contractile forces, work and other mechanical properties (Josephson, 1985; Josephson, 1993; Willmer *et al.*, 2004).

1.2.5.1.1 Isometric muscle performance

In vitro investigations can investigate numerous properties of the musculature, under various conditions. The assessment of isometric muscle performance provides a measure of muscle performance when held at a constant length (Seow, 2013; Willmer *et al.*, 2004). This technique involves muscle preparations being dissected out, placed in an experimental chamber containing an appropriate physiological solution (such as Ringers) which is maintained at an appropriate physiological temperature; one end of the preparation is attached to a fixed mount, while the other is attached to an ergometer. The muscle is held at a constant length using a force clamp or hard device loading; this ensures the muscle does not shorten when electrically stimulated via electrodes within the chamber (Caruel and Truskinovsky, 2018; Olson and Marsh, 1993). Under these conditions twitch responses can be assessed through the application of a single electrical stimulus; this results in a rapid increase in muscular force before these return to resting levels (Close, 1972; Hartree and Hill, 1921; Willmer *et al.*, 2004). Tetanic responses, where multiple electrical stimuli are applied in close succession with summation of muscle force and/or tension occurring, can also be

investigated (Hartree and Hill, 1921; Homsher *et al.*, 1979; Willmer *et al.*, 2004). The plateau associated with tetanic responses represents the maximum force musculature can achieve through isometric means, this being termed the maximal isometric force (Hill, 1950; Homsher *et al.*, 1979; Willmer *et al.*, 2004).

Isometric properties of musculature depend upon both the electrical stimuli given and the underlying structural properties of muscle (Hill, 1950; Kier and Thompson, 2003; Luther *et al.*, 1995; Willmer *et al.*, 2004). To achieve maximal isometric force muscle length is optimised; this involves musculature being gradually stretched and measures of force taken (Josephson, 1985; Josephson, 1993; Milligan *et al.*, 1997). The maximal length for isometric force production is defined as that which achieves the greatest force with low passive forces (≤ 10 %) (Josephson, 1985; Josephson, 1993; Milligan *et al.*, 1997). Optimisation of muscle length is of key importance for measurement of not only isometric properties, but also isotonic and cyclic properties of musculature, this is due to this process being a means to maximise sarcomere length (Close, 1972; Thompson *et al.*, 2014; Willmer *et al.*, 2004). Sarcomere length determines the degree of overlap between the thick and thin filaments and the potential number of cross-bridges and therefore maximum force that can be achieved by the musculature (Campbell and Reece, 2008; Willmer *et al.*, 2004).

These isometric approaches enable measures of twitch kinetics, twitch force and stress, as well as the twitch:tetanus ratio, to be obtained. These data provide important information relating to muscle function, particularly how fast or slow the muscle is able to respond to stimuli, and the maximal stress a muscle is able to produce (Altringham and Block, 1997; Willmer *et al.*, 2004), while the twitch:tetanus ratio provides an insight into internal processes and structure of musculature, with higher ratios representing similarities between twitch and tetanic responses, such similarities are thought to relate to calcium processing as well as the density and diameter of muscle fibres (Celichowski and Grottel, 1993; Ruegg, 1987). Such measures of twitch kinetics have been investigated by a number of authors, with Altringham and Block (1997) noting the twitch kinetics of myotomal musculature largely depended upon muscle depth in both yellowfin tuna (*Thunnus albacares*) and bonito (*Sarda*

chiliensis), with twitch kinetics being significantly impacted by temperature (Altringham and Block, 1997).

1.2.5.1.2 Dynamic muscle performance

The assessment of muscle during dynamic contractions can be determined through isotonic or isovelocity approaches (Milligan *et al.*, 1997; Rome *et al.*, 1990; Willmer *et al.*, 2004). These techniques build upon the isometric techniques described in section 1.2.5.1.1 by allowing muscle preparations to shorten against a given load; this is achieved using a load clamp or soft loading device which is used to alter the force a muscle is able to achieve; this is usually given as a fraction of the force achieved during an isometric tetanus (Caruel and Truskinovsky, 2018; Marsh and Bennett, 1985; Willmer *et al.*, 2004). These different relative forces allow the muscle to shorten at different velocities; this relationship is termed the force-velocity relationship (Figure 9), and describes how the velocity of shortening is inversely related to force, with muscle contracting against zero shortening at its maximum shortening velocity (V_{max}) (Caruel and Truskinovsky, 2018; Olson and Marsh, 1993).

The force-velocity relationship represents the trade-off between muscle force and the velocity of shortening, this is as a result of the formation of cross-bridges, where at higher shortening velocities there is a lesser degree of cross-bridge formation, cross-bridges which are attached may however dragged beyond equilibrium positions resulting in negative force (resistance). These two processes result in less force being produced at higher shortening velocities (Huxley, 1974; Seow, 2013). This relationship is generally described as a negative hyperbolic (Hill, 1938) or more recently as negative hyperbolic-linear (Marsh and Bennett, 1986). The work of Marsh and Bennett (1986) noted muscle which produces high forces was better described by a hyperbolic linear relationship (Equation 1) than Hill's equation. Figure 9 shows an example force-velocity relationship where greater force is achieved at lower shortening velocities.

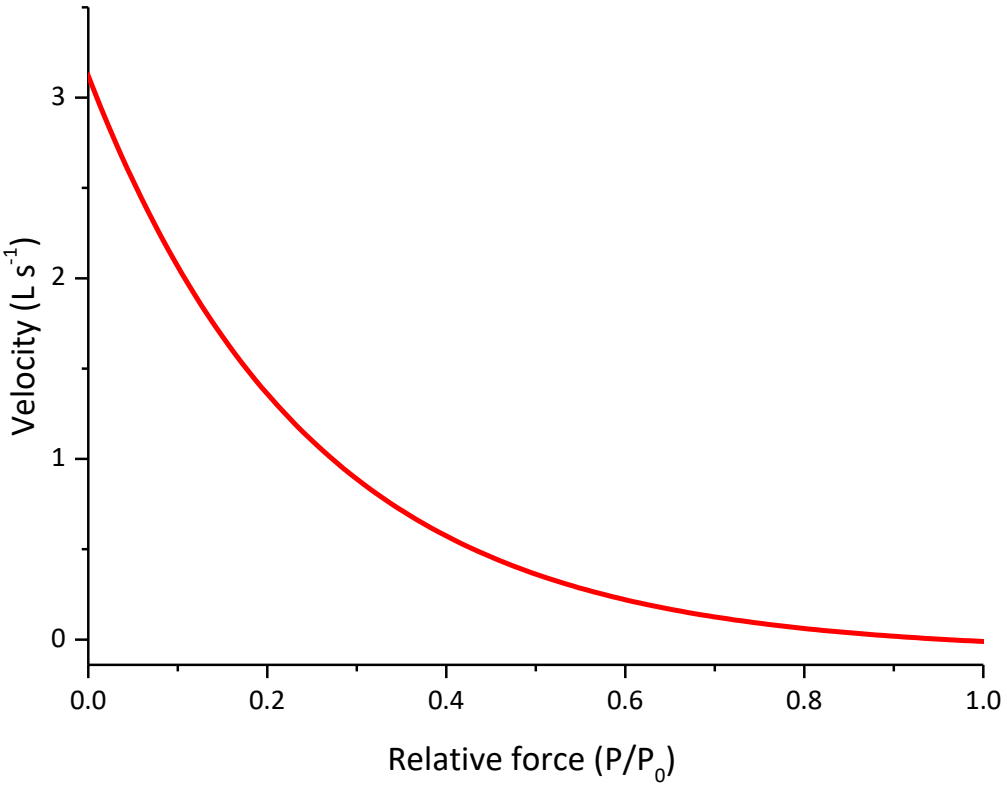

Figure 9. Typical relationship between muscle force and the velocity of shortening. Relationships are typically fit to either a negative hyperbolic (Hill, 1938) or a negative hyperbolic-linear (Marsh and Bennett, 1986). V_{max} is achieved at zero force, maximal force is achieved with zero length changes (isometric conditions).

$$V = [B(1 - P/P_0)/(A+P/P_0)]+C(1 - P/P_0)$$

Equation 1. The hyperbolic-linear equation. *V* is the velocity of muscle shortening and *P* is the force produced by musculature, P_0 is the maximum isometric force of musculature. A, B and C represent constants. (Marsh and Bennett, 1986)

The force-velocity relationship can be used to estimate the maximal work and power a muscle is capable of achieving (Hill, 1938; Marsh and Bennett, 1986). This is however likely an overestimate of how a muscle performs during locomotion, where cyclical muscle activity is more representative of how animals use muscles during locomotion. Cyclical contractions involve both muscle lengthening and shortening, the inclusion of both lengthening and shortening phases enables the work input to lengthen the

muscle to be included in estimating muscular work. This results in work and power generally being lower than the values obtained from force-velocity experiments, such values are however more likely to reflect muscle function *in vivo* (Josephson, 1985; Willmer *et al.*, 2004). Cyclical activity can be measured using the work loop technique, allowing the assessment of muscle performance under a more natural set of conditions (Josephson, 1985).

1.2.5.1.3 Cyclic muscle performance

The action of many locomotory muscles do not generally adhere to simple shortening responses as measured through the force-velocity relationship, instead muscle activity is cyclic in nature whereby muscle is lengthened before shortening occurs (Josephson, 1985; Josephson, 1993; Marsh and Olson, 1994). The measurement of muscle performance during such cyclic processes can be achieved using the work loop technique (Josephson, 1985). This technique differs somewhat to the techniques described in sections 1.2.5.1.1 and 1.2.5.1.2, like the previous techniques the work loop technique uses an ergometer with muscle preparations attached at one end; unlike these techniques length is changed cyclically involving both lengthening and shortening phases. When utilising work loops, waves typically begin and end at a resting position, this is the point in a cycle where a muscle is typically at rest (not producing active force), this is sometimes defined as the mid-point of the cycle, but where these measures are based on *in vivo* data this may not be the case. During a work loop activity begins from the resting position of the muscle, if this were to begin at the midpoint, the muscle may be lengthened, a stimulus delivered (producing force) and the muscle then shortens. Under other situations shortening and force production may begin immediately, with muscle resting in a position which would enable shortening to occur upon activation. Various aspects of a work loop experiment, such as the cycle frequency (*f;* the number of cycles over a certain period of time, denoted in hertz (Hz)), strain amplitude (the extent of an oscillation in muscle length, measured from the resting position), the proportion of the cycle shortening, phase duration (time delay between stimulation and length change), train duration (time over which stimuli are delivered) and the number of cycles, can be adjusted, enabling mechanical work

and power to be measured during various scenarios. As well as these mechanical properties, the cycles of lengthening and shortening can also be amended to fit various wave forms such as sinusoids or sawtoothes, which differ in the lengthening-shortening times (Alexander, 2003; Josephson, 1985). These various properties enable work loops to be amended to fit measures taken *in vivo*, or to maximise the mechanical properties of the musculature. The data obtained from such studies enables the calculation of the net work per cycle through the measurement of the area of the loop produced (Figure 10), or alternatively through taking the work input to lengthen the muscle from the work output during shortening (Johnson and Johnston, 1991; Josephson, 1985; Willmer *et al.*, 2004). The direction the of the loop is also indicative of if the muscle is producing positive or negative work, whereby counter-clockwise loops represent positive work while clockwise represent negative work (James *et al.*, 1996; Josephson, 1985; Willmer *et al.*, 2004). The power produced by a muscle can be calculated by multiplying the work produced by a muscle by its cycle frequency (James *et al.*, 1996; Josephson, 1985).

Work loops provide much more informative information upon the function of muscles than isotonic and isometric measures. The degree of positive or negative power production produced by musculature is lost under isotonic measures due to maximal stimulation (Josephson, 1985; Josephson, 1993). Work loops provide informative insight into the role of muscles during such cyclic responses, where some muscles may produce negative power such as those involved in stabilisation, whereas others provide the positive power required for movement (Altringham and Johnston, 1990; James *et al.*, 1996; Josephson, 1985).

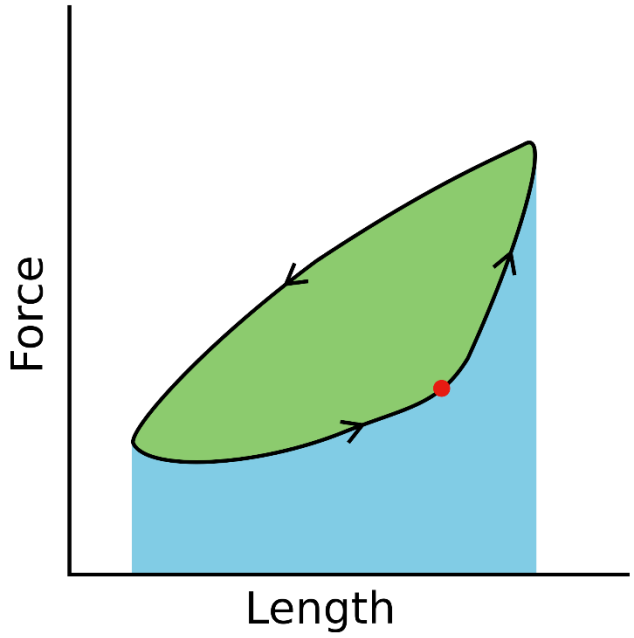

Figure 10. Representative work loop. Negative work is done as the muscle is lengthened while positive work is done during shortening (Josephson, 1985). The area of the loop represents the net work per cycle (shown in green). This example loop is counter clockwise, representing positive net work. The blue area beneath the loop represents work lost through passive and active resistance. Image adapted from Mokele (2011; https://commons.wikimedia.org/wiki/File:Work_Loop.svg) under a Creative Commons licence.

1.2.5.2 *In vivo* approaches

The use of *in vivo* measurements of muscle length change and activity patterns are often used to design *in vitro* experiments to replicate muscle's operating conditions during locomotion. The use of *in vivo* approaches alone is however somewhat limited due to challenges in measuring force (Fleming and Beynnon, 2004; Schellenberg *et al.*, 2015). These limitations derive from not only technological limitations, but also the requirements of some *in vivo* technologies to be implanted, requiring surgery, these implantation processes can sometimes damage tissues, and alter ligament and joint function (Fleming and Beynnon, 2004). Implanted technologies such as differential variable reluctance transducers (DVRTs) are often used in human (*H. sapiens*) knee or

elbow joints to measure strain and micromotion. Felming and Beynnon (2004) note these technologies can impact the function of knee joints where full extension of the knee joint can lead to implants impinging against the roof of the intercondylar notch. Along with these potential risks, and impacts *in vivo* approaches are not suitable for all muscles or organisms, with strain gauges usually requiring a rigid attachment point, making them unsuitable for animals lacking rigid skeletons, such as those of soft bodied animals (Fleming and Beynnon, 2004; Tobalske and Dial, 2000). As well as this, the insertion of strain gauges must be at a certain point, with variations impacting the action of muscle upon gauges, leading to differential measures of strain among individuals (Tobalske and Dial, 2000).

Despite the limitations of *in vivo* approaches, a variety of techniques have been developed, ranging from the strain gauges briefly discussed above (Jackson and Dial, 2011; Tobalske and Dial, 2000), to sonomicrometry (Ellerby and Askew, 2007; Jackson and Dial, 2011) and electromyography (Kier *et al.*, 1989). These techniques differ in their application and information obtained, electromyography (EMG) enables the activation pattern of musculature to be measured through the measurement of changes in local muscle potential during depolarisation (Askew and Marsh, 2001; Kier *et al.*, 1989; Lee *et al.*, 2013; Uyeno and Kier, 2007). Sonomicrometry utilises signal-generating piezoelectric crystals to provide insight into the length changes of muscle during movement. The ultrasound waves are created in the piezoelectric material by applying a voltage – this travels through the muscle and, at the 2nd crystal, a voltage is produced. Distance between crystals calculated from time and speed of sound in muscle (Coughlin *et al.*, 1996a; Moo *et al.*, 2017; Thompson *et al.*, 2014). With this being used to assess the length changes of muscle, as well as the velocity of such processes (Coughlin *et al.*, 1996a; Ellerby and Askew, 2007; Moo *et al.*, 2017). Finally, strain gauges provide direct measures of muscular force through attachment to tendons, bones or other rigid structures of animals (Harrison *et al.*, 2010; Smith and Hylander, 1985; Tobalske and Dial, 2000).

These *in vivo* techniques have been utilised using a variety of different animals, with Marsh and Olson (1994) noting *in vivo* muscle performance of the bay scallop adductor

(*Argopecten irradians*) was slightly lower than that measured *in vitro* through the work loop technique. Moo *et al.* (2017) utilised a variety of *in vivo* approaches to assess muscular shortening velocity, power and excitation responses during jumping in northern leopard frogs (*Lithobates pipiens*), where sonomicrometry, EMG and a tendon force transducer (strain gauge) were all utilised; this provided an insight into muscle length change, velocity, power of the frog plantaris longus muscle, with Moo *et al.* (2017) noting frog escape responses powered by the plantaris longus muscle produced high peak power through a dynamic catch mechanism during jumping.

As a result of the limitations of *in vivo* techniques, particularly the limits in measuring muscular force, and thus work/power, the parameters identified *in vivo* can be applied through *in vitro* techniques, providing a greater insight into mechanical performance (Askew and Marsh, 2001; Marsh and Olson, 1994). Comparisons between measures made *in vivo* and *in vitro* reveal *in vitro* measures are generally higher, with this likely resulting from both the optimisation of the mechanical properties *in vitro*, as well as the loss of constraints (such as acting against other muscles or tissues) outside the body of the animal (Marsh and Olson, 1994).

1.2.6 Transfer efficiency of muscle

The transfer efficiency is used here to describe the proportion of mechanical work from the muscles which is transferred into useful hydrodynamic work in the wake of an animal. Locomotory systems which achieve high transfer efficiency, where a high proportion of the mechanical energy is transferred to the wake of the animal, waste less mechanical energy than those where internal losses are high (Muller and van Leeuwen, 2006; Yalcinkaya *et al.*, 2016). The calculation of transfer efficiency requires knowledge of the muscle mechanical performance as well as knowledge upon the energy input into the environment, as such specialised equipment or techniques are generally required (Muller and van Leeuwen, 2006; Yalcinkaya *et al.*, 2016).

Measurements of transfer efficiency as defined here are somewhat lacking in the literature. Muller and van Leeuwen (2006) highlighted this limitation within the current knowledge upon undulatory swimming in fishes; recent work has begun to address this *in silico*, with Yalcinkaya *et al* (2016) estimating the mechanical efficiency of longfin squid (*L. brevis*) mantle muscle is 36.8 % during jet propulsion swimming.

1.3 Energy to the environment

The movement of animals through water is achieved through a variety of means (Alexander, 2003; Maddock *et al.*, 1994; Vogel, 1994), but all these locomotive strategies rely upon displacing water to create thrust (Alexander, 2003; Vogel, 1994). The displacement of water can be achieved through an assortment of mechanisms, as such animals have developed a range of locomotor strategies to take advantage of these locomotory processes. Of these various locomotor processes key strategies include the undulatory swimming seen by many fish (Muller and van Leeuwen, 2006), the jet propulsion swimming exhibited by various invertebrate lineages such as jellyfish (Demont and Gosline, 1988) and cephalopod molluscs (Wells and O'Dor, 1991), and the use of cilia seen at a smaller scale in many zooplankton (Alexander, 2003).

Free swimming animals utilise the energy from their muscles to create movement (Gerry and Ellerby, 2014). The energy put into the wake of an animal to create thrust is the driver of this process. Thrust can be created through a variety of means, this thesis will focus on the creation of thrust through jet propulsion, a swimming modality used by many invertebrate lineages (Alexander, 2003).

1.3.1 Swimming through jet propulsion

Swimming through jet propulsion is seen across a variety of invertebrate taxa such as the cephalopods, including both coleoids, such as the squid (O'Dor and Webber, 1986; Wells and O'Dor, 1991), and shelled *Nautilus* (Neil and Askew, 2018), cnidarians such

as jellyfish (Dabiri, 2009; Demont and Gosline, 1988), and bivalves such as scallops (Bailey and Johnston, 2005; Neil, 2016). The production of a jet is achieved through the compression of a fluid-filled cavity by surrounding musculature (Mill and Pickard, 1975; Sutherland and Madin, 2010; Thompson *et al.*, 2010). While the basic mechanisms of jet propulsion systems are the same, the morphology and path of fluid flow differs between different animals, but can be broadly categorised into three mechanisms. The first involves water entering through the front of the animal and leaving at the rear, this mechanism creates jets which act more as a stream and lack the intermittent nature of the other two mechanisms (Alexander, 2003; Sutherland and Madin, 2010). Such a mode of jet creation is seen in the salps, such as *Pegea confoederata*, *Weelia cylindrica* and *Cyclosalpa affinis*, (Sutherland and Madin, 2010). The jet propulsion of hydromedusan jellyfish, such as the red-eye jellyfish (*Polyorchis penicillatus*) is somewhat simpler than that of salps where water is taken in and expelled through the same orifice (the subumbrellar surface) (Demont and Gosline, 1988; Satterlie, 2011). The jet propulsion system of cephalopods involves water being taken in and expelled through two separate orifices (the collar flaps and siphon). As a result of the periodic intake and exhaust phases associated with jet propulsion swimming these systems typically involve periods of acceleration and deceleration (Anderson *et al.*, 2001; Bartol *et al.*, 2001; O'Dor, 2002), resulting in fluctuations in swimming velocity. The high mechanical costs associated with propelling a small volume of water at high velocity to achieve thrust, as well as the increased drag or mass associated with increasing chamber volume, have led to the conclusion of jet propulsion swimming being an inefficient mode of locomotion, particularly when compared to the undulatory swimming of teleosts (O'Dor and Webber, 1986), which involves the acceleration of a relatively larger volume of water to a lower velocity to achieve an equivalent thrust. Such differences are thought to afford teleosts lower mechanical costs, as well as less variable drag during routine swimming activities (O'Dor and Webber, 1991; Wells, 1994). Section 1.3.5 outlines the various methodologies in the calculation of propulsive efficiency, these equations highlight the refill phase of jet propulsion swimming is of key importance in understanding efficiency in jet propulsion, a limitation not seen in other modes of locomotion, limiting the usefulness of traditional efficiency calculations (See Section 1.3.5).

1.3.2 The efficiency of jet propulsion swimming

The long held assumption of jet propulsion being inefficient mode of locomotion has been brought into question by recent studies. Bartol *et al* (2009a; b) found the jets of brief (*Lolliguncula brevis*) and longfin squid (*D. pealeii*) showed differences in jet structure which seemed to impact upon propulsive efficiency. The work of Bartol *et al.* (2009) defined these jets as two "modes", jet mode I was characterised by a single isolated vortex ring while those of jet mode II were characterised as more elongate jet structures (Figure 11). The smaller isolated jets achieved greater propulsive efficiency than more elongate jets, with the suggestion this occurred as a result of turbulence within the fluid. These jet structures have been noted across a variety of species such as the chambered *Nautilus* (*Nautilus pompilius*) (Neil and Askew, 2018) and king scallops (*Pecten maximus*) (Neil, 2016).

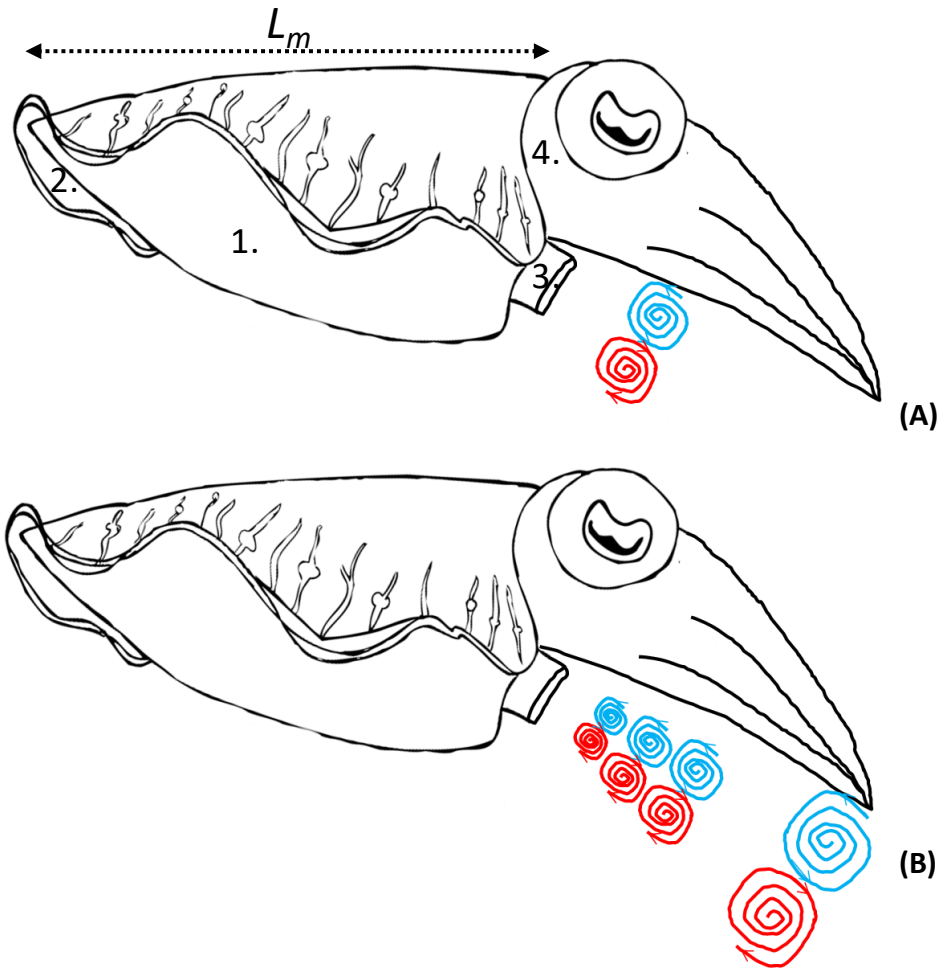

Figure 11. The underlying structure of jets of mode I (A) and II (B). Jets of mode I result from a single isolated jet vortex, while mode II jets result from a leading vortex followed by a series of interconnected jet vortices. Key anatomical details involved in locomotion are labelled as: 1. The mantle; 2. Fins; 3. The siphon; 4. The collar flaps; and L_m the mantle length. Figure adapted from Bartol *et al.* (2009); Cuttlefish image adapted from Downey (2009; https://www.flickr.com/photos/psd/3403881805) under a Creative Commons licence.

These structural characteristics of jet vortices are thought to play a key role in the thrust these impart (and thus the propulsive efficiency achieved by animals) (Bartol *et al.*, 2009a; Linden and Turner, 2004; Vogel, 1994). This seems to bring into question why these different jet structures are formed if those isolated jet vortices are more efficient than more elongate structures (Linden, 2011). Work with mechanically

generated jets has noted the energy input into a jet plays a key role in this, where a single jet vortex can only accept a finite amount of energy before the structure begins to breakdown (Linden and Turner, 2004). This seems to suggest animals producing more elongate jet structures are inputting a greater amount of energy per jet than those producing isolated vortices. Aside from this, several studies have demonstrated that juvenile animals appear to produce these isolated structures before these become more and more elongate and chaotic in nature (Anderson and Grosenbaugh, 2005; Bartol *et al.*, 2009a; Bartol *et al.*, 2009b). The changes in jet structure seem to relate to both the energy input, as suggested from mechanically generated jets (Linden, 2011; Linden and Turner, 2004), but also as a result of changes in the flow environment inhabited by animals (Herschlag and Miller, 2011; Ngo and McHenry, 2014; Shan and Dimotakis, 2006). The flow environment an animal finds itself in is explained through the use of Reynold's numbers (*Re*), these dimensionless numbers are the ratio of inertial forces to viscous forces, providing information about how fluid flows around animals, and the viscosity of the water animals are swimming through (Muller and van Leeuwen, 2006; Ngo and McHenry, 2014). Most animals inhabit laminar flow environments as juveniles before moving to more turbulent flow environments as adults (Muller and van Leeuwen, 2006). These changes in flow environments impact the efficiency with which animals can move through environments, as well as influencing the amount of energy which must be put into the wake to achieve thrust (Dabiri, 2009; Muller and van Leeuwen, 2006). Indeed, more turbulent environments are associated with an increased need for locomotive energy to achieve thrust, as well as increased streamlining to reduce the impacts of drag and other forces (Dabiri, 2009; Jones *et al.*, 2007; Muller and van Leeuwen, 2006).

Studies upon the structure of jets are widespread, ranging from the structure of mechanically generated jets (Linden, 2011; Linden and Turner, 2004) to the structure of the jets of various animals (Dabiri, 2009). These studies have revealed the jet modes outlined by Bartol *et al* (2009) seem to be a common feature among animals with cephalopods such as the longfin (*D. pealeii*) and brief (*L. brevis*) squid (Bartol *et al.*, 2009a; Bartol *et al.*, 2009b), nautilus (*N. pompilius*) (Neil and Askew, 2018), jellyfish species (Dabiri, 2009), and salp species (Sutherland and Madin, 2010). These different

jet modes (outlined in Figure 11) are thought to be influenced by the flow environments inhabited by animals, with Reynolds numbers appearing to be an important measure in determining the effectiveness of jet vortices. Herschlag and Miller (2011) suggested the jet propulsion swimming of idealised jellyfish was impacted by *Re*, where larger *Re* resulted in more rapid decay of forward velocity; as such this seems to necessitate the input of greater proportions of energy as animal Reynolds numbers increased (Herschlag and Miller, 2011; Shan and Dimotakis, 2006); this seems to explain the breakdown of jet structure associated with jet mode II, and the observation of only these elongate forms in larger squid (Anderson and Grosenbaugh, 2005; Anderson *et al.*, 2001; Bartol *et al.*, 2009a).

1.3.3 Molluscan locomotion

The diversity of molluscs has resulted in a range of locomotory strategies being employed by various different lineages. The locomotion can be broadly divided into three key modes: the crawling strategies seen by many gastropods and *Octopus* (Denny, 1980; Levy *et al.*, 2015; Yekutieli *et al.*, 2005). The use of fins and whole bodies to produce undulatory swimming, as seen in some cephalopods, such as the giant Australian cuttlefish (*Sepia apama*) (Aitken and O'Dor, 2004), as well as gastropods such as the hooded nudibranch *(Melibe leonina*) (Newcomb and Watson, 2002). The third strategy, jet propulsion swimming, is seen in all cephalopods (Bartol *et al.*, 2001; Helmer *et al.*, 2017; Wells and O'Dor, 1991), as well as in some bivalves, such as the scallops (Marsh *et al.*, 1992) and fragile file clams (*Limaria fragilis*) (Baldwin and Lee, 1979). The range of locomotive strategies employed by molluscs reflect the differences in evolutionary history of different lineages, as well as the adaptive constraints these animals find themselves under (Sanchez *et al.*, 2018).

The locomotion of cephalopod molluscs utilises all the key locomotive elements seen in molluscs, the propulsive systems of all cephalopods are described as being “dual-mode”; in the octopodiforms, such as the common octopus (*Octopus vulgaris*), crawling with arms and jet propulsion form this dual-mode system (Kazakidi *et al.*, 2015; Sfakiotakis *et al.*, 2015). Decapodiforms, including the squid and cuttlefishes,

utilise a slightly different dual-mode system consisting of undulatory swimming using fins located at the periphery of the mantle, and jet propulsion swimming (Bartol *et al.*, 2001; Jastrebsky *et al.*, 2016; Stewart *et al.*, 2010). Swimming through jet propulsion is common among all cephalopods, with some cephalopods able to create jets through both the presumably ancestral mechanism, whereby water is taken into the mantle cavity and expelled through the siphon (Neil and Askew, 2018; Wells and O'Dor, 1991), as well as through the action of modified arms (Sfakiotakis *et al.*, 2015). In the common (*Octopus vulgaris*) and algae octopuses (*Abdopus aculeatus*) the arms are joined by a thin membrane enabling an additional mechanism by which an animal can propel itself. These morphological structures enable a second type of jet propulsion, in which the contraction of the arms reduces the internal volume of the cavity created between the arms and membrane, forcing water out and creating jets (Sfakiotakis *et al.*, 2015).

Despite the variety of morphological and behavioural characteristics seen in cephalopod molluscs, investigations to understand the propulsive systems in these animals has largely focused upon the inshore squids (Family *Loliginidae*) (Anderson and Grosenbaugh, 2005; Bartol *et al.*, 2009a; Thompson *et al.*, 2010). The behaviour and morphology of such animals is dominated by jet propulsion swimming. The swimming mechanics of other decapodiform cephalopods have received less attention (Helmer *et al.*, 2017; Jastrebsky *et al.*, 2016). The cuttlefishes (Family *Sepiidae*) represent another major lineage of cephalopods with a set of unique morphological and behavioural features when compared to the previously investigated squids (Sanchez *et al.*, 2018; Wells and O'Dor, 1991). The behaviour of cuttlefish is dominated by predator avoidance through mechanisms of adaptive camouflage, and as such much research has focused upon this aspect of cuttlefish behaviour (Hanlon, 2007). The locomotion of cuttlefish has received limited attention but is thought to be dominated by the action of the fins upon the periphery of the mantle (Helmer *et al.*, 2017; Jastrebsky *et al.*, 2016). These fins are involved in the slow routine movements of animals, while the jet locomotor plays a key role in escape and more rapid swimming (Aitken and O'Dor, 2004; Jastrebsky *et al.*, 2016).

1.3.4 Visualisation of flow

In assessing the dynamics and efficiency of swimming mechanics these wakes can be measured through techniques such as particle image velocimetry (Bartol *et al.*, 2009b; Katija *et al.*, 2015). This technique involves seeding water or other media with small neutrally buoyant particles, these particles are illuminated using a light sheet. Animals are induced to swim through this and the movement of the particles in the wake tracked using a high-speed camera.

PIV has been used across a variety of disciplines to study the wake structure of both animals and mechanically generated vortices (Dabiri, 2009; Linden, 2011). Such studies have provided insight into the hydrodynamics associated with a range of different locomotive styles, ranging from the jet propulsion swimming of cephalopods (Anderson and Grosenbaugh, 2005; Bartol *et al.*, 2009a; Neil and Askew, 2018), jellyfish (Neil, 2016) and scallops (Neil, 2016) to the undulatory swimming of many teleosts (Bottom *et al.*, 2016; Gemmell *et al.*, 2016; Tytell and Lauder, 2004).

1.3.5 Propulsive efficiency

In understanding the locomotion of animals, a key concept is that of propulsive efficiency. Propulsive efficiency explains the proportion of the energy input into the water which is transferred to useful forward momentum. The calculation of propulsive efficiency typically uses three key components: the swimming velocity of animals ($\bar{U}$), the velocity of the fluid within the jets produced by animals ($\bar{u}_j$), and the velocity with which water refills the cavity from which it was expelled ($\bar{u}_r$). How these components are used differs between different calculation methods. Three commonly used methods for calculating propulsive efficiency are presented here: the rocket efficiency calculation (Equation 2), the Froude efficiency calculation (Equation 3) and the whole cycle efficiency calculation (Equation 4); these mechanisms of calculation all differ in their effectiveness and the assumptions made. Of these methodologies, perhaps the most simplistic is to calculate efficiency through the rocket equation:

$$\eta_r = \frac{2\bar{U}\bar{u}_j}{\bar{u}_j{}^2 + \bar{U}^2}$$

Equation 2. The rocket efficiency calculation. Where $\bar{U}$ signifies the velocity of the animal, and $\bar{u}_j$ is the jet velocity (Alexander, 2003; Weymouth and Triantafyllou, 2013).

The rocket and Froude equations are somewhat limited when applied to jet propulsion swimming as only forward momentum is accounted for, where $\bar{U}$ and $\bar{u}_j$ are used, but the intake processes ($\bar{u}_r$) are ignored; such intake processes are typically seen during the jet propulsion swimming of animals, highlighting why these methodologies may overestimate the efficiency of animal locomotion (Alexander, 2003; Anderson and Demont, 2000). Froude efficiency is noted by Anderson and Demont (2000) to be the most widely used in the study of animal propulsive efficiency:

$$\eta_f = \frac{2\bar{U}\bar{u}_j}{(\bar{U} + \bar{u}_j)^2}$$

Equation 3. The Froude efficiency calculation. Where $\bar{U}$ signifies the velocity of the animal, and $\bar{u}_j$ is the jet velocity (Alexander, 2003; Anderson and Demont, 2000).

This equation uses the same variables as the rocket equation ($\bar{U}$ and $\bar{u}_j$), but produces somewhat lower values. Anderson and Demont (2000) noted this equation is prone to overestimation during cephalopod jet propulsion swimming, perhaps as a result of differences between cephalopod swimming and airscrew propeller systems. Of the three methods for calculating propulsive efficiency presented here, the whole cycle efficiency is perhaps the most appropriate estimate of propulsive efficiency (Alexander, 2003; Anderson and Grosenbaugh, 2005):

$$\eta_{wc} = \frac{2\bar{U}\bar{u}_j}{2\bar{U}\bar{u}_j + \bar{u}_r{}^2 + \bar{u}_j{}^2}$$

Equation 4. The whole cycle efficiency calculation. Where $\bar{U}$ signifies the velocity of the animal, $\bar{u}_j$ is the jet velocity and $\bar{u}_r$ the refill velocity (Alexander, 2003; Anderson and Demont, 2000; Anderson and Grosenbaugh, 2005).

This equation is a modification of the η_r equation, where the acceleration of fluid during the intake phase ($\bar{u}_r$) is included, this is thought to give a more accurate

estimate of the efficiency of locomotion, as it accounts for both the intake and exhaust phases associated with jet propulsion swimming (Alexander, 2003; Anderson and Demont, 2000).

Previous work utilising the whole-cycle efficiency calculation has revealed efficiency values are much higher in chambered nautilus (*N. pompilius*) than squid species. With Anderson and Demont (2000) noting the propulsive efficiency of longfin squid (*D. pealeii*) was between 34 and 48 %, while Neil and Askew (2018) noted the propulsive efficiency of chambered nautilus (*N. pompilius*) was somewhat higher being between 37 and 86 %.

1.4 Summary

This thesis investigates the underlying mechanics and energetics of the jet propulsive system of European common cuttlefish (*Sepia officinalis*), with the aim of determining the efficiency with which energy is transferred from chemical energy into useful work in the environment. This was achieved through three key experimental protocols. The first investigates the structure and hydrodynamics of cuttlefish jet propulsion swimming, utilising particle image velocimetry to visualise the jets produced during free swimming in newly hatched and juvenile cuttlefish. This PIV data is then used to calculate the propulsive efficiency of animals through utilisation of the whole cycle efficiency calculation. This is followed by an investigation into the mechanical properties of the circular muscle of the cuttlefish mantle, specifically quantifying the physiological properties of the muscles under isometric, isotonic as well as cyclic conditions, and how these change between juvenile and adult stages. The data from this chapter is then used to calculate the transfer efficiency of muscle, this being the proportion of the available mechanical energy which makes it into the wake of the animal. The final data chapter measured changes in three key biochemicals (L-arginine, L-arginine phosphate and ATP) in response to a series of cyclic muscle contractions, and the efficiency with which biochemical energy is transferred into useful mechanical work by the mantle muscles. Taken together these data chapters enable the calculation of the total proportion of energy from ATP which is transferred into useful

movement, providing the most complete investigation into the energy transduction chain during locomotion to date.

Chapter 2 investigates the jet propulsion swimming of the European common cuttlefish (*S. officinalis*). This chapter aimed to expand current knowledge by providing an insight into the swimming mechanics employed by cuttlefish at two key stages: as newly hatched animals (≤7 days old), and as juveniles (3 months old). The wake structure and hydrodynamics of jets produced were investigated, and hydrodynamic efficiency calculated for each age group. These data enabled the scaling dynamics of cuttlefish jet propulsion swimming to be investigated, as well as a greater understanding of jet propulsion in these animals. The calculation of an animal's propulsive efficiency enabled an understanding of the proportion of energy in the wake which resulted in forward momentum, providing a key part of the energy transduction chain.

Chapter 3 investigates the mechanical function of the obliquely striated muscle of the cuttlefish mantle. Through this work the ontogenetic scaling of obliquely striated muscle function was investigated during juvenile and adult stages of cuttlefish. As well as this, the muscle performance under cyclical contractions was investigated, providing the first insight into cyclic muscle performance of this muscle type, and in cephalopod molluscs. Data derived from these cyclic contractions was used in the calculation of transfer efficiency along with information from Chapter 2 relating to energy in the wake, this provided empirical data for another key part of the energy transduction chain, enabling an understanding of how much of the mechanical energy made it into the wake of the animal.

The final data chapter (Chapter 4) investigates the changes in key metabolites (L-arginine, L-arginine phosphate and ATP) and contractile efficiency under a range of cycle frequencies which simulate jet propulsion swimming. This data taken with that obtained in previous chapters enables the estimation of the efficiency with which

chemical energy is converted into forward momentum, providing the most complete estimate of the locomotive energy transduction chain to date.

Chapter 2. The hydrodynamics of jet propulsion swimming in European cuttlefish: wake structure and propulsive efficiency

2.1 Abstract

Cuttlefish (*Sepia officinalis*) use jet propulsion swimming for activities ranging from migratory journeys and foraging to interactions with conspecifics and predators, jets result from the transfer of energy from locomotory muscles to the surrounding water, ultimately resulting in movement. Swimming by jet propulsion is generally considered to be inefficient, as relatively small volumes of water are propelled at high velocity to produce thrust, compared to undulatory swimmers. During jet propulsion swimming, jets that maximise thrust while minimising energy costs are considered optimal. Here the structure of jets produced by cuttlefish and their propulsive efficiency were investigated in newly hatched and late juvenile cuttlefish. Wake structure was determined using particle image velocimetry (PIV). Cuttlefish jets could be categorised qualitatively into two jet types: jets consisting of an isolated vortex ring, or jets consist of a vortex ring followed by a trailing jet. No relationship was found between jet type and the animal's swimming velocity and no significant difference in propulsive efficiency between jet types. However, propulsive efficiency did increase with increasing swimming speed for both jet types (ranging from approximately 0.40 to 0.95). The jets of newly hatched animals were dominated by the isolated vortex rings, while juvenile animals exhibited both types of jet structure. Propulsive efficiency and swimming speed were significantly higher in hatchling animals compared to juveniles, with newly hatched animals swimming more rapidly than juveniles across swim orientations. The impact of swimming orientation upon swimming speed was only noted in hatchlings, where posterior-first swimming was significantly faster than anterior-first swimming. Propulsive efficiency was unaffected by swimming orientation. These differences in propulsive efficiency and swimming mechanics between hatchlings and juveniles may arise from the different flow regimes (as predicted through Reynold's numbers) inhabited by animals. These different flow regimes impact the energy use of animals as a result of frictional forces, where more

turbulent environments are associated with increased energy expenditure as animals must overcome increased resistance on top of existing demands, to create the thrust required for movement.

2.2 Introduction

The cuttlefish (*Sepiidae*) represent a distinct evolutionary lineage within the cephalopod molluscs, having retained an internalised shell (termed the cuttlebone) and diverged from other decapodiform cephalopods early during their diversification (Sanchez *et al.*, 2018). As a result of their evolutionary history, cuttlefish show unique morphological and behavioural adaptations to their ecological niche. Cuttlefish behaviour is dominated by crypsis, where chromatic elements within the animal's skin are used to avoid detection by predators and prey (Hanlon, 2007). Cuttlefish swim using either jet propulsion, powered by the muscles of the mantle cavity, or by undulatory swimming, powered by the fins on the periphery of the mantle. These two locomotive modes work both independently and in concert giving cuttlefish locomotive flexibility in speed and manoeuvrability (Helmer *et al.*, 2017; Jastrebsky *et al.*, 2016).

Jet propulsion swimming is traditionally thought to be an inefficient mode of transport due to the energy losses associated with generating momentum by expelling a small volume of water at high velocity rather than moving a larger volume of water at lower velocity to achieve similar levels of thrust (Krieg and Mohseni, 2015; Weymouth and Triantafyllou, 2013). Despite these perceived inefficiencies, jet propulsion remains a key element in cephalopod locomotion, perhaps as a result of this system enabling rapid thrust creation, which is likely of key importance in prey capture and escape responses (Wells and O'Dor, 1991). Previous work on cephalopod swimming has given mixed results in terms of the propulsive efficiency of this locomotive system; Neil and Askew (2018) found the efficiency of *Nautilus pompilius* jet propulsion swimming was between 0.30-0.76 (Neil and Askew, 2018), while work with squid has noted this falling between 0.42-0.49 (Anderson and Grosenbaugh, 2005). These differences in

propulsive efficiency suggest refinement of this locomotor system may differ between different cephalopod lineages.

In producing movement, energy is transferred from the locomotory muscles into the surrounding medium to create thrust. The mechanism by which jet propulsion creates thrust involves water being taken into an enclosed cavity, before musculature reduces the size of the cavity, forcing water out (Figure 12; Krieg and Mohseni, 2015; Weymouth and Triantayfyllou, 2013). These mechanisms by which cephalopods swim through jet propulsion have been described in detail across various studies (Anderson *et al.*, 2001; Bartol *et al.*, 2001; Kier and Thompson, 2003; Neil and Askew, 2018). The process can be broken down into two phases: the first of which is the intake phase, where action of the radial muscles of the mantle cavity (Figure 13) causes the mantle to expand, increasing intramantle volume and reducing internal pressure. As a result of decreased intramantle pressure, the collar flaps open allowing water to flow into the mantle cavity. During this process animals are able to increase the intake into the mantle cavity by up to 30 % through “hyperinflation”, however the underlying muscular dynamics facilitating this process are largely unknown (Kier and Schachat, 2008; Weymouth and Triantafyllou, 2013). Kier and Schachat (2008) suggest this hyperinflation results from the flexibility afforded to cephalopods through the structure of obliquely striated musculature. Once the mantle cavity is filled, the second phase involves circular muscle contraction which forces the collar flaps shut, meaning water can only escape through the siphon (Figure 12). This expelled water acts to create thrust, propelling the animal through the water.

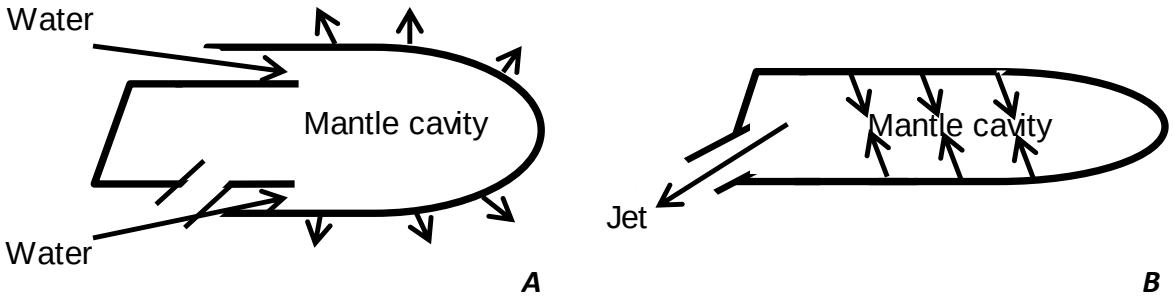

Figure 12. Simplified diagram showing the mechanisms involved in the creation of a jet by a typical cephalopod. A. Shows the intake phase where radial muscles and elastic mechanisms cause the intramantle area to increase, reduced internal pressure allows water to enter the mantle cavity through the collar flaps. B. Shows the mechanisms involved in the creation of a jet, where circular muscles contract reducing available space, and increasing pressure within the mantle cavity and forcing collar flaps shut. Water is forced out of the mantle cavity through the siphon. The siphon can be rotated 180 ° below the body of the animal (Jastrebsky, 2015), enabling animals to move both forwards, backwards and sideways through jet propulsion.

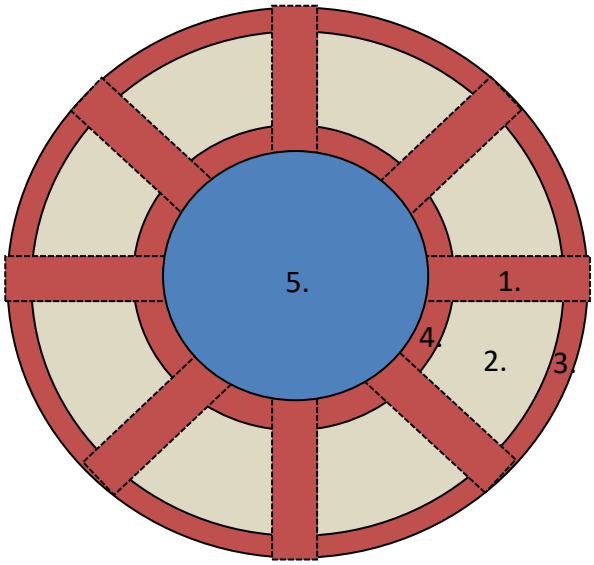

Figure 13. Simplified diagram showing the arrangement of muscle fibres through the cephalopod mantle. Circular muscle fibres (2., 3. and 4.) run circumventially around the mantle cavity in three distinct layers termed the superficial (3. and 4.) and central (2.). Superficial layers are dominated by aerobic fibres and thought to be involved in routine swimming, the central core is dominated by anaerobic fibres. These circular fibres are interspliced by radial muscle fibres (1.), radial musculature runs from the inner to the outer mantle antiparallel to the circular fibres. Intramantle area (5.) is altered through the action of the surrounding muscle tissues.

The displacement of water by animals during swimming is opposed by the surrounding water through viscous and inertial forces (Mauguit *et al.*, 2010; Muller and van Leeuwen, 2006). The ratio of inertial and viscous forces can be visualised through the use of Reynolds numbers (*Re*). These dimensionless numbers explain the relative importance of these forces, which depend on animal size, velocity and kinematic viscosity (Mauguit *et al.*, 2010; Ngo and McHenry, 2014; Voesenek *et al.*, 2018). As animals increase in size the flow environments inhabited may also change, many small or newly hatched animals inhabit laminar flow regimes (*Re* <1000), these flow regimes are characterised by fluid flows in parallel layers with no disruption within these layers of flow, within the laminar flow environment animals benefit from high momentum diffusion and low momentum convection leading to a reduction in drag and associated

frictional forces (Muller and van Leeuwen, 2006; Ngo and McHenry, 2014). Flow regimes *Re* >3000 are inhabited by larger animals, these flow regimes are characterised as turbulent flow environments with chaotic changes in pressure and flow velocity. Within these environments animals experience increased drag and friction due to interactions with the skin and shed vortices. This leads to increased energetic demands to overcome these forces (Gazzola *et al.*, 2014). Animals inhabiting intermediate flow regimes (termed the laminar-turbulent transition; *Re* 1000-3000) experience environments which have increased turbulence when compared to laminar environments, with associated increases in energetic demands (Ngo and McHenry, 2014). Many animals overcome these limitations associated with the transition from laminar flows to more turbulent flows through specific adaptations, where particular limbs or areas associated with locomotion may show differential growth to other body areas (Alexander, 1999; Gould, 1966), which may result in reduced drag through streamlining, greater muscle mass to facilitate in the production of power, as well as specific adaptations to reduce drag or create lift. The ontogeny of cuttlefish sees these animals pass from the laminar flow regime as hatchlings, to the turbulent regime as adults; with *Re* ranging from 100 in hatchlings to 20,000 in adult animals (Aitken and O'Dor, 2004).

The current understanding of cephalopod hydrodynamics is heavily dominated by measures of loliginid jet propulsion swimming, this work aims to expand upon this knowledge by investigating the jet propulsion swimming of the European common cuttlefish (*S. officinalis*). The key aim of this work was to investigate the hydrodynamics of cuttlefish jet propulsion swimming, through the quantification of wake structure and propulsive efficiency in cuttlefish during early ontogeny. Based upon previous work it is hypothesised: (i) the jet propulsion swimming of cuttlefish will be more efficient than that of loliginid squids and *Nautilus* as a result of neutral buoyancy, and the lack of restrictive external shells; (ii) The wake structure of cuttlefish jets will fall into discrete categories as described in other jet propelled organisms and these categories will differ in the ratio of jet length to jet diameter; (iii) Smaller cuttlefish will be more efficient as a result of reduced drag and differences in flow regimes.

2.3 Methods

2.3.1 Animals

European cuttlefish eggs were taken as by-catch upon fishing gear by: (i) JHC research, Poole, Dorset, UK; (ii) The Native Marine Centre, Weymouth, Dorset, UK; (iii) Centre de Recherches en Environnement Côtier, Université de Caen, Luc sur Mer, Normandie, France; and (iv) RK Stride, Christchurch, Dorset, UK, during June 2015 (i, ii, and iii) and May 2016 (iv) in the English Channel. Eggs were housed in recirculating artificial saltwater systems (see section 2.3.1.1) at the University of Leeds at a temperature of 19 ± 1 °C as this temperature maximises development speed while avoiding premature hatching (Bouchaud, 1991). Once eggs began hatchling temperature was gradually decreased to 15 ± 1 °C. Animals were fed twice daily using size-appropriate live foods: live enriched *Artemia salina* (Vitalis live food enrichment, World Feeds ltd, Thorne, Derbyshire, UK; Peregrine Livefoods, Magdalen Laver, Essex, UK); *Mysis* shrimp (*Mysis spp*.; Aquadip VOF, Oss, North Brabant, The Netherlands; Essex Marine Aquatics, Wickford, Essex, UK); and river shrimp (*Palaemon varians*; Aquatic Live fish foods, Woodford, London, UK). Cuttlefish used in experiments were either hatchlings (<7 days old at the time of experiments) or juveniles (3 months old at the time of experiments).

2.3.1.1 Animal housing facilities

Recirculating artificial saltwater facilities used to house all cuttlefish were maintained at a salinity of 32 ± 1 PSU (Cefas, 2012) using Aqua One Reef synthetic (Kong's (Aust.) Pty Ltd, Sydney, NSW, Australia) formulated in deionised water. Animals were housed in size-matched groups in 478.4, 357.9 and 288.8 litre (length × width × height; 1300 x 800 x 460; 910 x 690 x 570 and 890 x 590 x 550 mm) aquaria with each tank holding up to 150 hatchling animals, or 50 juvenile animals.

Water quality was monitored to ensure suitable ranges were maintained; temperature (15 ± 1 °C) and salinity (32 ± 1 PSU) were monitored twice-daily; pH (7.8-8.1) and nitrogenous compounds were monitored monthly (NH_4^+ ≤ 0.5 mg L^{-1}; NO_2^-: ≤ 0.2 mg L^{-1}; NO_3^- ≤ 80 mg L^{-1}). 25% water changes were carried out twice per week. The maintained parameters for temperature and salinity fell within the natural range of animals in the English channel at the time eggs were collected (10.8-16.7 °C; 31.89-34.49 PSU) (Cefas, 2012).

2.3.2 Wake visualisation and analysis

Cuttlefish were individually captured and hatchlings moved to a 44 litre (l × w × h; 460 x 310 x 310 mm) experimental tank, and juveniles to a 126 litre (l × w × h; 610 x 460 x 450 mm) experimental tank. Water parameters in these tanks matched those of the holding tanks exactly (15 ± 1°C, 32 ± 1 PSU), with the water being additionally seeded with aluminium oxide particles (Acros Organics, Pittsburgh, PA, USA) to visualise the wake (mean particle size 5 µm; seeding density of 30 mg per litre; following Dabiri, 2006).

To visualise the aluminium oxide particles, a 1 W continuous green (532 nm) laser (Shanghai Dream Lasers Technology Co., Ltd., Shanghai, China) directed through a Powell lens (Thorlabs, Inc., Newton, NJ, USA) was used to create a 1 mm thick vertical light sheet (Figure 14). The animal and its wake were recorded using a Photron FASTCAM SA3 (Photron USA, San Diego, CA, USA) high speed camera (1024 x 1024 pixels, 500 frame s^{-1}; shuttered at $^1/_{500}$ frame s^{-1}) orientated with the recording plane parallel to the light-sheet.

As cuttlefish typically rest upon the benthos, a modification of the methods employed by Karson *et al.* (2003) were used to induce animals to swim through the laser light sheet. A tunnel composed of a Perspex® back and base, and black plastic sides (l x w x h; 160 x 55 x 60 mm (hatchling); 250 x 100 x 100 mm (juvenile)) was positioned at the top of the laser sheet; animals were placed in this prior to each swim (Karson *et al.*,

2003). This design proved effective in inducing animals to swim out of the tunnel and horizontally through the tank while descending towards the tank bottom. The use of a tunnel ensured animals would swim through the laser light sheet as the tunnel only had one side which was not sealed, ensuring animals swam out and through the laser light sheet. This however did not allow any control of swimming orientation, where animals could choose to swim either anterior- or posterior-first. To reduce stress and avoid fatigue, animals were subjected to no more than 5 swim attempts per day. Following each trial ventilation rate was often observed to increase; animals were allowed to rest upon the tank bottom for up to 15 minutes, until ventilation rate returned to pre-swimming levels. If ventilation rates showed little reduction, animals were returned to holding tanks to recover for 12–24 hours.

Fluid movements were determined by recording illuminated particles (PIVlab v1.41 (Thielicke, 2014; Thielicke and Stamhuis, 2014a; Thielicke and Stamhuis, 2014b); MATLAB R2017a; The Mathworks Inc., Natick, MA, USA). PIVlab uses a cross correlation technique with adaptive multi-pass (3) processing to analyse image pairs and track particle movement between frames. Prior to detailed analysis, sequences were pre-processed using a contrast-limited adaptive histogram equalisation tool, enhancing contrast. Next, data were smoothed using the *smoothn* function (Damian-Garcia smoothing), and adaptive multi-pass processing, using a total of three passes, was used in tracking particle movements, the initial integration window was 64 x 64 pixels, the second was 32 x 32 pixels and a final integration window of 16 x 16 pixels, each pass had a 50 % overlap with the previous pass. A standard deviation filter was used to remove vectors that were more than 7 deviations away from the mean flow of the jets. Missing vectors were interpolated using a boundary value solver, giving a smooth interpolation that tended towards the average boundary velocities.

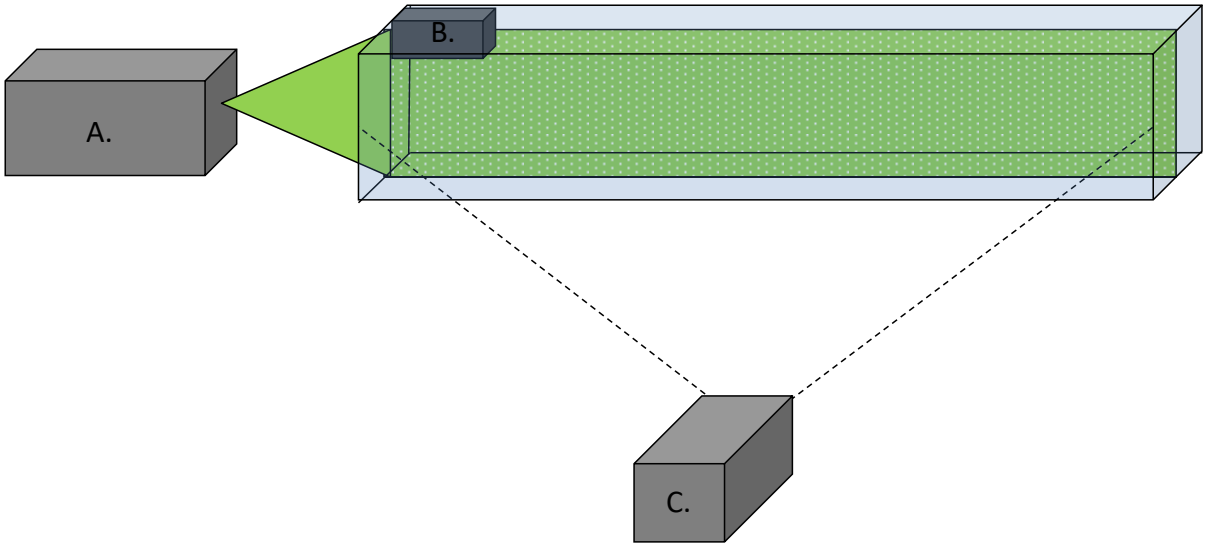

Figure 14. Typical setup for the PIV experiments.A vertical laser light sheet was projected through the tank illuminating aluminium oxide particles. A "tunnel" (B.) composed of a Perspex® base and back, with black plastic sides, was placed at the top of the chamber and cuttlefish placed within this prior to swimming through the laser light sheet. This chamber ensured cuttlefish could only swim out and through the laser light sheet. A. Shows the location of the laser and C. shows the location and viewing angle of the high speed video camera.

2.3.3 Jet properties and propulsive efficiency

Jet area (A_j) was calculated using D_j, the diameter of the vortex ring measured from the two peaks of vorticity that make up the ring. Due to the changeable orifice area of cephalopods, this method gave an average funnel diameter, and thus funnel area.

$$A_j = \pi \left(\frac{D_j}{2}\right)^2$$

Equation 5.

Measures of L_j (jet vortex length) and D_j (jet vortex diameter) were also used to calculate the L_j/D_j ratio. L_j and D_j were measured following Neil and Askew (2018), where L_j was measured as the extent of the vorticity field along the jet centreline which exceeded the background flow vorticity by 20%, D_j was measured from the two peaks of vorticity that make up the vortex ring. Previous work has noted this ratio can provide information relating to thrust generation and jet modes (Bartol *et al.*, 2009a; Dabiri, 2009; Neil and Askew, 2018).

Jet thrust (*T*), is the force propelling the animal and equals the rate of change of momentum in the surrounding fluid, and was calculated as (Anderson and Demont, 2000):

$$T = \rho \bar{u}_j{}^2 A_j$$

Equation 6.

where the density of seawater (1025 kg m^{-3}) is ρ, $\bar{u}_j$ is the average jet velocity calculated by taking the time average of the average jet core velocity during the jet period, A_j is the area of the jet.

Average body velocity during jetting ($\bar{U}$) was calculated as:

$$\bar{U} = \frac{d_{jet}}{t}$$

Equation 7.

where the swim distance over one jet (d_{jet}) was divided by the jet period (t). From this, the time average body velocity in body lengths per second (U_{Body}) was calculated, this involved dividing $\bar{U}$ by the mantle length (L_m).

$$U_{Body} = \frac{\bar{U}}{L_m}$$

Equation 8.

Whole cycle propulsive efficiency was calculated as follows (Alexander, 2003):

$$\eta_{wc} = \frac{2\bar{U}\bar{u}_j}{2\bar{U}\bar{u}_j + \bar{u}_r{}^2 + \bar{u}_j{}^2}$$

Equation 9.

Where $\bar{U}$ is the time average velocity of the animal, $\bar{u}_r$ is the refill velocity and $\bar{u}_j$ the mean jet velocity. Calculated following Alexander (2003).

Refill velocity ($\bar{u}_r$) was estimated following Neil and Askew (2018) as:

$$\bar{u}_r = \frac{\bar{u}_j A_j t_j}{A_r t_r}$$

Equation 10.

Assuming the amount of water released during a jet event is equal to the amount of water taken in, refill orifice area (A_r) was estimated from the radius of the collar flaps (r_{cf}). Orifice area is circular in nature running around the head of the animal (Bone *et al.*, 1994; King and Adamo, 2006).

$$A_r = \pi r_{cf}{}^2$$

Equation 11.

Drag was estimated as (Bartol *et al.*, 2001; O'Dor *et al.*, 1986):

$$D = 0.5 C_d \rho (0.25\pi L_m{}^2)\bar{U}^2$$

Equation 12.

Where the drag coefficient (C_d) was assumed to be 0.47, assuming the frontal area of animals was spherical, and L_m was used to calculate the surface area of animals.

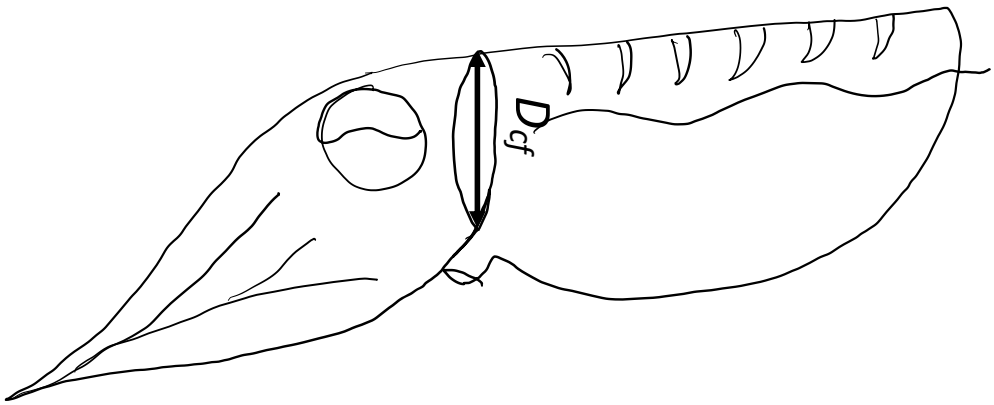

Figure 15. Simplified diagram outlining the data taken to estimate refill area. D_{cf} is the diameter of the collar flap, from which r_{cf} was derived. The mantle flaps form a circle around the head region with an attachment behind the eyes; water flows into the mantle cavity across a large area encircling the mantle.

Slip (*S*), the inverse of hydrodynamic efficiency, was calculated as the ratio of $\bar{u}_j/\bar{U}$ following Bartol *et al.*, 2009. Reynolds numbers were calculated following Alexander (2003) (Equation 13) and Strouhal numbers (Equation 14) were calculated following Triantafyllou *et al.* (1991):

$$Re = \frac{\rho \bar{U} L_m}{\mu}$$

Equation 13.

Where ρ is the density of seawater (1025 kg m^{-3}), $\bar{U}$ is the swimming speed of animals, and μ is the dynamic viscosity of seawater (0.00115 Ns m^{-2}).

$$St = \frac{f D_j}{\bar{U}}$$

Equation 14.

The jet diameter was used in the calculation as this gives the width of the wake in jet propelled swimmers.

2.3.4 Swimming kinematics

Swimming kinematics were determined over the course of several jet cycles by tracking the change in position every 10 frames (equivalent to every 0.02 seconds), this was achieved using the ImageJ plugin MTrackJ (Meijering *et al.*, 2012; Schneider *et al.*, 2012). The animal's eye was used as a reference point during the tracking process. Noise within the positional data were reduced following Bomphrey *et al.* (2009), and data used to visualise changes in velocity during animal swimming. This was achieved using an autocorrelation function to determine an appropriate cut off frequency (determined in 1 Hz steps) based upon the model fit, where residuals are used to determine the differences between the fitted model and the data. In this signal-plus-white noise model, a good fit for the signal will yield residuals which are white noise; if the autocorrelation looks like the autocorrelation of white noise this means the underlying signal has been well fit, while none of the signal has been lost to into the residuals. This filtered positional data was used to calculate the instantaneous velocity of animals during free-swimming.

2.3.5 Statistical analysis

Statistical tests were conducted in R 3.1.1, IBM SPSS Statistics 24 and OriginPro 9.1. All swimming sequences were used in data analysis, with individual cuttlefish included as a random variable. All data were tested for normality and homogeneity prior to statistical analysis. Where models were used quantile-quantile (q-q) plots of model residuals were checked to ensure these fit the normal distribution. A critical p value of 0.0017 was used to indicate significant differences between models and null models; this p value was chosen following a Bonferroni correction for multiple testing to reduce type I errors (Armstrong, 2014). A Bonferroni correction was selected as alternative procedures (such as the False Discovery rate) are less stringent in avoiding type I errors. Parametric tests were used on all data which met the assumptions of normality. Data which did not meet the assumptions of normality were log or arcsine transformed to meet these assumptions; where data could not be transformed

nonparametric tests were used. Statistical significance was determined using general linear models in R (Bates, 2015; Kuznetsova, 2017). Individual cuttlefish were included as a random factor, accounting for instances of repeated measures. Curve fitting was carried out using the curve estimation function in IBM SPSS Statistics 24, which selected the most appropriate fit for data based upon R^2 values. Scaling relationships were determined using the allometric fit function in OriginPro 9.1, where the goodness of fit was determined using Chi square tests.

2.4 Results

2.4.1 Animal morphology and swimming kinematics

A total of 244 jet events (from 124 unique sequences) were obtained from 38 hatchling (7.9 - 12.8 mm; mean (± sd) of 6 ± 4 jets per animal (ranging between 2 and 18); and 2 ± 2 jets per sequence (ranging between 1 and 12)) and 17 juvenile cuttlefish (20.8 - 40 mm; mean (± sd) of 3 ± 2 jets per animal (ranging between 2 and 9) and 2 ± 1 jets per sequence (ranging between 1 and 3)). Animals exhibited two swimming orientations, 'anterior-first' (AF) and 'posterior-first' (PF), in both age groups. Swimming orientation affected relative swimming speed, with this interacting with animal age- hatchlings swam at greater relative speeds than juveniles (AF: ~67 % faster; PF: ~44 % faster) in both orientations (X^2 47.29, df 2, p <0.001; see Table 1; Figure 16). Differences in swimming speed may relate to differences in drag forces. Drag forces were significantly higher during anterior-first swimming in newly hatched animals than during posterior-first swimming (X^2 26.88, df 1, p <0.001; Table 1; Figure 17), but showed no interaction with swimming orientation in juveniles (X^2 0.59, df 1, p 0.45; Table 1; Figure 17). Age-specific differences in drag forces were noted, where older (and larger) animals had significantly higher drag than newly hatched animals (X^2 56.1, df 1, p <0.001; Table 1; Figure 17). The relationship between swimming orientation, animal age and drag forces did not show a significant interaction (X^2 0.143, df 1, p 0.71). Despite these differences in swimming speed and drag forces, propulsive efficiency (Hatchlings: X^2 1.42, df 1, p 0.23; Juveniles: X^2 0.06, df 1, p 0.81; see Table 1) thrust (Hatchlings: X^2 0.98, df 1, p 0.23; Juveniles: X^2 0.32, df 1, p 0.57; see Table 1) and

slip (Hatchlings: X^2 0.79, df 1, p 0.37; Juveniles: X^2 0.14, df 1, p 0.71; see Table 1) were unaffected by swimming orientation. Further analysis revealed these two age groups differed in Reynolds numbers (*Re*), where hatchling cuttlefish had significantly lower *Re* than juveniles (X^2 54.89, df 1, p <0.001; Table 1).

Table 1. Morphology and swimming kinematics of hatchling and juvenile cuttlefish in relation to swimming orientation. Cycle frequency was defined as 1 ÷ t (jet period, defined as the whole jet cycle (mantle contraction and refill phases)). BL s^{-1} was calculated as $\bar{U}$ (body velocity) ÷ L_m (mantle length); L_m was used to define body length due to the consistency of this measure resulting from the rigid cuttlebone. Values are mean ± sd.

	Hatchling		Juvenile	
	Anterior-first	*Posterior-first*	*Anterior-first*	*Posterior-first*
Mantle length (mm)	10.52 ± 1.04	10.89 ± 1.10	31.78 ± 0.45	28.25 ± 0.36
Cycle frequency (Hz)	2.92 ± 0.91	3.95 ± 1.68	1.24 ± 0.49	1.65 ± 0.77
Swimming speed (BL s^{-1})	4.35 ± 1.68	7.26 ± 4.18	2.91 ± 1.26	3.21 ± 1.50
Reynolds number (Re)	435 ± 197	787 ± 500	2536 ± 1132	2325 ± 1285
Strouhal number (St)	0.47 ± 0.21	0.38 ± 0.20	0.18 ± 0.19	0.14 ± 0.08
Drag (mN)	8.86 ± 4.65	16.61 ± 11.43	154.17 ± 82.29	128.5 ± 81.07
Whole cycle propulsive efficiency (η_{wc})	0.87 ± 0.08	0.89 ± 0.07	0.76 ± 0.14	0.75 ± 0.16
Thrust (mN)	0.19 ± 0.61	0.30 ± 0.63	7.75 ± 8.68	7.29 ± 11.43
Slip	0.26 ± 0.23	0.23 ± 0.19	0.68 ± 0.53	0.75 ± 0.68
Jet velocity (cm s^{-1})	3.74 ± 4.31	5.78 ± 5.36	24.86 ± 22.75	24.43 ± 17.76

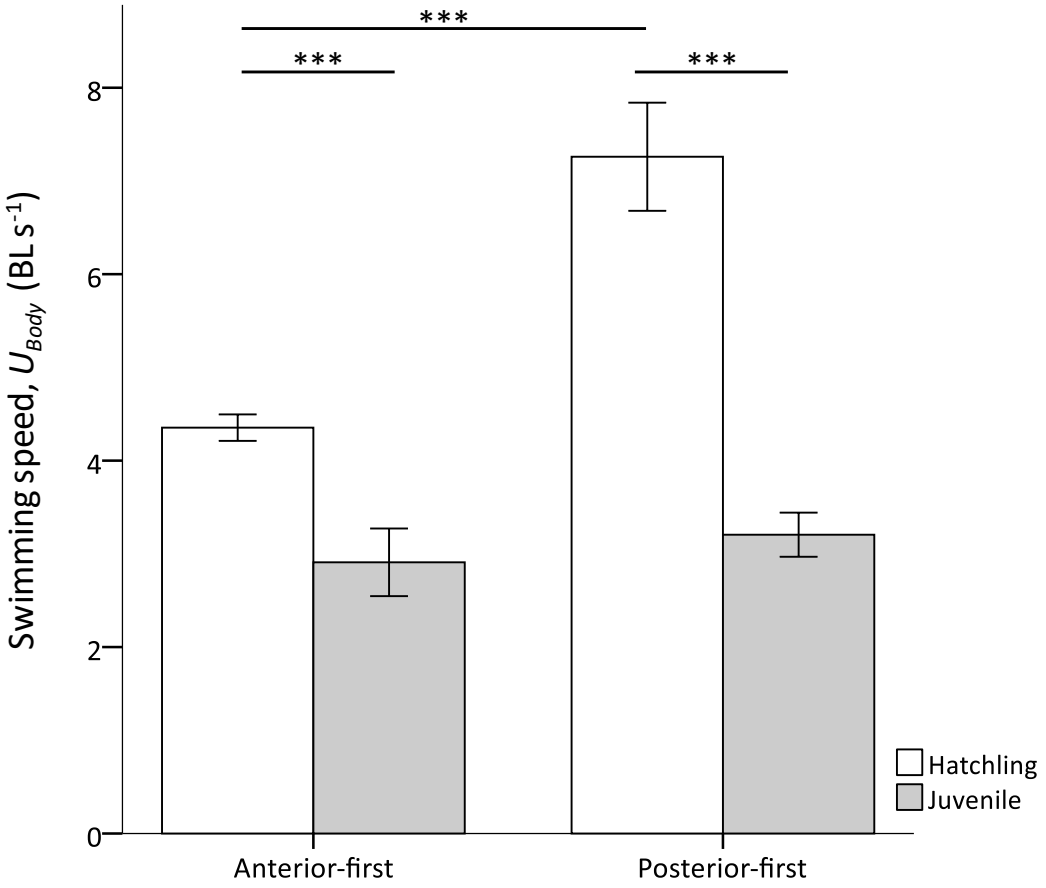

Figure 16. The mean swimming speed of hatchling and juvenile cuttlefish swimming anteriorly or posteriorly. Significant differences are indicated by *, error bars represent ± sem.**

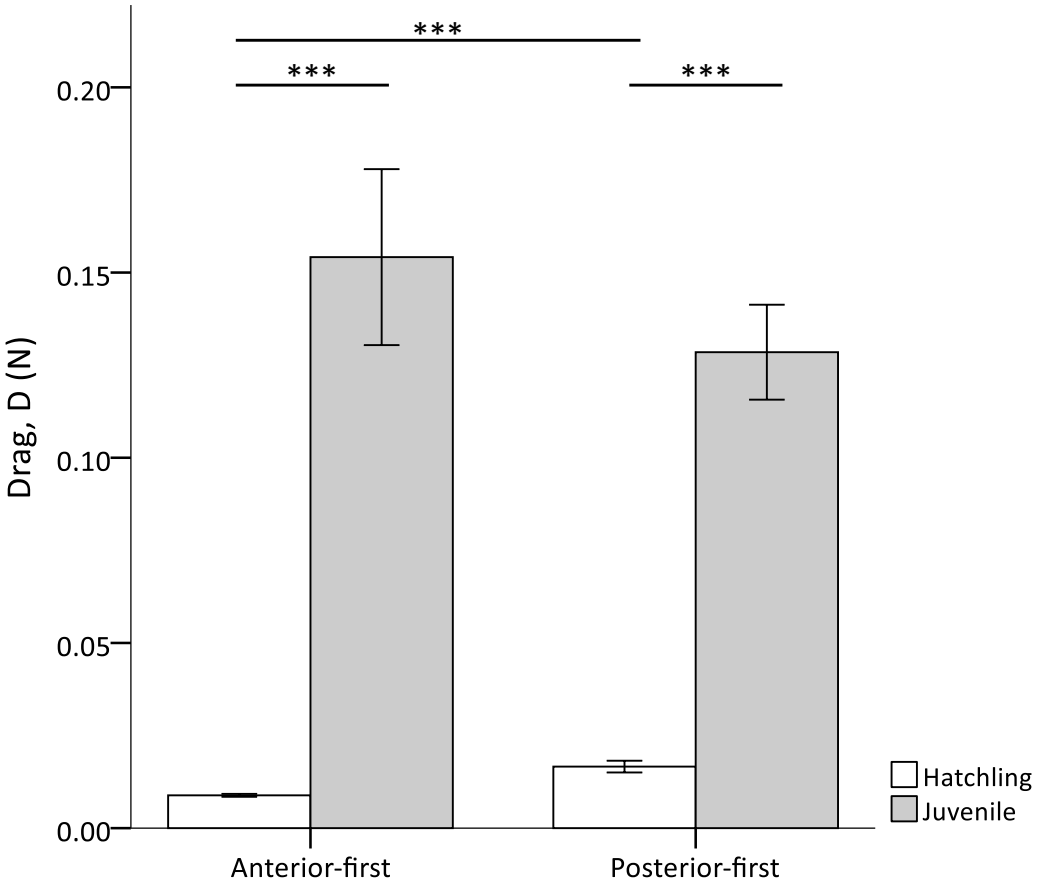

Figure 17. The estimated mean drag forces experienced by juvenile and hatchling cuttlefish during anterior- or posterior-first swimming. Estimates assume a drag coefficient of 0.47, this likely differs in cuttlefish, and may differ between the two swimming orientations. Significant differences are indicated by *, error bars represent ± sem.**

To further assess the kinematics of swimming cuttlefish, a subsample of sequences obtained from juvenile animals were used (n = 10). These revealed the mean duty cycle (the proportion of the swimming cycle made up of the power stroke) was 0.52 ± 0.25 (0.23 – 0.66), with the mantle contraction period lasting 0.44 ± 0.32 s (0.16 - 1.13 s; defined as the period over which a jet was being produced), and mantle refill lasting 0.39 ± 0.22 s (0.11 - 0.86 s; assumed to be the period between jet events). As a result of the measuring methodology differentiation between refill and relaxation was not possible. The duty cycle showed minor differences between swim orientations, with duty cycles associated with anterior-first swimming being somewhat higher, and more variable (0.49 ± 0.16; 0.23 – 0.66), than animals swimming posterior-first (0.40 ± 0.06;

0.28 – 0.47), the duty cycle did not differ significantly between swim orientations (X^2 1.92, df 1, p 0.166). The speed of the animal fluctuated over the course of a swimming cycle, increasing during the mantle contraction period and decreasing during the relaxation, refilling phase (Figure 18).

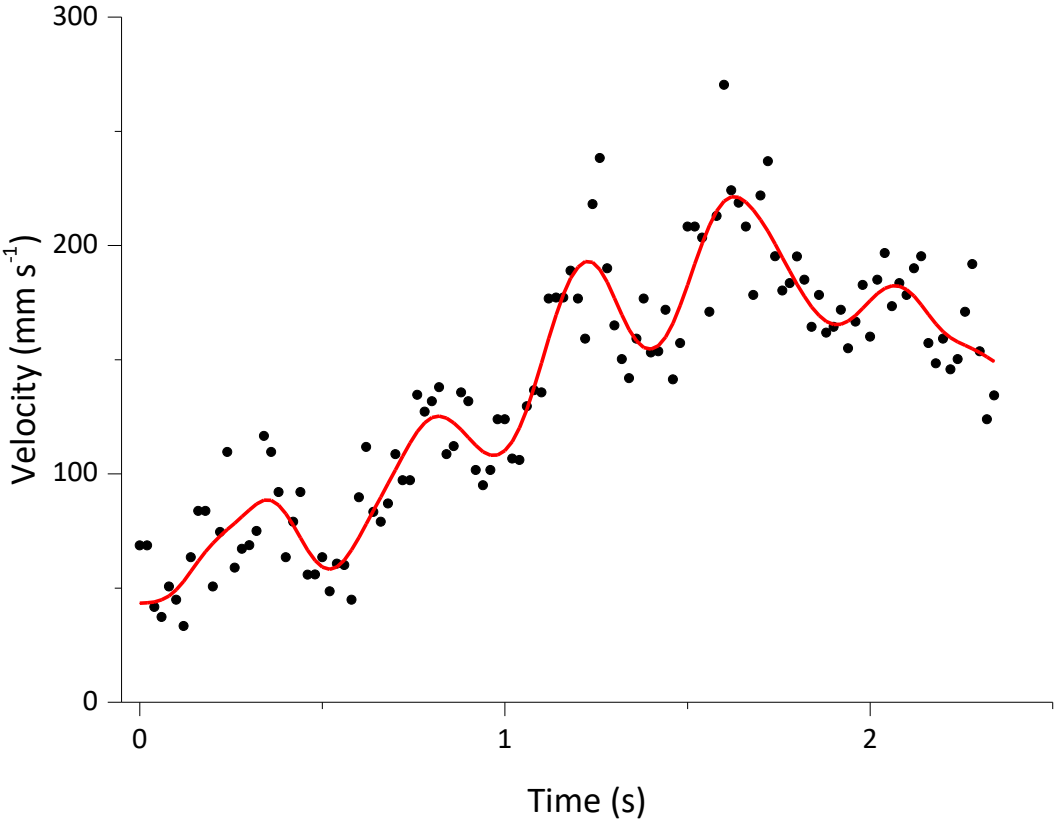

Figure 18. Example profile of changes in velocity of a swimming cuttlefish. Raw data is shown in black, and smoothed data in red. Noise within data were reduced smoothed following Bomphrey *et al.* (2009). Reductions in velocity likely represent the jet intake phases, while increases in velocity represent jet exhaust phases.

2.4.2 Wake structure

Two categories of jet were produced: the first consisted of a single isolated vortex while the second jets consisted of a leading jet vortex followed by a trailing jet (Figure 19). These two jet structures were termed jet mode I and II following previous nomenclature (Bartol *et al.*, 2009a). Both jet modes observed were seen in both hatchling and juvenile animals. However, the jets produced by hatchlings were dominated by jet mode I (95.34% were jet mode I and 4.66% jet mode II). Whereas juveniles utilised both jet modes (42.31% jet mode I and 57.69% jet mode II).

The rarity of jets of jet mode II in hatchlings precluded analysis of differences in jet modes for this size class, therefore all comparisons between jet modes are for juvenile animals only. It was noted previously that swimming orientation may impact aspects of locomotion. Prior to any analyses upon wake structure, the impact of swimming orientation upon jet modes was analysed: swimming orientation and jet mode use appear to be unconnected (X^2 1.668, df 1, p 0.197; Table 2), further analysis to ascertain if swimming orientation impacted any other aspects of locomotion revealed swimming orientation did not significantly impact thrust (X^2 0.023, df 1, p 0.879), swimming speed (X^2 0.091, df 1, p 0.763), jet cycle frequency (X^2 1.382, df 1, p 0.24), whole cycle propulsive efficiency (X^2 0.102, df 1, p 0.75), drag (X^2 0.923, df 1, p 0.334), or slip (X^2 0.138, df 1, p 0.71) in juvenile animals (see Table 1). The average L_j/D_j for juvenile animals was 4.22 ± 0.37; when divided by jet mode, it was found that the L_j/D_j of jet mode I (3.69 ± 0.28) was not significantly lower than in jet mode II (5.31 ± 0.28; X^2: 8.87, df 1, p 0.003). Jet modes had no significant affects upon thrust (X^2 1.968, df 1, p 0.161), whole cycle propulsive efficiency (X^2 1.60, df 1, p 0.689), swimming speed (X^2 2.505, df 1, p 0.114), cycle frequency (X^2 2.504, df 1, p 0.114), drag (X^2 0.724, df 1, p 0.395) or slip (X^2 0.415, df 1, p 0.519).

Table 2. Differences in L_j/D_j of juvenile cuttlefish swimming either anterior- or posterior-first. Values are mean ± sd. L_j is the jet length and D_j is the jet diameter.

	Anterior-first	Posterior-first
Jet mode I	3.63 ± 1.85	3.64 ± 1.22
Jet mode II	5.77 ± 2.09	5.55 ± 3.05

Most differences observed were between the two age classes rather than as a result of the two observed jet modes. Using standardised measures of jet velocity and body velocity, smaller animals were significantly faster swimmers than larger animals (X^2: 13.846, df 1, p <0.001).

The jets of cuttlefish showed no relationship between swimming speed and jet angle (X^2 0.299, df 1, p 0.585; Figure 20). Cycle frequency did however show a positive correlation with swimming speed in hatchlings (Anterior-first: *F* 24.69, df 1, p <0.001; Posterior-first: *F* 19.8, df 1, p <0.001; Figure 21), this relationship was not seen in juvenile cuttlefish (Anterior-first: *F* 0.792, df 1, p 0.395; Posterior-first: *F* 7.262; df 1, p 0.01; Figure 21).

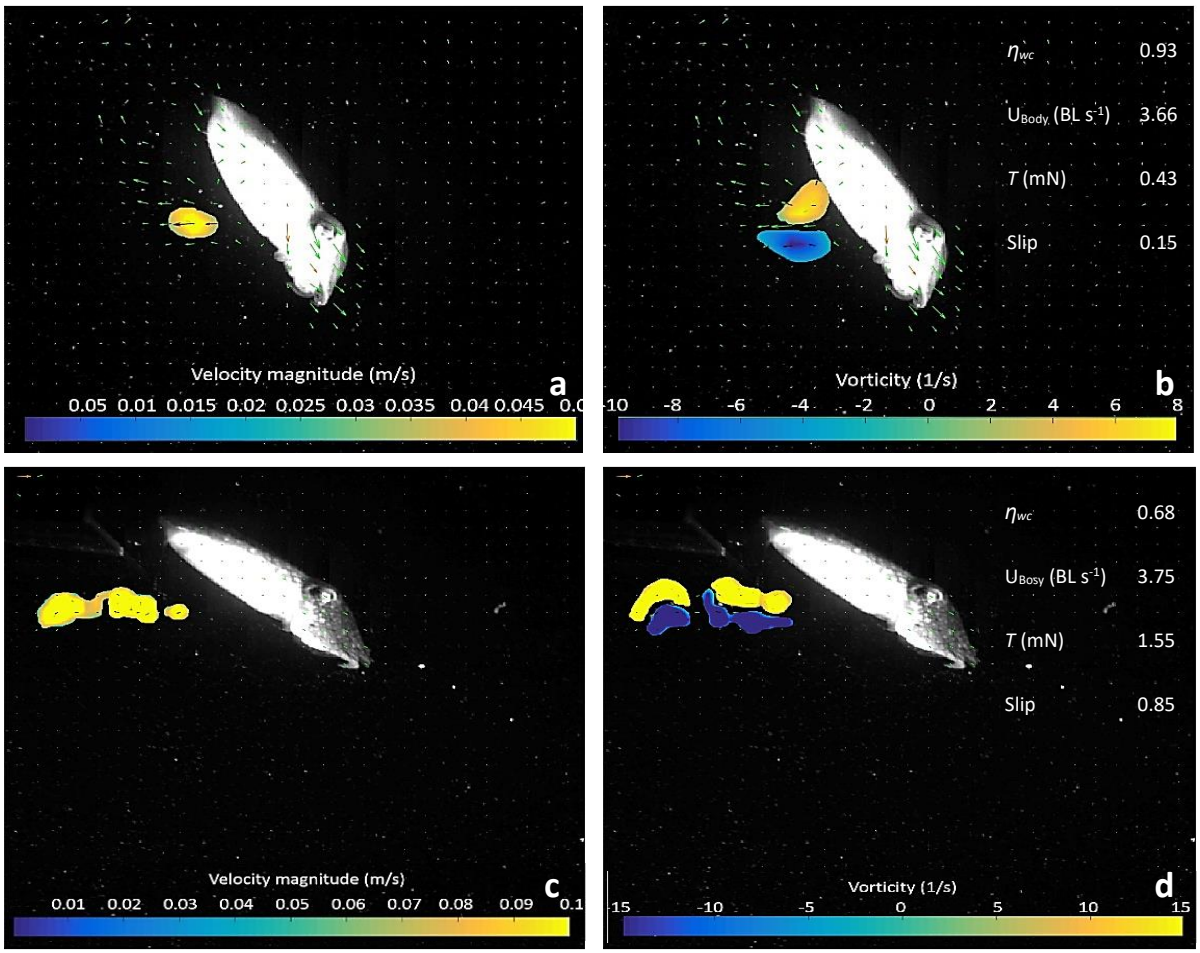

Figure 19. Comparisons of instantaneous flow and vorticity between jet modes I (a, b) and II (c, d) . Both animals are swimming in the anterior-first orientation, examples used are for illustrative purposes only to enable differences in wake structures to be visualized. The difference in the scale bars (and associated factors) between the examples is not representative of the data as a whole where jet velocity and vorticity were broadly similar between jet modes . Note the fluid is rolled into an isolated vortex ring during mode I jets (a), while this is more elongate during mode II jets (c). The red and blue regions on vorticity plots represent clockwise and counterclockwise rotation of water.

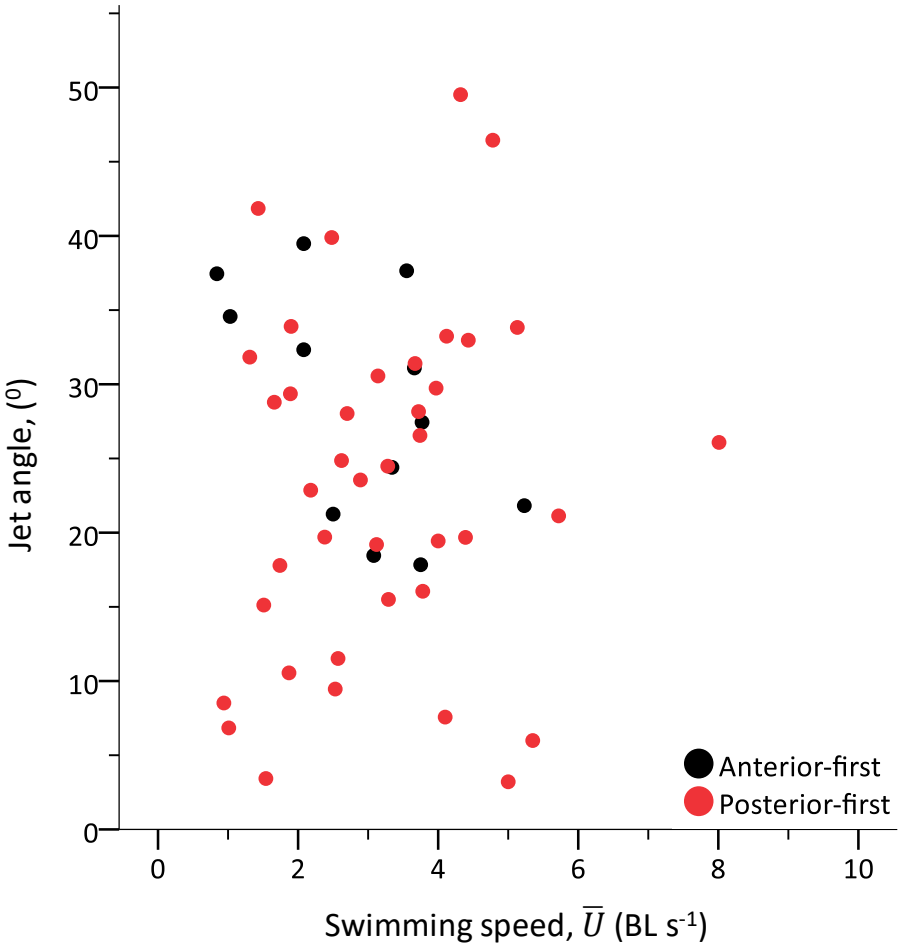

Figure 20. The relationship between relative swimming speed and jet angle of juvenile cuttlefish. Swim orientation is highlighted in black (anterior-first) or red (posterior-first).

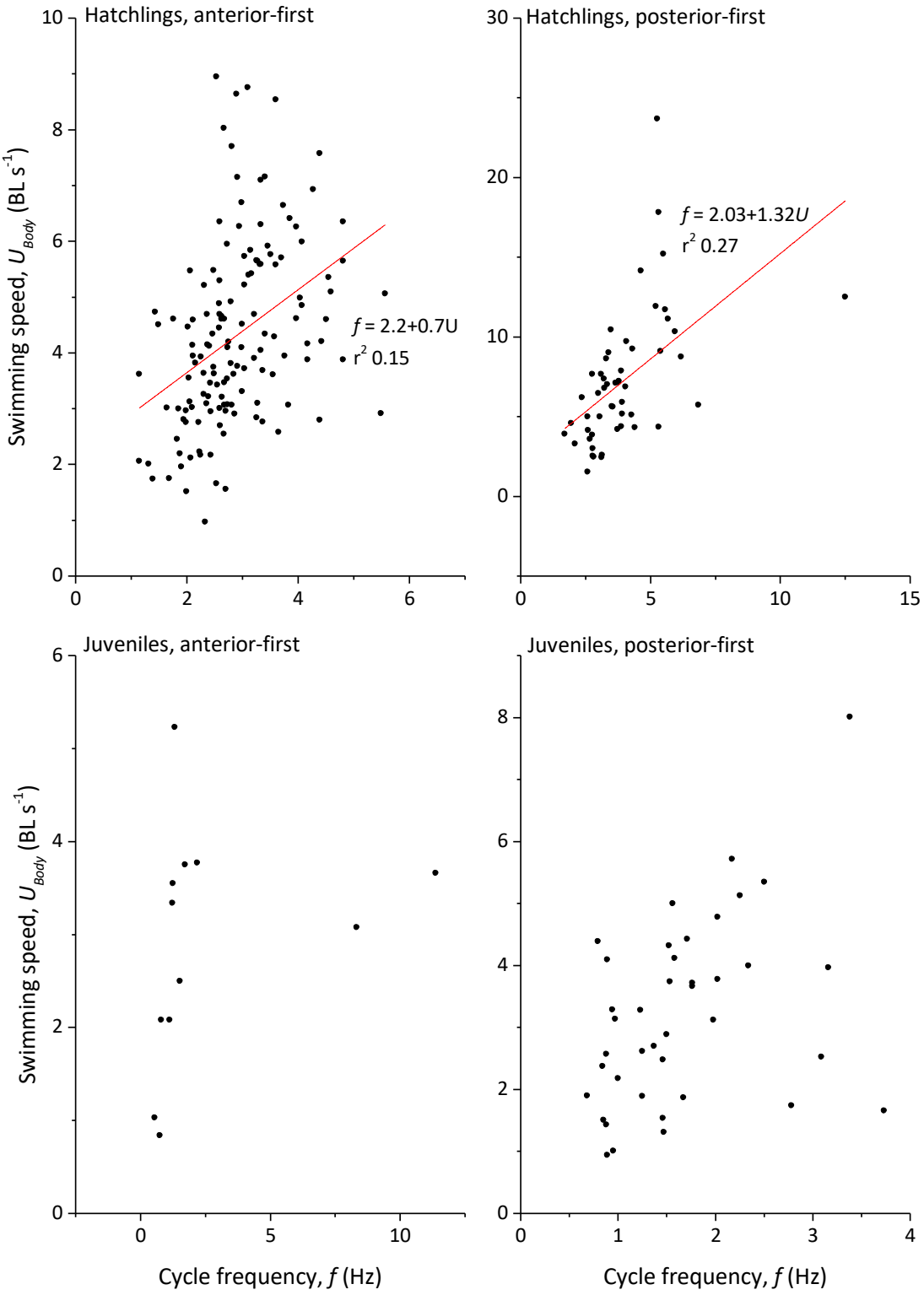

Figure 21. Relationship between cycle frequency and animal swimming speed.

Data are divided between animal age and swimming orientation. Swimming speed and cycle frequency interacted in hatchlings swimming in either orientation.

2.4.3 Whole cycle propulsive efficiency

Whole cycle propulsive efficiency and animal swim velocity showed a significant exponential relationships (Table 3; Figure 22), with propulsive efficiency increasing rapidly to ~5BL/s before reaching a plateau. This relationship was largely similar across age groups and swim orientations, with hatchling anterior-first swimming ranging between 0.44-0.99, posterior-first swimming ranging between 0.59-0.99, while juvenile whole cycle efficiency ranged between 0.50-0.96 during anterior-first swimming and 0.23-0.96 during posterior-first swimming (Table 3; Figure 22). Despite the similarities in range and peak efficiencies, the mean propulsive efficiency was significantly higher in hatchlings than juveniles (X^2 24.944, df 1, p <0.001), swim orientation was noted to only have minor (insignificant) effects (X^2 0.398, df 1, p 0.528) upon model parameters, and was therefore removed from analyses. Analysis upon the affects of swim orientation alone revealed propulsive efficiency was unaffected by swim orientation (X^2 0.086, df 1, p 0.769). There was no significant difference in whole cycle propulsive efficiency between the two jet modes (X^2 0.177, df 1, p 0.674), however cycle frequency showed a strong relationship with swimming speed (Figure 21). Slip, the inverse of propulsive efficiency, was significantly lower in hatchlings than juveniles (X^2: 21.915, df 1, p <0.001) and showed a strong negative relationship with swimming speed across the two age classes (Table 3).

2.4.4 Allometric scaling of cuttlefish swimming

Where significant differences were observed between the mean values for hatchling and juvenile locomotive performance (η_{wc}, U_{Body}, Re, f; see sections 2.4.1 and 2.4.3) scaling relationships with respect to mantle length were determined. This revealed cycle frequency, propulsive efficiency and swimming speed did not strongly scale with increasing mantle length (Figure 23; Table 4; Table 5), while Reynolds numbers increased with increased mantle length (Figure 23; Table 4), particularly in hatchling animals (Table 5).

Table 3. Regression results for selected parameters. Regression type selected based upon best-fit for data. U_{Body} is the swimming speed of animals in body lengths per second, η_{wc} is the whole cycle propulsive efficiency, L_j/D_j is the ratio of jet length (L_j) and jet diameter (D_j), and S represents slip.

Comparison	Regression type	F	P	R^2	Equation
U_{Body} on η_{wc}	I	166.573	<0.001*	0.512	$\eta = 0.978 + -0.465 \div U_{Body}$
U_{Body} on η_{wc} (hatchlings)	L	180.126	<0.001*	0.487	$\eta = \exp^{(-0.001 + -0.550 \div U_{Body})}$
U_{Body} on η_{wc} (juveniles)	L	39.609	<0.001*	0.442	$\eta = \exp^{(-0.022 + -0.721 \div U_{Body})}$
U_{Body} on S	I	180.086	<0.001*	0.531	$S = -0.119 + 1.773 \div U_{Body}$
U_{Body} on S (hatchlings)	I	77.272	<0.001*	0.419	$S = 0.014 + 0.98 \div U_{Body}$
U_{Body} on S (juveniles)	I	48.151	<0.001*	0.491	$S = -0.033 + 1.884 \div U_{Body}$

L= Logistic regression; I= inverse regression, d.f = 1, * denotes significant relationships.

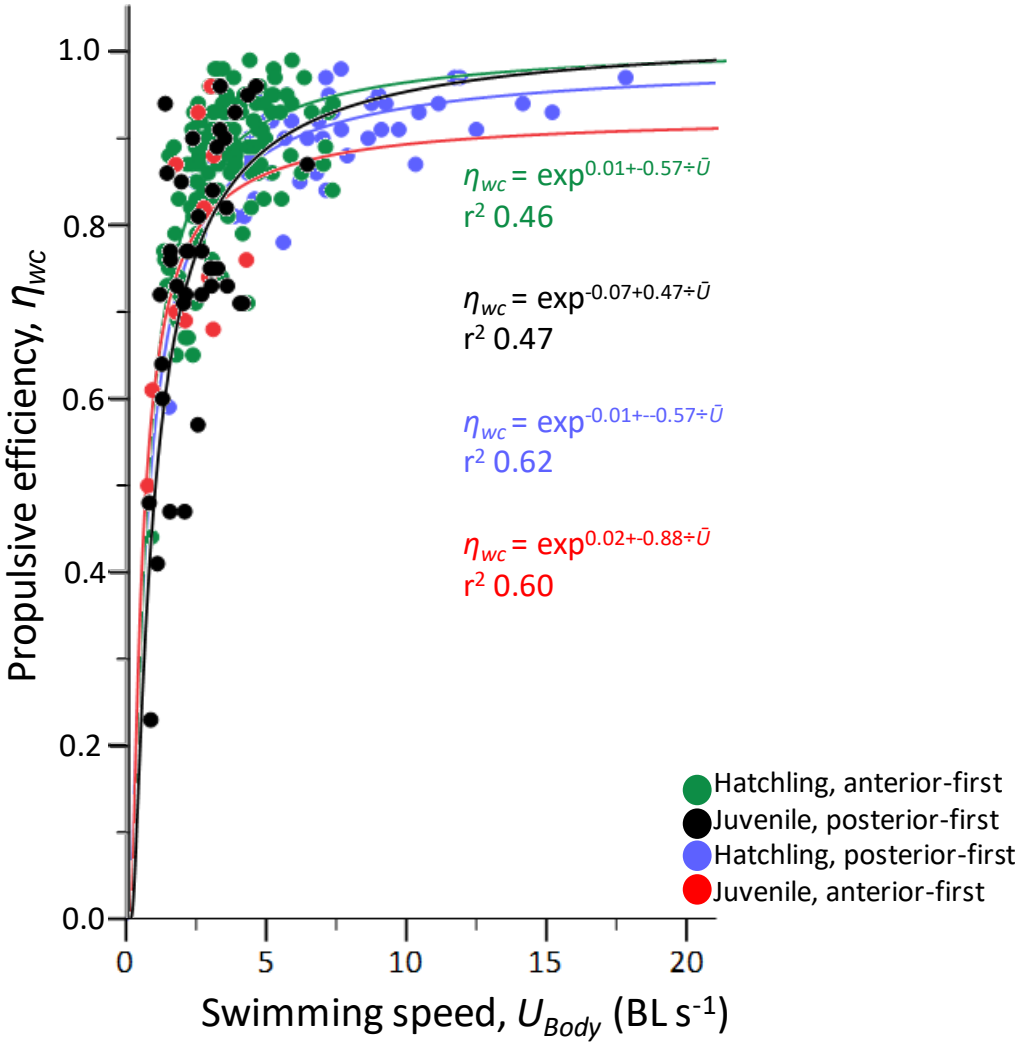

Figure 22. Relationship between animal swimming speed and propulsive efficiency in hatchling and juvenile cuttlefish. Relationships are fit using a logistic regressions ($y=\exp^{a+b\div x}$), model selection is based upon best fit as denoted through r^2 values.

Table 4. Allometric scaling relationships of swimming parameters with respect to mantle length of cuttlefish. Significant relationships are highlighted in bold.

Relationship	a	b (± sem)	r^2	p
f	3.25	-0.46 ± 0.1	0.11	NS
η_{wc}	2.65	-0.13 ± 0.02	0.15	NS
U_{Body}	5.16	-0.38 ± 0.11	0.06	NS
Re	**489**	**1.48 ± 0.08**	**0.64**	**<0.001**

Table 5. Allometric scaling relationships of swimming parameters with respect to mantle length of hatchling and juvenile cuttlefish. Significant relationships are highlighted in bold.

	Hatchling				Juvenile			
	a	***b (± sem)***	***r^2***	***p***	***a***	***b (± sem)***	***r^2***	***p***
f	3.19	0.08 ± 0.28	0.005	NS	0.82	0.78 ± 0.95	0.006	NS
η_{wc}	0.87	0.17 ± 0.06	0.031	NS	0.52	0.35 ± 0.2	0.04	NS
U_{Body}	4.9	0.8 ± 0.41	0.014	NS	4.26	-0.29 ± 0.46	0.01	NS
Re	**428**	**3.04 ± 0.46**	**0.2**	**<0.001**	518	1.42 ± 0.48	0.15	NS

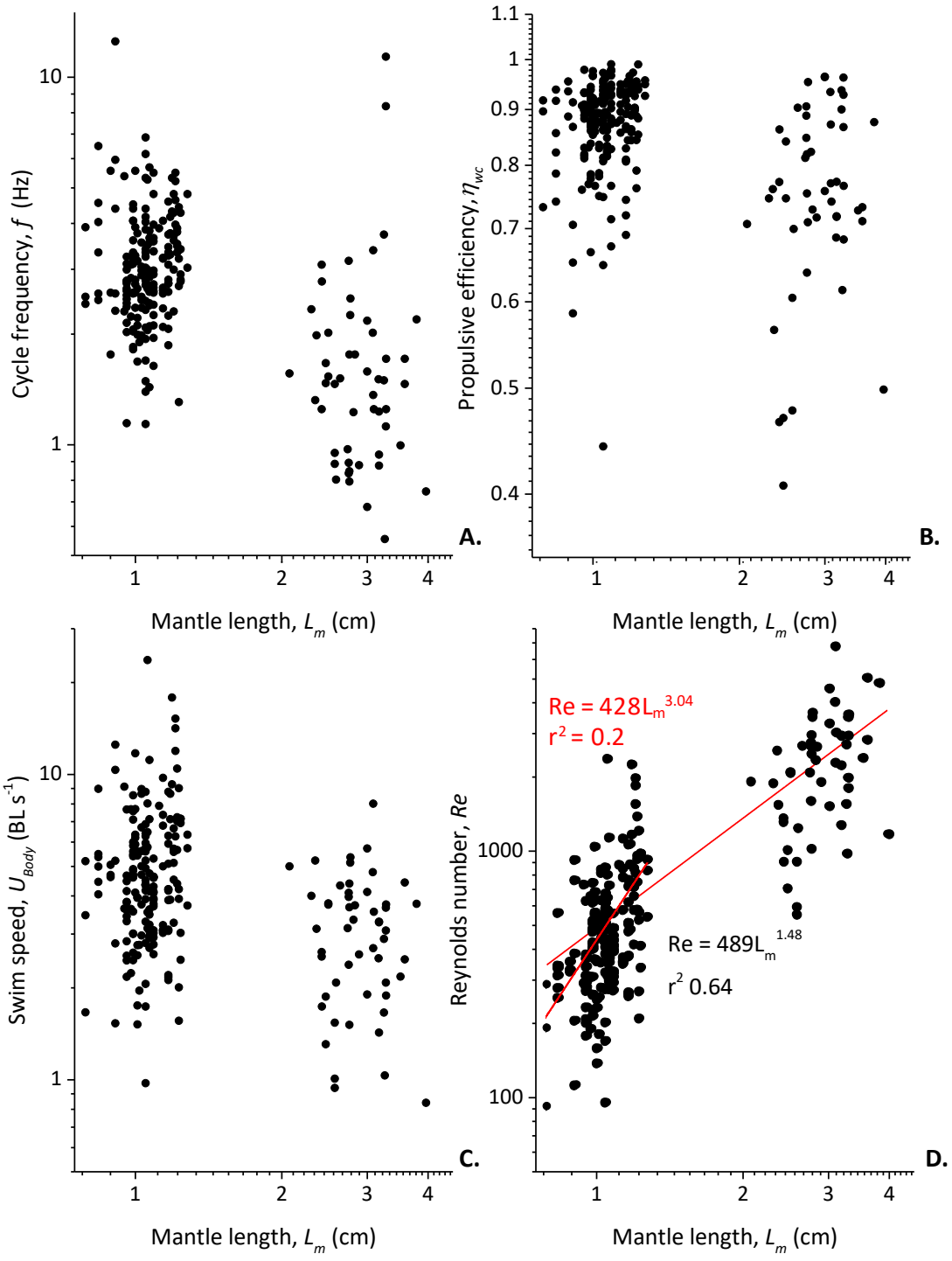

Figure 23. Allometric relationships between mantle length and selected swimming parameters. *f*, η_{wc} and $\overline{U}$ all declined with increased L_m, but no relationships were significant. *Re* increased with L_m, this occurred within hatchlings (line equation displayed in red) and overall (line equation displayed in black

2.5 Discussion

The jet propulsion system of cuttlefish plays a key role in many behaviours, such as predator evasion. Here it was found the propulsive efficiency was high (up to 99 %), with this declining as animals increased in length. This represents some of the highest measures of propulsive efficiency in cephalopods to date (Anderson *et al.*, 2001; Bartol *et al.*, 2008; Neil and Askew, 2018). Taken with measures of swimming performance and jet structure, this work builds upon our current knowledge of locomotion in cuttlefish (Helmer *et al.*, 2017; Jastrebsky *et al.*, 2016; Scatà *et al.*, 2017), through reporting quantitatively the structure of the wake and the propulsive efficiency of cuttlefish during jet propulsion swimming.

2.5.1 Wake structure

Cuttlefish were able to produce two jet types, defined by the differences in wake structure. These jet "modes" appear to exist on a continuum from isolated vortex rings through to trailing jets, this range of structures likely has hydrodynamic effects, with a key driver likely being the initial energy added to the fluid as it is ejected from the mantle cavity (Bartol *et al.*, 2009a; Linden and Turner, 2004). The existence of these two jet modes has been noted across various species which utilise jet propulsion swimming, such as brief squid (*L. brevis*) (Bartol *et al.*, 2009a), chambered nautilus (*N. pompilius*) (Neil, 2016; Neil and Askew, 2018), and king scallops (*Pecten maximus*) (Neil, 2016). Why these different wake structures occur is throught to be a result of how energy is added to the wake of an animal. Linden (2011) noted jet vortices created via a piston motor system would produce these two jet types as a result of how much, and how quickly, energy is added to the fluid. This occurs as a result of vortex rings being able to only accept a finite amount of energy before being "pinched-off", once this energy is added the remaining fluid forms an elongate, or trailing jet. These structural differences typically impact upon the propulsive efficiency of animals, where trailing jet vortices show increased turbulence, reducing the energy from the jet which is transferred into useful momentum (Deravi *et al.*, 2014; Linden and Turner, 2004). Experimental evidence of these impacts upon propulsive efficiency and thrust

have been noted by Bartol *et al.* (2009a), this study noted the use of different jet modes impacted the propulsive efficiency of brief squid (*L. brevis*), where jet mode I was significantly more efficient than jet mode II with mean values (± sd) of 69 ± 14 (36 – 91 %) when using jet mode I, and 59 ± 14 % (27 – 83 %) when using jet mode II (Bartol *et al.*, 2009a). While jet mode II was less efficient Bartol *et al.* (2009a) noted these jets created a greater amount of thrust. However, the structure of jets may also change throughout an animal's ontogeny as a result of changes in flow environment (Anderson and Grosenbaugh, 2005; Herschlag and Miller, 2011). This study noted jet mode did not have any significant effects upon aspects of locomotor performance such as swimming speed, cycle frequency, whole cycle propulsive efficiency or drag, suggesting cuttlefish are able to compensate for the differences in jet modes observed in brief squid in some way. It should however be noted the drag coefficient used in the calculation of drag here unlikely matches the true drag coefficient of cuttlefish, with this likely differing between swimming orientations, Tabatabaei *et al.* (2015) estimated the drag coefficient of squid swimming posterior-first would be ~0.004, though it is expected anterior-first swimming will come with increased drag. However, it was noted newly emerged cuttlefish used jet mode I in excess of 90% of the time, with jet mode II becoming increasingly common as animals increased in size. Bartol *et al.* (2009a) noted a similar pattern during the ontogeny of brief squid (*L. brevis*), where animals with mantle lengths <5 cm showed a greater reliance upon jet mode I, with reliance upon jet mode II increasing through ontogeny. This pattern seems to be in agreement with the findings of Andersson and Grosenbaugh (2005), where adult longfin squid (*D. pealeii*) produce elongate jets and never pulsed vortex rings, while longfin squid hatchlings (Bartol *et al.*, 2009b), and juvenile brief squid (*L. brevis*) (Bartol *et al.*, 2009a) produce the two jet modes observed in juvenile cuttlefish. These studies seem to suggest animals may transition from using jet mode I, to an intermediate stage before jets become more elongate. This seems to be supported when looking at the Reynolds numbers of animals and the flow environments inhabited. Newly emerged cuttlefish inhabit a laminar flow environment, within this environment momentum diffusion is high, meaning animals within this flow regime benefit from shedding isolated vortex rings. As animals increase in size they move further towards more turbulent flows, and with this the jets shed become more turbulent. As only newly hatched and juvenile animals were tested during this study this hypothesis

remains untested. However, previous studies with squid, which are morphologically similar to cuttlefish, have demonstrated this, suggesting a similar strategy may be employed by cuttlefish.

The differential use of jet modes, and flow environments seems to have enabled hatchling cuttlefish to move with increased speed relative to larger animals. Smaller animals generally move with increased speed relative to their larger counterparts. This results from a variety of factors, ranging from the underlying metabolism and muscular mechanics to smaller animals perhaps needing increased speed as a result of increased predation pressures associated with small size (Hanlon and Messenger, 1988).

2.5.2 Propulsive efficiency

Whole cycle propulsive efficiency did not vary between the two jet modes. The lack of a difference between jet modes is somewhat surprising when considering previous work both with squid and mechanically generated jets, which has shown mode II jet structure increases drag, reducing efficiency and thrust (Bartol *et al.*, 2009a; Linden, 2011). The lack of differentiation between jet modes in cuttlefish suggests animals can compensate for the theoretical inefficiencies of mode II jets in some way. Previous work with *Nautilus* found that propulsive efficiency did not vary between the two jet modes (Neil and Askew, 2018). However, propulsive efficiency did affect locomotor performance in cuttlefish, with swimming speed increasing with increasing propulsive efficiency, across all swimming orientations. It was also found that swimming orientation had a greater impact on the swimming speed of newly hatchled animals than jet mode. This relationship was also noted by Bartol *et al.* (2001; 2009a), where propulsive efficiency increased with increased swimming speed in brief squid (*L. brevis*) across both swimming orientations, the jet propulsion swimming of *Nautilus* showed a similar situation, where, despite the average speed being higher during posterior-first swimming compared to anterior-first swimming, whole cycle propulsive efficiency remained similar across both both orientations (Neil, 2016; Neil and Askew, 2018). This difference between swimming orientation and swimming speed likely arises due to siphon bending during anterior-first swimming where the siphon is bent back on itself,

resulting in turbulence within the fluid flowing through it, impacting upon the available energy which can be fed into the jet itself (Keulegan and Beij, 1937; Vogel, 1994). As well as this, animals swimming posterior-first may have a lower frontal area and therefore lower drag when the siphon is aligned parallel to the body axis rather than when the siphon is bent during anterior-first swimming. These differences in swimming speed may also relate to the different behaviours exhibited when animals swim either anteriorally or posterially. Anterior-first swimming is used during exploratory behaviours and are associated with a more saccadic movement strategy, whereas posterior-first swimming favours unidirectional speed, suggesting that this mode may be more important in escaping potential threats such as predators or conspecific rivals (Helmer *et al.*, 2017). These differences in propulsive efficiencies between swimming orientations may also be explained by the differences in Strouhal numbers (*St*). Taylor *et al.* 2003 suggested animals maximise their propulsive efficiency over a narrow range of *St* (between 0.2 and 0.4), while Eloy 2012 further modelled this noting a slightly larger range (between ~0.17 and 0.65). This seems to suggest cuttlefish are maximising their propulsive efficiency in terms of *St*. The decline in *St* noted here between hatchling and juvenile animals (see Table 1) seems to be a common feature as animals increase in size, where larger animals see an increase in body length coupled with a decrease in cycle frequency (Eloy, 2012; Taylor *et al.*, 2003).

2.5.3 Scaling of animal swimming mechanics and hydrodynamics

As cuttlefish increase in size, the mean swimming speed and the jet cycle frequencies decline. Despite this, jet cycle frequency and relative swimming speed did not show strong allometric scaling (scaling as $L_m^{-0.46}$ and $L_m^{-0.38}$ respectively). This is perhaps surprising given the trend towards decreasing cycle frequency seen elsewhere, where work has noted the tailbeat frequency in fishes and marine mammals, stride frequency in terrestrial organisms, wingbeat frequency in vertebrates and insects, and foot wave cycle frequency in molluscs (Heglund and Taylor, 1988; Hemmert and Baltzley, 2016; Nudds *et al.*, 2004; Quillin, 1999; Unwin and Corbet, 1984) all decline with increased body length. Watanabe *et al.* (2012) compiled the swim parameters of a 23 different fish species (11 teleosts and 12 elasmobranches). Analysis of these data revealed

tailbeat frequency declined with increased body length (L_b) as $L_b^{-0.55}$. Species-specific comparisons reveal tailbeat frequency scales as $L_b^{-0.59}$ in rainbow trout (*O. mykiss*) (Webb *et al.*, 1984), $L_b^{-0.13}$ in dace (*Leuciscus leuciscus*) (Bainbridge, 1958), $L_b^{-0.47}$ in goldfish (*Carassius auratus*) (Bainbridge, 1958), $L_b^{-0.12}$ in marsh frog tadpoles (*Limnodynastes peronii*) (Wilson and Franklin, 2000) and $L_b^{-0.22}$ in yellowbelly rockcod (*Notothenia neglecta*) (Archer and Johnston, 1989), while wing stroke cycle frequency scales as $L_b^{-0.86}$ among penguin species (Sato *et al.*, 2010). These scaling exponents show the same general trend as seen with cuttlefish, where the frequency with which locomotory events, be those jets, tailbeats or otherwise, decrease with increased body length. While similarities were noted in the scaling of cycle frequency and tailbeat frequency, the scaling of swimmng speed was far less pronounced in cuttlefish, the data compiled by Watanabe *et al.* (2012) suggested swimming speed (in BL s^{-1}) scaled as $L_b^{-0.80}$ in fishes, while swimming speed scaled as $L_b^{-0.62}$ in diving seabirds (Watanabe *et al.*, 2011), $L_b^{-0.73}$ in pinnipeds (Watanabe *et al.*, 2011), $L_b^{-0.71}$ in whales (Watanabe *et al.*, 2011), $L_b^{-0.75}$ in penguins (Sato *et al.*, 2010), $L_b^{1.34}$ in marsh frog tadpoles (*L. peronii*) (Wilson and Franklin, 2000) and $L_b^{-0.34}$ in yellowbelly rockcod (*N. neglecta*) (Archer and Johnston, 1989). Comparisons with other jet propulsion swimmers reveals swimming speed scales as $L_m^{-0.58}$ in opalescent inshore squid (*Doryteuthis opalescens*) paralarvae (Vidal *et al.*, 2018). These scaling exponents reported among other lineages suggest swimming speed scales less dramatically in cuttlefish than in other lineages. Such differences may relate to the larger size range of animals used, as well as the different flow environments and growth dynamics seen among animals.

The observed pattern of declining jet, tailbeat or wingbeat frequency with increased body size seen across lineages is thought to result from a variety of factors. Gazzola *et al.* (2014) noted the flow regime of aquatic animals plays a key role in determining locomotor performance, where the relative swimming speed of an animal scaled as $Re^{-0.25}$ (Gazzola *et al.*, 2014). While the flow environment may explain a proportion of the observed changes in swimming speeds among animals, morphological, physiological and behavioural aspects of animal locomotion are also of key importance. Hill (1950) provided some of the first insight into the scaling of animal locomotion. Hill (1950) proposed animal stride frequency would scale with mass as

$m_b^{-0.33}$. Niklas (1994) provided a cross-species analysis investigating how body mass scales with body length, this revealed mass scaled as $L_b^{2.95}$ (Niklas, 1994), this suggests stride frequency should scale with body length as $L_b^{-0.98}$ if Hill's geometric similarity model holds true, while elastic similarity models suggest a scaling exponent of $L_b^{-0.35}$ (Quillin, 1998), and stress similarity models predict stride frequency sclaes as L_b^0 (Quillin, 1998). These data suggest tailbeat, wingbeat and jet cycle frequencies fall between these extremes, with animals such as dace (*L. leuciscus*) scaling in a manner more closely aligned to stress similarity models, penguin wingbeat frequencies scaled more closely to geometric similarity models. Interestingly, the majority of fishes and cuttlefish seemed to fall somewhere between the predictions of the elastic and geometric similarity models. Geometric similarity models predict animals maintain geometry throughout growth, while elastic similarity models suggest animals increase diameter more rapidly than length. The observation here of animals falling between these two models is perhaps unsurprising when considering animal growth, where many animals do not grow uniformly, with differences in the growth of locomotory musculature or structures; indeed Trueman and Packard (1968) note larger jet-propelled organisms benefit from increased numbers of muscle fibres and a larger mantle cavity, this increase in mantle volume is seen in cuttlefish not only as a result of growth, but also as a reduction in the relative area occupied by the cuttlebone (Nixon and Mangold, 1998). Increased intramantle area, and muscle volume enables animals to eject more water per jet event, and create higher velocity jet vorticies (Trueman and Packard, 1968).

The changes in propulsive efficiency noted to occur from hatchling to juvenile stages (where a significant decline was seen), likely relates to the differential flow regimes encountered by the two age groups (Vogel, 1994). As noted previously, Reynold's numbers showed strong positive scaling with mantle length, when looking at these numbers, it appears hatchling animals inhabit a laminar flow environment. These flow environments enhance locomotion through the production of isolated jet vortices as a result of reduced drag and frictional forces. The larger animals used here inhabit the transitional zone between laminar flow and turbulent flows, as a result drag forces are increased upon animals, which may explain the lower propulsive efficiencies seen here (Muller and van Leeuwen, 2006; Ngo and McHenry, 2014). This transition between

flow regimes may also, in part, explain the the differences in jet structure, where more turbulent flows are associated with longer, trailing jets, such a situation is seen with brief squid (*L. brevis*) where animals at intermediate sizes (3 – 9 cm) produce the two jet modes observed in cuttefish (Bartol *et al.*, 2009a) with mode I jets being more efficient than mode II jets. As animals increase in size jet structure begins to breakdown leading to elongated emissions of fluid with waves of instability as seen in longfin squid (*D. pealeii*) of ~30 cm mantle length (Anderson and Grosenbaugh, 2005; Bartol *et al.*, 2009a). In the size range of animals investigated here, cuttlefish locomotion transitions from a high reliance upon mode I jets to incorporating mode II jets into their locomototion with increased size. It is unclear if the structure of jets produced by animals continues to alter as size increases, however, previous work with longfin squid (*D. pealeii*) has demonstrated the use of discrete jet vortices becomes increasingly rare as animals increase in size (Anderson and Grosenbaugh, 2005). These changes in jet structure and propulsive efficiency as animals increase in size may be compensated for by changes in locomotion, where cuttlefish become increasingly reliant upon undulatory propulsion from the fins, which is generally thought to be more efficienct than jet propulsion swimming. The changes in jet structure noted here as animals progress through different flow regimes were also noted by Katija *et al.* (2015) in the jet propulsion swimming of clapper hydroid medusae (*Sarsia tubulosa*). This study noted that animals used three distinct jet modes as they increased in size; between *Re* 10 – 30 elongated isolated jet vortices were observed, at *Re* 30 – 100 jet structures analagous to those of jet mode I were produced, and when *Re* > 100 jet structures analagous to those of jet mode II are generated. These different jet structures and their strong association with Reynolds numbers (and thus flow regime) (Katija *et al.*, 2015), suggest the transitions observed in cuttlefish are equivalent to those seen in clapper hydroids and squid.

During jet propulsion swimming, the exhaust phase accounted for 52 % of the cycle, while the water intake phase was slightly shorter at 48 % of the cycle, these exhaust and intake phases were largely unaffected by swim orientation, where exhaust phases accounted for 49 % during anterior-first swimming and 40 % during posterior-first swimming. A similar duty factor was found in jet propulsion swimming in the chambered nautilus (52 % of the jet cycle period (Neil and Askew, 2018)), with similar

minor differences between anterior-first (50 % of the jet cycle period) and posterior-first swimming (52 % of the jet cycle period). This pattern did not appear to be true across all cephalopods with the duty factor of Boston squid (*Illex illecebrosus*) ranging between 39 and 43 % (Webber and O'Dor, 1986). Wider comparisons reveal the duty factor of king scallops (*P. maximus*) was somewhat lower than these cephalopod lineages at 36 % (Neil, 2016), while the duty factor of bell jellies (*Polyorchis penicillatus*) was substantially higher at 84 % (Demont and Gosline, 1988). The similarities between cuttlefish and nautilus seem to suggests the jet propulsor may be used in a similar manner by these two lineages, like cuttlefish, nautilus are neutrally buoyant, relying upon the production of jet vortices solely for locomotive purposes. More closely related squid species use jet propulsion for both locomotive purposes, the creation of dynamic lift, as well as being coupled with respiration, which may explain the slightly higher duty cycles of these animals (O'Dor, 2002; O'Dor and Webber, 1991; Webber and O'Dor, 1986). While jet propulsion is an important aspect of jet propulsion swimming in cephalopods, it must be noted that cuttlefish use this in conjunction with the fins which are on the perhipery of the mantle cavity. The degree to which cuttlefish use jet propulsion in conjunction with their fins was not explicitly measured here, with it being difficult to visualise fins and jets simultaneously. It was noted some fin movement was seen in sequences (a total of 5 sequences) where animals had moved out of the laser-light sheet and were swimming more slowly. This usually occurred as animals approached the bottom of tanks, perhaps suggesting a role in slowing animals, or in searching for a resting position. Russell and Steven (1930) noted the fins of common cuttlefish (*S. officinalis*) were heavily used during slower swimming, while the jet propulsive system also contributed, but with increasing speed the contribution of the fins became less important (Russell and Steven, 1930). Investigations into how the action of fins affects locomotion and propulsive efficiency have presented a mixed picture, where Stewart *et al.* 2010 noted the fins of brief squid (*L. brevis*) act to create lift, as well as leading to both increases and decreases in the propulsive efficiency of animal swimming (by up to ~10 %), with this interacting with the swimming speed, where the contribution of the fins seems to decrease with increased swimming speed, perhaps as a result of drag (Stewart *et al.*, 2010). These studies suggest the role of the fins can be significant, but seems to be largely speed-

specific, further work should aim to assess this, providing key information about the interactions of these locomotive systems, and how this impacts propulsive efficiency.

2.6 Summary

Through the course of this chapter the swimming mechanics and underlying hydrodynamics of cuttlefish jet propulsion swimming have been investigated. This has provided one of the first insights into the jet propulsion of these animals with the data upon swim kinematics noting a strong relationship between animal size and the speed at which they swim, and the frequency with which jets are produced. The detailed analysis conducted upon the duty cycles of these animals reveals these are very similar to the observations seen in other cephalopods, particular the nautilus. The wake structure of cuttlefish jet propulsion swimming consisted of two key jet types: termed jet mode I and II. These jet modes differed in structure, where jet mode I was characterised by having a single isolated jet while mode II consisted of a leading vortex followed by a more elongate jet structure. These different jet modes did not appear to impact the propulsive efficiency of animals; propulsive efficiency and swim speed seemed to be more heavily impacted by the swim orientation and age of animals. It was noted here the propulsive efficiency and swim speed were significantly higher in hatchling animals when compared to juveniles. These differences in efficiency and swim mechanics between hatchlings and juveniles may arise from the different flow environments inhabited by animals. The next chapter builds upon this one investigating the underlying muscle mechanics, this provides key information about how musculature functions, the work output and enables the transfer efficiency (proportion of mechanical work which results in useful movement) to be estimated.

Chapter 3. The mechanical properties of the cuttlefish jet locomotor muscle

3.1 Abstract

The European cuttlefish (*Sepia officinalis*) utilise the circular muscle surrounding the mantle cavity during jet propulsion swimming. To develop a greater insight into the locomotion of these animals, it is important to understand the underlying mechanical properties of this musculature, and how these properties change during ontogeny. The mechanical properties of a bundle of muscle fascicles were determined during isometric, isotonic and cyclic length changes *in vitro*, at two life stages: juveniles and adults. Under isometric conditions, the time to peak twitch and half relaxation times increased with increasing body size, scaling as $L_m^{0.28}$ and $L_m^{0.59}$ respectively. The maximum velocity of shortening (V_{max}) and power ratio was similar across the size range studied. During sinusoidal cyclical contractions, the optimum frequency for maximum net work and maximum net power declined from the juvenile to adult stages. Such similarities highlight the scaling of cephalopod mantle muscle may meet many of the assumptions of Hill's (1950) geometric similarity model, suggesting the contractile features of cuttlefish mantle muscle are uncoupled from animal size, with the absolute power available for burst swimming in cuttlefish increasing with increased body size.

3.2 Introduction

Active movement is essential to the survival of many animals, playing a role in key processes such as avoiding predation, finding mates, catching prey, and performing key lifetime events, such as migrations (Alexander, 1999; Seebacher and Walter, 2012). Locomotor performance is under selective pressure and is in part determined by muscle mechanical performance (Roberts *et al.*, 2011; Seebacher *et al.*, 2015), where

mechanical performance explains how effectively energy from the locomotory muscles, and elastic structures, is transferred into useful work on the environment (Roberts *et al.*, 2011). In order to create movement, muscle tissues require an input of metabolic energy. Metabolic rates have an upper limit, where energy must be spread across all processes, including locomotion and key processes, such as growth and reproduction (Fu *et al.*, 2018; Seebacher and Walter, 2012). This upper limit to metabolic processes places selective pressure on animals to minimise energy expenditure, ensuring all processes can continue; as such locomotive systems can become more refined, minimising energetic losses while maximising useful work (Rossi *et al.*, 2018; Seebacher and Walter, 2012). While locomotor refinement is favoured for many routine activities, responses involved in escape or other non-routine activities may instead maximise performance over the energetic costs of such processes (Askew and Marsh, 2002; Jackson and Dial, 2011; James and Johnston, 1998). This presents a key trade-off where animals maximise locomotory power over the energetic demands, with these energetic costs being outweighed by costs associated with predation or antagonistic interactions (Vanhooydonck *et al.*, 2014; Wilson and James, 2004; Wilson *et al.*, 2002).

As animals increase in size, muscle performance must scale accordingly to ensure animals can perform key behaviours, such as locomotion (Jackson and Dial, 2011; Seebacher and Walter, 2012). The muscle contraction frequencies of larger animals are generally slower than those of smaller individuals, and this is seen across taxa with larger animals showing lower stride (Heglund and Taylor, 1988; Heglund *et al.*, 1974), wingbeat (Nudds *et al.*, 2004; Unwin and Corbet, 1984) and tailbeat (Bainbridge, 1958; Videler and Wardle, 1992) frequencies than smaller animals. The mechanistic hypothesis proposed by Hill (1950) assumes muscular stress, strain and density are independent of body size with differences in power output resulting from the scaling of frequency (Hill, 1950; Jackson and Dial, 2011). This hypothesis highlights the understanding of how frequency scales is of key importance in understanding the scaling of power. In reducing the muscle operating frequency, animals are able to maintain muscular power throughout ontogeny. Hill (1950) predicted muscle contractile frequency, relative power and the relative maximum shortening velocity

(V_{max}) would scale with body mass as $M_b^{-0.333}$, $M_b^{0.333}$ and $M_b^{-0.333}$, where scaling is determined in relation to body length, these parameters scale somewhat differently as $L_b^{-0.982}$, $L_b^{0.982}$ and $L_b^{-0.982}$ respectively (Niklas, 1994). While these scaling models may be appropriate for many animals, Quillin (1999) highlighted animals with hydrostatic skeletons may not necessarily scale in the same manner as animals with more rigid skeletons, this results from geometric and static stress similarity models not being mutually exclusive for these skeletons. Such non-conformity to traditional models is thought to result from musculature within these systems acting as both a locomotive and skeletal element, where musculature provides the support needed for body walls, as well as acting to compress cavities for locomotive purposes (Quillin, 1999). These functional and skeletal roles likely impact the allometry of musculature, with muscle mass and density increasing with increased animal size, with this not necessarily following geometry as a result of conflicting structural requirements. This difference between the muscle mechanics of animals with hydrostatic skeletons and those with fixed endo- and exoskeletal systems has been demonstrated in earthworms (*Lumbricus terrestris*) where stride frequency scaled as $M_b^{-0.07}$, while stride length and crawl speed scaled as $M_b^{0.41}$ and $M_b^{0.33}$. These scaling exponents suggest earthworm locomotion does not wholly match the predictions of Hill's (1950) mechanistic hypothesis, with frequency appearing to more closely match the parameters of the elastic similarity models. Wider comparisons paint a mixed picture, with the wingbeat frequency of orchid bees (Euglossini) scaling with body mass as $M_b^{-0.347}$ (Casey *et al.*, 1985), while the shortening velocity of Atlantic cod (*Gadus morhua*) myotomal muscle scales with body length as $L_b^{-0.79}$. Elastic similarity models predict cycle frequency will scale as $M_b^{-0.12}$, while speed and stride lengths should scale as $M_b^{0.25}$ and $M_b^{0.37}$ (McMahon, 1973; Quillin, 1999). Quillin (1998) noted crawl speed seemed to be in agreement with stress similarity models in earthworms with speed scaling as $M_b^{0.40}$, stride lengths scaling $M_b^{0.40}$, and stride frequency as M_b^0. This presents a confused picture of scaling in this muscle type. However, Quillin (1999) concluded that the locomotion of earthworms met the assumptions of the mechanistic hypothesis, as earthworms maintain similar movement (in BL s^{-1}) patterns, where body wall strains were independent of body mass, suggesting these patterns are maintained through differences in activation frequency alone.

The structure and function of an animal's musculature is a result of its ecology as well as the underlying muscular systems on which selection can act. Soft-bodied animals, such as molluscs, annelids, and nematodes, lack the hard skeletons of vertebrates and arthropods, as a result musculature acts both structurally and as a locomotive element (Quillin, 1999; Yekutieli *et al.*, 2005). This obliquely striated muscle can accommodate large dimensional changes, and typically acts against fluid-filled body cavities (Chapman, 1958; Yekutieli *et al.*, 2005). However, this muscular system does not typically accommodate movements similar to those seen in animals with more rigid skeletal systems as a result of these animals lacking jointed appendages, this results in many molluscs, annelids and nematodes locomoting through crawling (Chapman, 1958; Denny, 1980; Quillin, 1999). During such movements the banana slug (*Ariolimax columbianus*) produces a series of muscular waves on the ventral surface of the foot, to aid in movement gastropod molluscs also produce pedal mucus. The energetic costs of operating such musculature is similar to that of vertebrate muscle, however the relative speed achieved by animals is much lower, while muscle operation is primarily anaerobic (Denny, 1980). Despite the dominance of locomotion through crawling associated with obliquely striated muscle, cephalopod molluscs utilise this muscle during jet locomotion swimming. Cephalopods exemplify the role co-evolution can play in refining a locomotor system, where the coleoid cephalopods (cuttlefish, octopus and squid) have developed complex behaviours and a refined jet propulsion system which is powered through the action of obliquely striated muscle (Chapter 1; Hanlon and Messenger, 1996; Kier and Thompson, 2003). The mantle muscle of the European cuttlefish is one such example of how cephalopods utilise this muscle type. The structure of decapodiform cephalopod mantle muscle has been described in detail by various authors (Figure 13; Kier and Schachat, 2008; Kier and Thompson, 2003; Shaffer and Kier, 2012), where fast and slow twitch fibres are in distinct layers, and seem to have distinct functions, with slow-twitch fibres involved in routine swimming and respiration, while fast-twitch fibres are primarily involved in escape responses (Bartol *et al.*, 2001; Kier and Schachat, 2008; Kier and Thompson, 2003). This structural organisation allows the mechanical properties of different muscle types to be explored in isolation. Despite this understanding of muscle structure, little work has addressed

ontogenetic scaling of obliquely striated muscle or investigated muscle performance during cyclical length changes that are used during swimming. Thompson *et al.* (2014) did however provide some insight into the scaling of this musculature, noting cephalopods lack the myosin isoforms seen in vertebrates, with force modulation by the obliquely-striated muscle of cephalopods resulting from variations in thick filament instead.

Current understanding of muscle function in cephalopods has focused upon isometric and isotonic contractile properties, and largely restricted to longfin (*Doryteuthis pealeii*) (Thompson *et al.*, 2010; Thompson *et al.*, 2008) and European common (*Alloteuthis subulata*) squid (Milligan *et al.*, 1997; Rogers *et al.*, 1997), with some more limited work on European common cuttlefish (*Sepia officinalis*) (Curtin *et al.*, 2000; Milligan *et al.*, 1997; Rogers *et al.*, 1997). This work noted cephalopod obliquely striated muscle behaves in much the same way as vertebrate cross striated muscle, with isometric stimulation resulting in both twitch and tetanic responses. This relative difference between twitch and tetanus force generation was less pronounced than typically reported in typical vertebrate musculature, e.g. twitch:tetanus ratio of longfin squid mantle muscle is 0.58 ± 0.03 (Thompson *et al.* 2010), compared to 0.12 ± 0.01 in mouse soleus muscle (Askew and Marsh, 1997). In inshore squid species, mantle muscle shows a force-velocity relationship typical of vertebrate skeletal muscle, with shortening velocity being inversely related to load (Milligan *et al.*, 1997; Thompson *et al.*, 2010). Despite this understanding of muscle function in squid, current understanding of how muscular function scales in cephalopods remains largely unexplored. Thompson *et al.* (2010) offered some limited insight into how muscle function scales in longfin squid (*D. pealeii*), noting the maximum velocity of muscle shortening (V_{max}) was substantially higher in paralarval squid than adult animals. In this chapter the mechanics of the central mitochondria poor (CMP) muscle fibres of the cuttlefish mantle and the scaling of performance between the juvenile and adult stages of development, were investigated.

The work presented in this chapter expands upon the current knowledge of cephalopod muscle function by investigating muscle performance during cyclical

contractions. These cyclic contractions are more representative of the way in which the muscle operates during swimming than either isometric or isotonic contractions, where cyclical contractions involve both muscle lengthening and shortening, whereas isotonic contractions typically only investigate muscle shortening; the inclusion of both the lengthening and shortening phases enables the work input to lengthen the muscle to be included in estimating muscular work. As well as this, this work builds upon current knowledge relating to the scaling of cephalopod musculature, and provides further insight into the isometric and isotonic properties of cuttlefish mantle musculature.

To summarise, this chapter uses the mantle muscle of the European cuttlefish to achieve two key aims: (i) provide an understanding of the ontogenetic scaling of obliquely striated muscle function, and (ii) investigate muscle performance under cyclical contractions. These aims were investigated through several hypotheses: (i) the isometric contractile properties will differ between adult and juvenile mantle muscle, with musculature expected to respond and relax more rapidly in juveniles than adults as a result of differences in thick filament length, (ii) shortening velocity is expected to negatively scale with muscular force, where more rapid muscle shortening limits the amount of crossbridges which can form, and thus the force produced by musculature; crossbridge formation and cycle frequency are expected to interact, with greater force produced at lower cycle frequencies as a result of increased time for crossbridges to form, (iii) maximum velocity of shortening will negatively scale with animal size as seen with other fast-twitch musculature. (iv) musculature will respond to cyclic contraction in a similar manner to striated muscle, (v) contractile frequency will impact muscular work and power, with the plateau expected to shift towards lower frequencies with increased animal size; (vi) optimal frequency for maximum power will match the jet cycle frequency in free-swimming animals. The results collected here also in conjunction with those collected in Chapter 2 enabled the calculation of the efficiency with which energy from musculature was transferred into useful momentum in whole animals.

3.3 Methods

3.3.1 Animals

3.3.1.1 Juvenile cuttlefish

European cuttlefish eggs were taken as by-catch upon fishing gear by RK Stride, Christchurch, Dorset, UK, during May 2016 in the English Channel. Eggs were housed in recirculating artificial saltwater systems (see section 3.3.1.3) at the University of Leeds at a temperature of 19 ± 1 °C as this temperature maximises development speed while avoiding premature hatching and malformation (Bouchaud, 1991). Once eggs begun hatchling temperature was gradually decreased to 15 ± 1 °C. Animals were fed twice daily using size-appropriate live foods: live enriched *Artemia salina* (Vitalis live food enrichment, World Feeds ltd, Thorne, Derbyshire, UK; Peregrine Livefoods, Magdalen Laver, Essex, UK), *Mysis* shrimp (*Mysis spp*.; Aquadip VOF, Oss, North Brabant, The Netherlands; Essex Marine Aquatics, Wickford, Essex, UK), and river shrimp (*Palaemon varians*; Aquatic Live fish foods, Woodford, London, UK). Cuttlefish were reared until a mantle length of 30 - 45 mm was reached in groups of 100 animals.

3.3.1.2 Adult cuttlefish

Cuttlefish were captured off the south coast of the UK (Poole Harbour, Poole, Dorset, UK) using Cuttlefish traps by JHC research during April 2016. Animals were maintained in recirculating artificial saltwater systems at the University of Leeds in size-matched groups of 3 to 5 animals. Facilities were maintained at a temperature of 11 ± 1 °C, matching the parameters of the site from which animals were taken. Animals were fed twice daily using langoustine (*Nephrops norvegicus*), tiger prawns (*Penaeus monodon*) or live shore crab (*Carcinus maenas*; Tacklebox mail order, Worthing, West Sussex, UK).

3.3.1.3 Animal housing facilities

Recirculating artificial saltwater facilities used to house all cuttlefish were maintained at a salinity of 32 ± 1 PSU (Cefas, 2012) using Aqua One Reef synthetic (Kong's (Aust.) Pty Ltd, Sydney, NSW, Australia) formulated in deionised water. Animals were housed in size-matched groups in 478.4, 357.9 and 288.8 litre (length × width × height; 1300 x 800 x 460; 910 x 690 x 570 and 890 x 590 x 550 mm) aquaria.

Water quality was monitored to ensure suitable ranges were maintained; temperature and salinity were monitored twice-daily; pH and nitrogenous compounds were monitored monthly. 25% water changes were carried out twice per week for tanks housing juveniles, and daily for adult tanks, 50% water changes took place in the event of animals inking. The maintained parameters for temperature and salinity fell within the natural range of animals in the English channel at the time eggs or animals were collected (10.8-16.7 °C; 31.89-34.49 PSU) (Cefas, 2012).

3.3.2 Muscle preparation

Contractile properties of mantle musculature were measured using a bundle of muscle fibres dissected from the central zone of the ventral mantle; this zone was approximately 40% of the mantle length, measured from the tip of the ventral mantle. Cuttlefish were euthanized in accordance with schedule 1 of the Animals in Scientific Procedures Act (1986); animals were anaesthetised in 3.5% magnesium chloride hexahydrate (VWR chemicals, Radnor, PN, USA; Flurochem ltd, Hadfield, Derbyshire, UK) prior to destruction of neuronal tissues (the brain, vertical and optical lobes) via pithing.

Measures of mantle length, and total length (defined as the length of the mantle + the distance to the beak), were taken using digital callipers or a 30 cm ruler. From this, the region of dissection was calculated and dissected out. Sections were further dissected

to select only the central zone of the muscle. Muscle dissections were carried out within chilled (11 °C) artificial seawater. A stainless steel ring was attached to each end of the muscle preparation using suture thread (2-0 USP, Black braided silk non-absorbable, non-sterile surgical suture, LOOK surgical specialities corporation, Reading, PA, USA). The muscle preparation was placed in a flow-through Perspex® chamber; one end was attached to a fixed mount and the other to the arm on an ergometer via the stainless steel rings (Aurora Scientific Dual-mode lever system model 300B-LR, Aurora Scientific Inc., Aurora, ON, Canada; Figure 24). The chamber was continually circulated with artificial seawater at 11 ± 0.5 °C saturated with 100% oxygen, artificial seawater was used rather than Ringer's solution as cuttlefish are continually immersed in seawater with poorly vascularised musculature (following Milligan *et al.* (1997)).

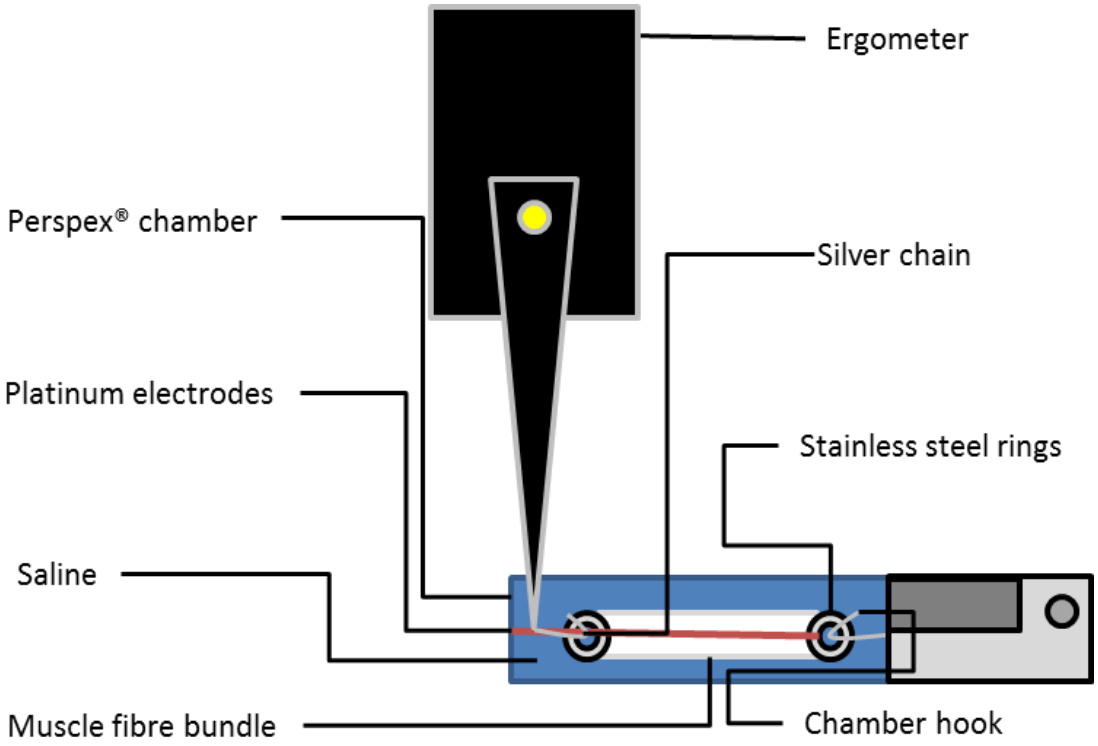

Figure 24. Schematic diagram showing dissected cuttlefish muscle bundle within the muscle rig setup. Muscle bundles were tied at both ends and stainless steel rings attached before one end was hooked onto the experimental chamber and the other to an ergometer. The chamber was circulated with artificial seawater and maintained at 11 ± 0.5 °C. Stimulation of muscle bundles was achieved via platinum electrodes.

3.3.3 Isometric contractile properties

Following dissection, muscle preparations were held at a constant length, and left for one hour to recover from the dissection process (following Olson and Marsh, 1993). The length of the muscle preparation was optimised for maximum active twitch force via a series of isometric twitches at different lengths (L_0). Muscle was allowed to rest for 3 minutes between successive twitch contractions. An isometric tetanic contraction was achieved using a 500 ms train of stimuli (pulse width 0.2 ms) delivered at a stimulation frequency of 50 Hz (following Milligan *et al.* 1997). Muscle preparations were given 5 minutes to rest between tetani to allow recovery. Peak twitch force (P_{tw}),

time to peak force (tP_{tw}), and time to half relaxation (RT_{50}) were recorded for the isometric twitch which yielded the highest force. Peak isometric tetanic force (P_0) was also recorded for each isometric tetanus. Twitch and tetanic stress profiles were smoothed using Fast Fourier Transformations with a low pass filter, cut-off frequencies were determined using an in-built algorithm in OriginPro which automatically selected an appropriate cut-off frequency, this process determines cut off frequencies as: $f_{cutoff} = \frac{1}{2n\Delta t}$, where Δt is time spacing between data points and n is the number of points. FFT filters were chosen to remove high-frequency noise present within data.

3.3.4 Isotonic contractile properties

3.3.4.1 The force-velocity relationship

In determining the force-velocity relationship, muscle bundles were subject to a series of after-loaded isotonic contractions at a stimulation frequency of 50 Hz. A control isometric tetanus was carried out after every three isotonic contractions, with a 5 minute rest period between each contraction. A linear decline in force was assumed between control contractions, and this was used to represent force relative to P_0. Force was noted to decline between 10 and 20 % with each subsequent contraction. In determining the force-velocity curves, force was expressed relative to P_0; velocity was determined from length changes with respect to time, where length change was determined as the change in length from zero to the maximum force achieved during a particular contraction. Relationships were fit to the hyperbolic-linear curve (following Marsh and Bennett, 1986) using IgorPro (version 7.00, WaveMetrics Inc., Portland, OR, USA) to determine the maximum shortening velocity (V_{max}), power ratio (calculated as $\Pi_i/V_{max}P_0$; following Marsh and Bennett, 1985) and maximal isotonic muscular power (Π_i). The hyperbolic-linear curve was used as this provided a good fit for the data and met many of the conditions outlined by Marsh and Bennett (1986).

3.3.5 Cyclic contractile properties

3.3.5.1 The work-loop technique

The muscle was stimulated *via* parallel platinum wire electrodes running along the full length of the muscle at a stimulation frequency of 50 Hz (pulse width 0.2 ms) at a time and for a duration that maximised net power output, parameters which yielded maximum power output were determined through preliminary testing, details of the tested parameters are detailed in Appendix 1. Each muscle preparation was subject to five cycles of sinusoidal length changes at cycle frequencies ranging from 0.6 to 2 Hz (see Table 6) and strain amplitude of 0.075 L_0, this strain amplitude was selected based upon preliminary testing at 1 Hz, which revealed maximum work and power were achieved when using this strain amplitude in association with other parameters (See Appendix 1 for a full breakdown of all parameters tested). The optimum phase was found to be invariant and was kept constant at 100 ms prior to peak length (See Appendix 1 for further details). Control work loops at a cycle frequency of 1 Hz were performed periodically to monitor and allow correction for decline of the preparation; where control power had declined >45% below previous measurements, the muscle was left to rest for 1 hour to allow muscle to recover to pre-fatigue levels. The net mechanical power output was calculated as the average of cycles 3 and 4, these cycles were selected as cycles 1 and 2 would sometimes result in large spikes in activity and slower relaxation times than subsequent work loops (See Appendix 2 for example work loops and traces of muscular force against time).

At the end of the experiment, the muscle preparation was removed, the sutured ends of the muscle were removed, and excess saline was removed from the muscle by lightly blotting the muscle with tissue. The wet mass of the muscle was then determined in grams to two decimal places using an electronic balance. The measured wet mass was used in the normalisation of isometric and isotonic power outputs, as well as calculation of muscle stress. The muscle density was assumed to be 1060 kg m^{-3} (Mendez and Keys, 1960).

Table 6. Modified parameters used for work loop experiments. The cycle frequency and train duration were modified during cyclic muscular work. Parameters at a cycle frequency of 1 Hz were used as control stimuli.

Cycle frequency (Hz)	Train duration (ms)
0.6	800
0.8	475
1.0	350
1.2	260
1.4	200
1.6	85
1.8	72
2.0	65

3.3.6 *In vivo* estimation of muscle strain

Using a modification of the methods of Girgenrath and Marsh (1997) *in vivo* muscle length was estimated from swim sequences. This was achieved by measuring the changes in the diameter of the cuttlefish mantle as animals swam through a tank. The swim sequences used were a sub-set of sequences described in Chapter 2, these sequences were recorded using a Photron FASTCAM SA3 (Photron USA, San Diego, CA, USA) high speed camera (1024 x 1024, 500 frame s^{-1}; shuttered at $^{1}/_{500}$ frame s^{-1}) mounted perpendicular to the experimental tank (l × w × h; 610 x 460 x 450 mm; volume = 126 l). To ensure changes in diameter could be estimated, a calibration image (a 14 mm grid) was taken prior to each swim sequence.

Sequences were analysed using ImageJ 1.48 (Schneider *et al.*, 2012). ImageJ enabled images to be imported and stacked into a video using the virtual stack function. Prior to analysis the scale was set, and the frames over which the jet cycle took place identified. In calculating muscle length changes, the diameter was measured at 5 specific points of the jet cycle, these were (1) prior to a jet event starting, (2) 50% through the jet exhaust phase, (3) the end of the jet exhaust phase, (4) 50% through the refill phase and (5) at the end of the refill phase. The contraction phase was defined as the period over which a jet was being produced, while the refill phase was assumed to be the time between two jet events taking place. As a result of these definitions, the refill and relaxation phases could not be differentiated during this study.

In estimating changes in the muscle length cuttlefish were assumed to be circular. The mantle circumference was estimated as:

$$C_m = \pi d_m$$

Where C_m is the mantle circumference and d_m is the mantle diameter. Data upon the jet cycle period was also collected, enabling the duty cycle, the time associated with the jet period, and jet cycle frequency to be calculated. Changes in C_m were used to estimate strain as:

$$Strain = \frac{\Delta C_m}{C_{m_{max}}}$$

Where the change in mantle circumference (ΔC_m) was calculated using maximum (C_{mmax}) and minimum mantle circumferences. The maximum mantle circumference was used as a reference value, to which changes in circumference were compared.

3.3.7 Statistical analysis

Data were analysed using Igor Pro (Version 7.00, WaveMetrics Inc., Portland, OR, USA), IBM SPSS Statistics 24 (International Business Machines Corporation, Armonk, NY, USA), Minitab 17 (Minitab Inc., State College, PA, USA) and OrginPro 9.1 (OriginLab

Corporation, Northampton, MA, USA). All data were tested for normality and homogeneity prior to statistical testing; if data were non-normally distributed these were transformed to meet these assumptions via log or arcsine transformation; data which could not be transformed, or where transformation was inappropriate, were tested for statistical differences using nonparametric tests. A critical p value of 0.0013 was used to indicate significant differences following a Bonferroni correction for multiple testing in an attempt to reduce type I errors (Armstrong, 2014). A Bonferroni correction was selected as alternative procedures (such as the False Discovery rate) are less stringent in avoiding type I errors. Where simple comparisons were made t-tests or Mann-Whitney U tests were used, Wilcoxon signed rank tests were used to investigate the decline of twitch:tetanus ratios due to repeated measures. ANOVA with Tukey post-hoc tests were used to test for differences in work or power output of muscle between cycle frequencies. The goodness of fit of models was determined using Chi square tests.

3.4 Results

Cuttlefish showed a 5-fold increase in mantle length from the juvenile to adult stages investigated here (from 44 to 201 mm). With juveniles being significantly smaller than adult animals (Juvenile: 45.4 ± 1.1 mm, n=5; Adult: 166.9 ± 23.9 mm, n=8; t 14.46; df 7, $p < 0.001$). All data collected here have been summarised in Table 7, along with comparisons to other lineages.

3.4.1 Isometric contractile properties

Contraction times, twitch and tetanic stresses and the twitch:tetanus ratio did not differ significantly between preparations from juvenile and adult animals (Table 7). The plateau of tetanic contractions was not particularly pronounced, with muscle relaxing quickly following a tetanus (Figure 25). The twitch:tetanus ratio decreased over the duration of the study (Table 8) in both adult and juvenile preparations, the manner in which this declined cannot be described in detail as twitch responses were only

measured at the beginning and end of experiments. The relatively higher loss of twitch contractile force compared to tetanus force was not related to changes in tP_{tw} and RT_{50}.

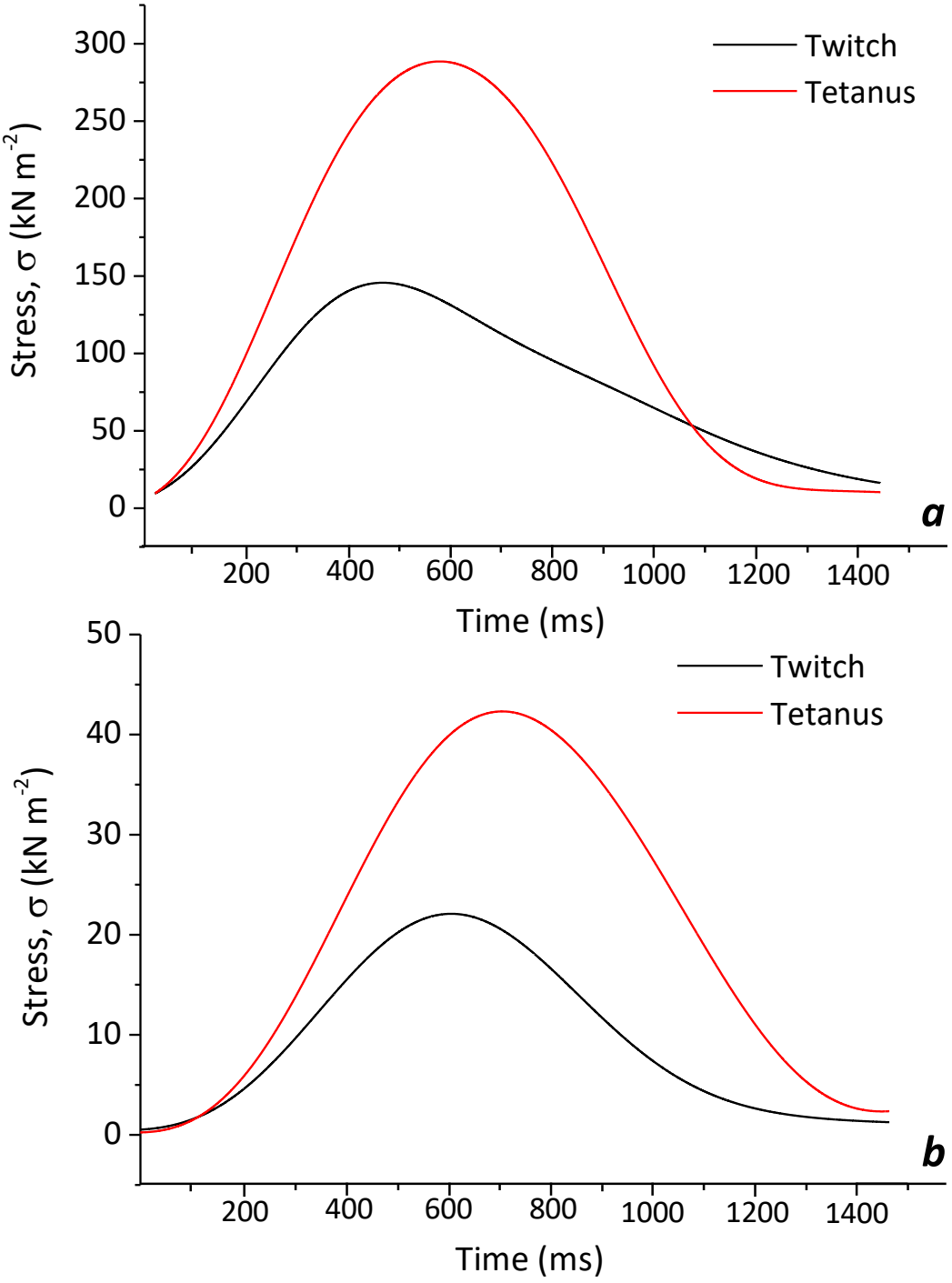

Figure 25. Example twitch and tetanic stress profiles from one adult (a) and juvenile (b) mantle preparation. Twitch (black line) and tetanic (red line) contractions are shown. The muscular stress during these particular contractions was: σ_{tw} 141.06 kN m^{-2} and σ_0 273.52 kN m^{-2} in the adult preparation and σ_{tw} 24.11 kN m^{-2} and σ_0 43.20 kN m^{-2} in the juvenile preparation. Data were smoothed using a FFT filters with a cut off frequency of 2.5 Hz.

Table 7. Contractile properties of the locomotory musculature of several mollusc species. All measures from European species were carried out at 11 ± 0.5 °C. All data are shown as means ± sd

		Juvenile cuttlefish (*S. officinalis*)	Adult cuttlefish (*S. officinalis*)*	Cuttlefish (*S. officinalis*)	Common squid (*Alloteuthis subulata*)	Longfin squid (*D. pealeii*) paralarva	Longfin squid (*D. pealeii*)	Bay scallop (*Argopecten irradians*)
Isometric	σ_{tw} (kN m^{-2})	48 ± 27	84 ± 37	35 ± 21	43 ± 16	-	-	21 ± 2.9
	σ_0 (kN m^{-2})	68 ± 51	144 ± 76	226 ± 50	262 ± 39	119 ± 15	216 ± 22 290 ± 59	24 ± 3.7
	P_{tw}/P_0	0.75 ± 0.13	0.62 ± 0.18	0.10 ± 0.05	0.18 ± 0.02	-	0.18 ± 0.1 0.58 ± 0.03	0.89 ± 0.04
	tP_{tw} (ms)	257 ± 39	371 ± 94	205 ± 56	92 ± 25	127 ± 28	143 ± 58	135 ± 22
	RT_{50} (ms)	257 ± 28	677 ± 221	484 ± 111	187 ± 61	57.4 ± 4.7	175 ± 99	160 ± 22
Isotonic	V_{max} (L s^{-1})	2.54 ± 0.67	2.27 ± 0.58	-	2.43 ± 0.31	9.1 ± 3.7	5.1 ± 1.2	5.35 ± 0.32
	P/P_0	0.10 ± 0.04	0.30 ± 0.11	-	-	-	-	0.39 ± 0.02
	Maximum Π_i (W kg^{-1})	13.87 ± 7.01	21.12 ± 17.67	-	18.3 ± 4.81	-	-	-
	Power ratio	0.14 ± 0.08	0.23 ± 0.18	-	-	-	-	0.11 ± 0.01
Cyclic	Peak cyclic frequency	2 Hz	1.4 Hz	-	-	-	-	1.92 ± 0.22
	Maximum Π_c (W kg^{-1})	23.76 ± 14.82	14.79 ± 8.09	-	-	-	-	34 ± 2

		*Juvenile cuttlefish (*S. officinalis*)*	*Adult cuttlefish (*S. officinalis*)*	*Cuttlefish (*S. officinalis*)*	*Common squid (*Alloteuthis subulata*)*	*Longfin squid (*D. pealeii*) paralarva*	*Longfin squid (*D. pealeii*)*	*Bay scallop (*Argopecten irradians*)*
	Temperature (°C)	11 ± 0.5	11 ± 0.5	11 ± 0.5	11 ± 0.5	20 ± 0.2	20 ± 0.2	10
Reference		This study	This study	1, 2	1, 2	4	3, 4	5, 6

List of abbreviations: σ_{tw} Twitch stress; σ_0 Tetanic stress; P_{tw}: Peak twitch force; P_0; Peak tetanic force; P_{tw}/P_0: Twitch:tetanus ratio; tP_{tw}: Time to peak twitch force; RT_{50}: Half relaxation time following a twitch; V_{max}: Maximum velocity of muscle shortening at zero force; Π_i: Net isotonic muscular power; Π_c Net cyclic muscular power

[1]Milligan *et al.* 1997; [2]Rogers *et al*, 1997; [3]Thompson *et al*, 2008; [4]Thompson *et al*, 2010; [5]Olson and Marsh, 1993; [6]Marsh and Olson, 1994

**Adult cuttlefish were in a fecund state during this study*

Table 8. Differences in P_{tw}/P_0 following exercise of mantle musculature. The ratio declines as a result of musculature losing its ability to twitch following exercise. No significant differences between pre- and post-exercised muscle were found; adult and juvenile muscle showed no significant differences in P_{tw}/P_0 in either pre- or post-exercised samples.

Age class	P_{tw}/P_0 (Pre-exercise)	P_{tw}/P_0 (Post-exercise)	Test statistic
Juvenile	0.75 ± 0.13	0.19 ± 0.13	W = -2.524, df 8, p 0.012
Adult	0.62 ± 0.16	0.06 ± 0.05	

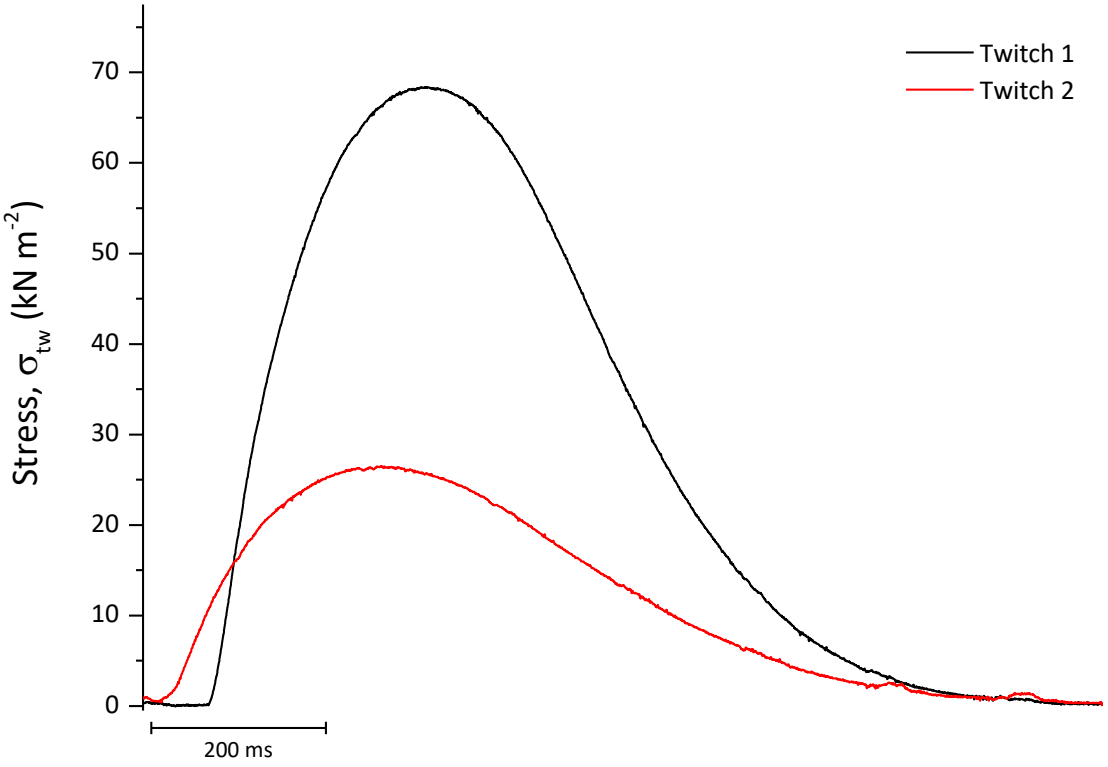

Figure 26. Example profiles from two twitch contractions from a 13 mm juvenile preparation. Initial twitches reached P_{tw} and relaxed more rapidly than subsequent stimuli, with subsequent stimuli achieving lower stresses. Data were smoothed using FFT filtering with cut-off frequency of 0.125 Hz.

3.4.2 Isotonic contractile properties

3.4.2.1 The force-velocity relationship

An inverse relationship between velocity of shortening and the relative force produced by the mantle musculature of cuttlefish was noted (see Figure 27 for mean relationship). The maximum velocity of shortening (V_{max}) and power ratio showed no significant change with age. The maximum isotonic power, though higher on average in adult animals, showed no significant differences between cuttlefish age classes.

Table 9. Parameters of the hyperbolic linear equations for juvenile and adult mantle muscle preparations. Presented as means ± sem. Chi-Square values signify the goodness of model fit, where lower values highlight data which better fits the hyperbolic linear equation.

	Juvenile	Adult
A	0.88 ± 0.07	0.70 ± 0.16
B	4.12 ± 0.62	3.31 ± 0.89
C	1.68 ± 0.24	1.60 ± 0.35
Chi Square	0.03 ± 0.01	0.07 ± 0.03
V_{max} (L s^{-1})	2.54 ± 0.30	2.27 ± 0.24
Power ratio	0.14 ± 0.03	0.23 ± 0.08
Relative force at max power	0.74 ± 0.02	0.8 ± 0.004
Velocity at max power (L s^{-1})	0.12 ± 0.03	0.09 ± 0.02
n	5	6

Power ratio was calculated as $\Pi_i/V_{max}P_0$. The power ratio describes the degree of curvature of the force-velocity relationship (Marsh and Bennett, 1985).

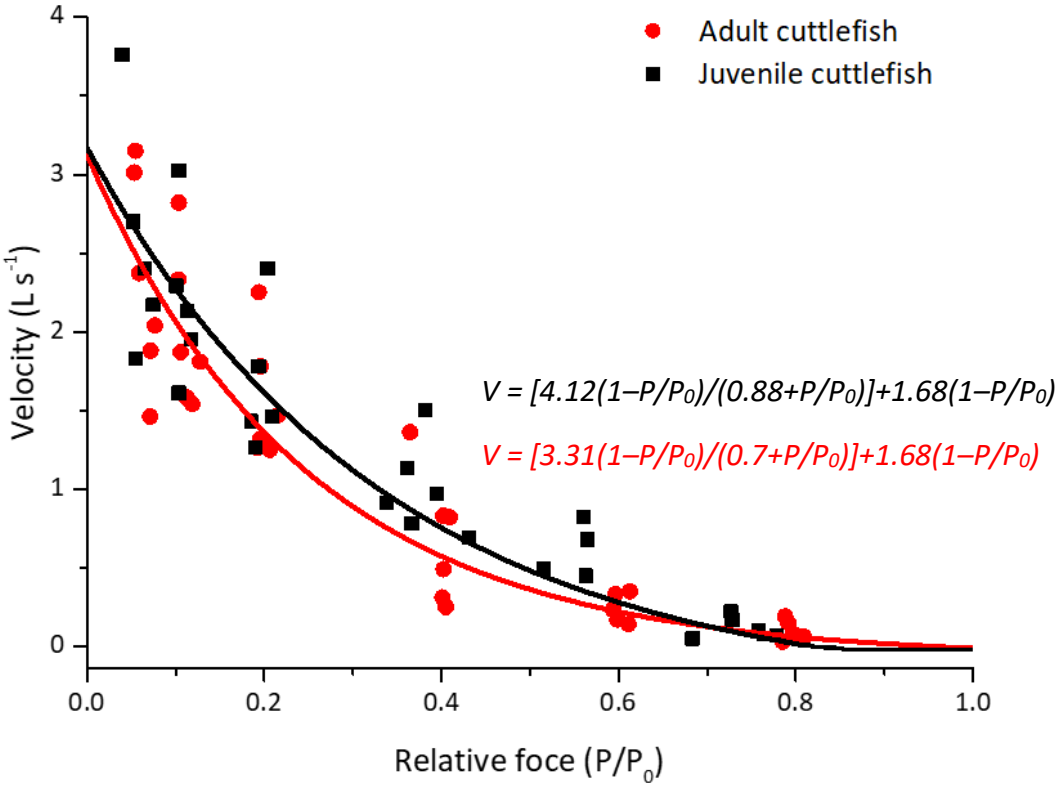

Figure 27. Mean relationship between relative force and velocity of shortening from 5 juvenile (displayed in black) and 6 adult (displayed in red) cuttlefish preparations. Data fit according to the hyperbolic-linear equation: V = [B(1 – *P/P0*)/(A+*P/P0*)]+C(1 – *P/P0*); the mean equation for each group is displayed.

3.4.3 Scaling dynamics of mantle muscle function

The relationship between animal size (given as mantle length (L_m)) with isometric, isotonic and cyclic contractile properties of the mantle musculature fit allometric relationships (Table 10; Table 11; Figure 28).

Table 10. Allometric scaling relationships of isometric and isotonic contractile properties and mantle length of cuttlefish. Significant relationships are highlighted in bold.

y	Units	r^2	a	b (± sem)	p
σ_0	**kN m^{-2}**	**0.25**	**7.09**	**0.6 ± 0.3**	**<0.001**
$P_{tw}:P_0$	-	0.13	1.41	-0.16 ± 0.1	NS
tP_{tw}	**ms**	**0.32**	**89.83**	**0.28 ± 0.12**	**<0.001**
RT_{50}	**ms**	**0.45**	**31.63**	**0.59 ± 0.23**	**<0.001**
V_{max}	L s^{-1}	0.08	3.13	-0.06 ± 0.12	NS
P/P_0	-	0.02	0.06	0.31 ± 0.02	NS
Π_i	W kg^{-1}	0.1	1.02	0.61 ± 0.43	NS
Π_c	W kg^{-1}	0.05	3.86	0.18 ± 0.24	NS

***List of abbreviations**: σ_0 – tetanic stress; $P_{tw}:P_0$ – twitch:tetanus ratio; tP_{tw} – time to peak twitch; RT_{50} – half relaxation time following a twitch; V_{max} – maximum velocity of shortening; P/P_0 – relative force at which maximum power is produced, Π_i - maximum isotonic power, Π_c – maximum cyclic power.*

Table 11. Allometric scaling relationships of isometric and isotonic contractile properties and mantle length of juvenile and adult cuttlefish. Significant relationships are highlighted in bold.

	Juvenile				Adult			
	a	*b (± sem)*	r^2	*p*	*a*	*b (± sem)*	r^2	*p*
σ_0	2.08 x 10^{-4}	3.4 ± 12.9	0.3	NS	**6.87 x 10^{-6}**	**3.28 ± 0.87**	**0.72**	**<0.001**
$P_{tw}:P_0$	3.49 x 10^{-6}	3.22 ± 3.4	0.01	NS	205.7	-1.14 ± 0.66	0.24	NS
tP_{tw}	**6.55**	**-5.68 ± 1.09**	**0.88**	**<0.001**	117.3	0.23 ± 0.72	0.15	NS
RT_{50}	**402**	**-0.12 ± 2.5**	**0.33**	**<0.001**	132444	-1.03 ± 0.85	0.05	NS
V_{max}	565	-1.42 ± 6	0.31	NS	0.006	1.14 ± 0.59	0.38	NS
P/P_0	4.66	-5.68 ± 24.48	0.3	NS	86.4	-1.11 ± 0.92	0.07	NS
Π_i	5.22 x 10^{-4}	2.67 ± 11.37	0.3	NS	**9.13 x 10^{-16}**	**7.25 ± 2.48**	**0.81**	**<0.001**
Π_c	2.8 x 10^{-12}	7.82 ± 23.82	0.4	NS	**1.05**	**0.5 ± 1.89**	**0.23**	**<0.001**

List of abbreviations: *σ_0 – tetanic stress; $P_{tw}:P_0$ – twitch:tetanus ratio; tP_{tw} – time to peak twitch; RT_{50} – half relaxation time following a twitch; V_{max} – maximum velocity of shortening; P/P_0 – relative force at which maximum power is produced, Π_i - maximum isotonic power, Π_c – maximum cyclic power.*

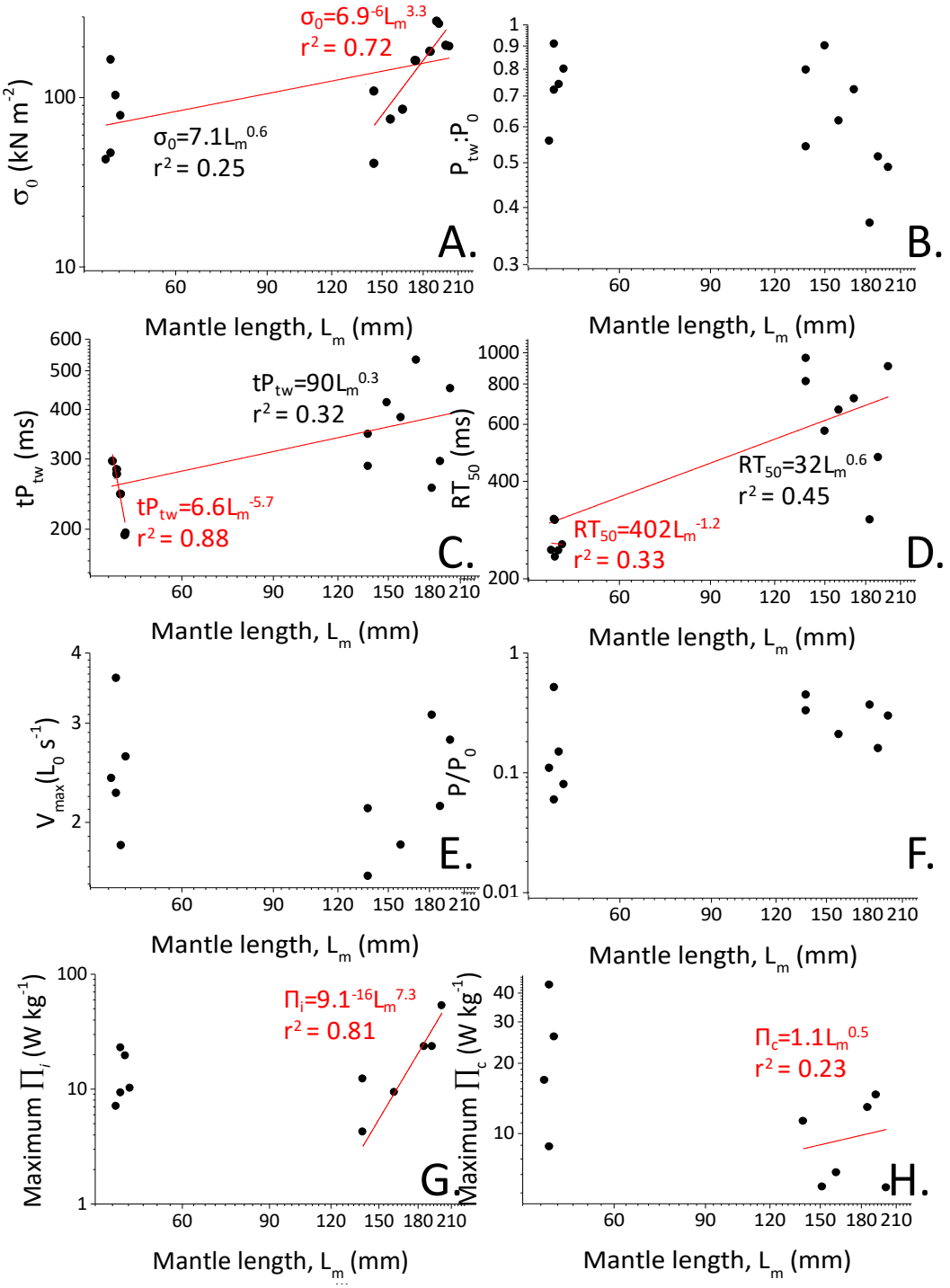

Figure 28. Scaling relationships between mantle length and mechanical properties of cuttlefish musculature. A. Peak tetanic stress, B. The twitch:tetanus ratio, C. Time to peak twitch force, D. Half-relaxation time following a twitch, E. Maximum velocity of shortening, F. Power ratio, G. Maximum isotonic power and H. Maximum cyclic power. Scaling exponents for all preparations are shown in black, where within-group scaling occurred this is shown in red, values shown to 1 dp.

3.4.3.1 Muscle performance during cyclical contractions

The net cyclic power (Π_c) of juvenile preparations ranged from 1.2 to 43.33 W kg^{-1}, with net cyclic power increasing at higher frequencies (Figure 29). Preparations from adult animals ranged from 1.12 to 28.82 W kg^{-1}, and showed a polynomial relationship where preparations reached a plateau between 0.8 and 1.2 Hz. Peak net muscular power was achieved at a frequency of 1.4 Hz in adult animals, and 2 Hz in juveniles, with respective mean net powers of 14.79 ± 8.09 W kg^{-1} and 23.76 ± 14.82 W kg^{-1} (Table 7). Net muscular power did not significantly differ between cycle frequencies in juvenile (*F* 2.24, df 6, p 0.07) and adult preparations (*F* 3.23, df 5, p 0.02). Comparisons of the net power-frequency relationships of the two age classes revealed no significant differences between the two curve fits (*F* 16, df 2, 8, p 0.009), with neither animal age (*F* 8.11, df 1, p 0.007) nor cycle frequency (*F* 371, df 7, p 0.18) impacting relationships.

The net muscular work at different cycle frequencies showed a similar relationship to muscular power, where a plateau was reached between 1.4 and 2 Hz in juvenile preparations, and 0.8 and 1.4 Hz in adult preparations (Figure 30). Peak net muscular work was achieved at 1.4 in juvenile preparations and 1.2 Hz in adult preparations, with respective mean work of 10.42 ± 3.09 J kg^{-1} and 10.91 ± 1.79 J kg^{-1}, these mean net work measurements did not differ significantly between juvenile and adult preparations (*U* 17, df 11, p 0.792). Cycle frequencies did not significantly affect peak muscular work in juvenile (*F* 1.01, df 6, p 0.44) and adult (*F* 0.98, df 5, p 0.45) animals.

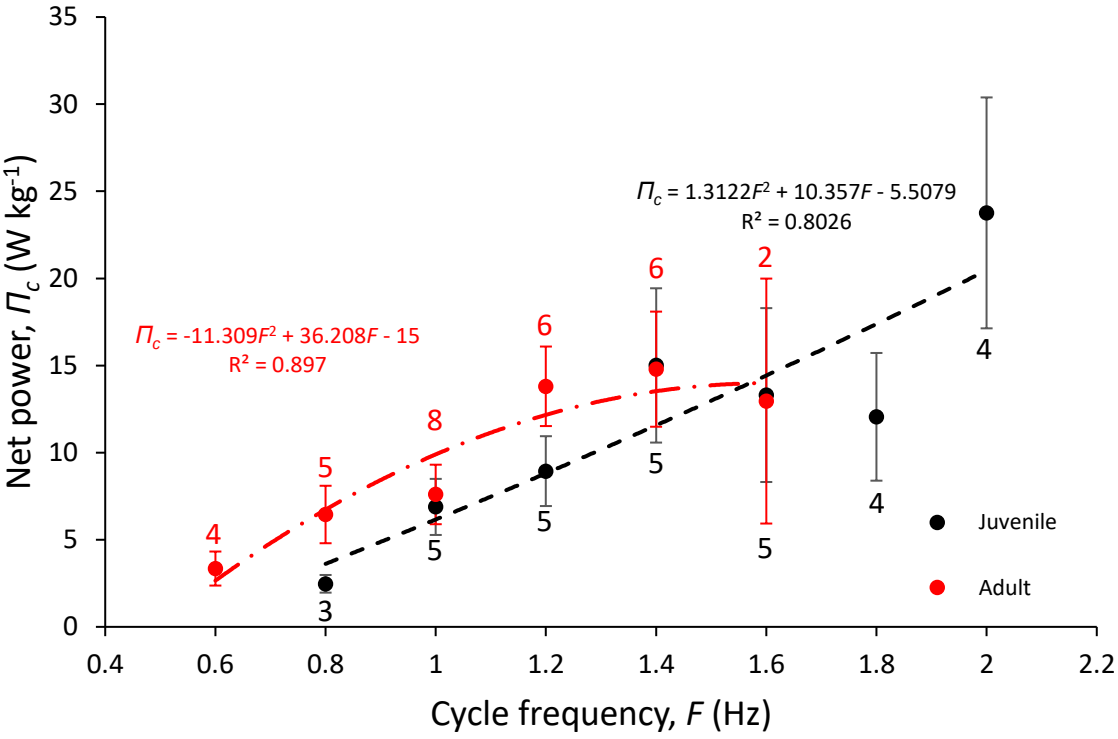

Figure 29. Relationship between mantle muscle cycle frequency and net muscular power of juvenile (black) and adult (red) preparations subject to sinusoidal work. Data fit to second order polynomials. Error bars represent ± sem. Equations of polynomials and R^2 values are displayed. Pairwise comparisons revealed no significant differences between groups. The number of preparations from which results were obtained are displayed above or below the relevant points.

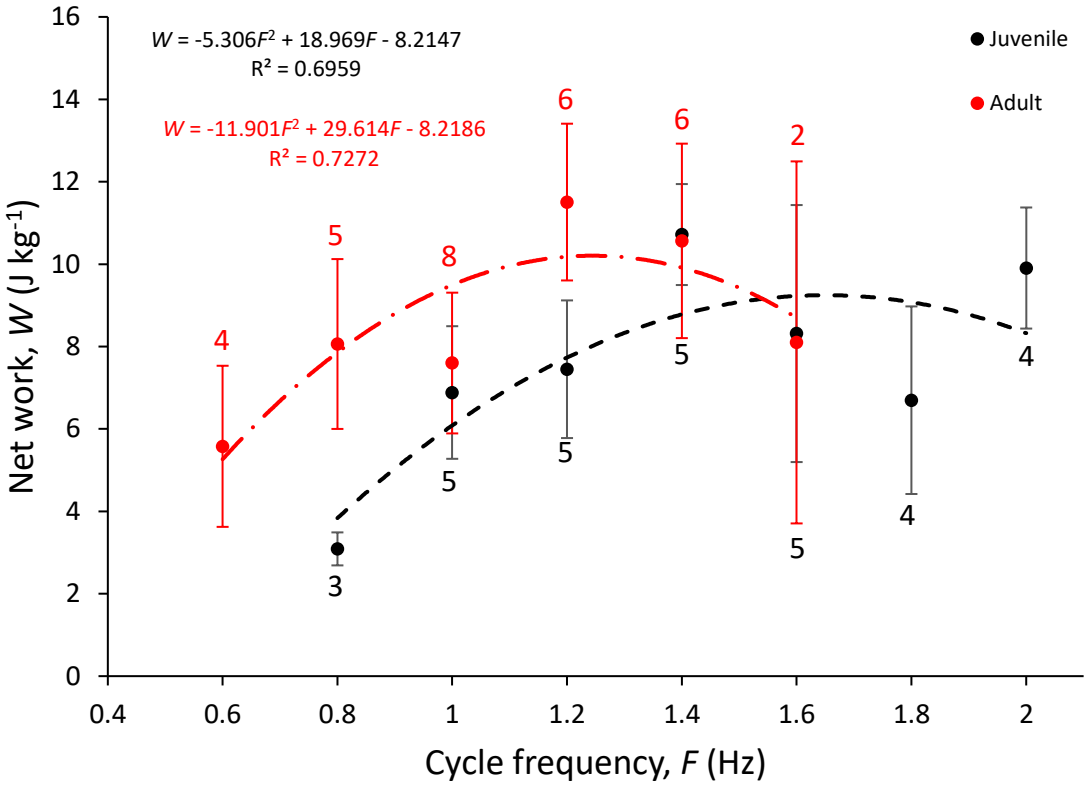

Figure 30. Relationship between mantle muscle cycle frequency and net muscular work of juvenile (black) and adult (red) preparations subject to sinusoidal work. Data fit to second order polynomials. Error bars represent ± sem. Equations of polynomials and R^2 values are displayed. Pairwise comparisons revealed no significant differences between groups. Numbers above or below each value denote the number of preparations from which data are obtained.

3.4.3.1.1 The muscular stress during cyclical contractions

The maximum stress of muscle undergoing cyclic contractions was very similar to that produced during isometric tetanic contractions at the cycle frequency which produced maximal work in juvenile animals (1.4 Hz; Figure 31). Peak muscular stress seen during cyclic contractions (91.98 ± 21.58 kN m^{-2}) was marginally higher than peak stress during isometric tetani (87.98 ± 22.73 kN m^{-2}; *U* 10, df 10, p 0.69), the average stress during cyclic contractions (calculated as: $\sigma_c = \frac{\Pi_c}{Strain \times F}$ (Ellington, 1985), where Π_c is

the muscular power and *F* is the cycle frequency), was marginally lower than tetanic contractions (51.04 ± 15.06 kN m^{-2}; *U* 19, df 10, p 0.22). During adult cyclic contractions the muscular stress at the cycle frequency which produced maximal work was marginally lower than that produced during an isometric tetanus at 105 ± 53 kN m^{-2} (P_0: 144 ± 76 kN m^{-2}; *U* 26, df 12, p 0.24), the average stress during cyclical activity was much lower (64 ± 26 kN m^{-2}; *U* 33, df 12, p 0.015). Generally, the muscular stress decreased as cycle frequency increased in adult preparations, while remaining largely similar across frequencies in juvenile preparations; stresses produced during isometric contractions were not dissimilar to those produced during cyclic contractions (Figure 31).

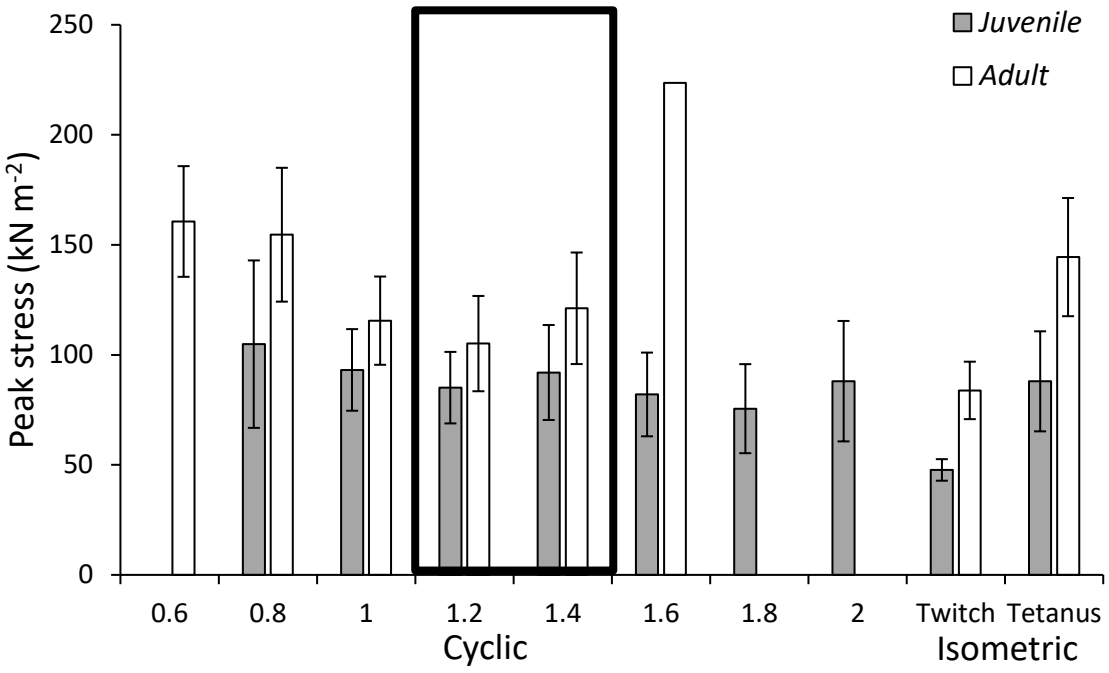

Figure 31. The peak (± sem) stress of mantle muscle preparations during cyclic and isometric stimuli. The cycle frequencies of 1.2 and 1.4 Hz are highlighted as these represent the frequencies over which muscular work was greatest in adult (1.2 Hz) and juvenile (1.4 Hz) muscle preparations. Where error bars are absent this is due to only one preparation been tested at this frequency.

3.4.4 *In vivo* muscle activity

Analysis of changes in the diameter of the mantle, used as a proxy for muscle shortening, revealed the mantle musculature shortened at an average velocity of 0.53 ± 0.36 L s^{-1} (range 0.12-1.25 L s^{-1}). Based upon the force-velocity relationship this suggests relative forces of between 20 and 80%. During free-swimming, overall strain (relative to maximum mantle circumference) was on average 0.19 ± 0.12 (range 0.09-0.31), with a jet contraction lasting 0.44 ± 0.33 s (0.16-1.13 s), and mantle refill 0.39 ± 0.24 s (0.11-0.86 s). This gave a duty cycle of 51.79 ± 26.72 % (22.62 - 83.43 %) and a cycle frequency of 1.39 ± 0.71 Hz (0.70 - 2.92 Hz).

3.5 Discussion

3.5.1 Contractile characteristics of obliquely striated musculature

During an animal's development the contractile properties may change as a result of changes in muscle ultrastructure and biochemistry, such as changes in muscle filament length, changes in the expression of myosin isoforms, and changes in the properties of associated connective tissues (Shaffer and Kier, 2012; Thompson and Kier, 2006).

Here, it was found that the contractile properties of cuttlefish mantle musculature differed between the two age classes investigated. The tP_{tw} positively scaled with mantle length as $L_m^{0.28}$, while RT_{50} scaled as $L_m^{0.59}$. Previous work with the mantle muscle of longfin squid (*D. pealeii*) has noted tP_{tw} and RT_{50} are more rapid during paralarval than adult stages (tP_{tw} is 11% and RT_{50} is 67% more rapid on average; Table 7; Thompson *et al.,* 2010). Previous work has noted cephalopods show continued addition of new muscle fibres, particularly fast-twitch fibres, throughout ontogeny, this ensures animals are able to maintain similar absolute muscular force throughout their growth, but may cause musculature to contract at lower velocities (Moltschaniwskyj, 1994; Moltschaniwskyj, 2004). Force modulation by the obliquely-striated muscle of cephalopods results from variations in thick filament length rather than through the

expression of different myosin isoforms (Thompson *et al.*, 2014). This increase in contractile speeds with increased length was coupled with a minor decline in the P_{tw}/P_0 ratio. Previous work has not explicitly explored how this changes through ontogeny, however the ratio seen here in adult animals (0.62) is very similar to that seen by Thompson *et al.* (2010) in brief squid (*L. brevis*; 0.58). Though, these ratios are comparatively high when compared to previous measurements (see Table 7), these previous measures may result from the decline in twitch responses by musculature over time (see Table 7 and Table 8). Thompson *et al.* (2010) noted a similar decline, suggesting the twitch response of cephalopod muscle declines with increased work. The underlying cause of this decline remains unclear but a likely hypothesis has been suggested by Marsh (1990), whose review noted that while most muscles show a strong correlation between V_{max} and deactivation rates, where tP_{tw} and P_{tw} are strongly correlated. Muscles where V_{max} and elasticity remain constant uncouple deactivation rates from twitch responses, where increasing the rate of deactivation leads to a reduction in tP_{tw} and P_{tw}, reducing P_{tw}/P_0 (Marsh, 1990). The results presented here could suggest cuttlefish mantle muscle maintains shortening velocity by increasing the rate at which Ca^{2+} is removed. Previous work has noted the elasticity of cuttlefish mantle musculature is particularly high, with as much as 80 % of the work for lengthening being met through recoil processes (Curtin *et al.*, 2000). This could support the hypothesis of Marsh (1990) and the findings here where the elasticity of muscle allows for increased Ca^{2+} removal to maintain muscle function. The process of Ca^{2+} removal is however active, suggesting energy expenditure may be increased during such activity. Ca^{2+} seems to be primarily taken up within myomuscular junctions between muscle fibres (Milligan *et al.*, 1997), with previous work noting Ca^{2+} flux within cephalopod muscles blocks myomuscular junctions (Bone *et al.*, 1982; Zullo *et al.*, 2017). Work has yet to address this empirically, suggesting cephalopod musculature may provide an avenue to further investigate if the suggestions of Marsh (1990) hold true. Taken together these results could highlight the involvement of this muscle in escape responses, Marsh (1990) noted the contractile frequency of bay scallops (*A. irradians*) is primarily related to the deactivation rate, with cycle frequency (measured through the rate of shell opening/closing) remaining constant when facing a predatory threat. Marsh (1990) suggested changes in V_{max} would more likely be related to overcoming inertial forces

than changes in cycle frequency, with changes in V_{max} unlikely in muscle with a high degree of elasticity as a result of recoil processes.

The tetanic responses of this muscle did not produce a clear plateau as may be expected in vertebrate striated muscle. Comparisons reveal this plateau is not present within the mantle muscle of European common squid (*A. subulata*) (Milligan *et al.*, 1997), longfin squid (*D. pealeii*) (Thompson *et al.*, 2010; Thompson *et al.*, 2008), and European common cuttlefish (*S. officinalis*) (Milligan *et al.*, 1997). These previous studies used a slightly shorter train of stimuli (200 ms), though Milligan *et al.* (1997) did investigate the effect of increased stimulation upon preparations of European common squid musculature. From this it was noted a 500 ms train of stimuli would enable musculature to reach maximal stimulation with muscle force reaching a short plateau as seen here. This could suggest the lack of a plateau results from how this muscle responds to stimulation, or may be an artefact of the experimental design, further work may be required to understand if tetani are simply brief within this muscle type (as suggested by Milligan *et al.* 1997), or if other factors may be influencing these responses.

Investigations into the force-velocity relationship of cephalopod muscle are somewhat more widespread than those looking at isometric properties alone. The relative velocity of shortening of cuttlefish mantle muscle declined with increased load, as found in vertebrate striated muscle, as well as the obliquely striated musculature of other cephalopods. The shortening velocity of cephalopod obliquely striated muscle is thought to be slower than the striated muscle of vertebrates and some invertebrate lineages, with the bulk of this difference arising from slower relaxation times when compared to cross-striated muscle (Millman, 1967), here the maximum shortening velocity was on average between 2.3 and 2.5 L s^{-1}, which is similar to that of other European cephalopods, such as the common squid (2.43 ± 0.11 L s^{-1}) (Milligan *et al.,* 1997; Table 7). Isotonic measures have also been taken from the funnel musculature of cephalopods and these studies have revealed very similar contractile properties to those recorded in mantle musculature, with the relative V_{max} of longfin squid (*D. pealeii*) funnel musculature is 2.15 ± 0.26 L s^{-1} (Rosenbluth *et al.*, 2010). This measure seems to be in agreement with measures taken in mantle musculature. The similarities

in mechanical properties between funnel and mantle musculature is perhaps unsurprising given these muscles are both of the same muscle type and involved in the same locomotory reflex. Table 7 details the contractile properties of the locomotory musculature of various cephalopods and scallops, it is clear from this that V_{max} varies between species, animal sizes, and likely temperature; this suggests more work may be required to ascertain the impacts of scaling and temperature upon isotonic contractile properties of cephalopod musculature. Comparisons with the velocity at which the muscles of other animals shorten when held at similar temperatures reveal shortening occurs more rapidly in both the white myotomal muscle of dogfishes (*Scyliorhinus canicula*), shortening as 3.8 ± 0.2 L s^{-1} at 12 °C (Curtin and Woledge, 1993b), and the adductor muscle of bay scallops (*Argopecten irradians*) shortening as 5.35 ± 0.13 at 10 °C (Olson and Marsh, 1993). These differences are not particularly pronounced, but seem to suggest the hypothesis of Millman (1967) may be in part true. The impacts of temperature upon the velocity with which muscle shortens are well documented, with Olson and Marsh (1993) noting V_{max} increases with increased temperature in the adductor of bay scallops, as the measures taken in other cephalopods are at higher temperatures, this may suggest similar shortening velocities may occur if similar temperatures were used; though this has yet to be tested empirically.

3.5.1.1 Ontogenetic scaling of mechanical performance

The contractile properties of cuttlefish mantle musculature scaled with mantle length. With isometric contractile properties such as tP_{tw} and RT_{50} scaling positively with mantle length as $L_m^{0.28}$ and $L_m^{0.59}$ respectively (see Table 10 for more details). Such scaling relationships have not been previously investigated in cephalopod molluscs necessitating wider comparisons. Comparisons with Atlantic cod (*Gadus morhua*) and shorthorn sculpin (*Myoxocephalus scorpius*) abdominal myotome muscle reveal tP_{tw} scales with body length as $L_b^{-0.05}$ and $L_b^{0.31}$, while RT_{50} scaled as $L_b^{0.44}$ and $L_b^{0.67}$ (Altringham and Johnston, 1990; James *et al.*, 1998); the scaling of RT_{50} noted in Atlantic cod and shorthorn sculpin is very similar to the data presented here in cuttlefish, suggesting shortening responses may be similar between these muscle types. Interestingly, the scaling of tP_{tw} in the musculature of Atlantic cod is barely

present, while tP_{tw} responses of sculpin muscle are very similar to those of cuttlefish mantle muscle. These observed differences in isometric scaling of cod and sculpin musculature are likely linked to how muscle fibres are recruited during development, and how muscle is used by animals. James *et al.* (1998) and James and Johnston (1998) both highlighted the behaviour of shorthorn sculpin is that of an ambush predator, with the swimming dynamics dominated by C-starts and escape responses. This behaviour mirrors that of cuttlefish suggesting mechanical similarities may result from similar selective pressures upon the locomotive muscle of these species.

While the isotonic mechanical properties of cephalopod musculature have been more widely investigated, scaling exponents are still lacking. Here it was noted V_{max} did not appear to scale with body length ($L_m^{-0.06}$) in cuttlefish, comparisons reveal scaling is far more pronounced in Atlantic cod (*G. morhua*; $L_b^{-0.79}$) (Anderson and Johnston, 1992) and shorthorn sculpin (*M. scorpius*; $L_b^{-0.66}$; $L_b^{-0.34}$) (James *et al.*, 1998; James and Johnston, 1998) locomotory musculature, and bluegill (*Lepomis macrochirus*; $L_b^{-0.28}$) (Carroll *et al.*, 2009) suction feeding musculature. The suction feeding musculature of largemouth bass (*Micropterus salmoides*; $L_b^{-0.011}$) (Carroll *et al.*, 2009) however seemed to lack any scaling relationship. The lack of scaling of V_{max} in cuttlefish musculature is somewhat similar to that of largemouth bass suction feeding musculature, Carroll *et al.* (2009) suggested the isometric growth of largemouth bass feeding muscle likely explained the similarities in contractile properties during growth. Previous work has suggested muscle recruitment occurs throughout the lifecycle of cephalopods, with allometric recruitment noted between hatchling and juvenile stages, and isometric recruitment in larger animals (Moltschaniwskyj, 2004), this seems to support the similarities noted here, suggesting shortening velocity is maintained as a result of how muscle fibres are recruited. The scaling of isotonic power output of adult cuttlefish mantle musculature positively scaled with mantle length as $L_m^{7.25}$, comparisons with the scaling of power output of the suction feeding muscles of bluegills (*L. macrochirus*) and largemouth bass (*M. salmoides*) reveals much lower exponents of $L_b^{0.08}$ and $L_b^{-0.13}$ (Carroll *et al.*, 2009), likely reflecting functional differences between these muscle types. Comparisons with locomotory musculature reveal much lower scaling exponents in the anterior abdominal myotome muscle of shorthorn sculpin (*M.*

scorpius; $L_b^{2.31}$) (James and Johnston, 1998). The scaling of muscular power in adult cuttlefish was much more pronounced as that of shorthorn sculpin, but muscular power did not scale strongly in juvenile preparations, or from juvenile to adult stages. The differences in scaling between age groups may reflect functional differences or developmental changes, it is also possible adult animals being in a fecund state may have influenced the results seen. The differences in power output between sculpin and cuttlefish may reflect differences between the muscle types and locomotory mechanisms, where sculpin swim through undulatory mechanisms and cuttlefish through jet propulsion, which likely differ in the underlying power requirements due to functional differences.

3.5.1 Performance of obliquely striated muscle under cyclical contractions

Obliquely striated muscle is common among invertebrate lineages, playing key roles in the locomotion of these species. The movements of animals are typically cyclical, where contractile waves spread throughout muscles and are repeated at regular intervals. The locomotion of molluscs, such as cephalopods and gastropods result from the action of this muscle type, where in the banana slug (*Ariolimax columbianus*) muscular waves travel anteriorly throughout the muscular pedal of the foot (Denny, 1981). This study is the first to investigate muscle performance during cyclical length changes that simulate swimming.

3.5.1.1 Interspecific comparisons

The frequency over which cuttlefish mantle musculature achieved maximum net work and net power declined from juvenile to adult stages. Hill (1950) noted animal muscle, and associated metabolism, is generally faster in smaller animals than their larger counterparts. Despite this decline in cycle frequency, net cyclic power did not scale overall with mantle length, nor was any scaling noted in juvenile cuttlefish, scaling was however noted in adult animals (scaling as $L_m^{0.5}$). Anderson and Johnston (1990) found animal length and cyclic contractile properties of isolated superficial hypaxial abdominal myotomes of Atlantic cod (*Gadus morhua*) were closely linked, where

muscular power declined as $L_b^{-0.40}$ with increased length, while the peak cycle frequency declined with body length as $L_b^{-0.52}$ (Altringham and Johnston, 1990). Similarly, the optimal cycle frequency of iliofibularis muscle of desert iguanas (*D. dorsalis*) declines with increased animal mass as $M^{-0.237}$. However, work output of this musculature increased as animals body mass increased (Johnson *et al.*, 1993). Johnson *et al.* (1993) noted the optimal cycle frequency of desert iguana iliofibularis muscle remained largely similar from hatchling to adult stages. Johnson *et al.* (1993) proposed such similarities suggest the musculature of desert iguanas (*D. dorsalis*) meets many of the assumptions of Hill's (1950) geometric similarity model (Hill, 1950; Johnson *et al.*, 1993), where muscle work and contractile features are independent of body size. The similarity of the muscle dynamics and scaling seen here suggest a similar situation may exist in cuttlefish. However, strain was kept constant during this work as part of the optimisation of muscle performance, which may not reflect the situation seen *in vivo*. Thompson *et al.* (2008) noted strain differed with jet type, with much higher strain during escape jets than routine swimming in longfin squid (*D. pealeii*). This variability in strain suggests more work is needed to fully understand scaling dynamics of this musculature, and to fully emulate length changes during more natural situations. Quillin (1998) noted the obliquely striated musculature of molluscs and other invertebrate lineages is unlikely to fit previously proposed scaling models perfectly as a result of the dual-function of this muscle type. Previous work with earthworms (*L. terrestris*) has noted Hill's geometric similarity model best describes the scaling dynamics of obliquely striated muscle function, where strain is independent of body mass, suggesting these patterns are maintained through differences in activation frequency alone (Hill, 1950; Quillin, 1998; Quillin, 1999). This model would assume the absolute power available for burst swimming in cuttlefish increases with increased body size, while minor differences may arise as a result of non-geometric growth. Trueman and Packard (1968) noted jet propulsion swimming favours larger animals due to increased intramantle area, here it was noted the power achieved by the musculature of larger animals was greater than that of juveniles at similar cycle frequencies. This seems to suggest cuttlefish maintain similar jet-propulsion swimming mechanics throughout ontogeny, with this being driven by similarities in underlying muscle function.

The generation of work and power by adult cuttlefish mantle muscle showed an inverse U-shaped relationship where muscular power and work increased with increasing cycle frequency up to a point, at this point a plateau was reached before muscular power and work declined, the power curves are slightly right-shifted compared to the work curves, this is expected as power is a product of work and frequency. Juvenile preparations show a slightly different power relationship, with power increasing with increased cycle frequencies, this may suggest the plateau for muscular power was not found during this study. Comparisons reveal the relationship seen in adult preparations is typical of muscle undergoing cyclic activity, with similar relationships noted in the flight muscle of tobacco hawkmoths (*Manduca sexta*) (Stevenson and Josephson, 1990), the abdominal myotomes of Atlantic cod (*G. morhua*) (Altringham and Johnston, 1990), the Soleus and EDL muscles of mice (*Mus musculus*) (Askew and Marsh, 1997), the iliofibularis of desert iguanas (*Dipsosaurus dorsalis*) (Swoap *et al.*, 1993) and the white myotomal muscle of dogfishes (*S. canicula*) (Curtin and Woledge, 1993b). While these relationships were similar, the operating frequencies of cuttlefish musculature was much lower than that of vertebrates, with cuttlefish muscle operating maximally at frequencies ranging between 1 and 2 Hz; vertebrate muscle operating at similar temperatures, such as the dorsal fin muscle of Northern pipefish (*Syngnathus fuscus*) and lined seahorses (*Hippocampus hudsonius*) operates maximally at much higher frequencies of 20 Hz (pipefish) and 30 Hz (seahorses) at 10 °C (Ashley-Ross, 2002), while the red and pink myotomal muscle of scup (*Stenotomus chrysops*) operate maximally at 2.5 and 3-4 Hz at 10 °C (Coughlin *et al.*, 1996b; Rome and Swank, 1992), and the white myotomes of shorthorn sculpin (*M. scorpius*) operate maximally between 5 and 7 Hz at 4 °C, and 8 – 13 Hz at 15 °C (Johnson and Johnston, 1991; Johnston and Temple, 2002). These differences between different swimming modalities highlight the underlying muscle mechanics affect the optimal parameters under which musculature functions; the relatively slow contractile frequencies noted here for cuttlefish muscle likely derive from how these animals swim, as well as the temperature. The work and power output of cuttlefish mantle muscle was largely unaffected by animal growth, however it was noted the muscle of larger cuttlefish operated at lower cycle frequencies to produce peak work and power

outputs, a similar situation is seen with the abdominal myotomes of Atlantic cod as these muscles show a leftward shift as animals increase in length, coupled with a broader plateau in smaller animals, but power output is greater in larger animals, possibly as a result of increased muscle mass (Altringham and Johnston, 1990).

This work noted muscle undergoing cyclic contraction fatigued rapidly, highlighting the anaerobic nature of this musculature (Kier and Schachat, 2008; Kier and Thompson, 2003). The use of anaerobic musculature is common among animals which perform high power escape behaviours, where the pectoralis muscle of blue-breasted quail (*Coturnix chinensis*), the iliofibularis muscle of desert iguanas (*D. dorsalis*), and the adductor muscle of scallops are all fuelled anaerobically (Askew and Marsh, 2002; Johnson *et al.*, 1993; Marsh and Olson, 1994). This presents a trade-off in locomotive flexibility, where animals can maximise short-term speed through recruitment of CMP fibres, however, this may limit available space to recruit SMR fibres. CMP fibres play a key role in the production of escape jets, where muscle capable of sustained activity is unrequired. This trade-off is well documented in nature, where the swim performance of Atlantic cod (*Gadus morhua*) shows individual variation, with animals favouring either burst performance or prolonged aerobic swimming (Reidy *et al.*, 2000). This trade-off likely differs between cephalopod lineages as a result of behavioural and/or physiological differences.

3.5.2 Limitations of this study

During the experiments presented here the temperature was maintained at 11 ± 0.5 °C. This temperature was chosen as a result of the sea temperature from which adult animals were captured. Juvenile animals were maintained at 15 °C to ensure animals reached the required size to carry out these experiments. This represents a 4 °C difference in the experimental and housing temperatures. The comparable work of Thompson *et al.* (2008; 2010) was undertaken at 20 ± 0.2 °C with animals housed at 14 °C representing a 6 °C difference. Thompson *et al.* note this temperature difference falls within that experienced naturally by the longfin squid; the 4 °C temperature difference of this study also falls within natural variability of sea temperatures within

the English Channel (Cefas, 2012; Huntance, 2010). Long term temperature trends, and their variability were reported by Huntance (2010), these data reveal the temperature variability within the English Channel can be as much as 5 °C over a typical 2 – 4 week period; this temperature variability suggests local ectotherms, such as cuttlefish, must accommodate rapid changes in temperature. Seibel *et al.* (1997) noted Californian and Hawaiian cephalopods which undergo diel migrations are able to cope with rapid temperature changes of between 5 – 10 °C. The ability of animals to accommodate such temperature changes was noted to be dependent upon the environment particular cephalopods inhabit, with cephalopods inhabiting deep-sea environments less able to cope with deviations in temperature (Seibel *et al.*, 1997).

Despite these local-level factors, it is nonetheless important to note these differences in experimental temperatures may have impacted upon the performance of the musculature. Studies of fish musculature have revealed changes in contractile properties, as well as a muscles aerobic capacity change with decreasing temperature (James, 2013; Johnston and Maitland, 1980). Such studies have revealed crucian carp (*Cyprinus carpio*) acclimated to high (28 ± 1 °C) or low (8 ± 1 °C) temperatures for 6 weeks alter how muscle fibres are recruited, particularly fast-twitch (anaerobic) fibres (Rome *et al.*, 1985). Cold acclimated fish recruit low-twitch fibres more rapidly at lower temperatures as a result of reduced mechanical power generated by slow-twitch fibres (Johnson and Johnston, 1991). These changes represent a change in the muscle structure, and are thought to be particularly pronounced in fast-twitch fibre types. The contractile properties of amphibian muscle however seem largely unaffected by acclimation temperature, with both isometric and isotonic contractile properties remaining stable across temperatures; the Sartorius muscle of both northern leopard frogs (*Rana pipiens*) and American toads (*Bufo americanus*) show no significant difference in the shortening velocity, tetanic tension, or maximum mechanical power, of animals maintained in cold (5 ± 1 (5 weeks); 12 ± 1 (8 months) °C) or warm (25 ± 1 (5 weeks); 28 ± 1 (8 months) °C) environments (Renaud and Stevens, 1984; Rome, 1983). The impacts of acclimation temperature on molluscan musculature has received limited attention, the work of Bailey and Johnston (2005) has demonstrated the mechanical properties of the adductor muscle of queen scallops (*Aequipecten*

opercularis) acclimated to 5, 10 or 15 °C were largely unaffected, with no significant impacts upon maximum shortening velocity, tension or power, nor did this impact other aspects of locomotion (such as jet velocity or thrust) (Bailey and Johnston, 2005); however the musculature of bivalve and cephalopod molluscs may differ, suggesting future work should address this current gap in knowledge, especially given changing temperatures associated with climate change.

The results presented here using preparations from adult animals may also be affected by these animals being in a breeding state, having been captured during the breeding season. Cuttlefish are semelparous, investing all energy and resources into reproductive activity prior to death, as such it is likely mechanical performance is affected by this (Allen *et al.*, 2017; O'Dor and Webber, 1991; Wells, 1994). Previous work has suggested cephalopods may degrade muscle tissues during these spawning events (Moltschaniwskyj, 1994; Moltschaniwskyj, 2004), with little-no feeding taking place. This may explain why results were so variable between adult preparations. Despite this, the results presented by Milligan *et al.* (1997) do show similar levels of variability and overlap with the results presented here, this is particularly evident in tetanic stress values, as well as twitch rise and relaxation times (Table 7). Looking more closely at the data presented in Table 7 the values of cephalopods appear to be variable across all the studies presented, with much less variability seen in bay scallops (*A. irradians*). The underlying reason for such variability may simply reflect smaller sample sizes, but may also reflect differences between muscle types, where the structure of obliquely striated muscle gives flexibilities not seen in other muscle types, which may see greater variation in muscle dynamics between animals (Kier and Schachat, 2008). Further work with larger sample sizes may be able to address these questions, and allow greater understanding of the flexibility bestowed upon animals with this muscle type.

Through the course of this study the *in vitro* parameters used were those which maximised the performance of the musculature; these parameters may however not perfectly match the situation seen *in vivo*. The *in vivo* estimates presented here suggest the strain of free-swimming animals was 0.19 ± 0.04, *in vitro* preparations used

a strain amplitude of 0.075, yielding a strain range of 0.15 (due to use of a sinusoid wave). The manner in which strain was calculated for whole animals (using changes in animal circumference) suggests the strain amplitude used here is not dissimilar to what would be expected (0.075 vs 0.095), suggesting the parameters used here to maximise muscle performance closely match the conditions seen in whole animals.

3.5.3 Transfer efficiency of muscular energy into the wake

While Hill (1950) and other scaling models (McMahon, 1973; Quillin, 1998) provide information on how muscular power scales, these models do not account for other forces which may influence how external forces influence the transfer of muscular power into useful momentum. Alexander (2005) highlighted the power required for swimming results from induced power, which is the power required to drive water backwards; parasite power, which describes the power required to overcome drag; and inertial power the power required to move appendages associated with movement. Parasite and inertial power are applicable to cephalopod jet propulsion swimming, but inertial power is not (Alexander, 2005). The ratio of parasite power to total available power (parasite power + induced power) is used to describe the Froude efficiency of animals; this measure of propulsive efficiency is thought to be less comprehensive than the whole cycle efficiency of animals, as presented in Chapter 2, as it does not account for the intake phase involved in jet propulsion swimming (Alexander, 2003; Anderson and Grosenbaugh, 2005). Alexander (2005) noted previous estimates of squid Froude efficiency are much lower than the undulatory swimming of fishes. This has been suggested to result from the transfer of mechanical energy to a small volume of water, Alexander (2005) therefore suggested measures of induced power (i.e. mechanical power) were needed to assess the efficiency of cephalopod locomotion.

Using the juvenile data from this chapter together with that from Chapter 2, an estimate of the transfer efficiency of muscle was taken. Transfer efficiency is used to describe the proportion of the mechanical energy from the musculature that is

transferred into the wake of the animal. These animals were similarly sized with the mantle length of juveniles from Chapter 2 being ~30-40 mm, and 44-47 mm here, experimental temperatures differed somewhat with the PIV experiments of Chapter 2 being carried out at 15 ± 1 °C, and the experiments here taking place at 11 ± 0.5 °C. Taking the data from this chapter upon the mechanical work generated by the mantle muscle during cyclical contractions. For each contraction cycle the mean work generated by the mantle musculature was 35.44 ± 5.29 mJ. The useful energy in the wake was 9.12 ± 1.08 mJ, giving a transfer efficiency of 25.74%. Note that there are a number of potential sources of error in the estimation of transfer efficiency. First, different animals of different sizes were used for the muscle contractile measurements and the wake analysis. Second, the mechanical work generated by the entire mantle muscle was estimated by scaling up that generated by a fascicle bundle to the mass of the whole mantle. Third, the strain used in the contractile measurements was arbitrary and may not reflect that used *in vivo*; also, there could be regional variation in strain *in vivo* as demonstrated in Guinea fowl (*Numida meleagris*) (Carr *et al.*, 2011), pigeons (*Columba livia*) (Dial and Biewener, 1993), and longfin squid (*D. pealeii*) (Thompson *et al.*, 2014). Fourth, the jets produced *in vivo* may not be from maximal swims, and finally experimental temperatures differed which may have influenced mechanical output. Despite these limitations, this represents the first estimate of this nature in cephalopod molluscs, and seems to be in agreement with the *in silico* study of Yalcinkaya *et al.* (2016) which suggests the transfer efficiency of brief squid (*L. brevis*) mantle muscle would be 24.82 %.

3.6 Summary

This chapter provided an insight into the how the mechanical properties of the obliquely striated muscle of the cephalopod mantle change from juvenile to adult stages. This revealed isometric contractile properties scaled with mantle length, with a decline in twitch kinetics, but shortening velocity remaining largely uncoupled from mantle length. Measures of cyclic muscle activity highlighted decreases in peak cycle frequencies. Overall muscle function did not strongly scale, suggesting the scaling of

cuttlefish mantle muscle may meet the assumptions of Hill's (1950) geometric similarity model, where the contractile features of cuttlefish mantle muscle are uncoupled from animal size, with the absolute power available for burst swimming in cuttlefish increasing with increased body size. The results of this chapter along with that of Chapter 2 were then used to calculate the transfer efficiency, revealing this was ~26%, highlighting much of the mechanical energy from musculature is not transferred into useful movement. The next chapter will further build upon the work presented in this chapter to investigate the underlying biochemical changes associated with mechanical work at selected cycle frequencies. This will enable a greater understanding of how muscle utilises energy, enabling the calculation of contractile efficiency (how effectively energy from ATP hydrolysis is converted into mechanical work). Taken together with the previous two chapters, this will enable the efficiency of the jet propulsive system to be estimated.

Chapter 4. The efficiency of the mantle muscle during cyclical contractions

4.1 Abstract

The mantle musculature of cephalopod molluscs plays a key role in both routine swimming and escape responses. The swimming behaviour of European common cuttlefish (*Sepia officinalis*) is characterised by slow swimming with the fins, while the jet is primarily involved in escape responses. The understanding of the efficiency with which biochemical energy is converted to mechanical work by muscles is of key importance, providing information relating to how effectively animals utilise available resources, and how this trades off against the production of mechanical power output during high performance activities. This study utilised an *in vitro* technique to cyclically contract cuttlefish mantle muscle at three frequencies (0.8, 1.4 and 2 Hz); muscle samples were then frozen and analysed biochemically to assess changes in three key metabolites: ATP, arginine and arginine-phosphate. ATP and arginine-phosphate significantly declined following cyclical contractions; with metabolite profiles differing between the three stimulation frequencies, muscle stimulated at lower frequencies utilised ATP and phosphagen stores more heavily than at higher frequencies. These metabolite changes were then used to estimate the contractile efficiency, the ratio of average mechanical work to average energy input from ATP metabolism, of musculature, revealing this did not differ significantly between the cycle frequencies tested. The proportion of the energy released from ATP hydrolysis which results in useful mechanical work (the contractile efficiency) was 26%. These data suggest that the mantle muscle of cuttlefish utilises a lower proportion of the input biochemical energy to produce useful mechanical work than other lineages.

4.2 Introduction

The movement of swimming animals results from an energy cascade during which chemical energy derived from food is ultimately transferred to the water as useful kinetic energy, generating thrust which moves the animal (Whipp and Wasserman, 1969). The energy imparted to the water is derived from the mechanical work generated by the an animal's musculature, and utilises chemical energy during crossbridge cycling and ion pumping (Baker *et al.*, 2010; Whipp and Wasserman, 1969). The availability of ATP often acts as a limiting factor upon how long muscular work (and thus movement) can continue. The processes of oxidative metabolism resynthesizes ATP, with the rate of ATP synthesis and depletion determining if processes can be fuelled wholly aerobically, or if anaerobic processes must be utilised with a period of aerobic recovery afterward (Askew and Marsh, 2002; Ballantyne, 2004; Di Santo *et al.*, 2017). The musculature associated with the production of escape behaviours typically consists of muscle fibres which contract rapidly and are able to produce appropriate force (Askew and Marsh, 2002). Such muscle types typically work anaerobically, as a result of reduced mitochondrial densities; maximising myofibrillar cross-sectional area to maximise force and power production by musculature (Askew and Marsh, 2002; Kier and Thompson, 2003; Willmer *et al.*, 2004), utilising available ATP and phosphagen reserves to fuel burst activity. Burst activity such as this is typically followed by a recovery stage, where animals aerobically restore metabolite levels to those before muscular activity occurred (Askew and Marsh, 2002; Ballantyne, 2004).

The transfer of chemical energy into mechanical energy, like all processes, involves inefficiencies, where energy is lost. These inefficiencies can occur through a variety of processes, such as the creation of heat as a result of incomplete energy transfer, and the creation of end products which inhibit muscular or enzymatic processes, amongst others. To better understand how effectively energy is utilised by animal musculature, several methodologies of calculating this have been suggested. Smith *et al.* (2005) reviewed the range of methodologies which have been established to calculate the efficiency with which chemical energy is transferred into mechanical energy. These

methodologies can be broadly divided into four key techniques (Figure 32). The first, termed the thermodynamic efficiency of cross-bridge cycling (η_{x-b}), estimates efficiency based upon the heat output of musculature, utilising knowledge of the heat produced by the hydrolysis of ATP. The second method, termed the initial efficiency (ε_i), is perhaps the most simplistic, where the mechanical work is divided by the Gibbs free energy or the change in enthalpy (Smith *et al.*, 2005; Whipp and Wasserman, 1969). Net efficiency (ε_{Net}) is similar to ε_i, but accounts for oxidative recovery processes. The final method, is the overall efficiency ($\varepsilon_{Overall}$). $\varepsilon_{Overall}$, builds further upon ε_{Net} through the inclusion of all metabolic processes, this being the inclusion of the basal metabolism as well as the processes being investigated to calculate the impact of mechanical work upon the uptake of oxygen or other metabolites (Smith *et al.*, 2005).

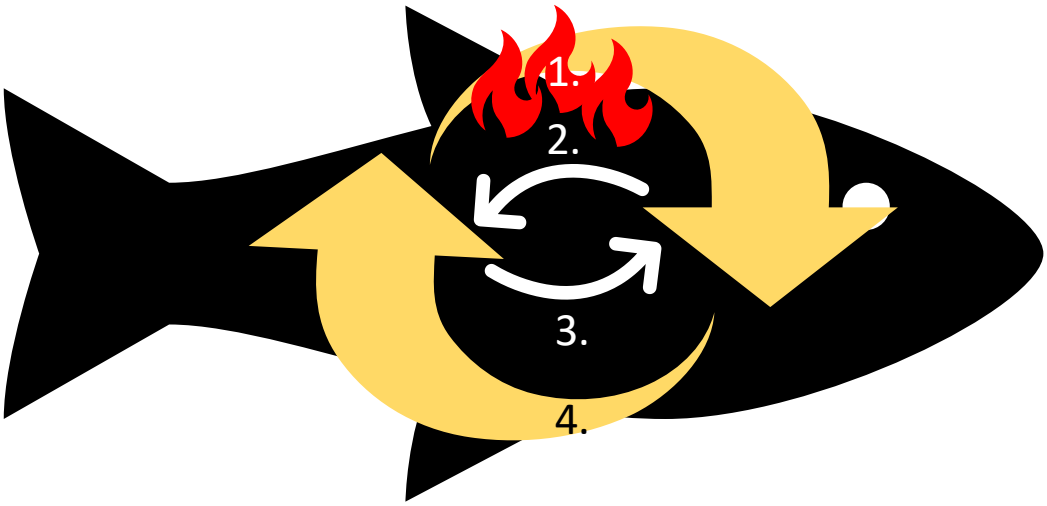

Figure 32. Diagram indicating the relationship between the different efficiency measures. 1. Indicates the heat produced by the catabolism of ATP during muscular activity (the thermodynamic efficiency of cross-bridge cycling). 2. Indicates the initial efficiency, where biochemical energy is converted to mechanical energy. 3. Indicates the aerobic recovery phase acting against the processes of 2. Taken together 2. and 3. yield the net efficiency. The overall efficiency takes the underlying metabolism of the animal into account (4.), overall efficiency is the sum of basal metabolism + the energy used for muscle activity + energy use through recovery processes (Smith *et al.*, 2005).

The efficiency with which such muscles are able to convert chemical energy into mechanical work is of key importance (Smith *et al.*, 2005). Muscles able to convert chemical energy into mechanical energy at a greater efficiency enables them to sustain contractile activity for longer periods of time without fatigue (Smith *et al.*, 2005; Whipp and Wasserman, 1969). Increased muscle efficiency may also impact upon the survival of animals, since energy that is not used during locomotion could be utilised for other key processes such as growth and reproduction (Alexander, 1999; Husak and Fox, 2008; Priede, 1977; Snell *et al.*, 1988). As such, selective pressures may exist to ensure locomotor systems remain as efficient as possible, particularly in environments where resources are limited or unpredictable (Aerts *et al.*, 2000; Alexander, 1999). Efficiency may however trade-off against the production of muscular power; where key processes, such as escaping predation or antagonistic interactions, may favour the production of power over efficiency (Vanhooydonck *et al.*, 2014; Wilson and James, 2004). This contractile efficiency is likely influenced by the cycle frequency of musculature, where Curtin and Woledge (1993) noted the fast-twitch fibres of dogfish (*Scyliorhinus canicula*) white myotomal muscle showed differences in initial efficiency at different cycle frequencies. The contractile efficiency of dogfish musculature showed a bell-shaped relationship between cycle frequency and contractile efficiency, with a distinct plateau at frequencies which produced the maximal net muscular power (Curtin and Woledge, 1993b). However, Curtin and Woledge (1996) noted muscular power and initial efficiency did not always align and suggested that there is a trade-off against one another, where the production of greater muscular power would be less efficient (more energetically costly) than producing lower muscular power (Curtin and Woledge, 1996).

The mantle musculature of the cephalopod molluscs plays a key role in both locomotion through jet propulsion, and respiration (O'Dor, 2002; Portner *et al.*, 1996). This musculature is arranged into two key types which are analogous to the fast- and slow-twitch fibres of vertebrates, with fast-twitch fibres located centrally, and slow-twitch fibres surrounding these (Kier and Thompson, 2003; Figure 13). The mantle musculature is primarily made up of fast-twitch anaerobic muscle fibres [termed central-mitochondria poor (CMP) fibres; Kier and Thomspon, 2003]. These fibres are

thought to power much of the muscle activity during jet propulsion swimming, particularly during escape swimming (Kier and Schachat, 2008; Thompson and Kier, 2002). Previous work has revealed that cephalopods fuel muscular contractions primarily through carbohydrate and protein metabolism (Storey and Storey, 1978), with little to no fat reserves present. During anaerobic activity cephalopods are thought to firstly utilise available ATP within the muscle before replenishing ATP though dephosphorylation of arginine-phosphate (ArgP) through the action of arginine kinase: ArgP + ADP + $H^+ \leftrightarrow$ ATP + Arg. As arginine levels begin to rise, and as a means of maintaining the redox balance within musculature, octopine is formed from arginine and pyruvate via the action of octopine dehydrogenase (Arginine + pyruvate + NADH + $H^+ \leftrightarrow$ Octopine + NAD^+ + H_2O) (Portner *et al.*, 1996; Storey and Storey, 1979). Previous work investigating how metabolites change during hypoxia and exercise in cuttlefish (*S. officinalis*) have revealed octopine is accumulated, while arginine-phosphate, arginine, and ATP are depleted (Capaz *et al.*, 2017; Storey and Storey, 1979).

In order to quantify efficiency, energy utilisation and mechanical work generation must both be measured. Measurement of energy utilisation in anaerobic musculature can be achieved in a variety of ways, which range from measures of thermal changes (Kretzschmar, 1975; Smith *et al.*, 2005), down to various biochemical techniques (Feala *et al.*, 2007; Lowry and Passonneau, 1972; Smith *et al.*, 2005), such as enzymatic processes, as used here. The anaerobic metabolism of cephalopod musculature is known to utilise ATP, arginine and arginine-phosphate to fuel contractile activity. To enable the measurement of changes in these metabolites, controlled conditions are required which mimic the cyclical contractions that occur during locomotion. These contractile conditions and use of *in vitro* approaches ensure mechanical work can be quantified, enabling the contractile efficiency of the musculature to be estimated.

The mantle musculature of the European cuttlefish (*S. officinalis*) was used to measure efficiency under a range of conditions which simulate jet propulsion swimming, a key step in understanding swimming energetics. It was hypothesised that cycle frequency would impact contractile efficiency, with cycle frequencies observed *in vivo* expected to be the most efficient.

4.3 Methods

4.3.1 Animals

Juvenile European cuttlefish were reared from eggs taken as by-catch upon fishing gear by RK Stride, Christchurch, Dorset, UK, during May 2016 in the English Channel. Eggs and hatchlings were maintained as described previously (Chapter 2; Chapter 3). Animals were housed in two recirculating artificial saltwater systems (Aqua One Reef synthetic, Kong's (Aust.) Pty Ltd, Sydney, NSW, Australia) of 357.9 litres (length × width × height; 91 x 69 x 57 cm), at a temperature of 11 ± 1 °C and salinity of 32 ± 1 PSU, this temperature was gradually decreased from 15 ± 1 °C once animals were three-months old. Animals were fed bi-daily on alternate days using live river shrimp (*Palaemon varians*; Aquatic Live fish foods, Woodford, London, UK). Cuttlefish were reared for 12 months under these conditions, with final group sizes consisting of up to 30 animals per tank.

Water quality was monitored to ensure suitable ranges were maintained; temperature and salinity were monitored twice-daily; pH (7.8-8.1) and nitrogenous compounds were monitored monthly ($NH_4 \leq 0.5$ mg L^{-1}; NO_2: ≤ 0.2 mg L^{-1}; $NO_3 \leq 80$ mg L^{-1}). 25% water changes were carried out twice per week. The maintained parameters for temperature and salinity fell within the natural range of animals in the English channel (10.8-16.7 °C; 31.89-34.49 PSU) (Cefas, 2012).

4.3.2 Muscle preparation

Muscle preparations were dissected out as described in Chapter 3. Briefly, this involved a bundle of fibres being dissected out (approximately 40% from the tip of the ventral mantle). Cuttlefish were euthanized in accordance of schedule 1 of the Animals in Scientific Procedures Act; animals were chilled to 4 °C in artificial seawater before the brain, vertical and optical lobes were destroyed by pithing. This alternate

procedure was used as opposed to the home office recommended approach (as used in Chapter 3) due to the distress caused by the administration of magnesium chloride.

Dissected sections were pared down to select the central zone of the muscle. Muscle dissections were carried out within artificial seawater. The dissected out preparations were tied at each end using suture thread (2-0 USP, Black braided silk non-absorbable, non-sterile surgical suture, LOOK surgical specialities corporation, Reading, PA, USA) and a stainless steel metal ring placed on each end. Preparations were then attached to one end of a Perspex chamber, and the other ring attached to the arm of an ergometer (see Figure 24; Aurora Scientific Dual-mode lever system model 300B-LR, Aurora Scientific Inc., Aurora, ON, Canada). Approximately 500 ml of artificial seawater at 11 ± 0.5 °C were recirculated through the flow-through muscle chamber.

Immediately following the addition of muscle preparations to the chamber a series of isometric twitches were used to optimise length to that which yielded the highest twitch force. Length was optimised as described previously (Chapter 3). Briefly this involved muscles being subject to brief stimuli and these being optimised to a length which gave peak active force. Once muscle length was optimal, preparations were subjected to cyclic contractions using the work-loop technique (Josephson, 1985). Each muscle was subject to sinusoidal length changes at one of three frequencies: 0.8, 1.4 or 2 Hz. The timing and duration of stimulation that maximised net power output previously determined (Chapter 3) were used. Frequencies were selected based on previous work which suggested 1.4 Hz closely matched *in vivo* observations of jet cycle frequency (1.39 Hz; Chapter 3). 0.8 and 2Hz were selected as frequencies above and below the *in vivo* cycle frequency.

Each muscle preparation was subject to a series of cycles at these frequencies. At 0.8 and 1.4 Hz preparations were subject to 15 cycles. The number of cycles was increased to 30 at 2 Hz as muscle force continued to increase up to the 15^{th} cycle. Following work loops, muscles were immediately removed from the experimental chamber, placed in a 1.5 ml micro tube (Sarstedt AG & Co. Kommanditgesellschaft, Nümbrecht,

Oberbergischer Kreis, Köln, Nordrhein-Westfalen, Germany), weighed and frozen in liquid nitrogen before being stored at -80 °C. The weighing and freezing process took 30 seconds in total, with recovery expected to be minimal over this time; Melzner *et al.* (2006) noted the recovery of the phosphagen pool following exercise is slow in cuttlefish, with the process taking between 150-200 minutes (recovery rate of 0.05—0.06 μmol g^{-1} min^{-1} at 15 °C) to return levels to levels recorded at rest (Melzner *et al.*, 2006). Each muscle preparation was paired with a control, non-exercised sample. These control samples were weighed and frozen under liquid nitrogen prior to the exercised preparation experiments taking place, and stored at -80 °C. A total of 25 preparations were used, of which 8 were subject to cycles at 0.8 Hz, 8 at 1.4 Hz, and 9 at 2 Hz.

Following each experiment, the remaining mantle muscle was dissected out and weighed (and added to the mass of the control and experimental muscle preparation) to give the total mass of the mantle musculature.

Data from cyclic contractions were used to determine net work and net power (as described in Chapter 3), the cycle average mechanical work output was determined as the average mechanical output of all muscle cycles, power was determined by multiplying work by the cycle frequency.

4.3.3 Sample preparation

Metabolites were freed from tissues using a modification of the methods of Olson and Marsh (in preparation); frozen muscle preparations were placed in 2 ml micro tubes (Eppendorf, Hamburg, Germany) and homogenised in 6 % perchloric acid (Honeywell Fluka, Honeywell International Inc., Morris Plains, NJ, USA) in 40 % ethanol (Sigma-Aldrich, St Louis, MO, USA; ratio of one part muscle to two parts solution) maintained at -20 °C for 20 minutes using a bead mill homogeniser (Qiagen TissueLyser LT, Qiagen, Hilden, North Rhine-Westphalia, Germany). Homogenised samples were then transferred to 1.5 ml micro tubes and centrifuged at 10,000 g for 30 minutes at room

temperature (Sigma 1-14 Microfuge, Sigma Laborzentrifugen GmbH, Osterode am Harz, Niedersachsen, Germany). The supernatant was then collected and neutralised with 0.125 volumes 3 M potassium carbonate (Fisher Chemical, Pittsburgh, PA, USA) in 50 mM MES buffer (Alfa Aesar, Haverhill, MA, USA). Neutralised samples were centrifuged again at 10,000 g for 15 minutes and the final supernatant collected and stored at -80 °C.

4.3.3.1 Measurement of ATP

The ATP content of samples was determined following Lowry and Passonneau (1972). ATP content of samples was determined through a two-step reaction, facilitated by the action of hexokinase and glucose-6-phosphate dehydrogenase:

ATP + Glucose → ADP + Glucose-6-Phosphate

[Hexokinase]

Glucose-6-Phosphate + $NADP^+$ → 6-phospho-glucono-1,5-lactone + NADPH + H^+

[Glucose-6-Phosphate dehydrogenase]

NADPH absorbs light at 340, with the increase in absorbance being used to determine the content of ATP as a result of stoichiometry of reactions.

The reaction mixture consisted of 25 mM Tris-HCl (Lonza, Castleford, W. Yorks., UK), 1 mM magnesium chloride (Fluorochem ltd. Hadfield, Derbs, UK), 0.5 mM dithiothreitol (DTT; Fluorochem), 1 mM glucose (Sigma-Aldrich), 0.5 mM NADP (Merck chemicals ltd., Darmstadt, Germany) and 50 µl neutralised homogenate in a final volume of 2 ml. The reaction was initiated by the simultaneous addition of 1 unit of glucose-6-phosphate dehydrogenase (G6Pdh) and 1 unit of hexokinase (HK; Sigma-Aldrich). Prior to the addition of G6Pdh and HK the absorbance was read at 340 nm, 1 cm light path (Ultrospec 2100 Pro UV/Visible spectrophotometer, Biochrom, Harvard Bioscience Inc., Holliston, MA, USA). 20 minutes after the addition of G6P and HK absorbance was re-read.

A blank was included in all runs to correct for any absorbance associated with materials within reaction mixtures and the cuvette itself, the blanks were at the same volume containing 50 µl water instead of homogenate.

4.3.3.2 Measurement of arginine and arginine phosphate

The content of arginine and arginine phosphate was determined within samples following Mira de Orduna (2001). Arginine content of samples were determined through a three-step reaction, facilitated by the action of arginase, urease and glutamate dehydrogenase:

Arginine + Water → Urea + Ornithine

[Arginase]

Urea + Water → $2NH_3 + CO_2$

[Urease]

2-Oxoglutarate + NADPH + NH_4^+ → Glutamate + $NADP^+$ + Water

[Glutamate dehydrogenase]

NH_3 disassociates in water to become NH_4^+:

$H_2O + NH_3 \rightarrow OH^- + NH_4^+$

NADPH absorbs light at 340 nm, with the decline in absorbance being used to determine the content of arginine as a result of stoichiometry of reactions.

Arginine phosphate (ArgP) content was determined using the same reaction pathways, with ArgP dephosphorylated using 1 M hydrochloric acid (following Morris and Adamczewska (2002); Fisher Chemical). Hydrochloric acid was added in the same ratio as muscle homogenate (i.e. 50 µl) and samples heated for 90 s at 100 °C. Samples were cooled before 50 µl of 1 M sodium hydroxide (Fisher Chemical) was added to neutralise.

Reactions were carried out using the K-large L-arginine assay kit (Megazyme ltd, Wicklow, Ireland). Each assay was carried out at room temperature, and made to a final volume of 1.345 ml; this contained 50 µl neutralised homogenate, 1 ml deionised water, 0.15 ml buffer solution (containing triethanolamine (TEA), polyvinylpolypyrrolidone (PVPP), α-ketoglutaric acid (α-KG), ADP, orthophosphoric acid, 2-oxoglutarate and sodium azide) , and 0.10 ml NADPH. Prior to any enzyme addition the solution was gently mixed and left 2 minutes, the absorbance was then measured at 340 nm, 1 cm light path. 10 µl of the glutamate dehydrogenase solution were then added, the cuvette inverted to mix, and the absorbance measured again after 5 minutes. 25 µl urease solution was then added and the cuvette inverted to mix, the absorbance was measured after 6 minutes. Finally 10 µl arginase solution was added to the cuvette, the cuvette inverted to mix, and the absorbance measured after 7 minutes or until absorbance became stable.

An internal blank was included in all runs to correct for any absorbance associated with materials within reaction mixtures and the cuvette itself, the blanks were at the same volume containing 50 µl water instead of homogenate.

Absorbance measures were converted to concentrations of metabolites in accordance with Beer's law, where the cuvette volume (*V*; ml), the molecular mass (M_r) of ATP (507.18 g mol^{-1}) or arginine (174.2 g mol^{-1}), the extinction coefficient of NADH (6.22 millimoles) or NADPH (6.3 millimoles) at 340 nm, light path (d; cm) and the sample mass (m_c; g) were used to calculate this as:

$$c = \frac{V \times M_r}{\varepsilon \times d \times m_c} \times \Delta Absorbance$$

Equation 15.

4.3.3.3 Estimation of ATP used during exercise

The changes in metabolite concentrations between control and worked musculature were used to estimate the total ATP use associated with cyclic muscle work. The stoichiometry of metabolic pathways allowed estimation as 3 moles ATP are produced per 2 moles of arginine lost and 1 mole of ATP is produced for every 1 mole of Arg-P dephosphorylated. Total mass specific ATP use was calculated as:

$$ATP_{total} = 1.5 \times \Delta[\text{Arginine}] + \Delta[\text{ArgP}] + \Delta[\text{ATP}]$$

Equation 16. Total ATP (ATP_{total}) use during exercise. Calculated from the changes in arginine, arginine-phosphate and ATP levels between control and worked muscle.

4.3.4 Contractile efficiency

The efficiency with which energy from ATP was transferred into mechanical work was calculated assuming the free energy from ATP hydrolysis was 45 kJ mol^{-1} (Portner *et al.*, 1996). In calculating contractile efficiency the ratio of free energy from ATP and the muscular work were used (Equation 17). Recovery was not accounted for in this calculation, and is expected to be minimal due to the slow metabolic rates of cuttlefish (Lamarre *et al.*, 2016; Speers-Roesch *et al.*, 2016), suggesting efficiency measures presented here mostly closely resemble initial efficiency calculations (Smith *et al.*, 2005; Whipp and Wasserman, 1969).

$$\eta_c = \frac{W_c}{W_m}$$

Equation 17. The contractile efficiency (η_c) was calculated as the ratio of cycle average mechanical work (W_c) output to the cycle average energy input (from ATP metabolism; W_m).

4.3.5 Statistical analysis

Data were analysed using IBM SPSS Statistics 24 (International Business Machines Corporation, Armonk, NY, USA). All data were tested for normality and homogeneity prior to statistical testing; as data were non-normally distributed and could not be transformed to meet these assumptions, data were analysed using nonparametric tests. Comparisons of metabolite concentrations between control and cyclically worked muscle preparations was achieved using Wilcoxon signed rank tests due to the paired nature of the data. Comparisons of the percentage change in metabolite concentrations between cycle frequencies were achieved using Kruskal-Wallis tests. Comparisons of ATP_{total} (Determined from equation 16) and derived parameters between cycle frequencies were determined using Kruskal-Wallis tests. Statistical significance was defined by a threshold of 0.05, a correction for multiple testing (e.g. Bonferroni) was not applied due to paired tests not influencing other tests (following the recommendations of Armstrong, 2014), and to avoid the risk of increasing type II errors in subsequent tests.

4.4 Results

4.4.1 Anaerobic metabolite concentrations

The metabolite profiles differed between the three cycle frequencies tested here, raw data values are reported in Table 12. A cycle frequency of 0.8 Hz resulted in significant declines in arginine-phosphate (ArgP) and ATP content between control and worked musculature (ArgP: *W* 2, n 8, p 0.025; ATP: *W* 3, n 9, p 0.021; Figure 33; Table 12). At 1.4 Hz arginine-phosphate levels significantly declined (*W* 10, n 8, p 0.023; Figure 33; Table 12), while at the highest frequency used (2 Hz) significant declines in arginine-phosphate were noted (*W* 2, n 9, p 0.025; Figure 33; Table 12). Despite differences in metabolite levels, the percentage change in ATP (*H* 0.325, df 2, p 0.85), arginine phosphate (*H* 4, df 2, p 0.135) and arginine (*H* 1.395, df 2, p 0.498) did not differ between cycle frequencies (Table 12).

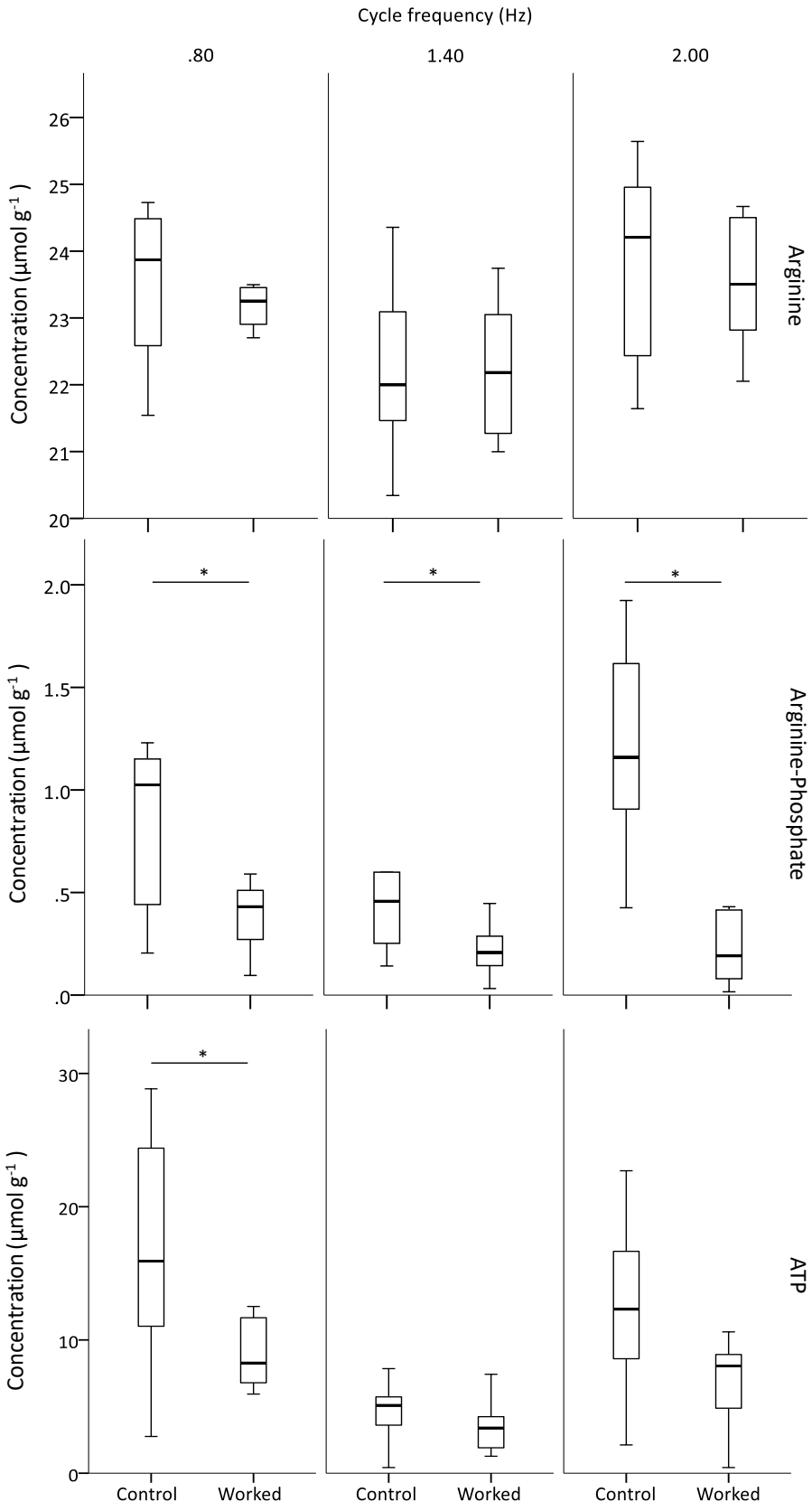

Figure 33. Boxplot showing the concentration of arginine, arginine-phosphate and ATP in control (unworked) and worked muscle (1 cycle at 0.8 (n=8), 1.4 (n=8) or 2 (n=9) Hz).* indicates significant differences between control and worked concentrations at the 0.05 level.

Table 12. Content of ATP, arginine phosphate and arginine present in control and exercised mantle preparations, as well as the percentage change in the mean metabolite levels. Bold text indicates significant differences between control and worked muscle samples, data presented ± sd.

Frequency (Hz)	ATP			Arginine phosphate			Arginine			n
	Control (µmol g^{-1})	Worked (µmol g^{-1})	Percentage change (%)	Control (µmol g^{-1})	Worked (µmol g^{-1})	Percentage change (%)	Control (µmol g^{-1})	Worked (µmol g^{-1})	Percentage change (%)	
0.8	**17.14 ± 9.28**	**9 ± 2.52**	**-47 ± 23**	**2.3 ± 4.55**	**0.51 ± 0.53**	**-69 ± 24**	21.04 ± 7.52	23.26 ± 0.54	+2 ± 7	8
1.4	5.29 ± 3.68	3.48 ± 1.69	-50 ± 28	**1.1 ± 1.73**	**0.26 ± 0.2**	**-54 ± 31**	20.64 ± 5.65	20.63 ± 4.99	-0.2 ± 6	8
2.0	12.49 ± 6.53	6.84 ± 3.27	-50 ± 27	**2.08 ± 2.76**	**0.23 ± 0.17**	**-75 ± 22**	23.81 ± 1.47	23.55 ± 0.96	-4 ± 6	9

4.4.2 Total anaerobic ATP use during exercise

The total ATP (ATP_{total}; calculated from Equation 16) consumed per cycle at 0.8 Hz was 0.98 ± 0.6 µmol g^{-1}, 0.4 ± 0.26 µmol g^{-1} at 1.4 Hz and 0.45 ± 0.45 µmol g^{-1} at 2 Hz. Total ATP use per cycle was significantly affected by cycle frequency (*H* 6.02, df 2, p 0.049; Table 13; Figure 35), ATP consumption rates were however unaffected by cycle frequency (*H* 0.962, df 2, p 0.618), where 0.78 ± 0.48 µmol s^{-1} were utilised at 0.8 Hz, 0.56 ± 0.36 µmol s^{-1} at 1.4 Hz and 0.91 ± 0.9 µmol s^{-1} at 2 Hz.

Table 13. Pairwise comparisons between cycle frequencies. Comparisons reveal significant differences in total ATP (ATP_{total}) consumption per cycle between 0.8 Hz and other cycle frequencies.

Comparison	Test statistic	Significance
1.4 vs 2 Hz	0.375	0.92
0.8 vs 2 Hz	7.931	0.033
0.8 vs 1.4 Hz	7.556	0.036

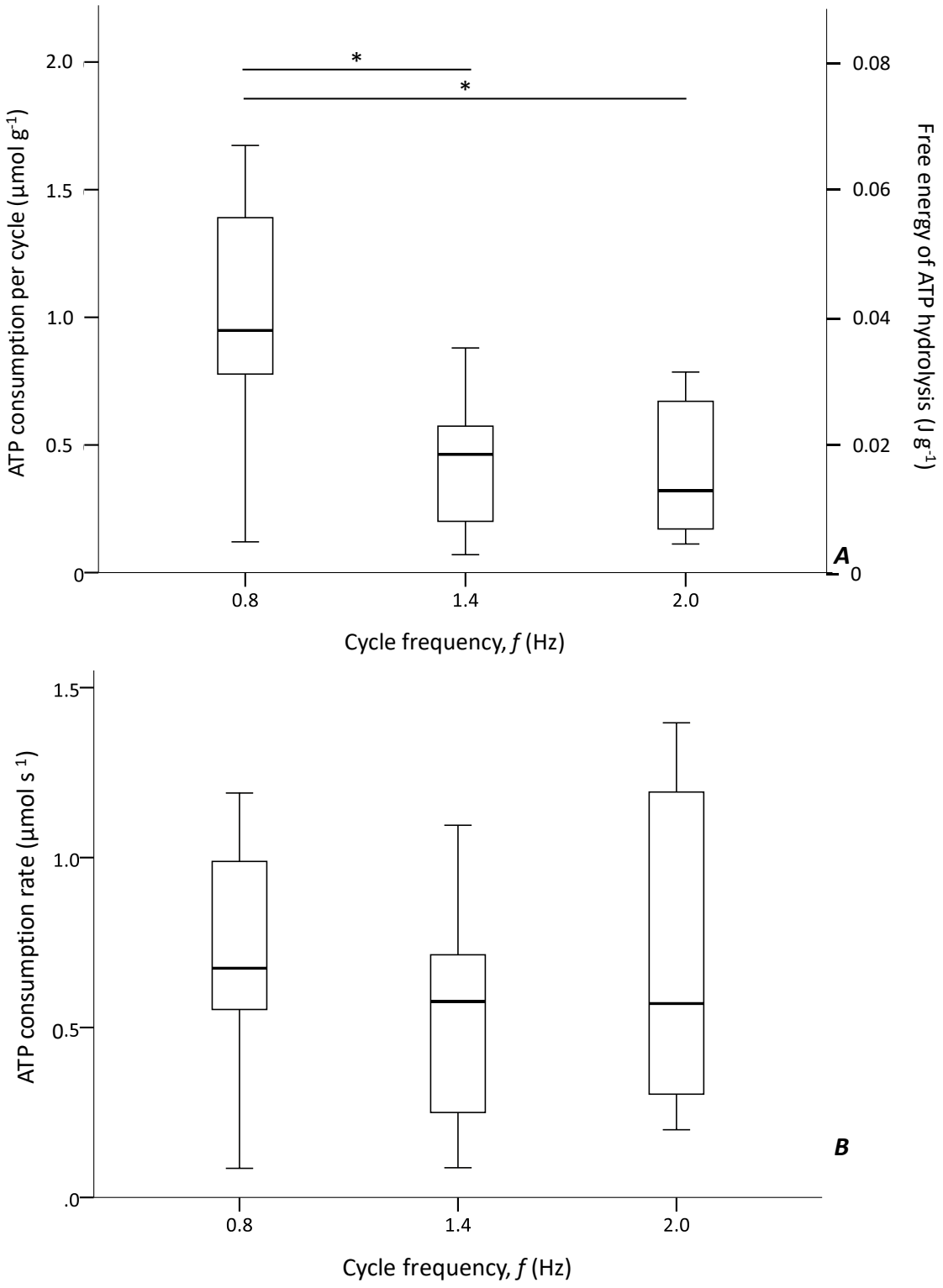

Figure 34. Boxplots showing the total ATP consumption by cuttlefish mantle muscle. A) ATP consumption per cycle and free energy from ATP hydrolysis, B) ATP consumption rate. ATP use per cycle and the free energy from ATP hydrolysis were significantly affected by cycle frequencies. ATP consumption rates did not differ significantly between cycle frequencies. * denotes significant differences at the 0.05 level.

4.4.3 Contractile properties of mantle musculature

The contractile properties of cuttlefish mantle musculature are described in detail in Chapter 3. To obtain the contractile efficiency of cyclic contraction of this musculature, the net work per cycle (W_c) was calculated, this revealed mean W_c was 0.004 ± 0.002 J g^{-1} (3.88 ± 1.82 J kg^{-1}; for a full breakdown of these data in J kg^{-1} and comparisons to Chapter 3 data, see Appendix 3), work per cycle did not significantly differ between the cycle frequencies tested here (*H* 0.284, df 2, p 0.868; Figure 35).

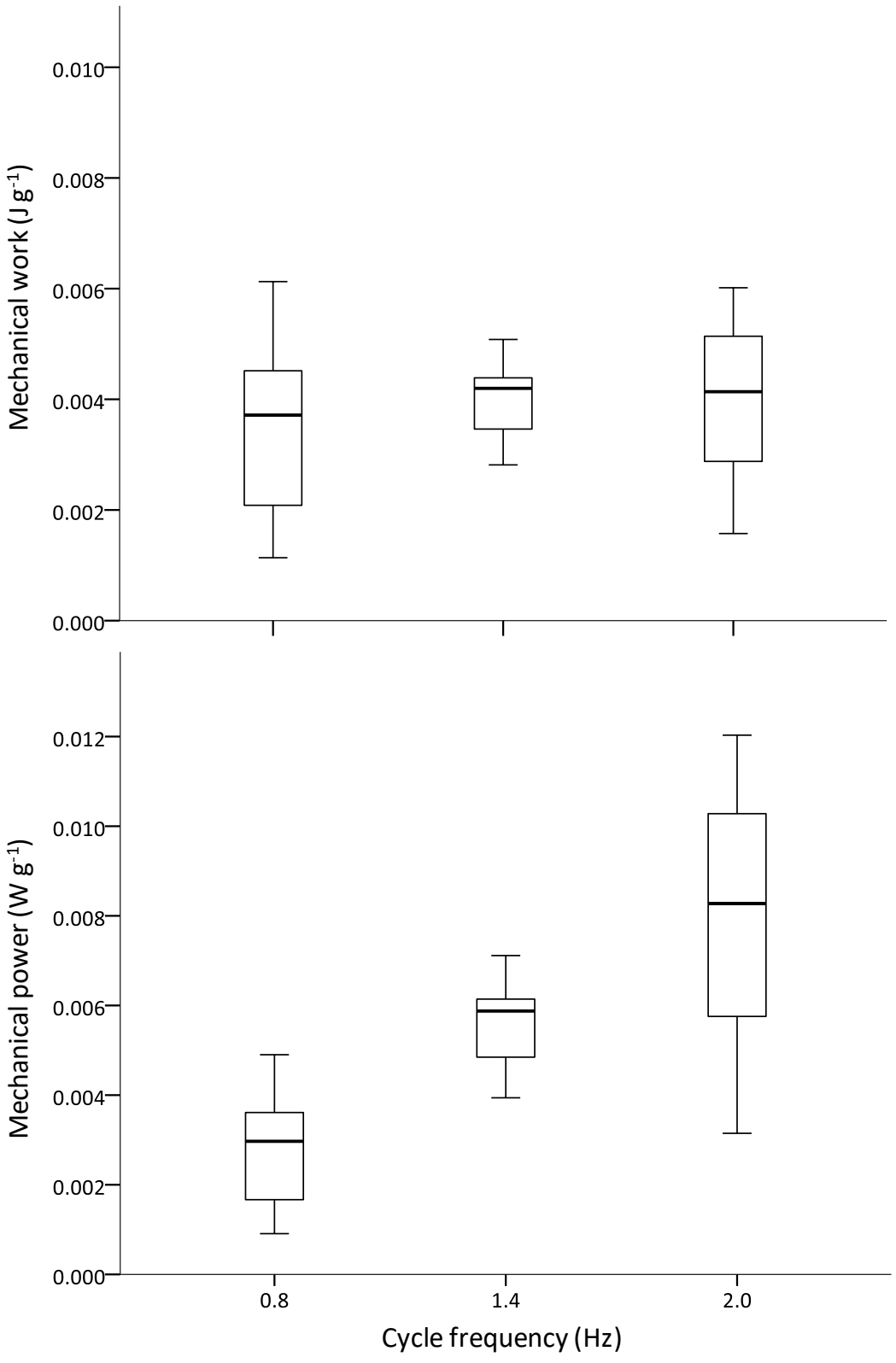

Figure 35. Boxplots of mechanical work and power per cycle at 0.8 (n=8), 1.4 (n=8) and 2 (n=9) Hz. Mean power per cycle increased with cycle frequency in these preparations.

4.4.4 Contractile efficiency

Contractile efficiency did not significantly differ between cycle frequencies (*H* 4.572, df 2, p 0.102; raw values are shown in Table 14). Data were pooled as a result, revealing the overall contractile efficiency of cuttlefish mantle muscle was 0.26 ± 0.26 (ranging between 0.03-0.88). The mean energy release from metabolites was 0.19 ± 0.18 J per cycle, with a mean mechanical work of 0.03 ± 0.02 J per cycle.

Table 14. Contractile efficiency at different muscle cycle frequencies. No significant differences were found between muscle cycle frequencies.

Cycle frequency (Hz)	Mean energy release from metabolites (J; ± sd)	Mean mechanical work (J; ± sd)	Mean contractile efficiency (± sd)	n
0.8	0.34 ± 0.21	0.03 ± 0.02	0.17 ± 0.2	8
1.4	0.08 ± 0.06	0.02 ± 0.01	0.29 ± 0.25	8
2	0.15 ± 0.13	0.03 ± 0.01	0.34 ± 0.33	9

4.5 Discussion

4.5.1 The contractile efficiency of cephalopod musculature

The efficiency with which biochemical energy is transferred into mechanical energy by the cuttlefish mantle muscle was 0.26 ± 0.05 (sem). Comparisons with theoretical work reveals the contractile efficiency of cuttlefish muscle is very similar to the expected contractile efficiency of brief squid (*L. brevis*) mantle muscle, where an efficiency of 0.23 was expected during escape responses and 0.28 during steady-state swimming (Yalcinkaya *et al.*, 2016). Wider comparisons with other molluscan lineages suggest cuttlefish musculature contractile efficiency falls short of other jet propelled molluscs,

such as spear (*Chlamys hastata*) and bay scallops (*Argopecten irradians*), where contractile efficiencies of the adductor muscle have efficiencies of 0.30 ± 0.03 and 0.37 ± 0.03 (Olson and Marsh, in preparation). These differences in mean contractile efficiency may reflect differences between these two lineages, where cuttlefish mantle muscle serves as both support and a locomotive element, unlike the adductor of scallops (Jereb and Roper, 2005; Lee *et al.*, 2014; O'Dor and Webber, 1991). Similarities in the range of contractile efficiency suggest this musculature has some similarities in its use and structure, likely as a result of both scallops and cuttlefish utilising muscle primarily for escape (Cheng *et al.*, 1996; Helmer *et al.*, 2017; Jastrebsky *et al.*, 2016), where muscle acts as one unit due to extensive coupling between muscle fibres (Kier and Thompson, 2003; Olson and Marsh, in preparation).

Wider comparisons with the musculature of vertebrates reveals measures of molluscan contractile efficiencies are somewhat lower. Curtin and Woledge (1993) revealed the contractile efficiency of dogfish (*S. canicula*) white myotomal muscle was 0.379 ± 0.022 (corrected to 0.41 by Smith *et al.* 2005), while the contractile efficiency of fast twitch fibres of mouse (*M. musculus*) soleus muscle was 0.34 ± 0.03 (Barclay, 1994). To enable further comparisons published values were corrected to remove the impact of recovery processes. Recovery was assumed to account for 61% of a measured value (Hinkle, 2005; Hinkle *et al.*, 1991), with this being used to correct the contractile efficiency as: $\eta_{c[est]} = (\varepsilon_{Overall}-((\varepsilon_{Overall}/100)*61))/\varepsilon_{Overall}$. This revealed the contractile efficiency of the sartorius muscle of edible frogs (*Rana esculenta*) was 0.4, while mammalian muscle was broadly similar with the extensor digitorum longus (EDL) muscle and soleus muscle of Wistar rats (*R. norvegicus*) with only 0.37 and 0.4 (Abbate *et al.*, 2002; Heglund and Cavagna, 1987). These results seem to highlight limited variability in the contractile efficiency of vertebrate muscle. However, when compared with molluscan muscle, efficiency seems greater in vertebrates, where a greater proportion of the chemical energy is converted into mechanical work. This difference may arise for a variety of factors, such as the differences in muscle structure and function, but may also arise as a result of differential metabolic profiles among muscle types (Willmer *et al.*, 2004). Indeed Curtin and Woledge (1993a,b) found that the initial efficiency of aerobic red muscle fibres of the dogfish (*S. canicula*) myotomal muscle

was ~10% higher than white muscle fibres (0.51 vs 0.41) (Curtin and Woledge, 1993a; Curtin and Woledge, 1993b; Smith *et al.*, 2005). Such differences between muscle types are likely related to how musculature is used, where musculature involved in burst performance usually has high phosphagen stores (Portner *et al.*, 1996; Seebacher and Walter, 2012) enabling musculature to act quickly and maximise mechanical work. Such musculature can maximise efficiency in the short-term, but this efficiency may be offset by post-exercise recovery being required, and muscle rapidly fatiguing, the results with dogfish suggest that while this musculature can have comparable efficiencies to other vertebrate muscle types, this still seems to fall short of fuelling muscle aerobically.

The low contractile efficiency of cuttlefish mantle muscle is perhaps the lowest value recorded to date (Smith *et al.*, 2005). The underlying cause of this low efficiency seems to stem from inefficient transfer of the energy released from ATP hydrolysis into useful mechanical work. Comparisons with fast-twitch muscle of other lineages (worked at similar temperatures) reveals the power output of cuttlefish muscle is very similar, where the white myotomal muscle of dogfish (*S. canicula*) worked cyclically at 12 °C was able to achieve muscular powers of up to ~20 W kg^{-1} (Curtin *et al.*, 2010). Cuttlefish mantle muscle worked at 11 °C achieved very similar values of up to ~25 W kg^{-1} (Chapter 3). Why cuttlefish muscle is less efficient is unclear, but likely represents a trade-off, where efficiency is traded in favour of the production of power. Askew and Marsh (2002) suggest animals which rely upon burst performance may favour high power output in the short term to maximise responses. Given the role of the mantle muscle in escape responses, it seems the production of short-term power would be favoured over the efficiency of such a system; the work of Curtin *et al.* (2010) notes the power output of slow-twitch myotomal muscle is 75 % lower than the power output of fast-twitch muscle (5 vs 20 W kg^{-1}), with this amounting to a 10 % difference in contractile efficiency (Curtin and Woledge, 1993a; Curtin and Woledge, 1993b). A similar situation may exist in cuttlefish, where routine swimming is more efficient, with this likely also influenced by the dual-mode nature of the cuttlefish locomotive system, where routine swimming is likely aided by switching from jet to undulatory (fin) locomotion. It is clear more work is needed to assess the efficiency of slow-twitch

musculature of cuttlefish, and how this relates to the fast-twitch muscle investigated here.

4.5.1.1 The impact of cycle frequency on contractile efficiency

The contractile efficiency of cuttlefish mantle musculature did not differ significantly between the three cycle frequencies used (see Table 14). This suggests cycle frequency may not be strongly coupled to contractile efficiency in cuttlefish, though the lack of differentiation may result from the relatively narrow band of frequencies tested or the high variability of results, suggesting more work is needed to establish if contractile frequency and efficiency are connected or independent of one-another. Barclay (1994) noted the efficiency of mouse soleus varied with cycle frequency, with this being particularly evident during aerobic contractions, where a 22 % difference was noted between the lowest efficiencies (0.30 ± 0.03; 0.5 Hz) and the highest efficiencies (0.52 ± 0.01; 3 Hz). Curtin and Woledge (1993a, b; 1996) noted a similar situation, where cycle frequency impacted contractile efficiency. The limited difference seen here may be related to how muscle fibres are recruited and contraction is controlled; cephalopod musculature is known to show extensive coupling between fibres, with this aiding in the rapid and coordinated contraction of the mantle (Bone *et al.*, 1982; Milligan *et al.*, 1997; Zullo *et al.*, 2017). Under such situations, an all-or-nothing response by the musculature of the mantle is seen; this is likely during escape responses, where animals are known to jet while shielding their direction of travel through the release of ink clouds or pseudomorphs (Bush and Robison, 2007; Wood *et al.*, 2010; Wood *et al.*, 2008), under such situations maximising the efficiency of muscular contraction is likely to trade-off against increasing the likelihood of survival.

4.5.2 The impact of work on metabolite levels

In fuelling muscle anaerobically cephalopods utilise the available ATP before moving onto available arginine-phosphate and arginine (Capaz *et al.*, 2017; Storey and Storey, 1979). As a result, availability of these molecules needs to be high to fuel this

musculature; arginine stores are substantially higher than those of arginine-phosphate and ATP within this musculature, these high arginine levels, and equally high glycogen stores within cuttlefish mantle musculature (Storey and Storey, 1979) likely play a key role in fuelling this musculature during burst activity. As part of this work it was noted the resting levels of these metabolites seemed to vary between preparations, Robertson (1965) provided one of the few comprehensive studies of the metabolites present within cephalopod muscle tissues, with this noting phosphates were stored in four forms within cephalopod tissues: inorganic phosphates (P_i); arginine phosphate; ATP; and hexose phosphate, variability of ATP levels could perhaps be explained by animals storing phosphates through one of these alternative routes (Robertson, 1965). Such variability in metabolites does however seem to be a common feature among cephalopods, with Grieshaber and Gade (1976) noting arginine phosphate and arginine levels within the mantle muscle of European common squid (*L. vulgaris*) varied by as much as 37.7 and 32.5 µmol g^{-1}, while Storey and Storey (1979) noted ATP, arginine phosphate and arginine varied between preparations, with deviations from the mean values of between 1.6 and 4.4 µmol g-1 in European common cuttlefish (S. officinalis). The underlying reason for this variability is unclear, but may relate to variability in the storage molecules used by animals, perhaps as a result of diet, different pathway use or differences in local muscle fibres (Grieshaber and Gäde, 1976; Robertson, 1965; Storey and Storey, 1979). Despite these differences in resting levels it was noted the changes in metabolite levels were remarkably similar. Here it was noted ATP and arginine-phosphate levels significantly declined as a result of exercise, changes in total arginine levels were less pronounced, perhaps as a result of replenishment through the action of arginine kinase, where arginine-phosphate is degraded to replenish ATP levels within the muscle tissue. Some information relating to metabolite levels may have been lost as a result of recovery processes. Previous work has noted recovery of energy stores is slow in the mantle muscle of cuttlefish (*S. officinalis*), where Melzner *et al.* (2006) noted recovery rates of between 0.05 and 0.06 µmol g^{-1} min^{-1} at 15 °C. The work carried out here was at a slightly lower temperature (11 ± 0.5 °C) which would likely reduce recovery rates further, as well as this all preparations were subject to the same 30 second interval between work loops and flash-freezing, suggesting the impacts of this process are minor.

4.5.2.1 Interspecific comparisons

The utilisation of available resources during exercise by cephalopod mantle musculature has previously been investigated using longfin squid (*D. pealeii*). Such studies have revealed significant declines in available ATP and arginine-phosphate following exercise, as well as significant increases in arginine (Storey and Storey, 1978). These results are in agreement with the findings here where both ATP and arginine-phosphate levels significantly declined while minor increases in arginine were noted. Storey and Storey (1978) noted the changes in arginine-related compounds and ATP levels were strongly linked to swimming, however levels of anaerobic end-products, notably octopine, did not seem to accumulate in squid musculature; this finding contrasts with that of Storey and Storey (1979) which found exhaustive exercise in cuttlefish leads to significant declines in ATP, arginine-phosphate while arginine and octopine accumulate within this musculature. This work is in agreement with both studies in noting declines in ATP and arginine-phosphate following exercise, and increases in arginine levels.

The decline in arginine-phosphate and ATP levels are a common feature during the swimming mechanics of many animals. Bailey *et al.* (2003) demonstrated arginine-phosphate levels would significantly decline as a result of exercise in three scallop species – the queen scallop (*Aequipecten opercularis*), king scallop (*P. maximus*) and Antarctic scallops (*Adamussium colbecki*). These changes in arginine-phosphate levels were strongly linked to the workload of the animal, with a greater number of claps more strongly depleting phosphagen levels (Bailey *et al.*, 2003). Bailey *et al.* (2003) found no relationship between ATP use and the workload of the muscle, with the suggestion this was being replenished from phosphagen stores within the musculature. The data presented here seem to broadly agree with these findings with pronounced arginine-phosphate depletion, however the overall decline of ATP in cuttlefish muscle was greater than the minor differences noted by Bailey *et al* (2003); this decline may be as a result of greater resting levels of ATP within the cuttlefish muscle measured here, though the resting levels of ATP in cuttlefish did show substantial variability. Relatively high levels of ATP within cuttlefish muscle likely

enable animals to quickly utilise this before more complex biochemicals are utilised. Similar results to those noted by Bailey *et al.* (2003) were seen with Christmas Island red crabs (*Gecarcoidea natalis*). Exercise in these crabs results in significant declines in arginine-phosphate levels while arginine levels significantly increase, similar to the findings of Bailey *et al.* (2003) ATP levels did not see any significant changes as a result of exercise, with the suggestion this results from replenishment through dephosphorylation of arginine-phosphate (Morris and Adamczewska, 2002).

This general pattern of phosphagen depletion and accumulation of metabolites is seen across taxa; unlike molluscs and arthropods, vertebrates utilise creatine phosphate as a phosphagen store. Underlying processes are broadly similar, with creatine accumulation occurring following exercise, as demonstrated in the crucian carp (*Carassius carassius*) where intensive exercise leads to significant increases in creatine levels (Johnston and Goldspink, 1973), while creatine-phosphate is utilised as a phosphagen store, as noted with skipjack tuna (*Katsuwonus pelamis*) where intensive exercise leads to a significant decline in phosphagen stores (Arthur *et al.*, 1992). Similarly, Dobson and Hochachka (1987) and Dunn and Johnston (1986) noted significant declines in creatine-phosphate and ATP levels, while creatine levels significantly increased in the white epaxial muscle of rainbow trout (*Oncorhynchus mykiss*) and the white muscle myotomes of yellowbelly rockcod (*Notothenia neglecta*) (Dobson and Hochachka, 1987; Dunn and Johnston, 1986). These findings seem to agree with the findings here. This seems to paint the general picture where the escape responses of animals are fuelled by through the utilisation of phosphagen and ATP stores, while other compounds, such as lactate and octopine are accumulated as end products as a means of maintaining the internal pH of musculature, but also as a means to ensure ATP levels are maintained.

4.5.3 Metabolite profiles and muscle cycle frequency

The frequency with which muscle preparations performed cyclical work seemed to impact the metabolite profiles of the musculature. During lower frequency work ATP stores were more heavily impacted, while at the highest frequency significant declines

were seen in arginine-phosphate. These changes in metabolite content are suggestive of differential underlying processes having taken place within the musculature to ensure ATP levels are maintained within the muscle, ensuring muscle activity can continue, these differences may however result solely from variation in the resting levels of metabolites, with the percentage changes in metabolites being similar across cycle frequencies.

4.5.3.1 Interspecific comparisons

This work is the first to directly address the role of cyclic muscle activity in cephalopod molluscs, and how this impacts metabolite profiles of this musculature, as a result no intraspecific comparisons can be made. Previous work investigating the impact of the number of cycles muscle undergoes and its metabolic profile reveals differences among species and between locomotive systems. Dobson and Hochachka (1987) noted the levels of creatine phosphate and ATP both declined as tail beat frequency increased in rainbow trout (*O. mykiss*). Similarly, Guppy *et al.* (1979) noted the use of ATP differed between steady and burst swimming in skipjack tuna (*K. pelamis*), where significant declines were noted during burst activity, but little difference occurred during steady swimming. Creatine-phosphate however declined under both scenarios suggesting the significant decline in ATP seen during burst swimming represents the utilisation of both freely available ATP and creatine-phosphate stores (Guppy *et al.*, 1979). Within the cuttlefish musculature lower cycle frequencies seemed to heavily utilise ATP, while higher frequencies seemed to replenish ATP levels through the utilisation of arginine-phosphate and possibly arginine. These results are perhaps unsurprising when considering the underlying processes within musculature, where higher cycle frequencies are associated with more rapid cross-bridge formation and decoupling (Abbate *et al.*, 2002; Whipp and Wasserman, 1969). The reduction in arginine levels suggest musculature may be beginning to utilise arginine to maintain ATP levels within the musculature through the action of octopine dehydrogenase, though the lack of significant declines suggests the ATP and arginine-phosphate levels within musculature fuel much of the burst performance. Octopine dehydrogenase plays an analogous role to lactate dehydrogenase in vertebrate musculature (Capaz *et*

al., 2017), work with skipjack tuna (*K. pelamis*) has demonstrated intensive exercise leads to the accumulation of lactate (Arthur *et al.*, 1992), minimal arginine utilisation suggests burst activity is primarily fuelled through the utilisation of available ATP and phosphagens in cuttlefish.

Through the course of this work the impact of cycle frequency upon the efficiency and metabolite profiles of cuttlefish mantle musculature were investigated. This revealed efficiency was largely unaffected by muscle cycle frequency, this similarity between cycle frequencies may reflect the underlying function of this muscle, where the creation of a jet requires the simultaneous activity of muscles throughout the mantle cavity. Previous work has also reported a plateau in muscular efficiency in relation to cycle frequency, the plateau region of efficiency vs frequency includes the mean frequency observed during free swimming, suggesting the contractile efficiencies are maximised at frequencies used by animals. It is expected that efficiency will decrease at lower and higher cycle frequencies than those investigated in this study, suggesting more work is needed to gain further insight into the contractile efficiency of cephalopod musculature; with particular emphasis upon the frequency at which efficiency starts to fall off, giving insight into the energetics of swimming when different jet frequencies are used. When looking in greater detail at these different cycle frequencies it became evident muscle cycle frequency led to differences in the metabolite profile of musculature, with lower frequencies appearing to more heavily utilise ATP and phosphagen stores. Taken together, these results reveal ATP and phosphagens fuel the contractile activity of cuttlefish muscle, with 26 % of the available energy released from ATP hydrolysis resulting in useful mechanical work.

4.6 Summary

Through the course of this work three key questions were explored using the mantle musculature of the European cuttlefish (*S. officinalis*). In answering the first of these it was noted intensive exercise resulted in significant declines in both ATP and arginine-phosphate, however arginine levels showed no significant changes, despite minor

increases. Secondly, the impact of muscle cycle frequency was explored, revealing lower cycle frequencies significantly affected ATP use per cycle, however this did not affect ATP consumption rates. Finally, the contractile efficiency of musculature was calculated revealing 26 % of the energy from metabolic processes within the muscle was transferred to mechanical processes. This is one of the lowest values reported to date, seeming to confirm jet propulsion as an inefficient mode of locomotion. Taken with the results of the previous two chapters, the efficiency of the system is estimated in the next chapter, with the implications of this discussed further.

Chapter 5. General Discussion

This thesis investigated the transduction of energy through the locomotive system of European cuttlefish (*S. officinalis*) from the biochemical level through to the transfer of mechanical power to the water, the key findings relating to the efficiency of the energy transduction chain are summarised in Figure 36. This has provided an insight into how these animals utilise energy stores to fuel muscle, the biomechanical properties of this musculature and how this scales, as well as hydrodynamics and wake properties of jets produced to move through the water.

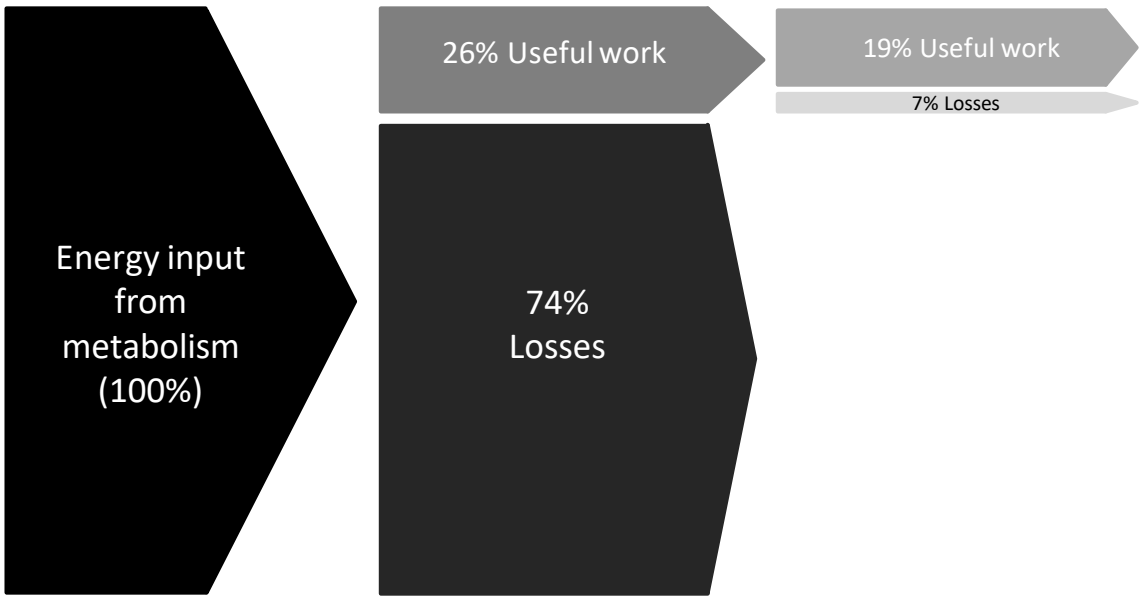

Figure 36. The energy cascade during contractile activity of the circular muscle of the cuttlefish mantle. Where the efficiency with which energy input from ATP hydrolysis is transferred into useful mechanical work is estimated to be 26 %, of this 19 % is transferred into useful propulsive work.

5.1 The contractile efficiency, and biochemical changes of mantle muscle during cyclical contractions

The work of muscle utilises chemical energy in the form of ATP (Willmer *et al.*, 2004). This ATP is supplied through underlying chemical processes within animal tissues, be

these aerobic or anaerobic. The activity of cephalopod mantle muscle is largely driven by anaerobic processes (Kier and Schachat, 2008; Kier and Thompson, 2003); such processes utilise available ATP within tissues before using energy stores held within muscles; these are usually in the form of phosphagens, fatty and/or amino acids and sugars (Morris and Adamczewska, 2002; Willmer *et al.*, 2004). The composition of storage molecules and the end products of anaerobiosis depends largely upon the particular animal and its evolutionary history. This work investigated the impact of cyclic muscular work upon three key metabolites within the mantle musculature of European common cuttlefish. Metabolites were selected based on previous work which noted ATP, arginine-phosphate and arginine play central roles in the anaerobic metabolism of molluscs, including the cephalopods (Bailey and Johnston, 2005; Baldwin and Lee, 1979; Storey and Storey, 1978; Storey and Storey, 1979). Unlike previous studies, this work utilised an *in vitro* approach to investigate the changes in these key metabolites; the use of an *in vitro* approach ensured interfering processes are removed and the number of contractile cycles more closely controlled. These results noted exercised muscle utilised available ATP, phosphagen, and, to a small degree, arginine stores to fuel muscle contraction. The resulting metabolic profiles differed somewhat between the three cycle frequencies tested, however, ATP consumption rates were unaffected. Despite these differences, cycle frequency did not significantly impact contractile efficiency, although an increase in efficiency was noted as cycle frequency increased. The lack of significant differences between contractile frequencies tested suggests this muscle responds in much the same way regardless of contractile frequency. The primary function of the cephalopod fast-twitch mantle muscle is to facilitate escape from predators (O'Dor, 2002); under such conditions muscle is likely to respond maximally to ensure escape is achieved. These escape responses are facilitated by other key behaviours, such as the release of ink clouds or pseudomorphs to distract predators and alert conspecifics, while hiding the escape path of animals (Bush and Robison, 2007; Derby, 2014; Wood *et al.*, 2010; Wood *et al.*, 2008). These scenarios are likely very energetically costly to animals, where the comparatively low efficiency of mantle musculature (~26 %), coupled with the release of melanin-based ink clouds is likely a significant energetic investment, suggesting efficiency may be traded in favour of maximising escape from predation. Interestingly, a trend towards increased contractile efficiency at higher cycle frequencies was noted,

suggesting more rapid escape responses may benefit from increased efficiency, though more work may be needed to investigate if this holds true.

Previous work examining the contractile efficiency of cephalopod mantle musculature is lacking; Yalcinkaya *et al.* (2016) provided some theoretical insight for brief squid (*L. brevis*) locomotion. This suggested contractile efficiency of the central mantle muscle was expected to be similar to what was observed in cuttlefish with this expected to be 23 % in brief squid. The value obtained here seems to largely be in agreement with the work of Yalcinkaya *et al.* (2016), suggesting the efficiency of cuttlefish mantle muscle behaves as predicted for other cephalopods. Wider comparisons reveal the contractile efficiencies of spear (*Chlamys hastata*) and bay scallops (*Argopecten irradians*) are somewhat higher (0.30 ± 0.03; 0.37 ± 0.03) (Olson and Marsh, in preparation). The similarities between predicted values and the values seen in cuttlefish suggest muscle mechanics may be largely similar between these two cephalopod lineages, though it is clear further work is needed to make more accurate comparisons, and further understand the locomotion and underlying physiology in cephalopods. Current understanding of cephalopod physiology, particularly that related to muscular work and anaerobiosis, is somewhat lacking. This work has provided an insight into how cephalopod mantle musculature responds to cyclical muscle contractions in terms of changes in key metabolites and contractile efficiency; it is clear more work is needed to build upon this, and provide further knowledge as to if the patterns seen in cuttlefish mantle musculature is true across cephalopods, or if differences between lineages exist. To further build upon this it is also evident wider knowledge upon the biochemistry and changes associated with exercise of obliquely striated muscle are needed. This muscle type is widespread across invertebrate lineages, yet little work upon its biochemistry and contractile properties exists.

5.2 The mechanical properties and scaling of cuttlefish muscle

The mantle muscle of the cephalopod molluscs plays a key role in locomotion, respiration and as a structural element (Kier, 1988; Kier and Thompson, 2003). The

central role this muscle plays in these processes highlights its importance to the cephalopods. This work has provided an insight into the mechanical properties of this musculature in juvenile and adult animals. Previous work with the mantle muscle of cuttlefish had only investigated its isometric properties, this work built upon this providing an insight into the isotonic properties, as well as the first insight into the cyclic properties of this musculature.

The isometric properties of cuttlefish muscle presented here showed the mantle muscle of juveniles reached tP_{tw} and RT_{50} significantly more rapidly than preparations from adult animals. Interestingly, tetanic responses and the twitch:tetanus ratio showed no significant differences with age; but tetanic stresses did show a weak allometric relationship. Through the course of this work it was noted the twitch:tetanus ratio would decline; a similar situation has been noted with the mantle muscle of longfin squid (*D. pealeii*); the decline in this ratio seems to relate to a decline in twitch responses by musculature (Thompson *et al.*, 2010). The underlying cause of this decline was not investigated here, but previous work upon cephalopod musculature has noted calcium flux within the muscle can act to close myomuscular junctions (Bone *et al.*, 1982; Zullo *et al.*, 2017), this action would act to decrease the local recruitment of muscle fibres, which would be particularly evident during twitch responses. Experiments investigating the isotonic contractile properties of this musculature revealed this relationship fit the hyperbolic-linear relationship of Marsh and Bennett (1986) in both adult and juvenile animals. The maximum velocity of shortening (V_{max}) and power ratio showed no significant decline with age. The lack of differentiation in muscle shortening velocity is perhaps surprising, but may relate to structural differences between the obliquely striated muscle of cuttlefish and vertebrate musculature, or the scaling dynamics of cuttlefish muscle growth. Current understanding of muscle growth in cephalopods has received limited attention, previous work has noted both muscle hyperplasia and hypertrophy seem to occur within the mantle musculature of cephalopods (Moltschaniwskyj, 1994; Moltschaniwskyj, 2004; Pecl and Moltschaniwskyj, 1997). The continued addition of new fibres throughout the entire lifespan of animals is particularly pronounced in the mitochondria poor fibres (Moltschaniwskyj, 1994). This addition of new fibres likely

influences the contractile properties of cephalopod musculature, however, the lack of detailed knowledge upon the muscle structure and how this scales throughout ontogeny could be a fruitful avenue for future research.

Building upon these isometric and isotonic measures the cyclic performance of this muscle was also measured. This provides the first estimate of cyclic performance in this muscle type while also noting minor decreases in the frequency over which cuttlefish mantle musculature achieved maximum work and power. Hill (1950) noted animal muscle, and associated metabolism, is generally faster in smaller animals than their larger counterparts, suggesting this observation of declining muscular contractile velocities and cycle frequencies is to be expected. The iliofibularis muscle of desert iguanas (*D. dorsalis*) showed a similar situation as that noted here where the optimal cycle frequency remained largely similar from hatchling to adult stages (Johnson *et al.*, 1993). Such similarities suggest cuttlefish mantle muscle meets many of the assumptions of Hill's (1950) geometric similarity model (Hill, 1950; Johnson *et al.*, 1993), where muscle work and contractile features are independent of body size.

5.3 The hydrodynamics and scaling of cuttlefish jet propulsion swimming

Through the course of this thesis the structure and hydrodynamics of cuttlefish jet propulsion swimming were investigated. This revealed cuttlefish were able to produce two jet modes. These jet modes were previously identified by Bartol *et al.* (2009a, b) in the brief and longfin squids. Much of the work following that of Bartol *et al.* (2009a, b) has noted these jet modes are common across lineages, with animals from jellyfish (Katija *et al.*, 2015; Neil, 2016), salps (Sutherland and Madin, 2010) and cephalopods (Bartol *et al.*, 2009a; Bartol *et al.*, 2009b; Neil and Askew, 2018) all noted to produce these different jet structures. Interestingly, this work noted a change in the prevalence of jet modes with increased animal size. Newly emerged animals produced nearly exclusively jets of mode I while more mature animals seemed to be utilising both jet mode I and II. This change in the prevalence of jet modes may relate to changes in the

flow environment inhabited by animals, the velocity of fluid transfer to the environment, or the interaction between these two.

The propulsive efficiency of cuttlefish jet propulsion swimming showed a positive correlation with swimming speed, but was largely unaffected by swimming orientation, despite swimming speed appearing to be impacted by this. The efficiency of jets ranged between 0.23 and 0.99; with this range being somewhat higher (0.59-0.99) in hatchlings when compared to juveniles (0.23-0.96). Despite the larger range in juveniles, the propulsive efficiency of cuttlefish locomotion was higher than previous measures taken in squid (0.29-0.44 and 0.34-0.48) (Anderson and Demont, 2000; Bartol *et al.*, 2008). Interestingly, the closest measures among the cephalopods come from the chambered nautilus, Neil and Askew (2018) suggested the high propulsive efficiency of nautiloids (up to ~0.7) may derive from their neutral buoyancy. Like the nautilus, cuttlefish are neutrally buoyant as a result of the cuttlebone, this internalised shell acts to maintain buoyancy through the diffusion of gases into small chambers within (Denton *et al.*, 1961; Sherrard, 2000). Unlike their externally shelled cousins, cuttlefish are less restricted in terms of their locomotion, able to move with increased speed, enabling cuttlefishes to inhabit environments unavailable to externally shelled nautilus (Chamberlain, 1990; Neil, 2016; Neil and Askew, 2018). The increased propulsive abilities bestowed upon cuttlefishes through the retention of cuttlebones may lead many to question why squid and octopus have lost or severely limited these structures. This becomes evident when looking at the habitats cuttlefish are able to inhabit; cuttlefishes are typically found in highly productive shelf seas, but are completely absent from the Americas (Xavier *et al.*, 2016). These shelf seas, while highly productive, are also very competitive environments, this has perhaps driven the cuttlefishes to develop the complex behaviours and camouflage seen today (Darmaillacq *et al.*, 2014; Hanlon, 2007). These competitive environments and high predation rates may also have driven the locomotion of cuttlefish, where retention of the cuttlebone seems to ensure jet propulsion is as efficient as possible. Retention of the cuttlebone has however restricted cuttlefishes to these shelf-sea habitats, where cuttlebones implode below 200 m (Sherrard, 2000). This restriction of cuttlebones has meant these are unsuitable for many squid species, where diurnal migrations or deep

sea environments are favoured to avoid predation (Rosa and Seibel, 2010; Trueblood and Seibel, 2013; Wells and O'Dor, 1991); it appears squid may have traded increased propulsive efficiency of this locomotor system in favour of predator evasion and the ability to inhabit a greater range of habitats.

5.4 How efficiently do cuttlefish utilise energy?

Taken together, these data have enabled the efficiency with which chemical energy is transferred into the water to be calculated. In Chapter 3, the amount of mechanical energy transferred to the water was calculated (termed the transfer efficiency), this revealed at least 26 % of this energy was transferred. However, the data from Chapters 2 and 4, enable an alternative method for calculating the total efficiency: $\eta_T = \eta_c \times \eta_{wc}$, where contractile efficiency is 0.26 ± 0.05 (sem; Chapter 4), and the mean propulsive efficiency of juvenile cuttlefish is 0.73 ± 0.02 (sem; Chapter 2), this yields an efficiency of 19% (Figure 36). This value is slightly lower than that calculated in Chapter 3, but accounts for biochemical energy use. This value is higher than the predicted value of longfin squid (*D. pealeii*; 6.87%), suggesting Yalcinkaya *et al.* (2016) may have underestimated the efficiency of the cephalopod jet propulsion. It is unclear if these differences reflect species-specific differences, or simply a result of model limitations. It is clear more empirical work is needed to solve this, and to give a clearer view of the efficiency of locomotion in animals. The value presented here likely represents the minimum efficiency, as the jets produced *in vivo* may not maximise efficiency. The propulsive efficiency, while high, did vary among individuals and age groups, suggesting a higher efficiency could be met by increased hydrodynamic efficiency, as well as aerobic inputs which were not measured here. Wider comparisons reveal the efficiency of undulatory swimming in rainbow trout (*O. mykiss*) is between 14.5-15.5 % (Webb, 1971), while the labriform swimming of bluegill sunfish (*Lepomis macrochirus*) ranges between 16 and 22 % (Jones *et al.*, 2007). The comparable efficiency of cephalopod jet propulsion swimming when compared to other modes of locomotion seems to stem from high propulsive efficiencies. Looking deeper it does appear the transfer of chemical energy into mechanical energy is lower than in other lineages

(Chapter 4); this is in agreement with the expectations in jet propulsion where propelling small volumes of water at high velocities is more costly than shedding vortices across the length of the body (Alexander, 2003; Maddock *et al.*, 1994).

5.5 Future work

The investigation into the biochemical properties of muscle presented here are limited by the number of metabolites measured. To gain a more complete insight into the biochemical changes associated with jet propulsion swimming in these animals metabolomics technologies could be utilised. The use of 'omics technologies would enable further understanding of how available chemical energy is utilised by the musculature of cephalopods, while also providing an insight into the full biochemistry of these muscles. As well as this, respirometry measures would enable the input of aerobic processes to be estimated, providing further information on the energetic demands and use of musculature, providing more detailed estimates of contractile efficiency. This work provided a comprehensive insight into the contractile properties of this musculature, however all experiments were performed *in vitro* with somewhat limited *in vivo* measures. Future *in vivo* studies could provide further insight into this system under more naturalistic conditions, technologies such as sonomicrometry and pressure gauges could be utilised to measure natural muscle length changes and the pressure changes associated with the jet process.

The work presented here upon the hydrodynamics of cuttlefish jet propulsion swimming presents the first insight into this system; the finding of two jet modes and the changes in their prevalence between the two age groups presents further questions as to how jet structure may relate to the size of animals. Previous work has noted the structure of older squid seem to be more elongate and chaotic in nature, however to date no comprehensive scaling studies have taken place. The work presented here suggests the increasing size of animals may have hydrodynamic effects, which could be investigated further in future. As well as this, the existence of these two jet modes could be reconstructed in greater detail through the utilisation of 3-D

volumetric flow analysis. Such studies would enable a greater understanding of these jet structures, and may also enable the contribution of the fins to be investigated. Here the fins of animals were not investigated, however, these likely play an important role in the locomotion, with Stewart *et al.* (2010) noting the fins of brief squid (*L. brevis*) impact the swim performance of animals both positively and negatively (Stewart *et al.*, 2010).

The estimation of the efficiency by which chemical energy is transferred into momentum presented here gives an indication of the efficiency of jet propulsion systems, this could be built upon through further insights into the efficiency with which biochemicals are obtained from food sources, providing an insight into the whole system. As well as this, it is clear more work is needed to provide more information across lineages to further understand the locomotion of animals.

References

Abbate, F., De Ruiter, C. J., Offringa, C., Sargeant, A. J. and De Haan, A. (2002). *In situ* rat fast skeletal muscle is more efficient at submaximal than at maximal activation levels. *Journal of Applied Physiology* **92**, 2089-2096.

Aerts, P., Van Damme, R., Vanhooydonck, B., Zaaf, A. and Herrel, A. (2000). Lizard locomotion: how morphology meets ecology. *Netherlands Journal of Zoology* **50**, 261-277.

Aitken, J. P. and O'Dor, R. K. (2004). Respirometry and swimming dynamics of the giant Australian cuttlefish, *Sepia apama* (Mollusca, Cephalopoda). *Marine and Freshwater Behaviour and Physiology* **37**, 217-234.

Alexander, R. M. (1999). Energy for animal life. Oxford: Oxford University Press.

Alexander, R. M. (2003). Principles of animal locomotion. Princeton, N.J., ; Woodstock: Princeton University Press.

Alexander, R. M. (2005). Models and the scaling of energy costs for locomotion. *Journal of Experimental Biology* **208**, 1645-1652.

Allen, J. J., Akkaynak, D., Schnell, A. K. and Hanlon, R. T. (2017). Dramatic Fighting by Male Cuttlefish for a Female Mate. *American Naturalist* **190**, 144-151.

Altringham, J. D. and Block, B. A. (1997). Why do tuna maintain elevated slow muscle temperatures? Power output of muscle isolated from endothermic and ectothermic fish. *Journal of Experimental Biology* **200**, 2617-2627.

Altringham, J. D. and Johnston, I. A. (1990). Scaling effects on muscle function - power output of isolated fish muscle-fibers performing oscillatory work. *Journal of Experimental Biology* **151**, 453-467.

Andersen, P. and Henriksson, J. (1977). Training induced changes in the subgroups of human type II skeletal muscle fibres. *Acta Physiologica Scandinavica* **99**, 123-125.

Anderson, E. J. and Demont, M. E. (2000). The mechanics of locomotion in the squid *Loligo pealei*: Locomotory function and unsteady hydrodynamics of the jet and intramantle pressure. *Journal of Experimental Biology* **203**, 2851-2863.

Anderson, E. J. and Grosenbaugh, M. A. (2005). Jet flow in steadily swimming adult squid. *Journal of Experimental Biology* **208**, 1125-1146.

Anderson, E. J., Quinn, W. and DeMont, M. E. (2001). Hydrodynamics of locomotion in the squid *Loligo pealei*. *Journal of Fluid Mechanics* **436**, 249-266.

Anderson, M. E. and Johnston, I. A. (1992). Scaling of power output in fast muscle-fibers of the atlantic cod during cyclical contractions. *Journal of Experimental Biology* **170**, 143-154.

Archer, S. D. and Johnston, I. A. (1989). Kinematics of labriform and subcarangiform swimming in the antarctic fish *Notothenia neglecta*. *Journal of Experimental Biology* **143**, 195-210.

Armstrong, R. A. (2014). When to use the Bonferroni correction. *Ophthalmic and Physiological Optics* **34**, 502-508.

Arthur, P. G., West, T. G., Brill, R. W., Schulte, P. M. and Hochachka, P. W. (1992). Recovery metabolism of skipjack tuna (*Katsuwonus pelamis*) white muscle - rapid and parallel changes in lactate and phosphocreatine after exercise. *Canadian Journal of Zoology-Revue Canadienne De Zoologie* **70**, 1230-1239.

Ashley-Ross, M. A. (2002). Mechanical properties of the dorsal fin muscle of seahorse (*Hippocampus*) and pipefish (*Syngnathus*). *Journal of Experimental Zoology* **293**, 561-577.

Askew, G. N. and Marsh, R. L. (1997). The effects of length trajectory on the mechanical power output of mouse skeletal muscles. *Journal of Experimental Biology* **200**, 3119-3131.

Askew, G. N. and Marsh, R. L. (2001). The mechanical power output of the pectoralis muscle of blue-breasted quail (*Coturnix chinensis*): the *in vivo* length cycle and its implications for muscle performance. *Journal of Experimental Biology* **204**, 3587-3600.

Askew, G. N. and Marsh, R. L. (2002). Muscle designed for maximum short-term power output: quail flight muscle. *Journal of Experimental Biology* **205**, 2153-2160.

Bailey, D. M. and Johnston, I. A. (2005). Scallop swimming kinematics and muscle performance: Modelling the effects of "within-animal'' variation in temperature sensitivity. *Marine and Freshwater Behaviour and Physiology* **38**, 1-19.

Bailey, D. M., Peck, L. S., Bock, C. and Portner, H. O. (2003). High-energy phosphate metabolism during exercise and recovery in temperate and antarctic scallops: An *in vivo* P-31-NMR study. *Physiological and Biochemical Zoology* **76**, 622-633.

Bainbridge, R. (1958). The speed of swimming of fish as related to size and to the frequency and amplitude of the tail beat. *Journal of Experimental Biology* **35**, 109-133.

Baker, J. S., McCormick, M. C. and Robergs, R. A. (2010). Interaction among skeletal muscle metabolic energy systems during intense exercise. *Journal of Nutrition and Metabolism* **2010**, 13.

Baldwin, J. and Lee, A. K. (1979). Contributions of aerobic and anaerobic energy production during swimming in the bivalve mollusc *Limaria fragilis* (Family Limidae). *Journal of Comparative Physiology* **129**, 361-364.

Ballantyne, J. S. (2004). Mitochondria: aerobic and anaerobic design-lessons from molluscs and fishes. *Comparative Biochemistry and Physiology B-Biochemistry & Molecular Biology* **139**, 461-467.

Barclay, C. J. (1994). Efficiency of fast-twitch and slow-twitch muscles of the mouse performing cyclic contractions. *Journal of Experimental Biology* **193**, 65-78.

Bartol, I. K., Krueger, P. S., Stewart, W. J. and Thompson, J. T. (2009a). Hydrodynamics of pulsed jetting in juvenile and adult brief squid *Lolliguncula brevis*: evidence of multiple jet 'modes' and their implications for propulsive efficiency. *Journal of Experimental Biology* **212**, 1889-1903.

Bartol, I. K., Krueger, P. S., Stewart, W. J. and Thompson, J. T. (2009b). Pulsed jet dynamics of squid hatchlings at intermediate Reynolds numbers. *Journal of Experimental Biology* **212**, 1506-1518.

Bartol, I. K., Krueger, P. S., Thompson, J. T. and Stewart, W. J. (2008). Swimming dynamics and propulsive efficiency of squids throughout ontogeny. *Integrative and Comparative Biology* **48**, 720-733.

Bartol, I. K., Patterson, M. R. and Mann, R. (2001). Swimming mechanics and behavior of the shallow-water brief squid *Lolliguncula brevis*. *Journal of Experimental Biology* **204**, 3655-3682.

Bates, D., Maechler, M., Bolker, B., Walker, S. (2015). Fitting linear mixed-effects models using lme4. *Journal of Statistical Software* **67**, 1-48.

Bone, Q. (1966). On the function of the two types of myotomal muscle fibre in elasmobranch fish. *Journal of the Marine Biological Association of the United Kingdom* **46**, 321-349.

Bone, Q., Brown, E. R. and Travers, G. (1994). On the respiratory flow in the cuttlefish (*Sepia officinalis*). *Journal of Experimental Biology* **194**, 153-165.

Bone, Q., Packard, A. and Pulsford, A. L. (1982). Cholinergic innervation of muscle-fibers in squid. *Journal of the Marine Biological Association of the United Kingdom* **62**, 193-199.

Bottom, R. G., Borazjani, I., Blevins, E. L. and Lauder, G. V. (2016). Hydrodynamics of swimming in stingrays: numerical simulations and the role of the leading-edge vortex. *Journal of Fluid Mechanics* **788**, 407-443.

Bouchaud, O. (1991). Energy consumption of the cuttlefish *Sepia officinalis* L. (Mollusca, Cephalopoda) during embryonic development, preliminary-results. *Bulletin of Marine Science* **49**, 333-340.

Burr, A. H. J. and Gans, C. (1998). Mechanical significance of obliquely striated architecture in nematode muscle. *Biological Bulletin* **194**, 1-6.

Bush, S. L. and Robison, B. H. (2007). Ink utilization by mesopelagic squid. *Marine Biology* **152**, 485-494.

Campbell, N. A. and Reece, J. B. (2008). Biology. San Francisco: Pearson Benjamin Cummings.

Capaz, J. C., Tunnah, L., MacCormack, T. J., Lamarre, S. G., Sykes, A. V. and Driedzic, W. R. (2017). Hypoxic induced decrease in oxygen consumption in cuttlefish (*Sepia officinalis*) is associated with minor increases in mantle octopine but no changes in markers of protein turnover. *Frontiers in Physiology* **8**.

Carr, J. A., Ellerby, D. J. and Marsh, R. L. (2011). Function of a large biarticular hip and knee extensor during walking and running in guinea fowl (*Numida meleagris*). *Journal of Experimental Biology* **214**, 3405-3413.

Carroll, A. M., Ambrose, A. M., Anderson, T. A. and Coughlin, D. J. (2009). Feeding muscles scale differently from swimming muscles in sunfish (Centrarchidae). *Biology Letters* **5**, 274-277.

Caruel, M. and Truskinovsky, L. (2018). Physics of muscle contraction. *Reports on Progress in Physics* **81**.

Casey, T. M., May, M. L. and Morgan, K. R. (1985). Flight energetics of *Euglossine* bees in relation to morphology and wing stroke frequency. *Journal of Experimental Biology* **116**, 271-289.

Cefas. (2012). Sea temperature and salinity trends, vol. 2016. https://www.cefas.co.uk/cefas-data-hub/sea-temperature-and-salinity-trends/: Centre for Environment, Fisheries and Aquaculture science.

Celichowski, J. and Grottel, K. (1993). Twitch/tetanus ratio and its relation to other properties of motor units. *Neuroreport* **5**, 201-204.

Chamberlain, J. A. (1990). Jet propulsion of *Nautilus* - a surviving example of early paleozoic cephalopod locomotor design. *Canadian Journal of Zoology-Revue Canadienne De Zoologie* **68**, 806-814.

Chapman, G. (1958). The hydrostatic skeleton in the invertebrates. *Biological Reviews of the Cambridge Philosophical Society* **33**, 338-371.

Cheng, B., Tobalske, B. W., Powers, D. R., Hedrick, T. L., Wang, Y., Wethington, S. M., Chiu, G. T. C. and Deng, X. Y. (2016). Flight mechanics and control of escape manoeuvres in hummingbirds. II. Aerodynamic force production, flight control and performance limitations. *Journal of Experimental Biology* **219**, 3532-3543.

Cheng, J. Y., Davison, I. G. and DeMont, M. E. (1996). Dynamics and energetics of scallop locomotion. *Journal of Experimental Biology* **199**, 1931-1946.

Close, R. I. (1972). The relations between sarcomere length and characteristics of isometric twitch contractions of frog sartorius muscle. *The Journal of Physiology* **220**, 745-762.

Coughlin, D. J. (2002). Aerobic muscle function during steady swimming in fish. *Fish and Fisheries* **3**, 63-78.

Coughlin, D. J., Burdick, J., Stauffer, K. A. and Weaver, F. E. (2001). Rainbow trout display a developmental shift in red muscle kinetics, swimming kinematics and myosin heavy chain isoform. *Journal of Fish Biology* **58**, 701-715.

Coughlin, D. J., Valdes, L. and Rome, L. C. (1996a). Muscle length changes during swimming in scup: Sonomicrometry verifies the anatomical high-speed cine technique. *Journal of Experimental Biology* **199**, 459-463.

Coughlin, D. J., Zhang, G. X. and Rome, L. C. (1996b). Contraction dynamics and power production of pink muscle of the scup (*Stenotomus chrysops*). *Journal of Experimental Biology* **199**, 2703-2712.

Curtin, N. A., Lou, F. and Woledge, R. C. (2010). Sustained performance by red and white muscle fibres from the dogfish Scyliorhinus canicula. *Journal of Experimental Biology* **213**, 1921-1929.

Curtin, N. A. and Woledge, R. C. (1993a). Efficiency of energy-conversion during sinusoidal movement of red muscle-fibers from the dogfish *Scyliorhinus canicula*. *Journal of Experimental Biology* **185**, 195-206.

Curtin, N. A. and Woledge, R. C. (1993b). Efficiency of energy-conversion during sinusoidal movement of white muscle-fibers from the dogfish *Scyliorhinus canicula*. *Journal of Experimental Biology* **183**, 137-147.

Curtin, N. A. and Woledge, R. C. (1996). Power at the expense of efficiency in contraction of white muscle fibres from dogfish *Scyliorhinus canicula*. *Journal of Experimental Biology* **199**, 593-601.

Curtin, N. A., Woledge, R. C. and Bone, Q. (2000). Energy storage by passive elastic structures in the mantle of *Sepia officinalis*. *Journal of Experimental Biology* **203**, 869-878.

Dabiri, J. O. (2009). Optimal vortex formation as a unifying principle in biological propulsion. *Annual Review of Fluid Mechanics* **41**, 17-33.

Darmaillacq, A.-S., Dickel, L. and Mather, J. A. (2014). Cephalopod cognition. Cambridge: Cambridge University Press.

Demont, M. E. and Gosline, J. M. (1988). Mechanics of jet propulsion in the hydromedusan jellyfish, *Polyorchis penicillatus* .2. energetics of the jet cycle. *Journal of Experimental Biology* **134**, 333-345.

Denny, M. (1980). Locomotion - the cost of Gastropod crawling. *Science* **208**, 1288-1290.

Denny, M. W. (1981). A quantitative model for the adhesive locomotion of the terrestrial slug, *Ariolimax columbianus*. *Journal of Experimental Biology* **91**, 195-217.

Denton, E., Gilpin-Brown, J. and Howarth, J. (1961). The osmotic mechanism of the cuttlebone. *Journal of the Marine Biological Association of the United Kingdom* **41**, 351-363.

Deravi, L. F., Magyar, A. P., Sheehy, S. P., Bell, G. R. R., Maethger, L. M., Senft, S. L., Wardill, T. J., Lane, W. S., Kuzirian, A. M., Hanlon, R. T. *et al.* (2014). The structure-function relationships of a natural nanoscale photonic device in cuttlefish chromatophores. *Journal of the Royal Society Interface* **11**.

Derby, C. D. (2014). Cephalopod ink: Production, chemistry, functions and applications. *Marine Drugs* **12**, 2700-2730.

Di Santo, V., Kenaley, C. P. and Lauder, G. V. (2017). High postural costs and anaerobic metabolism during swimming support the hypothesis of a U-shaped metabolism–speed curve in fishes. *Proceedings of the National Academy of Sciences* **114**, 13048-13053.

Dial, K. P. and Biewener, A. A. (1993). Pectoralis-muscle force and power output during different modes of flight in pigeons (*Columba livia*). *Journal of Experimental Biology* **176**, 31-54.

Dobson, G. P. and Hochachka, P. W. (1987). Role of glycolysis in adenylate depletion and repletion during work and recovery in teleost white muscle. *Journal of Experimental Biology* **129**, 125-140.

Domenici, P. and Blake, R. W. (1997). The kinematics and performance of fish fast-start swimming. *Journal of Experimental Biology* **200**, 1165-1178.

Donovan, D. A., Elias, J. P. and Baldwin, J. (2004). Swimming behavior and morphometry of the file shell *Limaria fragilis*. *Marine and Freshwater Behaviour and Physiology* **37**, 7-16.

Dunn, J. F. and Johnston, I. A. (1986). Metabolic constraints on burst-swimming in the Antarctic teleost *Notothenia neglecta*. *Marine Biology* **91**, 433-440.

Ellerby, D. J. and Askew, G. N. (2007). Modulation of pectoralis muscle function in budgerigars *Melopsitaccus undulatus* and zebra finches *Taeniopygia*

guttata in response to changing flight speed. *Journal of Experimental Biology* **210**, 3789-3797.

Ellington, C. P. (1985). Power and efficiency of insect flight-muscle. *Journal of Experimental Biology* **115**, 293-304.

Eloy, C. (2012). Optimal Strouhal number for swimming animals. *Journal of Fluids and Structures* **30**, 205-218.

Fagernes, C. E., Stenslokken, K. O., Rohr, A. K., Berenbrink, M., Ellefsen, S. and Nilsson, G. E. (2017). Extreme anoxia tolerance in crucian carp and goldfish through neofunctionalization of duplicated genes creating a new ethanolproducing pyruvate decarboxylase pathway. *Scientific Reports* **7**, 1-11.

Feala, J. D., Coquin, L., McCulloch, A. D. and Paternostro, G. (2007). Flexibility in energy metabolism supports hypoxia tolerance in *Drosophila* flight muscle: metabolomic and computational systems analysis. *Molecular Systems Biology* **3**.

Flammang, B. E. and Lauder, G. V. (2008). Speed-dependent intrinsic caudal fin muscle recruitment during steady swimming in bluegill sunfish, *Lepomis macrochirus*. *Journal of Experimental Biology* **211**, 587-598.

Fleming, B. C. and Beynnon, B. D. (2004). *In vivo* measurement of ligament/tendon strains and forces: A review. *Annals of Biomedical Engineering* **32**, 318-328.

Fongy, A., Romestaing, C., Blanc, C., Lacoste-Garanger, N., Rouanet, J. L., Raccurt, M. and Duchamp, C. (2013). Ontogeny of muscle bioenergetics in Adelie penguin chicks (*Pygoscelis adeliae*). *American Journal of Physiology-Regulatory Integrative and Comparative Physiology* **305**, 1065-1075.

Fu, S.-J., Peng, J. and Killen, S. S. (2018). Digestive and locomotor capacity show opposing responses to changing food availability in an ambush predatory fish. *The Journal of Experimental Biology*.

Fukutomi, M. and Ogawa, H. (2017). Crickets alter wind-elicited escape strategies depending on acoustic context. *Scientific Reports* **7**, 8.

Gazzola, M., Argentina, M. and Mahadevan, L. (2014). Scaling macroscopic aquatic locomotion. *Nature Physics* **10**, 758-761.

Gemmell, B. J., Fogerson, S. M., Costello, J. H., Morgan, J. R., Dabiri, J. O. and Colin, S. P. (2016). How the bending kinematics of swimming lampreys build negative pressure fields for suction thrust. *Journal of Experimental Biology* **219**, 3884-3895.

Gerry, S. P. and Ellerby, D. J. (2014). Resolving shifting patterns of muscle energy use in swimming fish. *PloS one* **9**.

Gerson, A. R. and Guglielmo, C. G. (2013). Energetics and metabolite profiles during early flight in American robins (*Turdus Migratorius*). *Journal of Comparative Physiology B-Biochemical Systemic and Environmental Physiology* **183**, 983-991.

Gillis, G. B. (1998). Neuromuscular control of anguilliform locomotion: Patterns of red and white muscle activity during swimming in the American eel *Anguilla rostrata*. *Journal of Experimental Biology* **201**, 3245-3256.

Gosline, J. M., Steeves, J. D., Harman, A. D. and Demont, M. E. (1983). Patterns of circular and radial mantle muscle-activity in respiration and jetting of the squid *Loligo opalescens*. *Journal of Experimental Biology* **104**, 97-109.

Gould, S. J. (1966). Allometry and size in ontogeny and phylogeny. *Biological Reviews* **41**, 587-638.

Greidinger, A. (2012). Swimming kinematics and force-velocity relationship of the obliquely striated longitudinal muscles in the body wall of the ribbon leech (*Erpobdella obscura*). In *Department of Biology*, vol. BSc (Hons). Lancaster, PA, USA: Franklin and Marshall College.

Greig, C. A. and Jones, D. A. (2016). Muscle physiology and contraction. *Surgery (Oxford)* **34**, 107-114.

Grieshaber, M. and Gäde, G. (1976). The biological role of octopine in the squid,Loligo vulgaris (Lamarck). *Journal of Comparative Physiology* **108**, 225-232.

Guppy, M., Hulbert, W. C. and Hochachka, P. W. (1979). Metabolic sources of heat and power in tuna muscles .2. Enzyme and metabolite profiles. *Journal of Experimental Biology* **82**, 303-320.

Haba, A. (2016). The functional morphology and ontogeny of the nuchal retractor muscle in the Atlantic long-fin squid (*Doryteuthis pealeii*). *Franklin & Marshall College*.

Hanlon, R. (2007). Cephalopod dynamic camouflage. *Current Biology* **17**, 400-404.

Hanlon, R. T. and Messenger, J. B. (1988). Adaptive coloration in young cuttlefish (*Sepia officinalis*) - the morphology and development of body patterns and their relation to behavior. *Philosophical Transactions of the Royal Society of London Series B-Biological Sciences* **320**, 437-487.

Harrison, S. M., Whitton, R. C., Kawcak, C. E., Stover, S. M. and Pandy, M. G. (2010). Relationship between muscle forces, joint loading and utilization of elastic strain energy in equine locomotion. *Journal of Experimental Biology* **213**, 3998-4009.

Hartree, W. and Hill, A. V. (1921). The nature of the isometric twitch. *Journal of Physiology-London* **55**, 389-411.

Hawley, J. A. (2002). Adaptations of skeletal muscle to prolonged, intense endurance training. *Clinical and Experimental Pharmacology and Physiology* **29**, 218-222.

Heglund, N. C. and Cavagna, G. A. (1987). Mechanical work, oxygen-consumption, and efficiency in isolated frog and rat muscle. *American Journal of Physiology* **253**, 22-29.

Heglund, N. C. and Taylor, C. R. (1988). Speed, stride frequency and energy-cost per stride - how do they change with body size and gait. *Journal of Experimental Biology* **138**, 301-318.

Heglund, N. C., Taylor, C. R. and McMahon, T. A. (1974). Scaling stride frequency and gait to animal size - mice to horses. *Science* **186**, 1112-1113.

Helmer, D., Geurten, B. R. H., Dehnhardt, G. and Hanke, F. D. (2017). Saccadic movement strategy in common cuttlefish (*Sepia officinalis*). *Frontiers in Physiology* **7**.

Hemmert, H. M. and Baltzley, M. J. (2016). Intraspecific scaling relationships between crawling speed and body size in a Gastropod. *Biological Bulletin* **230**, 78-84.

Herschlag, G. and Miller, L. (2011). Reynolds number limits for jet propulsion: A numerical study of simplified jellyfish. *Journal of Theoretical Biology* **285**, 84-95.

Hessel, A. L. and Nishikawa, K. C. (2017). The hip-twist jump: A unique mechanism for jumping in lungless salamanders. *Journal of Herpetology* **51**, 461-467.

Hickman, C. P. (2009). Animal diversity. Boston, Mass. ; London: McGraw-Hill Higher Education.

Hill, A. V. (1938). The heat of shortening and the dynamic constants of muscle. *Proceedings of the Royal Society Series B-Biological Sciences* **126**, 136-195.

Hill, A. V. (1950). The dimensions of animals and their muscular dynamics *Scientific Progress* **38**, 200-230.

Hinkle, P. C. (2005). P/O ratios of mitochondrial oxidative phosphorylation. *Biochimica Et Biophysica Acta-Bioenergetics* **1706**, 1-11.

Hinkle, P. C., Kumar, M. A., Resetar, A. and Harris, D. L. (1991). Mechanistic stoichiometry of mitochondrial oxidative-phosphorylation. *Biochemistry* **30**, 3576-3582.

Homsher, E., Kean, C. J., Wallner, A. and Garibian-Sarian, V. (1979). The time-course of energy balance in an isometric tetanus. *The Journal of General Physiology* **73**, 553-567.

Huntance, J. (2010). Temperature and salinity. London: DEFRA on behalf of the United Kingdom Marine Monitoring and Assessment Strategy (UKMMAS) Community.

Husak, J. F. and Fox, S. F. (2008). Sexual selection on locomotor performance. *Evolutionary Ecology Research* **10**, 213-228.

Huxley, A. F. (1974). Muscular-contraction - review lecture. *Journal of Physiology-London* **243**, 1-43.

Ipata, P. L. and Balestri, F. (2012). Glycogen as a fuel: metabolic interaction between glycogen and ATP catabolism in oxygen-independent muscle contraction. *Metabolomics* **8**, 736-741.

Jackson, B. E. and Dial, K. P. (2011). Scaling of mechanical power output during burst escape flight in the Corvidae. *Journal of Experimental Biology* **214**, 452-461.

James, R. S. (2013). A review of the thermal sensitivity of the mechanics of vertebrate skeletal muscle. *Journal of Comparative Physiology B* **183**, 723-733.

James, R. S., Cole, N. J., Davies, M. L. F. and Johnston, I. A. (1998). Scaling of intrinsic contractile properties and myofibrillar protein composition of fast muscle in the fish *Myoxocephalus scorpius* L. *Journal of Experimental Biology* **201**, 901-912.

James, R. S. and Johnston, I. A. (1998). Scaling of muscle performance during escape responses in the fish *Myoxocephalus scorpius* L. *Journal of Experimental Biology* **201**, 913-923.

James, R. S., Young, I. S., Cox, V. M., Goldspink, D. F. and Altringham, J. D. (1996). Isometric and isotonic muscle properties as determinants of work loop power output. *Pflugers Archiv-European Journal of Physiology* **432**, 767-774.

Jastrebsky, R. A. (2015). Kinematics and hydrodynamics of cephalopod turning performance in routine swimming and predatory attacks. *Old Dominion University*.

Jastrebsky, R. A., Bartol, I. K. and Krueger, P. S. (2016). Turning performance in squid and cuttlefish: unique dual-mode, muscular hydrostatic systems. *Journal of Experimental Biology* **219**, 1317-1326.

Jayne, B. C. and Lauder, G. V. (1994). How swimming fish use slow and fast muscle-fibers - implications for models of vertebrate muscle recruitment. *Journal of Comparative Physiology a-Sensory Neural and Behavioral Physiology* **175**, 123-131.

Jenni-Eiermann, S. (2017). Energy metabolism during endurance flight and the post-flight recovery phase. *Journal of Comparative Physiology a-Neuroethology Sensory Neural and Behavioral Physiology* **203**, 431-438.

Jereb, P. and Roper, C. F. E. (2005). Cephalopods of the world: an annotated and illustrated catalogue of cephalopod species known to date. Rome: Food and Agriculture Organisation of the United Nations.

Johnson, T. P. and Johnston, I. A. (1991). Power output of fish muscle-fibers performing oscillatory work - effects of acute and seasonal temperature-change. *Journal of Experimental Biology* **157**, 409-423.

Johnson, T. P., Swoap, S. J., Bennett, A. F. and Josephson, R. K. (1993). Body size, muscle power output and limitations on burst locomotor performance in the lizard *Dipsosaurus dorsalis*. *Journal of Experimental Biology* **174**, 199-213.

Johnston, I. A. and Goldspink, G. (1973). A study of the swimming performance of the Crucian carp *Carassius carassius* (L.) in relation to the effects of exercise and recovery on biochemical changes in the myotomal muscles and liver. *Journal of Fish Biology* **5**, 249-260.

Johnston, I. A. and Maitland, B. (1980). Temperature-acclimation in crucian carp, *Carassius carassius* L., morphometric analyses of muscle-fiber ultrastructure. *Journal of Fish Biology* **17**, 113-125.

Johnston, I. A. and Temple, G. K. (2002). Thermal plasticity of skeletal muscle phenotype in ectothermic vertebrates and its significance for locomotory behaviour. *Journal of Experimental Biology* **205**, 2305-2322.

Jones, E. A., Lucey, K. S. and Ellerby, D. J. (2007). Efficiency of labriform swimming in the bluegill sunfish (*Lepomis macrochirus*). *Journal of Experimental Biology* **210**, 3422-3429.

Josephson, R. K. (1985). Mechanical power output from striated-muscle during cyclic contraction. *Journal of Experimental Biology* **114**, 493-512.

Josephson, R. K. (1993). Contraction dynamics and power output of skeletal-muscle. *Annual Review of Physiology* **55**, 527-546.

Karson, M. A., Boal, J. G. and Hanlon, R. T. (2003). Experimental evidence for spatial learning in cuttlefish (*Sepia officinalis*). *Journal of Comparative Psychology* **117**, 149-155.

Kasumovic, M. M. and Seebacher, F. (2018). Casual movement speed but not maximal locomotor capacity predicts mate searching success. *Journal of Evolutionary Biology* **31**, 438-445.

Katija, K., Colin, S. P., Costello, J. H. and Jiang, H. S. (2015). Ontogenetic propulsive transitions by *Sarsia tubulosa* medusae. *Journal of Experimental Biology* **218**, 2333-2343.

Kazakidi, A., Vavourakis, V., Tsakiris, D. P. and Ekaterinaris, J. A. (2015). A numerical investigation of flow around octopus-like arms: near-wake vortex patterns and force development. *Computer Methods in Biomechanics and Biomedical Engineering* **18**, 1321-1339.

Keulegan, G. H. and Beij, K. H. (1937). Pressure losses for fluid flow in curved pipes. *Journal of Research of the National Bureau of Standards* **18**, 89-114.

Kier, W. M. (1988). The arrangement and function of molluscan muscle. In *The mollusca: Form and function*, vol. 1 eds. E. R. Trueman K. M. Wilbur and M. R. Clarke). Oakland, California, USA: Elsevier Academic Press.

Kier, W. M. and Schachat, F. H. (2008). Muscle specialization in the squid motor system. *Journal of Experimental Biology* **211**, 164-169.

Kier, W. M., Smith, K. K. and Miyan, J. A. (1989). Electromyography of the fin musculature of the cuttlefish *Sepia officinalis*. *Journal of Experimental Biology* **143**, 17-31.

Kier, W. M. and Thompson, J. T. (2003). Muscle arrangement, function and specialization in recent coleoids. *Berliner Palaobiol. Abh.* **3**, 141-162.

King, A. J. and Adamo, S. A. (2006). The ventilatory, cardiac and behavioural responses of resting cuttlefish (*Sepia officinalis* L.) to sudden visual stimuli. *Journal of Experimental Biology* **209**, 1101-1111.

Kraskura, K. and Nelson, J. A. (2018). Hypoxia and sprint swimming performance of juvenile striped bass, *Morone saxatilis*. *Physiological and Biochemical Zoology* **91**, 682-690.

Krauel, J. J., Ratcliffe, J. M., Westbrook, J. K. and McCracken, G. F. (2018). Brazilian free-tailed bats (*Tadarida brasiliensis*) adjust foraging behaviour in response to migratory moths. *Canadian Journal of Zoology* **96**, 513-520.

Kretzschmar, K. M. (1975). Heat production and metabolism during the contraction of mammalian skeletal muscle. *Journal of Supramolecular Structure* **3**, 175-180.

Krieg, M. and Mohseni, K. (2015). Pressure and work analysis of unsteady, deformable, axisymmetric, jet producing cavity bodies. *Journal of Fluid Mechanics* **769**, 337-368.

Kuznetsova, A., Brockhoff, P. B., Christensen, R. H. B. (2017). lmerTest: Tests in linear mixed effects models. *Journal of Statistical Software* **82**.

Lamarre, S. G., MacCormack, T. J., Sykes, A. V., Hall, J. R., Speers-Roesch, B., Callaghan, N. I. and Driedzic, W. R. (2016). Metabolic rate and rates of protein turnover in food-deprived cuttlefish, *Sepia officinalis* (Linnaeus 1758). *American Journal of Physiology-Regulatory Integrative and Comparative Physiology* **310**, 1160-1168.

Lee, D. G., Park, M. W., Kim, B. H., Kim, H., Jeon, M. A. and Lee, J. S. (2014). Microanatomy and ultrastructure of outer mantle epidermis of the cuttlefish, *Sepia esculenta* (Cephalopoda: Sepiidae). *Micron* **58**, 38-46.

Lee, S. S. M., Miara, M. D., Arnold, A. S., Biewener, A. A. and Wakeling, J. M. (2013). Recruitment of faster motor units is associated with greater rates of fascicle strain and rapid changes in muscle force during locomotion. *Journal of Experimental Biology* **216**, 198-207.

Levy, G., Flash, T. and Hochner, B. (2015). Arm coordination in octopus crawling involves unique motor control strategies. *Current Biology* **25**, 1195-1200.

Li, J. T., Li, W. T., Zhang, X. M. and He, P. G. (2018). Physiological and behavioral responses of different modes of locomotion in the whiteleg shrimp *Litopenaeus vannamei* (Boone, 1931) (Caridea: Penaeidae). *Journal of Crustacean Biology* **38**, 79-90.

Linden, P. F. (2011). The efficiency of pulsed-jet propulsion. *Journal of Fluid Mechanics* **668**, 1-4.

Linden, P. F. and Turner, J. S. (2004). 'Optimal' vortex rings and aquatic propulsion mechanisms. *Proceedings of the Royal Society B-Biological Sciences* **271**, 647-653.

Lowry, O. H. and Passonneau, J. V. (1972). A flexible system of enzymatic analysis: Academic Press.

Luther, P. K., Munro, P. M. G. and Squire, J. M. (1995). Muscle ultrastructure in the teleost fish. *Micron* **26**, 431-459.

Maddock, L., Bone, Q. and Rayner, J. M. V. (1994). Mechanics and physiology of animal swimming. Cambridge, UK: University of Cambridge Press.

Marsh, R. L. (1990). Deactivation rate and shortening velocity as determinants of contractile frequency. *American Journal of Physiology* **259**, 223-230.

Marsh, R. L. and Bennett, A. F. (1985). Thermal-dependence of isotonic contractile properties of skeletal-muscle and sprint performance of the lizard *Dipsosaurus dorsalis*. *Journal of Comparative Physiology B-Biochemical Systemic and Environmental Physiology* **155**, 541-551.

Marsh, R. L. and Bennett, A. F. (1986). Thermal-dependence of contractile properties of skeletal-muscle from the lizard *Sceloporus occidentalis* with comments on methods for fitting and comparing force-velocity curves. *Journal of Experimental Biology* **126**, 63-77.

Marsh, R. L. and Olson, J. M. (1994). Power output of scallop adductor muscle during contractions replicating the *in-vivo* mechanical cycle. *Journal of Experimental Biology* **193**, 139-156.

Marsh, R. L., Olson, J. M. and Guzik, S. K. (1992). Mechanical performance of scallop adductor muscle during swimming. *Nature* **357**, 411-413.

Maughan, R. J., Watson, J. S. and Weir, J. (1983). Strength and cross-sectional area of human skeletal-muscle. *Journal of Physiology-London* **338**, 37-49.

Mauguit, Q., Olivier, D., Vandewalle, N. and Vandewalle, P. (2010). Ontogeny of swimming movements in bronze corydoras (*Corydoras aeneus*). *Canadian Journal of Zoology-Revue Canadienne De Zoologie* **88**, 378-389.

McMahon, T. (1973). Size and shape in biology. *Science* **179**, 1201-1204.

Meijering, E., Dzyubachyk, D. and Smal, I. (2012). Methods for cell and particle tracking. *Methods in Enzymology* **504**, 183-200.

Melzner, F., Bock, C. and Poertner, H.-O. (2007). Allometry of thermal limitation in the cephalopod *Sepia officinalis*. *Comparative Biochemistry and Physiology a-Molecular & Integrative Physiology* **146**, 149-154.

Melzner, F., Bock, C. and Portner, H. O. (2006). Critical temperatures in the cephalopod Sepia officinalis investigated using in vivo P-31 NMR spectroscopy. *Journal of Experimental Biology* **209**, 891-906.

Mendez, J. and Keys, A. (1960). Density and composition of mammalian muscle. *Metabolism-Clinical and Experimental* **9**, 184-188.

Mill, P. J. and Knapp, M. F. (1970). Fine structure of obliquely striated body wall muscles in earthworm, *Lumbricus terrestris Journal of Cell Science* **7**, 233-261.

Mill, P. J. and Pickard, R. S. (1975). Jet-propulsion in Anisopteran dragonfly larvae. *Journal of Comparative Physiology* **97**, 329-338.

Milligan, B. J., Curtin, N. A. and Bone, Q. (1997). Contractile properties of obliquely striated muscle from the mantle of squid (*Alloteuthis subulata*) and cuttlefish (*Sepia officinalis*). *Journal of Experimental Biology* **200**, 2425-2436.

Millman, B. M. (1967). Mechanism of contraction in molluscan muscle. *American Zoologist* **7**, 583-591.

Moltschaniwskyj, N. A. (1994). Muscle-tissue growth and muscle-fiber dynamics in the tropical loliginid squid *Photololigo sp*. (Cephalopoda, Loliginidae). *Canadian Journal of Fisheries and Aquatic Sciences* **51**, 830-835.

Moltschaniwskyj, N. A. (2004). Understanding the process of growth in cephalopods. *Marine and Freshwater Research* **55**, 379-386.

Moo, E. K., Peterson, D. R., Leonard, T. R., Kaya, M. and Herzog, W. (2017). *In vivo* muscle force and muscle power during near-maximal frog jumps. *PloS one* **12**.

Morris, S. and Adamczewska, A. M. (2002). Utilisation of glycogen, ATP and arginine phosphate in exercise and recovery in terrestrial red crabs, *Gecarcoidea natalis*. *Comparative Biochemistry and Physiology a-Molecular and Integrative Physiology* **133**, 813-825.

Muller, U. K. and van Leeuwen, J. L. (2006). Undulatory fish swimming: from muscles to flow. *Fish and Fisheries* **7**, 84-103.

Mullowney, D., Morris, C., Dawe, E., Zagorsky, I. and Goryanina, S. (2018). Dynamics of snow crab (*Chionoecetes opilio*) movement and migration along the Newfoundland and Labrador and Eastern Barents Sea continental shelves. *Reviews in Fish Biology and Fisheries* **28**, 435-459.

Muniz, D. G., Baena, M. L., Macias-Ordonez, R. and Machado, G. (2018). Males, but not females, perform strategic mate searching movements between host plants in a leaf beetle with scramble competition polygyny. *Ecology and Evolution* **8**, 5828-5836.

Neil, T. R. (2016). Muscle mechanics and hydrodynamics of jet propulsion swimming in marine invertebrates. *University of Leeds*.

Neil, T. R. and Askew, G. N. (2018). Swimming mechanics and propulsive efficiency in the chambered nautilus. *Royal Society Open Science* **5**.

Newcomb, J. M. and Watson, W. H. (2002). Modulation of swimming in the gastropod *Melibe leonina* by nitric oxide. *Journal of Experimental Biology* **205**, 397-403.

Ngo, V. and McHenry, M. J. (2014). The hydrodynamics of swimming at intermediate Reynolds numbers in the water boatman (Corixidae). *Journal of Experimental Biology* **217**, 2740-2751.

Niklas, K. J. (1994). The scaling of plant and animal body-mass, length, and diameter. *Evolution* **48**, 44-54.

Nixon, M. and Mangold, K. (1998). The early life of *Sepia officinalis*, and the contrast with that of *Octopus vulgaris* (Cephalopoda). *Journal of Zoology* **245**, 407-421.

Nudds, R. L., Taylor, G. K. and Thomas, A. L. R. (2004). Tuning of Strouhal number for high propulsive efficiency accurately predicts how wingbeat frequency and stroke amplitude relate and scale with size and flight speed in birds. *Proceedings of the Royal Society B-Biological Sciences* **271**, 2071-2076.

O'Dor, R. (2002). Telemetered cephalopod energetics: swimming, soaring, and blimping. *Integrative and Comparative Biology* **42**, 1065-1070.

O'Dor, R. K., Foy, E. A., Helm, P. A. and Balch, N. (1986). The locomotion and energetics of hatchling squid *Illex illecebrosus*. *American Malacological Bulletin* **4**, 55-60.

O'Dor, R. K. and Webber, D. M. (1986). The constraints on cephalopods - why squid aren't fish. *Canadian Journal of Zoology-Revue Canadienne De Zoologie* **64**, 1591-1605.

O'Dor, R. K. and Webber, D. M. (1991). Invertebrate athletes - trade-offs between transport efficiency and power-density in cephalopod evolution. *Journal of Experimental Biology* **160**, 93-112.

Olson, J. M. and Marsh, R. L. (1993). Contractile properties of the striated adductor muscle in the bay scallop *Argopecten irradians* at several temperatures. *Journal of Experimental Biology* **176**, 175-193.

Olson, J. M. and Marsh, R. L. (in preparation). Efficiency of the adductor muscle in scallops during jet-propulsion.

Ono, S. (2014). Regulation of structure and function of sarcomeric actin filaments in striated muscle of the nematode *Caenorhabditis elegans*. *Anatomical Record-Advances in Integrative Anatomy and Evolutionary Biology* **297**, 1548-1559.

Ormerod, K. G., LePine, O. K., Abbineni, P. S., Bridgeman, J. M., Coorssen, J. R., Mercier, A. J. and Tattersall, G. J. (2017). *Drosophila* development, physiology, behavior, and lifespan are influenced by altered dietary composition. *Fly* **11**, 153-170.

Pearson, M. P., Spriet, L. L. and Stevens, E. D. (1990). Effect of sprint training on swim performance and white muscle metabolism during exercise and recovery in rainbow-trout (*Oncorhynchus mykiss*). *Journal of Experimental Biology* **149**, 45-60.

Pecl, G. T. and Moltschaniwskyj, N. A. (1997). Changes in muscle structure associated with somatic growth in *Idiosepius pygmaeus*, a small tropical cephalopod. *Journal of Zoology* **242**, 751-764.

Pette, D. and Staron, R. S. (2000). Myosin isoforms, muscle fiber types, and transitions. *Microscopy Research and Technique* **50**, 500-509.

Portner, H. O., Finke, E. and Lee, P. G. (1996). Metabolic and energy correlates of intracellular pH in progressive fatigue of squid (*L. brevis*) mantle muscle. *American Journal of Physiology-Regulatory Integrative and Comparative Physiology* **271**, 1403-1414.

Priede, I. G. (1977). Natural selection for energetic efficiency and the relationship between activity level and mortality. *Nature* **267**, 610.

Quillin, K. J. (1998). Ontogenetic scaling of hydrostatic skeletons: Geometric, static stress and dynamic stress scaling of the earthworm *Lumbricus terrestris*. *Journal of Experimental Biology* **201**, 1871-1883.

Quillin, K. J. (1999). Kinematic scaling of locomotion by hydrostatic animals: Ontogeny of peristaltic crawling by the earthworm *Lumbricus terrestris*. *Journal of Experimental Biology* **202**, 661-674.

Quillin, K. J. (2000). Ontogenetic scaling of burrowing forces in the earthworm *Lumbricus terrestris*. *Journal of Experimental Biology* **203**, 2757-2770.

Reidy, S. P., Kerr, S. R. and Nelson, J. A. (2000). Aerobic and anaerobic swimming performance of individual Atlantic cod. *Journal of Experimental Biology* **203**, 347-357.

Renaud, J. M. and Stevens, E. D. (1984). The extent of short-term and long-term compensation to temperature shown by frog and toad sartorius muscle. *Journal of Experimental Biology* **108**, 57-75.

Roberts, T. J., Abbott, E. M. and Azizi, E. (2011). The weak link: do muscle properties determine locomotor performance in frogs? *Philosophical Transactions of the Royal Society B-Biological Sciences* **366**, 1488-1495.

Robertson, J. D. (1965). Studies on the chemical composition of muscle tissue III: The mantle muscle of cephalopod molluscs. *Journal of Experimental Biology* **42**, 153-175.

Rogers, C. M., Nelson, L., Milligan, B. J. and Brown, E. R. (1997). Different excitation-contraction coupling mechanisms exist in squid, cuttlefish and octopod mantle muscle. *Journal of Experimental Biology* **200**, 3033-3041.

Rome, L. C. (1983). The effect of long-term exposure to different temperatures on the mechanical performance of frog-muscle. *Physiological Zoology* **56**, 33-40.

Rome, L. C., Funke, R. P., Alexander, R. M., Lutz, G., Aldridge, H., Scott, F. and Freadman, M. (1988). Why animals have different muscle-fiber types. *Nature* **335**, 824-827.

Rome, L. C., Loughna, P. T. and Goldspink, G. (1985). Temperature-acclimation - improved sustained swimming performance in carp at low-temperatures. *Science* **228**, 194-196.

Rome, L. C., Sosnicki, A. A. and Goble, D. O. (1990). Maximum velocity of shortening of three fibre types from horse soleus muscle: implications for scaling with body size. *The Journal of Physiology* **431**, 173-185.

Rome, L. C. and Swank, D. (1992). The influence of temperature on power output of scup red muscle during cyclical length changes. *Journal of Experimental Biology* **171**, 261-281.

Rosa, R. and Seibel, B. A. (2010). Metabolic physiology of the Humboldt squid, *Dosidicus gigas*: Implications for vertical migration in a pronounced oxygen minimum zone. *Progress in Oceanography* **86**, 72-80.

Rosenbluth, J., Szent-Gyorgyi, A. G. and Thompson, J. T. (2010). The ultrastructure and contractile properties of a fast-acting, obliquely striated, myosin-

regulated muscle: the funnel retractor of squids. *Journal of Experimental Biology* **213**, 2430-2443.

Rossi, G. S., Turko, A. J. and Wright, P. A. (2018). Oxygen drives skeletal muscle remodeling in an amphibious fish out of water. *The Journal of Experimental Biology*.

Ruegg, J. C. (1987). Excitation-contraction coupling in fast-twitch and slow-twitch muscle-fibers. *International Journal of Sports Medicine* **8**, 360-364.

Russell, F. S. and Steven, G. A. (1930). The Swimming of Cuttlefish. *Nature* **125**, 893.

Sanchez, G., Setiamarga, D. H. E., Tuanapaya, S., Tongtherm, K., Winkelmann, I. E., Schmidbaur, H., Umino, T., Albertin, C., Allcock, L., Perales-Raya, C. *et al.* (2018). Genus-level phylogeny of cephalopods using molecular markers: current status and problematic areas. *Peerj* **6**.

Sato, K., Shiomi, K., Watanabe, Y., Watanuki, Y., Takahashi, A. and Ponganis, P. J. (2010). Scaling of swim speed and stroke frequency in geometrically similar penguins: they swim optimally to minimize cost of transport. *Proceedings of the Royal Society B-Biological Sciences* **277**, 707-714.

Satterlie, R. A. (2011). Do jellyfish have central nervous systems? *Journal of Experimental Biology* **214**, 1215-1223.

Scatà, G., Darmaillacq, A.-S., Dickel, L., McCusker, S. and Shashar, N. (2017). Going up or sideways? Perception of space and obstacles negotiating by cuttlefish. *Frontiers in Physiology* **8**.

Schellenberg, F., Oberhofer, K., Taylor, W. R. and Lorenzetti, S. (2015). Review of modelling techniques for *in vivo* muscle force estimation in the lower extremities during strength training. *Computational and Mathematical Methods in Medicine*.

Schiaffino, S. and Reggiani, C. (1994). Myosin isoforms in mammalian skeletal muscle. *Journal of Applied Physiology* **77**, 493-501.

Schneider, C. A., Rasband, W. S. and Eliceiri, K. W. (2012). NIH Image to ImageJ: 25 years of image analysis. *Nature Methods* **9**, 671-675.

Seebacher, F., Little, A. G. and James, R. S. (2015). Skeletal muscle contractile function predicts activity and behaviour in zebrafish. *Journal of Experimental Biology* **218**, 3878-3884.

Seebacher, F. and Walter, I. (2012). Differences in locomotor performance between individuals: importance of parvalbumin, calcium handling and metabolism. *Journal of Experimental Biology* **215**, 663-670.

Seibel, B. A., Thuesen, E. V., Childress, J. J. and Gorodezky, L. A. (1997). Decline in pelagic cephalopod metabolism with habitat depth reflects differences in locomotory efficiency. *Biological Bulletin* **192**, 262-278.

Seow, C. Y. (2013). Hill's equation of muscle performance and its hidden insight on molecular mechanisms. *Journal of General Physiology* **142**, 561-573.

Sfakiotakis, M., Kazakidi, A. and Tsakiris, D. P. (2015). Octopus-inspired multi-arm robotic swimming. *Bioinspiration & Biomimetics* **10**, 22.

Shaffer, J. F. and Kier, W. M. (2012). Muscular tissues of the squid *Doryteuthis pealeii* express identical myosin heavy chain isoforms: an alternative mechanism for tuning contractile speed. *Journal of Experimental Biology* **215**, 239-246.

Shan, J. W. and Dimotakis, P. E. (2006). Reynolds-number effects and anisotropy in transverse-jet mixing. *Journal of Fluid Mechanics* **566**, 47-96.

Sherrard, K. M. (2000). Cuttlebone morphology limits habitat depth in eleven species of Sepia (Cephalopoda : Sepiidae). *Biological Bulletin* **198**, 404-414.

Shipley, O. N., Brownscombe, J. W., Danylchuk, A. J., Cooke, S. J., O'Shea, O. R. and Brooks, E. J. (2018). Fine-scale movement and activity patterns of Caribbean reef sharks (*Carcharhinus perezi*) in the Bahamas. *Environmental Biology of Fishes* **101**, 1097-1104.

Smith, K. K. and Hylander, W. L. (1985). Strain-gauge measurement of mesokinetic movement in the lizard *Varanus exanthematicus*. *Journal of Experimental Biology* **114**, 53-70.

Smith, N. P., Barclay, C. J. and Loiselle, D. S. (2005). The efficiency of muscle contraction. *Progress in Biophysics & Molecular Biology* **88**, 1-58.

Snell, H. L., Jennings, R. D., Snell, H. M. and Harcourt, S. (1988). Intrapopulation variation in predator-avoidance performance of Galápagos lava

lizards: The interaction of sexual and natural selection. *Evolutionary Ecology* **2**, 353-369.

Speers-Roesch, B., Callaghan, N. I., MacCormack, T. J., Lamarre, S. G., Sykes, A. V. and Driedzic, W. R. (2016). Enzymatic capacities of metabolic fuel use in cuttlefish (*Sepia officinalis*) and responses to food deprivation: insight into the metabolic organization and starvation survival strategy of cephalopods. *Journal of Comparative Physiology B-Biochemical Systemic and Environmental Physiology* **186**, 711-725.

Staniland, L. J., Ratcliffe, N., Trathan, P. N. and Forcada, J. (2018). Long term movements and activity patterns of an Antarctic marine apex predator: The leopard seal. *PloS one* **13**.

Stevenson, R. D. and Josephson, R. K. (1990). Effects of operating frequency and temperature on mechanical power output from moth flight-muscle. *Journal of Experimental Biology* **149**, 61-78.

Stewart, W. J., Bartol, I. K. and Krueger, P. S. (2010). Hydrodynamic fin function of brief squid, *Lolliguncula brevis*. *Journal of Experimental Biology* **213**, 2009-2024.

Storey, K. B. (1977). Tissue specific isozymes of octopine dehydrogenase in cuttlefish, S*epia officinalis* - roles of octopine dehydrogenase and lactate-dehydrogenase in *Sepia*. *Journal of Comparative Physiology* **115**, 159-169.

Storey, K. B. and Storey, J. M. (1978). Energy metabolism in the mantle muscle of the squid, *Loligo pealeii*. *Journal of Comparative Physiology* **123**, 169-175.

Storey, K. B. and Storey, J. M. (1979). Octopine metabolism in the cuttlefish, *Sepia officinalis* - octopine production by muscle and its role as an aerobic substrate for non-muscular tissues. *Journal of Comparative Physiology* **131**, 311-319.

Suarez, R. K., Lighton, J. R. B., Moyes, C. D., Brown, G. S., Gass, C. L. and Hochachka, P. W. (1990). Fuel selection in Rufous hummingbirds - ecological implications of metabolic biochemistry. *Proceedings of the National Academy of Sciences of the United States of America* **87**, 9207-9210.

Sutherland, K. R. and Madin, L. P. (2010). Comparative jet wake structure and swimming performance of salps. *Journal of Experimental Biology* **213**, 2967-2975.

Svetlichny, L., Larsen, P. S. and Kiorboe, T. (2018). Swim and fly: escape strategy in neustonic and planktonic copepods. *Journal of Experimental Biology* **221**, 9.

Swoap, S. J., Johnson, T. P., Josephson, R. K. and Bennett, A. F. (1993). Temperature, muscle power output and limitations on burst locomotor performance of the lizard *Dipsosaurus dorsalis*. *Journal of Experimental Biology* **174**, 185-197.

Taylor, G. K., Nudds, R. L. and Thomas, A. L. R. (2003). Flying and swimming animals cruise at a Strouhal number tuned for high power efficiency. *Nature* **425**, 707-711.

Thielicke, W. (2014). The flapping flight of birds - analysis and application. *PhD thesis* **Rijksuniversiteit Groningen**

Thielicke, W. and Stamhuis, E. J. (2014a). PIVlab - Time-resolved digital particle image velocimetry tool for MATLAB.

Thielicke, W. and Stamhuis, E. J. (2014b). PIVlab - Towards user-friendly, affordable and accurate digital particle image velocimetry in MATLAB. *Journal of Open Research software* **2**, e30.

Thompson, J. T., Bartol, I. K., Baksi, A. E., Li, K. Y. and Krueger, P. S. (2010). The ontogeny of muscle structure and locomotory function in the long-finned squid *Doryteuthis pealeii*. *Journal of Experimental Biology* **213**, 1079-1091.

Thompson, J. T. and Kier, W. M. (2002). Ontogeny of squid mantle function: Changes in the mechanics of escape-jet locomotion in the oval squid, *Sepioteuthis lessoniana* lesson, 1830. *Biological Bulletin* **203**, 14-26.

Thompson, J. T. and Kier, W. M. (2006). Ontogeny of mantle musculature and implications for jet locomotion in oval squid *Sepioteuthis lessoniana*. *Journal of Experimental Biology* **209**, 433-443.

Thompson, J. T., Shelton, R. M. and Kier, W. M. (2014). The length-force behavior and operating length range of squid muscle vary as a function of position in the mantle wall. *Journal of Experimental Biology* **217**, 2181-2192.

Thompson, J. T., Szczepanski, J. A. and Brody, J. (2008). Mechanical specialization of the obliquely striated circular mantle muscle fibres of the long-finned squid *Doryteuthis pealeii*. *Journal of Experimental Biology* **211**, 1463-1474.

Tobalske, B. W. and Dial, K. P. (2000). Effects of body size on take-off flight performance in the Phasianidae (Aves). *Journal of Experimental Biology* **203**, 3319-3332.

Toida, N., Kuriyama, H., Tashiro, N. and Ito, Y. (1975). Obliquely striated-muscle. *Physiological Reviews* **55**, 700-756.

Trueblood, L. A. and Seibel, B. A. (2013). The jumbo squid, *Dosidicus gigas* (Ommastrephidae), living in oxygen minimum zones I: Oxygen consumption rates and critical oxygen partial pressures. *Deep-Sea Research Part Ii-Topical Studies in Oceanography* **95**, 218-224.

Trueman, E. R. and Packard, A. (1968). Motor performances of some cephalopods. *Journal of Experimental Biology* **49**, 495-&.

Tytell, E. D. and Lauder, G. V. (2004). The hydrodynamics of eel swimming - I. Wake structure. *Journal of Experimental Biology* **207**, 1825-1841.

Unwin, D. M. and Corbet, S. A. (1984). Wingbeat frequency, temperature and body size in bees and flies. *Physiological Entomology* **9**, 115-121.

Uyeno, T. A. and Kier, W. M. (2007). Electromyography of the buccal musculature of octopus (*Octopus bimaculoides*): a test of the function of the muscle articulation in support and movement. *Journal of Experimental Biology* **210**, 118-128.

Vanhooydonck, B., James, R. S., Tallis, J., Aerts, P., Tadic, Z., Tolley, K. A., Measey, G. J. and Herrel, A. (2014). Is the whole more than the sum of its parts? Evolutionary trade-offs between burst and sustained locomotion in lacertid lizards. *Proceedings of the Royal Society B-Biological Sciences* **281**.

Vidal, E. A. G., Zeidberg, L. D. and Buskey, E. J. (2018). Development of swimming abilities in squid paralarvae: Behavioral and ecological implications for dispersal. *Frontiers in Physiology* **9**.

Videler, J. J. and Wardle, C. S. (1992). FIsh swimming stride by stride - speed limits and endurance *Reviews in Fish Biology and Fisheries* **2**, 358-358.

Voesenek, C. J., Muijres, F. T. and van Leeuwen, J. L. (2018). Biomechanics of swimming in developing larval fish. *Journal of Experimental Biology* **221**.

Vogel, S. (1994). Life in movng fluids: the physical biology of flow. Princeton ; Chichester: Princeton University Press.

Watanabe, Y. Y., Sato, K., Watanuki, Y., Takahashi, A., Mitani, Y., Amano, M., Aoki, K., Narazaki, T., Iwata, T., Minamikawa, S. *et al.* (2011). Scaling of swim speed in breath-hold divers. *Journal of Animal Ecology* **80**, 57-68.

Waters, R. E., Rotevatn, S., Li, P., Annex, B. H. and Yan, Z. (2004). Voluntary running induces fiber type-specific angiogenesis in mouse skeletal muscle. *American Journal of Physiology-Cell Physiology* **287**, 1342-1348.

Webb, P. W. (1971). The swimming energetics of trout II. Oxygen consumption and swimming efficiency. *Journal of Experimental Biology* **185**, 179-193.

Webb, P. W., Kostecki, P. T. and Stevens, E. D. (1984). The effect of size and swimming speed on locomotor kinematics of rainbow-trout. *Journal of Experimental Biology* **109**, 77-95.

Webber, D. M. and O'Dor, R. K. (1986). Monitoring the metabolic-rate and activity of free-swimming squid with telemetered jet pressure. *Journal of Experimental Biology* **126**, 205-224.

Wells, M. J. (1994). The evolution of a racing snail. *Marine and Freshwater Behaviour and Physiology* **25**, 1-12.

Wells, M. J. and O'Dor, R. K. (1991). Jet propulsion and the evolution of the cephalopods. *Bulletin of Marine Science* **49**, 419-432.

Westerblad, H., Allen, D. G. and Lannergren, J. (2002). Muscle fatigue: Lactic acid or inorganic phosphate the major cause? *News in Physiological Sciences* **17**, 17-21.

Wexler, Y., Wertheimer, K. O., Subach, A., Pruitt, J. N. and Scharf, I. (2017). Mating alters the link between movement activity and pattern in the red flour beetle. *Physiological Entomology* **42**, 299-306.

Weymouth, G. D. and Triantafyllou, M. S. (2013). Ultra-fast escape of a deformable jet-propelled body. *Journal of Fluid Mechanics* **721**, 367-385.

Whipp, B. J. and Wasserman, K. (1969). Efficiency of muscular work. *Journal of Applied Physiology* **26**, 644-648.

Wilbur, K. M. (1983). The Mollusca. New York ; London: Academic.

Willmer, P., Stone, G. and Johnston, I. A. (2004). Environmental physiology of animals. Malden, Mass. ; Oxford: Blackwell Pub.

Wilson, R. S. and Franklin, C. E. (2000). Effect of ontogenetic increases in body size on burst swimming performance in tadpoles of the striped marsh frog, *Limnodynastes peronii*. *Physiological and Biochemical Zoology* **73**, 142-152.

Wilson, R. S. and James, R. S. (2004). Constraints on muscular performance: trade-offs between power output and fatigue resistance. *Proceedings of the Royal Society B-Biological Sciences* **271**, 222-225.

Wilson, R. S., James, R. S. and Van Damme, R. (2002). Trade-offs between speed and endurance in the frog *Xenopus laevis*: a multi-level approach. *Journal of Experimental Biology* **205**, 1145-1152.

Wissocq, J. C. and Boilly, B. (1977). Obliquely striated and transversally striated muscles of a polychaete annelid - *Magelona papillicornis*. *Biologie Cellulaire* **29**, 183.

Woledge, R. C., Curtin, N. A. and Homsher, E. (1985). Energetic aspects of muscle contraction. London: Academic Press Limited.

Wood, J. B., Maynard, A. E., Lawlor, A. G., Sawyer, E. K., Simmons, D. M., Pennoyer, K. E. and Derby, C. D. (2010). Caribbean reef squid, *Sepioteuthis sepioidea*, use ink as a defense against predatory French grunts, *Haemulon flavolineatum*. *Journal of Experimental Marine Biology and Ecology* **388**, 20-27.

Wood, J. B., Pennoyer, K. E. and Derby, C. D. (2008). Ink is a conspecific alarm cue in the Caribbean reef squid, *Sepioteuthis sepioidea*. *Journal of Experimental Marine Biology and Ecology* **367**, 11-16.

Xavier, J. C., Peck, L. S., Fretwell, P. and Turner, J. (2016). Climate change and polar range expansions: Could cuttlefish cross the Arctic? *Marine Biology* **163**.

Yalcinkaya, B. H., Erikli, S., Ozilgen, B. A., Olcay, A. B., Sorguven, E. and Ozilgen, M. (2016). Thermodynamic analysis of the squid mantle muscles and giant axon during slow swimming and jet escape propulsion. *Energy* **102**, 537-549.

Yekutieli, Y., Sagiv-Zohar, R., Aharonov, R., Engel, Y., Hochner, B. and Flash, T. (2005). Dynamic model of the octopus arm. I. Biomechanics of the octopus reaching movement. *Journal of Neurophysiology* **94**, 1443-1458.

Zamora-Camacho, F. J. (2018). Locomotor performance in a running toad: roles of morphology, sex and agrosystem versus natural habitat. *Biological Journal of the Linnean Society* **123**, 411-421.

Zullo, L., Fossati, S. M., Imperadore, P. and Nödl, M.-T. (2017). Molecular determinants of cephalopod muscles and their implication in muscle regeneration. *Frontiers in Cell and Developmental Biology* **5**.

Appendix 1

Table 15. Parameters tested during the optimisation process. Work and power output recorded at test frequencies are shown, where parameters were maximal data is shown in Chapter 3. n=1 for each row.

Cycle frequency	Strain amplitude	Phase	Train duration	Work, W_c (J kg^{-1})	Power, Π_c (W kg^{-1})
0.5	0.075	-100	800	0.77	0.39
0.6	0.075	-100	660	2.01	1.21
0.6	0.075	-100	740	1.56	0.93
0.6	0.075	-100	850	2.07	1.25
0.6	0.075	-100	800	See Chapter 3	
0.8	0.075	-100	390	0.92	0.73
0.8	0.075	-100	425	0.48	0.39
0.8	0.075	-100	400	4.16	3.33
0.8	0.075	-100	375	3.36	2.69
0.8	0.075	-100	450	3.6	2.9
0.8	0.075	-100	475	See Chapter 3	
0.8	0.075	-100	575	2.07	1.65
1	0.05	-60	120	3.13	3.13
1	0.05	-80	140	3.99	3.99
1	0.05	-100	160	4.15	4.15
1	0.05	-100	200	4.99	4.99
1	0.05	-100	250	5.65	5.65
1	0.05	-100	300	5.98	5.98
1	0.05	-100	350	5.72	5.72
1	0.075	-100	350	See Chapter 3	
1	0.1	-100	350	5.2	5.2
1	0.075	-100	300	2.3	2.3
1	0.075	-100	400	5.61	5.61
1.2	0.075	-100	300	1.15	1.38

Cycle frequency	Strain amplitude	Phase	Train duration	Work, W_c (J kg^{-1})	Power, Π_c (W kg^{-1})
1.2	0.075	-100	260	See Chapter 3	
1.4	0.075	-100	200	See Chapter 3	
1.4	0.075	-100	150	3.29	4.6
1.6	0.075	-100	175	-2.91	-4.65
1.6	0.075	-100	125	-7.53	-12.05
1.6	0.075	-100	90	12.49	19.99
1.6	0.075	-100	85	See Chapter 3	
1.6	0.075	-100	65	0.77	1.24
1.8	0.075	-100	72	See Chapter 3	
2	0.075	-100	75	0.16	0.32
2	0.075	-100	25	-1.5	-3
2	0.075	-100	65	See Chapter 3	
2.5	0.075	-99	40	-2.01	-5.03
2.5	0.075	-50	30	-5.52	-13.8
2.5	0.075	-99	30	-2.81	-7.02
2.5	0.075	-99	50	1.02	2.55
2.5	0.075	-99	75	3.66	9.14
2.5	0.075	-99	65	3.79	9.47
3	0.075	-30	40	-3.53	-10.59
3	0.075	-30	15	-4.54	-13.62

Appendix 2

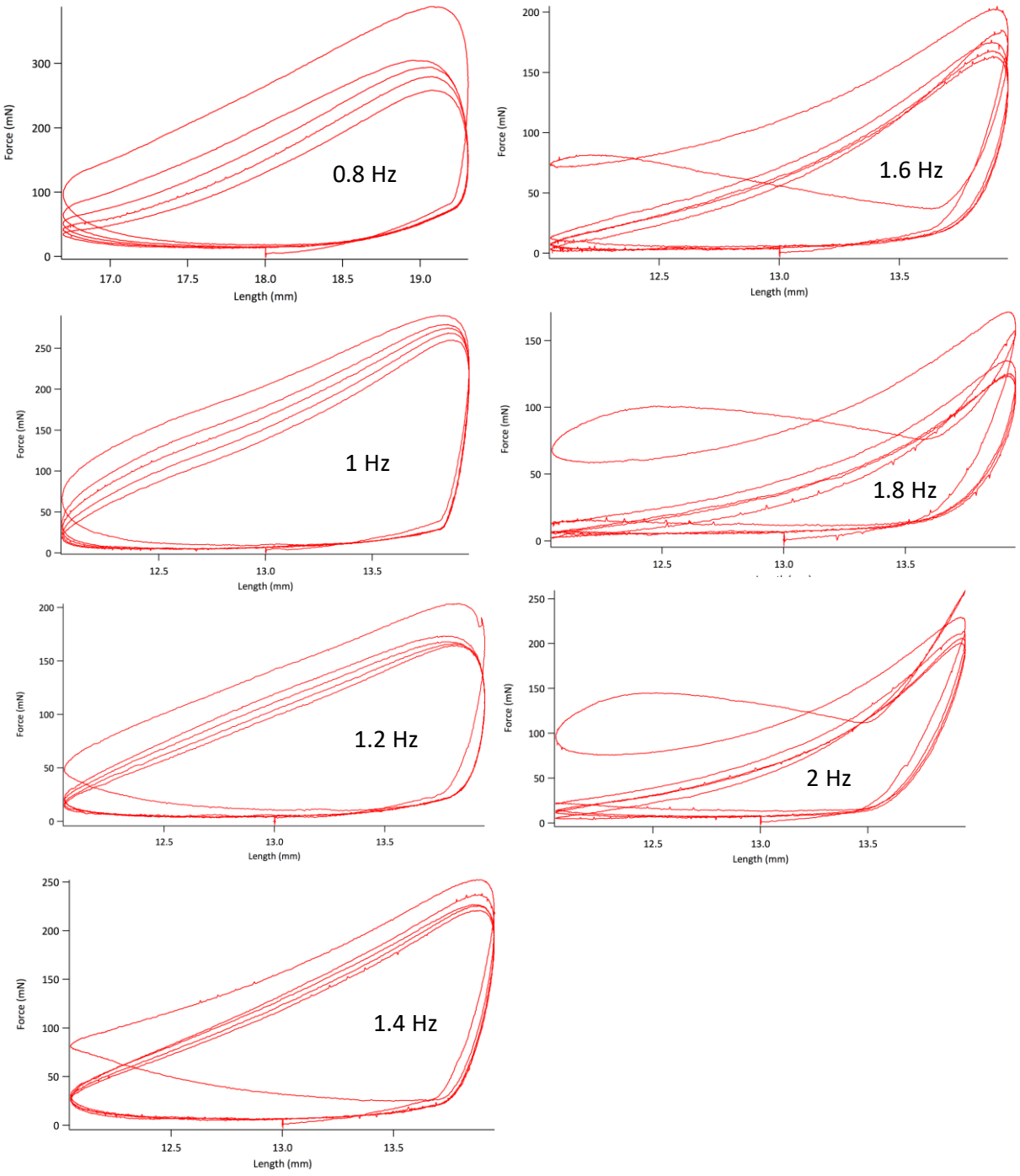

Figure 37. Example work loop traces from juvenile cuttlefish. Work loops show 5 loops at frequencies ranging from 0.8 to 2 Hz. Initial work loops did not relax properly which results in an unusual work loop shape, this is particularly pronounced at higher cycle frequencies.

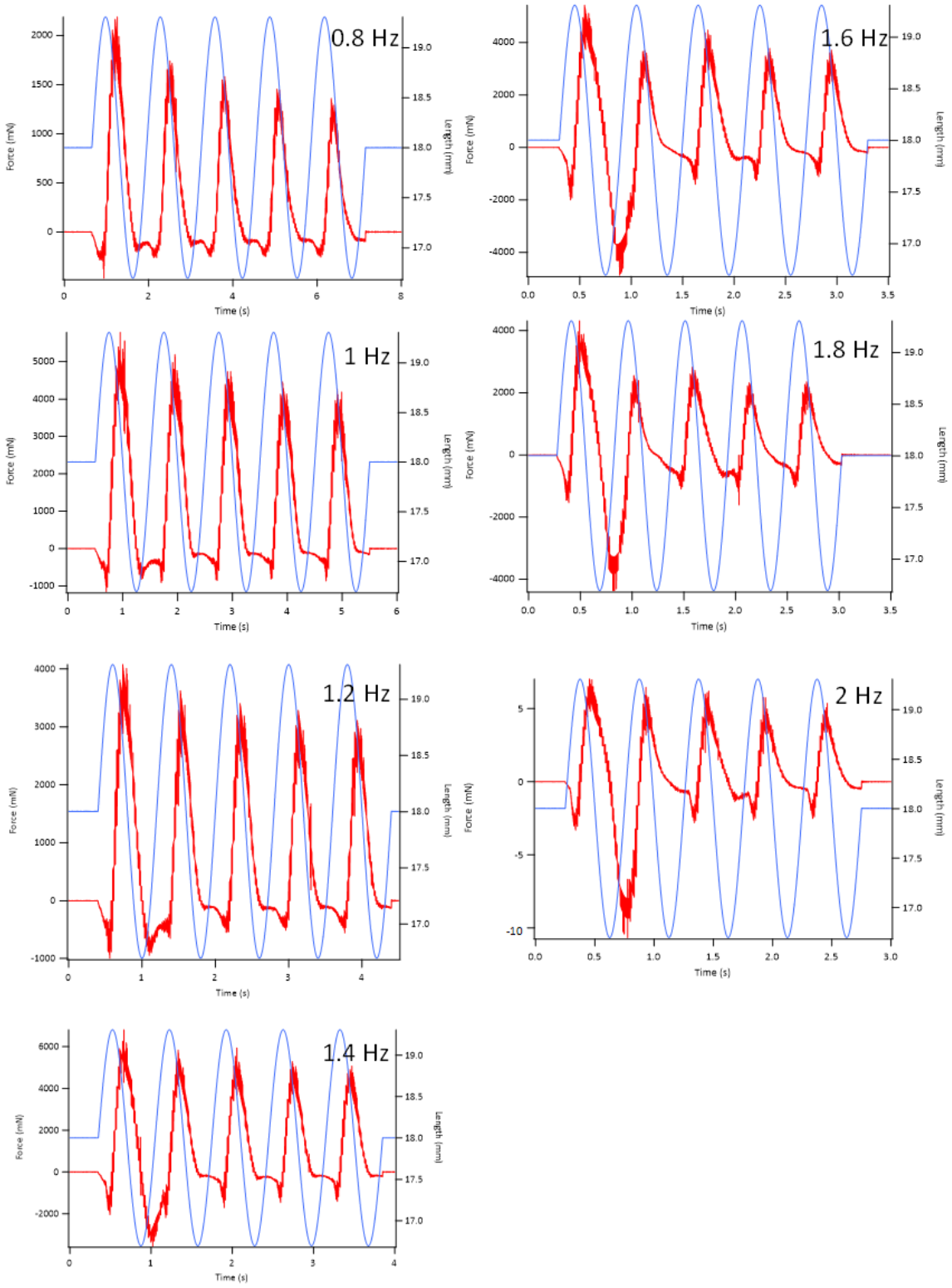

Figure 38. Example force produced by work loops ranging from 0.8 to 2 Hz. Data shown is from one juvenile preparation. Red lines indicate the raw force produced, and blue the changes in length during each consecutive work loop. As noted relaxation of loop one would sometimes result in negative force, with this being more pronounced at higher frequencies.

Appendix 3

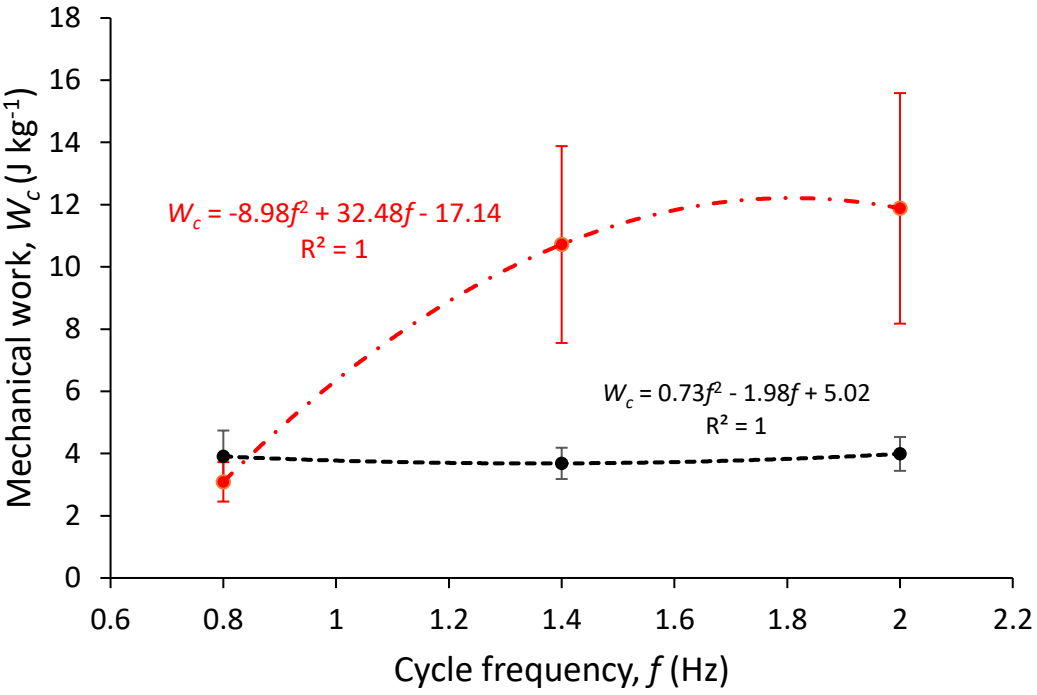

Figure 39. Comparison of the work output of muscle from juvenile preparations from Chapter 3 (red) and 4 (black) at 0.8, 1.4 and 2 Hz. Data presented ± sem.

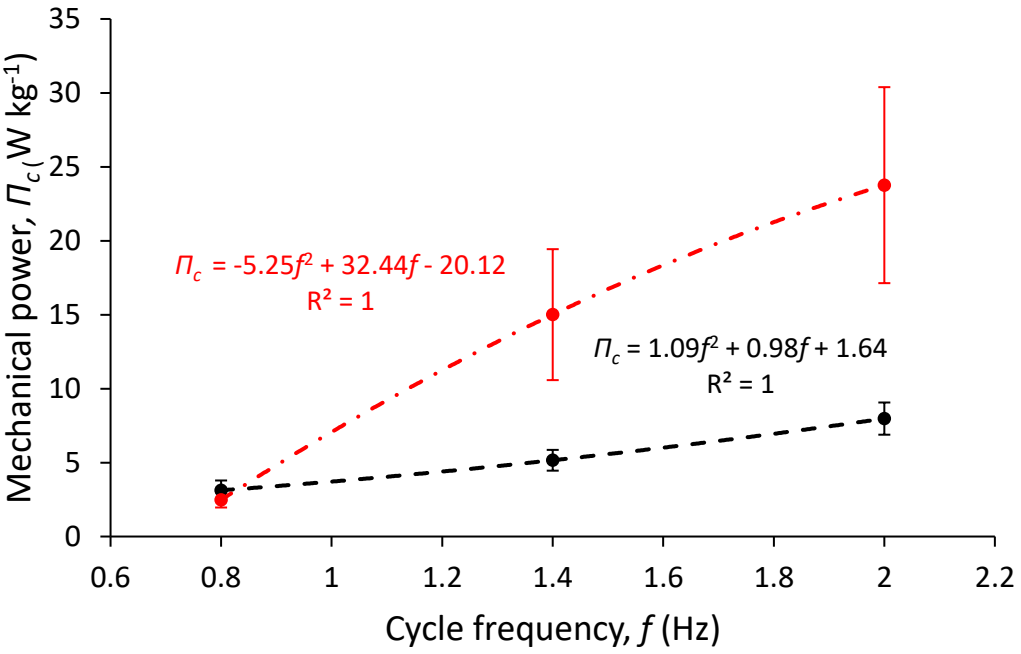

Figure 40. Comparison of the power output of muscle from juvenile preparations from Chapter 3 (red) and 4 (black) at 0.8, 1.4 and 2 Hz. Data presented ± sem.

Table 16. Comparison of the work and power output of juvenile preparations from Chapters 3 and 4. Number of preparations in each chapter is given in brackets. Data presented ± sd

Frequency, f (Hz)	Chapter 3		Chapter 4	
	W_c (J kg^{-1})	Π_c (W kg^{-1})	W_c (J kg^{-1})	Π_c (W kg^{-1})
0.8	3.1 ± 1.4 (3)	2.5 ± 0.9 (3)	3.9 ± 2.5 (9)	3.1 ± 2 (9)
1.4	10 ± 7.1 (5)	15 ± 9.9 (5)	3.7 ± 1.5 (9)	5.2 ± 2.1 (9)
2	11.9 ± 7.4 (4)	23.8 ± 14.8 (4)	4 ± 1.5 (8)	8 ± 3.1 (8)